ISSN 1444-8939

MAGNT RESEARCH REPORT NO. 6
December 2000

MORPHOLOGY, SYSTEMATICS AND EVOLUTION OF THE MARSUPIAL GENUS *NEOHELOS* STIRTON (DIPROTODONTIDAE, ZYGOMATURINAE)

PETER MURRAY, DIRK MEGIRIAN, THOMAS RICH,
MICHAEL PLANE, KAREN BLACK, MICHAEL ARCHER,
SUZANNE HAND AND PATRICIA VICKERS-RICH

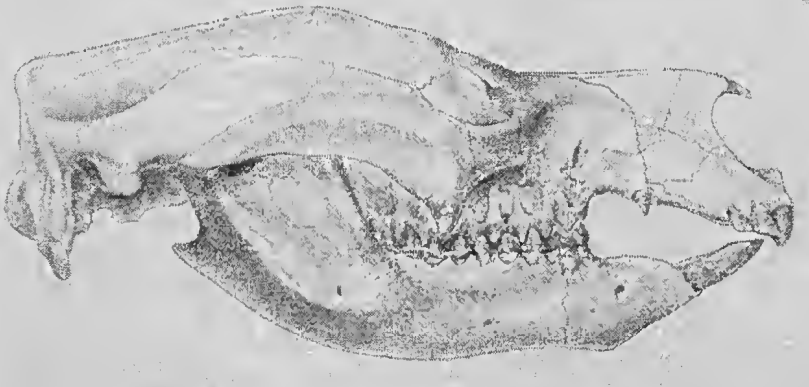

Museums and Art Galleries of the Northern Territory

MAGNT RESEARCH REPORT No. 6, December 2000

MORPHOLOGY, SYSTEMATICS AND EVOLUTION OF THE MARSUPIAL GENUS *NEOHELOS STIRTON* (DIPROTODONTIDAE, ZYGOMATURINAE)

PETER MURRAY, DIRK MEGIRIAN, THOMAS RICH, MICHAEL PLANE, KAREN BLACK, MICHAEL ARCHER, SUZANNE HAND AND PATRICIA VICKERS-RICH

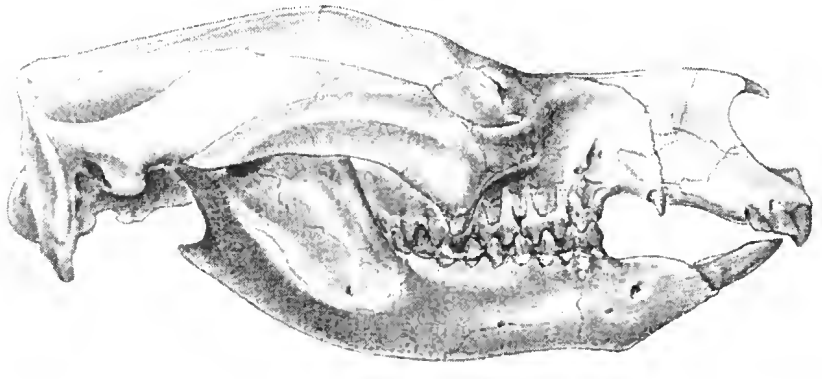

No part of this report may be reproduced without the written permission of the Director, Museums and Art Galleries of the Northern Territory.

MUSEUMS & ART GALLERIES OF THE NORTHERN TERRITORY

The Museums and Art Galleries of the Northern Territory Research Report series is a medium for the dissemination of the results of research undertaken by MAGNT staff in the fields of Natural Sciences, History and Culture. All contributions are reviewed internally by staff of the MAGNT.

First printed 15 December, 2000

ISSN 1444-8939

© 2000 Museums and Art Galleries of the Northern Territory. No part of this report may be reproduced without the written permission of the Director, Museums and Art Galleries of the Northern Territory.

Department of
Arts & Museums
Northern Territory Government

MORPHOLOGY, SYSTEMATICS AND EVOLUTION OF THE MARSUPIAL GENUS *NEOHELOS* STIRTON (DIPROTODONTIDAE, ZYGOMATURINAE)

PETER MURRAY[1], DIRK MEGIRIAN[2], THOMAS RICH[3], MICHAEL PLANE[4], KAREN BLACK[5], MICHAEL ARCHER[5], SUZANNE HAND[5] AND PATRICIA VICKERS-RICH[6]

[1] *Museum of Central Australia, PO Box 3521, Alice Springs NT 0870, AUSTRALIA*
[2] *Museum and Art Gallery of the Northern Territory, GPO Box 4646, Darwin NT 0801, AUSTRALIA*
[3] *Museum Victoria, PO Box 666E, Melbourne VIC 3001, AUSTRALIA*
[4] *PO Gundaroo NSW 2620, AUSTRALIA*
[5] *University of New South Wales, School of Biological Sciences, Sydney 2052 NSW, AUSTRALIA*
[6] *Monash University, Department of Earth Sciences, Clayton VIC 3168, AUSTRALIA*

FOREWORD

The contents of this report were originally submitted to *The Records of the Queen Victoria Museum* in 1995. Subsequent to peer review and acceptance for publication in December 1996, certain aspects of the paper had been presented elsewhere, and at the point of going to press, some co-authors felt that significant parts of the manuscript had been superseded. Rather than re-circulate the manuscript for another lengthy round of editorial revision (a process that had already spanned the greater part of a decade), it was decided to withdraw it from *The Records of the Queen Victoria Museum*. However, because some of the findings of this study had influenced subsequent research, but were not in circulation in a citable form, or readily available to others wishing to verify details, it was decided to present the accepted version of the original manuscript as a *MAGNT Research Report*.

The *MAGNT Research Report* series is not an ideal medium for publishing new taxa. Consequently, the manuscript has been minimally edited for present purposes so as not to introduce new taxonomic nomenclature. Three new *Neohelos* species are identified here only as *Neohelos* spA, spB and spC, and the text (but not the order of presentation) has also been adjusted so that *scottorrorum* remains in *Nimbadon*. Other taxa mentioned that were formally named after 1996 remain as they appeared in the original manuscript.

INTRODUCTION

Over the past three decades, since 1967 when R. A. Stirton first described *Neohelos tirarensis*, Australian vertebrate palaeontologists excavating at Bullock Creek, Northern Territory and Riversleigh, Queensland have recovered many additional specimens representing some new species of the previously rare *Neohelos* fossil material. As a result of our study, the genus *Neohelos* now incorporates four species: the type species *N. tirarensis* Stirton, and three new species informally designated *Neohelos* spA, *Neohelos* spB, and *Neohelos* spC. It is probable that *Nimbadon scottorrorum* also belongs in *Neohelos*. The excellent preservation and completeness of some of the material makes it possible to provide detailed descriptions of a Miocene zygomaturine genus previously known only from a few isolated teeth. The systematic framework for the Zygomaturinae established by Stirton and his colleagues is confirmed by new discoveries made since 1967. We interpret the structural succession within the genus *Neohelos* and its annectant genus *Kolopsis*, as a predominantly gradual evolutionary sequence. Three of the four species of *Neohelos* also provide a chronocline useful in biocorrelation.

Neohelos Stirton, 1967a, was described from five isolated teeth collected in 1962 from the Wipajiri Formation (formerly known as the Wipajiri Channel Sand) on the eastern shore of Lake Ngapakaldi, South Australia. Although the diagnostic specimen, a permanent upper third premolar (P^3) was missing its anterior half, Stirton inferred the presence of a parastyle on the type and then only known species, *Neohelos tirarensis*, from the basic similarity of its posterior half to those of complete specimens belonging to the diprotodontid genera *Plaisiodon* Woodburne, 1967a, *Kolopsis* Woodburne 1967a, *Kolopsoides* Plane, 1967, and *Zygomaturus* Owen, 1859.

Stirton, Woodburne and Plane (1967) went on to analyse a representative collection of diprotodontids from all of the Australian and New Guinean localities known at that time, resulting in the formulation of the basic outline of diprotodontid phylogeny in current use. While they were unable to provide any details about the overall appearance of *Neohelos tirarensis*, their 'stage-of-evolution' analysis of the morphology of the cheek teeth of the various diprotodontid species established the phylogenetic position of *Neohelos* within the subfamily Zygomaturinae, newly erected by the authors to accommodate the genera possessing a large parastyle and posterolingual cusp or hypocone on the P^3.

The zygomaturines thus became established as one of the most useful lineages for stage-of-evolution correlation of fossiliferous deposits in Australia. In 1967 *Neohelos* fossils represented the oldest and most structurally primitive forms within the subfamily. The generic name *Neohelos* is derived from Greek equivalents meaning 'new' (*neo*) + 'wart' (*helos*) referring to the presence of a hypocone on the P^3, specifically alluding to the evolutionary appearance of the structure. The remaining genera of diprotodontids that characteristically lacked a parastyle and a hypocone were assigned to either the Diprotodontinae (species with lophodont P^3 and divided parametacone) or the Nototheriinae (species with simple, bicuspid P^3 and an undivided parametacone).

The only subsequent change in the classification of the diprotodontids proposed by Stirton *et al.* (1967) has been the inclusion of the nototheres with the Diprotodontinae by Archer (1977). Recent work on the Diprotodontidae has concentrated on filling in the details of the established higher systematic construct. Although several new diprotodontid genera and species (some yet to be named) have been found since Stirton *et al.* (1967) (i.e. Rich *et al.*

1978, Flannery and Plane 1986, Murray 1990a-b, Flannery 1992, Hand *et al.* 1993, Murray *et al.* 1993) the genus *Neohelos*, which was originally central to our understanding of the phylogeny of the Zygomaturinae, has remained more or less in obscurity until now.

The initial reason for the lack of additional documentation for *Neohelos* was the rarity and fragmentary condition of *Neohelos* material from the type locality. In 1966, not long before Stirton *et al.* (1967) went to print, a new source of *Neohelos* fossil material was discovered at Bullock Creek, Northern Territory by C. Gatehouse (Plane and Gatehouse 1968). The newly found *Neohelos* material fully confirmed Stirton's diagnosis, which he was unable to appreciate due to his death in 1966. M. Plane, then of the Bureau of Mineral Resources, prepared a draft manuscript describing the Bullock Creek *Neohelos* as a new species named in honour of his colleague and mentor.

Meanwhile, more *Neohelos* fossil material was being recovered from Bullock Creek by T. and P. Rich, P. Murray and D. Megirian, and also from Riversleigh, Queensland by M. Archer and others, and from the type locality of *Neohelos tirarensis* at Lake Ngapakaldi by W. Clemens, M. Woodburne, M. Archer and others. The additional material seemed to show an unusually broad morphological range, some features of which could be attributed to a high individual variability, and some features of which seemed to indicate the presence of several species. On becoming aware of this new material and its variability, M. Plane withheld his manuscript from publication until the full range of available material could be examined and compared first hand.

In March 1988, all of the available *Neohelos* cranial material from the collections in the Museum of Victoria and Monash University, BMR (now AGSO, Australian Geological Survey Organisation), University of New South Wales and the Northern Territory Museum was assembled for examination at the Bureau of Mineral Resources in Canberra. It soon became apparent that the Bullock Creek *Neohelos* was a single, though highly variable, species distinct from *Neohelos tirarensis*. Most of the Riversleigh material compared closely with Wipajiri Formation *N. tirarensis*, though some fragments hinted at the existence of a possible second morphospecies, an impression eventually confirmed by continued collecting.

Here we describe three new species of *Neohelos*, add considerable information to the previously existing knowledge of *Neohelos tirarensis*, assess the morphological variability within the large sample from Bullock Creek, and discuss the evolutionary and biochronological significance of the new forms. The statistical analyses of *Neohelos* measurements (Appendix I) were prepared by T. Rich. The phylogeny of the Zygomaturinae, discussed in Murray (1991, 1992), Murray *et al.* (1993), and Hand *et al.* (1993), is extended from those studies in order to incorporate the new species and to develop a biochronological hypothesis for the Zygomaturinae that may continue to be useful in correlation. Following Luckett (1993), the molars are numbered M1-4. The anatomical terminology follows the appendix in Stirton, Woodburne and Plane (1967). Additional terms are listed in the key to abbreviations (Appendix 2).

ACKNOWLEDGMENTS

We thank the Managers of Camfield and Riversleigh Stations for their hospitality and continued interest and support; and express gratitude to our excavation teams composed of

numerous students and volunteers representing The Flinders University, University of New South Wales, The Riversleigh Society and Friends of Riversleigh. We gratefully acknowledge financial support from the National Estate Grants Program (Northern Territory), Australian Research Grant Scheme, Wang Australia, the Australian Geographic Society, National Estate Grants Program (Queensland), World Heritage Unit of the Department of Environment, Sports and Territories, Queensland National Parks and Wildlife Service, Waanyi People and Carpentarian Land Council, Century Zinc, Mt Isa Mines, Mt Isa Council, ICI Australia, Queensland Museum and Australian Museum. We are indebted to Drs William Clemens, Richard Tedford, Michael Woodburne and Tim Flannery for their valuable comments on the manuscript. We thank Lesley Kool and Michael Whitelaw (Monash University), Richard Brown (BMR), and Anna Gillespie (UNSW), for preparation of specimens.

PHYSICAL AND GEOLOGICAL SETTING

Wipajiri and Etadunna Formations, Lake Eyre Basin. The mid to late Cainozoic Lake Eyre Basin (*sensu* Wells and Callen 1986) lies in southern central Australia (Fig. 1). The oldest sediments comprise the late Oligocene / early Miocene Etadunna Formation, a 40 m thick succession of essentially lacustrine, but partly fluviatile origin. The Etadunna Formation rests unconformably on early Tertiary Eyre Formation of the Birdsville Basin. The Birdsville and Lake Eyre Basins are distinguished by contrasting structure, the older exhibiting greater deformation. The two basins are also separated by a long period of non-deposition, during which an extensive terminal weathered surface formed.

Green claystones and mudstones with a smectite-dolomite-palygorskite mineralogy are dominant lithologies of the Etadunna Formation. Massive, thick to thin beds of pale, light-grey to light-green dolomitic mudstones are useful marker horizons in the formation. Together they represent the lacustrine facies. Interbedded, usually lenticular, arenaceous claystone and argillaceous to quartzose sandstones represent fluviatile phases of deposition. In some cases these units are scoured into the lacustrine facies. Within the formation are minor hiatuses marked in part by sub-aerial exposure facies.

The Etadunna Formation is succeeded by erosional unconformity by the fluviatile channel-filling Wipajiri Formation, generally regarded as being of medial Miocene age. However, the Wipajiri Formation may be intraformational within the Etadunna: the duration of the hiatus between the two formations is not yet adequately established. Palaeomagnetic data suggest it may be of only short duration (Woodburne *et al.* 1993). The Wipajiri Formation is in turn succeeded by Pliocene and younger fluviatile, and ultimately in the Pleistocene, also by aeolian sediments, none of which contain *Neohelos*.

Within the Eyre Basin, only the Etadunna and Wipajiri Formations contain *Neohelos*. The Etadunna material is fragmentary and not diagnosable to species level. In spite of unresolved geochronological problems, the Etadunna and Wipajiri formations and their contained vertebrate faunas stand as a reference for the base of Australian continental mammal biochronology (Rich 1991, Woodburne *et al.* 1993, Megirian 1994).

Carl Creek Limestone, Karumba Basin. The Late Cretaceous to Holocene Karumba Basin covers the Gulf of Carpentaria region of Queensland and the Northern Territory (Fig. 2). Total sediment thickness is about 300 m, dominantly continental sand with minor silt

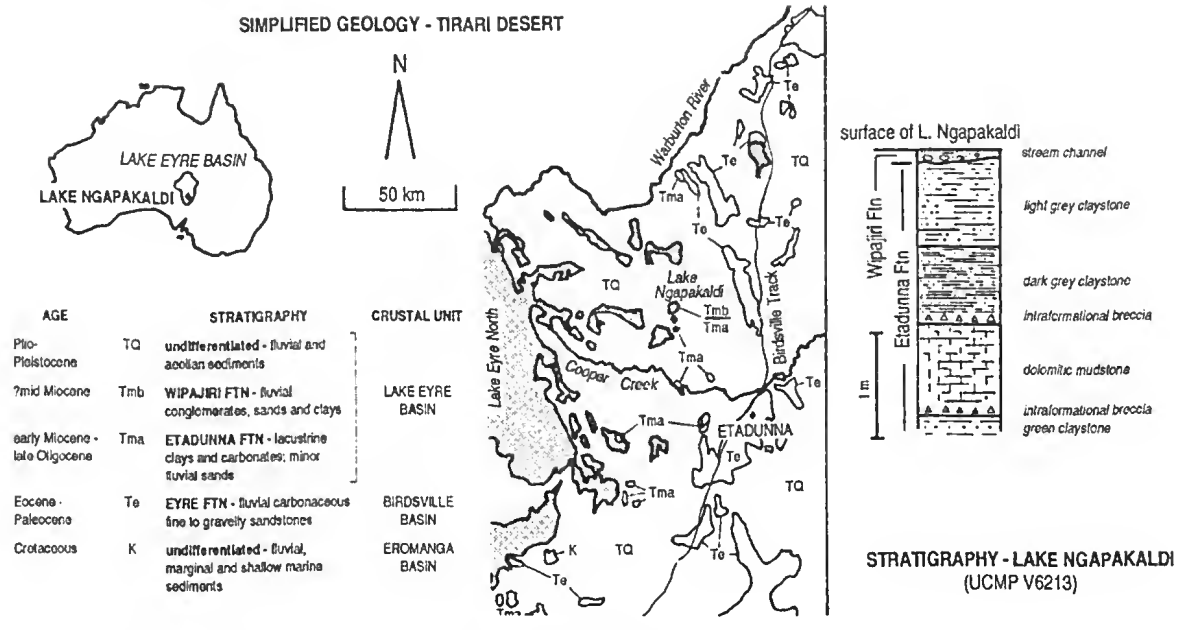

Fig. 1. Tirari Desert, South Australia. The Wipajiri Formation contains *N. tirarensis*. Geological map after Wells and Callen (1968: fig.1). Stratigraphic section at UCMP Vetebrate Locality V6213 (*N. tirarensis* type locality), Lake Ngapakaldi, after Stirton *et al.* (1967: fig. 2).

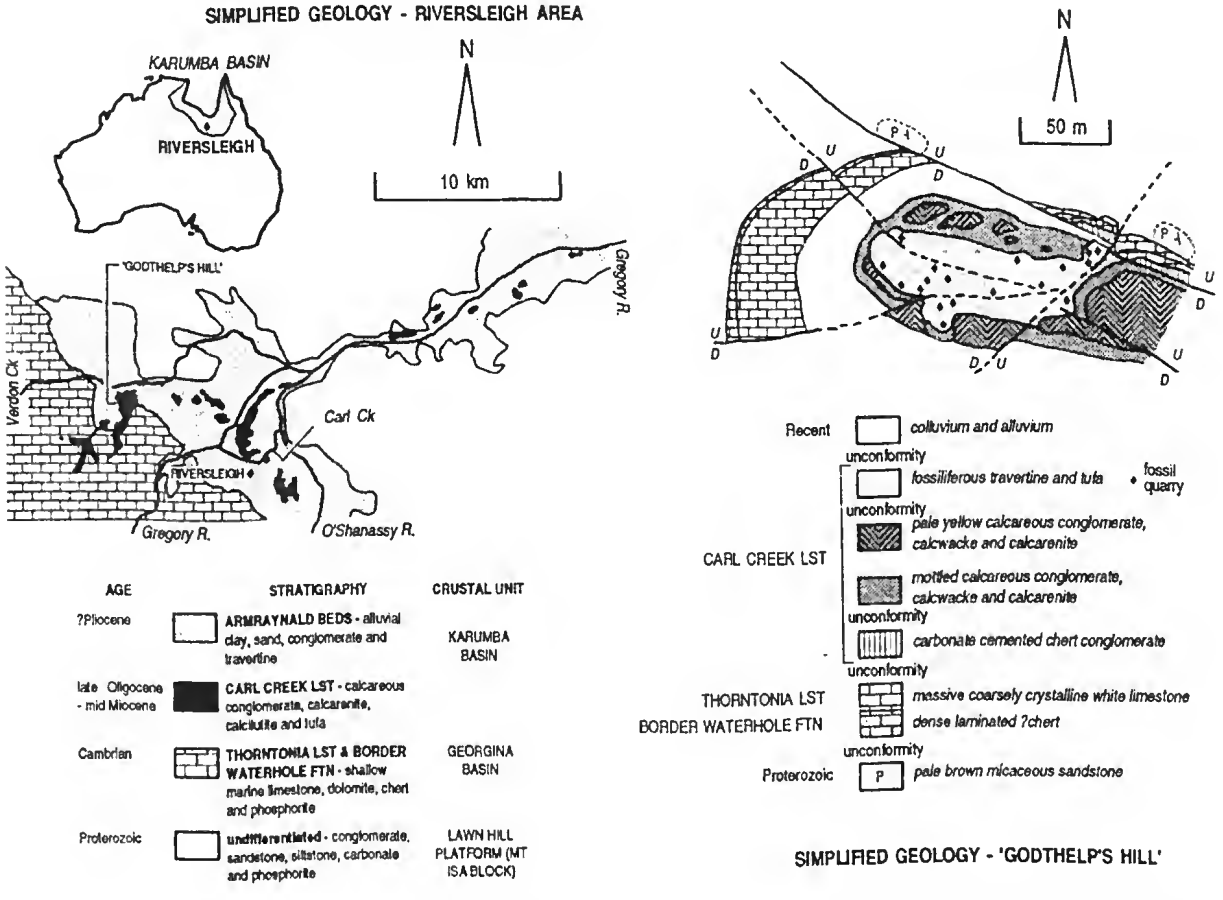

Fig. 2. Riversleigh area, northwestern Queensland. The Carl Creek Limestone contains three species of *Neohelos* plus *Nimbadon scottorrorum*. Four quarries at Godthelp's Hill (Upper, Inabeyance, Camel Sputum and Mike's Menagerie contain *N. tirarensis*. Riversleigh geology after Megirian (1992: fig. 3), Godthelp's Hill geology after Megirian (1992: fig. 7).

and clay, with some marine intercalations around the present onshore area. The development of the basin was cyclic, each cycle commencing with deposition, and finishing with an extended period of sub-aerial weathering, resulting in regionally extensive, deep-weathered profiles and terminal weathered surfaces.

The late Oligocene to mid Miocene Carl Creek Limestone is a small formation cropping out as a series of poorly bedded mesas along the Gregory River drainage system at the southern margin of the basin. The sedimentology of the deposit has not yet been published in detail. Most of the formation is composed of very pale orange to greyish-orange, very coarse to fine clastic limestones, altered by diagenesis into a typically crystalline state. Volumetrically minor, but palaeontologically important, are chemically and/or biologically mediated precipitates, specifically travertines and various classes of tufa. Erosional unconformities, sub-aerial exposure facies, scour and fill structures and lenticular bedforms, ranging from small to large scale, are common. These features, together with a lack of useful marker horizons, have so far not led to a satisfactory resolution of the lithostratigraphy of the formation as a whole.

Megirian (1992) interpreted the Carl Creek Limestone as a predominantly alluvial association composed of karst, tufa and calcareous lithoclastics (cf. the 'calclithites' of Folk 1959) deposited at or near the headwaters of a fluvial system. Others (Tedford 1967, Archer *et al.* 1989) favour a lacustrine environment of deposition for the bulk of the formation.

Camfield Beds. No regional study of the kind compiled for the Lake Eyre and Karumba Basins (Wells and Callen 1985, Smart *et al.* 1980) has been produced for the Victoria River region of the Northern Territory (Fig. 3), although the foundations for such a work, including the formal definition of a comparable Cainozoic sedimentary basin, may be found in unpublished geological survey records (e.g. Randal and Brown 1967, Swect *et al.* 1971), explanatory notes to the 1:250 000 geological map sheets for the area (Bultitude 1973) and Hay's (1967) study of ancient land surfaces of the Northern Territory.

Like the Carl Creek Limestone, the Miocene Camfield Beds are palaeo-valley fills. The Camfield Beds, which crop out along the Bullock Creek and Cattle Creek tributaries of the Camfield River, consist of calcareous siltstone, sandy siltstones, and silty sandstones conglomeratic limestone, calcimudstone, chalcedonic limestone and gypsiferous siltstone. Vertebrate fossils are concentrated in the limestone facies which Murray and Megirian (1992) interpret to have been deposited in fluviatile channels and associated billabongs: Randal and Brown (1967) postulated a normally saline lacustrine, lagoonal or estuarine environment of deposition, occasionally flooded by freshwater inflow.

Common factors. While the geological histories of various Cainozoic basins differ in their detail, there was, at a broad scale of about 10^7 year magnitude, a pattern of cyclic deposition over most of the continent. The physiography of the Australian landscape was largely established by the time the early Cretaceous seas receded from the continent. Erosion and continental sedimentation varied in intensity. When rates were low, deeply weathered profiles and extensive duricrust land surfaces of considerable stratigraphic importance formed, as shown in interregional correlation charts (e.g. Smart *et al.* 1980).

The sediments containing *Neohelos* consist of, or are interbedded with, carbonates (limestone, dolomite, or dolomitic limestone), which together comprise a subset of more extensively distributed limestone formations occurring in comparable depositional settings.

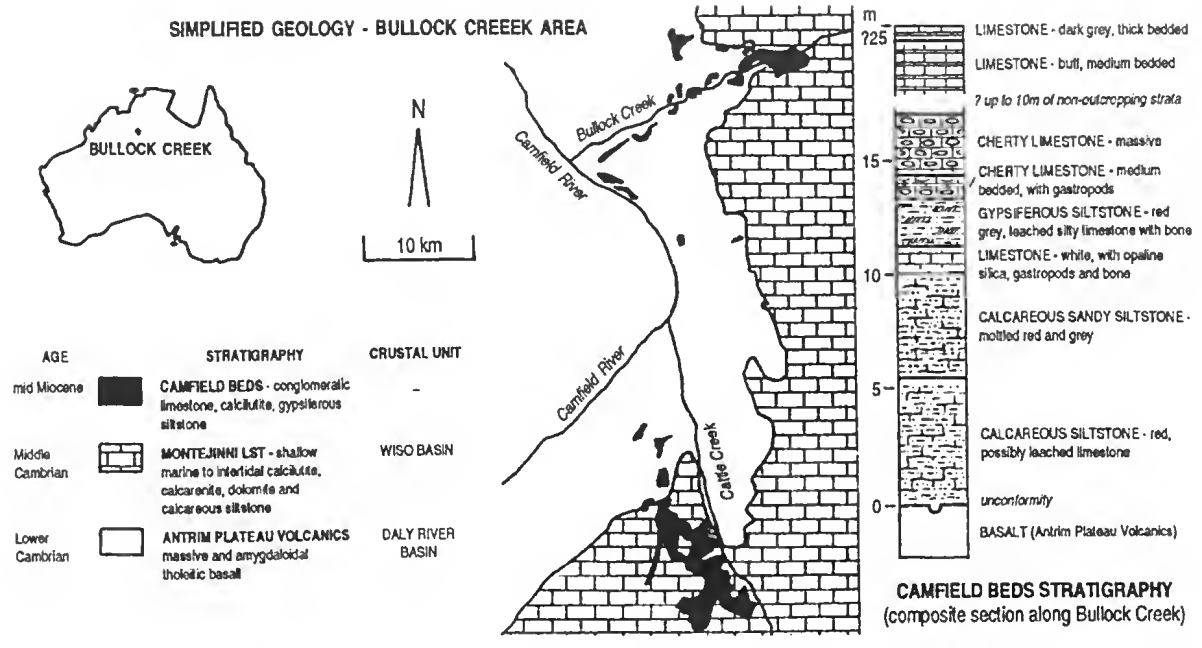

Fig. 3. Bullock Creek area, Northern Territory. Camfield Beds contain *Neohelos* spB only. Bullock Creek geology after Murray and Megirian (1992: fig. 1). Composite stratigraphic section along Bullock Creek after Randal and Brown (1967: 47).

The geographic, and to the extent that they can be currently resolved, temporal distributions of these formations suggests common factors in their genesis (Lloyd 1965, Megirian 1992). By consilience of induction McGowran and Li (1994) have proposed a causal relationship of the Carl Creek Limestone, Camfield Beds and Etadunna and Wipajiri Formations to the southern Australian marine 'Miocene oscillation', a phase of deposition spanning the latest Oligocene to middle Miocene Marsupial biochronology is one means of correlating between sedimentary basins. While *Neohelos* has previously been used in inter-regional biochronological correlation, the details are presented here for the first time.

SYSTEMATICS

Superorder MARSUPIALIA Illiger, 1811
Order DIPROTODONTIA Owen, 1866
Family DIPROTODONTIDAE Gill, 1872
Subfamily ZYGOMATURINAE Stirton, Woodburne and Plane, 1967

The extinct Family Diprotodontidae to which *Neohelos* belongs, is a diverse group of vombatomorphian marsupials united by the possession of relatively simple bilophodont molars, a transversely lobate, minimally bicuspid, oval to triangular P^3 and three upper and one lower incisor per quadrant (Fig. 4). Although subfamilial divisions of the Diprotodontidae were proposed in the late 1800s, the affinities of the various genera remained ambiguous until Stirton, Woodburne and Plane (1967) revised the family, recognising the subfamily Zygomaturinae as distinct from two newly ranked subfamilies, the Nototheriinae and the Diprotodontinae.

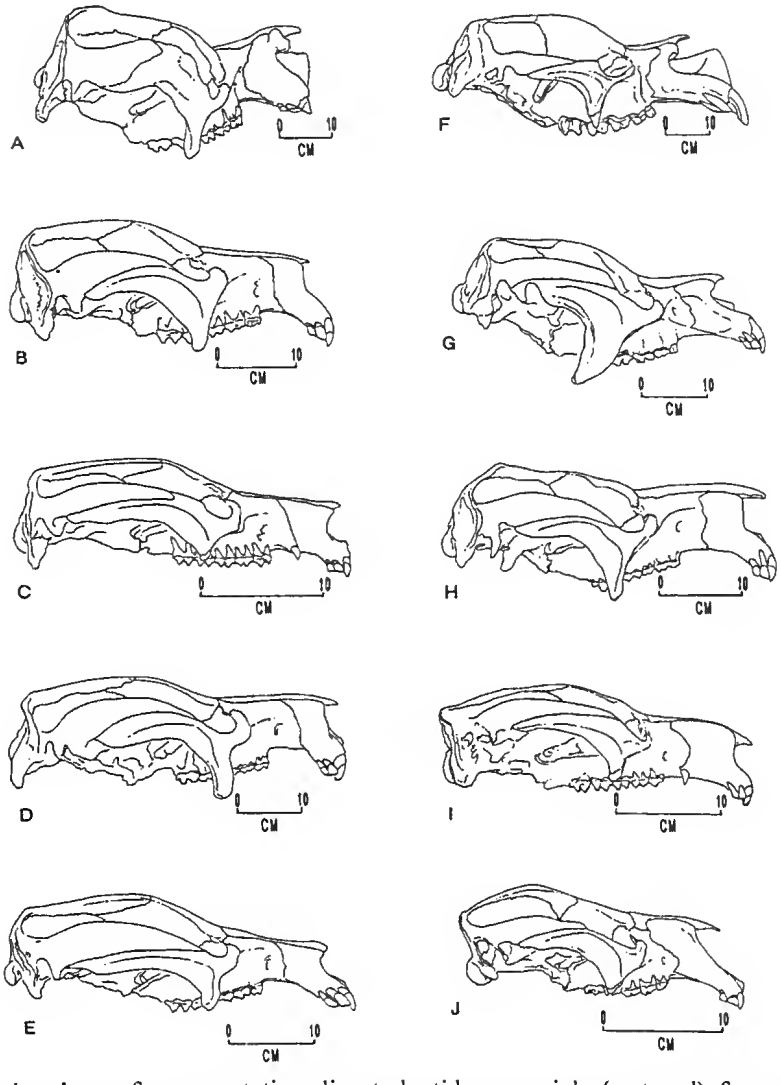

Fig. 4. Outline drawings of representative diprotodontid marsupials (restored) for comparison of overall form: **A**, *Zygomaturus trilobus*; **B**, *Kolopsis torus*; **C**, *Neohelos* spA (composite restoration; **D**, *Plaisiodon centralis*; **E**, *Alkwertatherium webbi*; **F**, *Diprotodon* sp.; **G**, *Euryzygoma dunense*; **H**, *Pyramios alcootense*; **I**, un-named ?zygomaturine species from Riversleigh, Queensland; **J**, *Ngapakaldia tedfordi.* Scale bars = 10 cm. G after photograph in Archer and Bartholomai (1978); F after photograph compliments of T. Rich; J after photograph in Archer *et al.* (1991: 217).

Stirton *et al.* (1967) considered the Nototheriinae to represent an intercalary lineage that gave rise to the Zygomaturinae through the addition of a large conical parastyle to the P^3. The Diprotodontinae were distinguished from the Nototheriinae by the differentiation of the paracone and metacone from a single large buccal cusp on the P^3, giving rise to a horseshoe-shaped lophodont pattern when the crown was worn. Because the P^3 of *Euryzygoma dunense*, a 'notothere', was structurally intermediate between the diprotodontine, *Diprotodon* and other nototheriines, Archer (1977) recommended suppression of the subfamily Nototheriinae.

Other than the inclusion of the Nototheriinae within the Diprotodontinae, Stirton *et al.*'s original diagnoses remain valid; but to which we append the following observations. Unknown to Stirton at the time, an epitympanic fenestra in the superficies meatus area similar to that *in Ngapkaldia tedfordi* Stirton is present among the more primitive genera of both subfamilies. The structure is diminished and eventually lost in the later, more derived

species of which he was aware and upon which he based his observation. In addition to the presence of a parastyle on the P^3 (Fig. 5) the Zygomaturinae is also distinguished apomorphically from the Diprotodontinae by the development of the ventral surface of the tympanic process within the alisphenoid. In the Diprotodontinae, the tympanic process is formed entirely within the squamosal, as in the Vombatidae (Fig. 6).

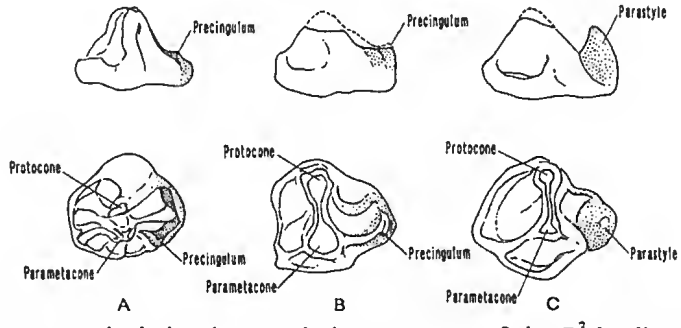

Fig. 5. Structural sequence depicting key evolutionary states of the P^3 leading to the Zygomaturinae: **A**, *Palorchestes azeal* (Palorchestidae); **B**, *Pyramios alcootense* (Diprotodontinae); **C**, *Alkwertatherium webbi* (Zygomaturinae).

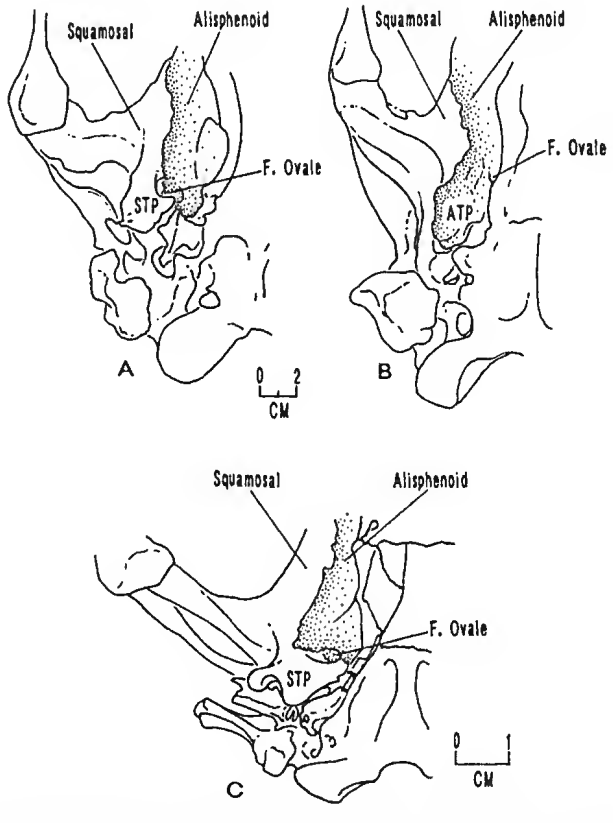

Fig. 6. Comparison of the tympanic wing structures in: **A**, *Pyramios alcootense* (Diprotodontinae); **B**, *Alkwertatherium webbi* (Zygomaturinae); **C**, *Vombatus ursinus* (Vombatidae).

Stirton *et al.* (1967) described the primary distinguishing feature of the subfamily Zygomaturinae as a large, complex, bulbous-outlined P^3 with four or five cusps. A three-cusped zygomaturine genus, *Alkwertatherium webbi* Murray (1990a) is now known, as anticipated by the Stirton *et al.* (1967) reconstructed structural succession based on the initial development of a parastyle, then a hypocone (*Neohelos, Plaisiodon*), followed by the division of the parametacone into a distinct paracone and a metacone (*Kolopsis, Kolopsoides, Zygomaturus*) (Fig. 7). The division or twinning of the parametacone arose independently in the Palorchestinae (*Palorchestes azeal*) and in the Diprotodontinae (some individuals of *Euryzygoma* and *Diprotodon* spp.).

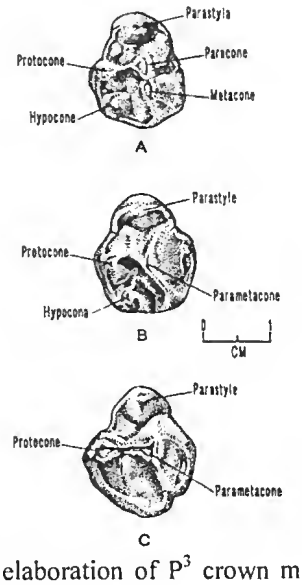

Fig. 7. Structural sequence showing elaboration of P^3 crown morphology in Zygomaturinae: **A**, *Kolopsis torus*; **B**, *Neohelos* spB; **C**, *Alwertatherium webbi.*

It is plainly evident from the morphology of the P^3 that *Neohelos* is structurally intermediate between the simpler, somewhat diprotodontine-like three-cusped condition in *Alkwertatherium* and the five-cusped condition of *Zygomaturus*. However, the actual phylogenetic position of *Neohelos* is not quite as transparent as its structure suggests. Two other genera with four-cusped P^3s are also present in the form of *Plaisiodon centralis* Woodburne 1967a and *Nimbadon* spp. (Hand *et al.* 1993). Moreover, it is probable that the division of the parametacone into two distinct cusps occurred more than once within the Zygomaturinae as indicated by *Kolopsoides cultridens* Plane, 1967, which shows closer affinity to *Plaisiodon* than to either *Neohelos* or *Kolopsis* (Murray 1990, 1992).

Neohelos Stirton, 1967a

Type species. *Neohelos tirarensis* Stirton, 1967a

Additional species. *Neohelos* spA; *Neohelos* spB ; *Neohelos* spC.

Revised generic diagnosis. Diprotodontids possessing a four-cusped P^3 with a distinct, isolated parastyle and hypocone; canines vestigial to absent. Trapezoidal M^1 with large parastyle and metastyle, crown approximately the same length as P^3: upper molars with wide interproximal contacts. Lower incisor with distinct ventrolabial longitudinal groove; M_1, paralophid strong; lower molars with weak metalophids and low, wide transverse valleys. All other zygomaturine genera are distinguished from *Neohelos* by the following character differences: unnamed (Riversleigh Gen. et sp. nov.) differs in having a feeble P^3 parastyle and in lacking a hypocone; *Alkwertatherium* differs in lacking a hypocone on P^3; *Nimbadon* differs in that the M^1 stylar corners are small and the interproximal contacts of molars are rounded and narrow; *Kolopsoides* differs in that the parastyle of P^3 is connected to the paracone by a high crest, the parametacone is divided and the hypocone is larger than the protocone; *Plaisiodon* differs in the absence of an anterolabial crest on the parastyle and absence of a mesostyle on P^3; *Kolopsis* differs in having fully differentiated paracone and metacone on P^3 and lacks a ventrolabial groove on I_1; genera *Zygomaturus*, *Maokapia* (and possibly *Hulitherium*, in which only a fragment of its P^3 is known) differ in that the P^3 parametacone is fully divided, the P^3 is much smaller than M^1 and the parastyle and metastyle of M^1 are reduced (Murray 1992) (Figs 8, 9; Table 1).

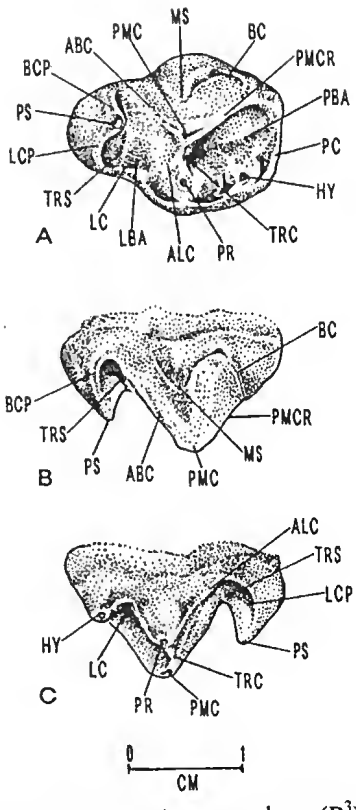

Fig. 8. Upper permanent premolar (P^3) of *Neohelos* spB (NTM P8695-141) showing typical structures of the crown.

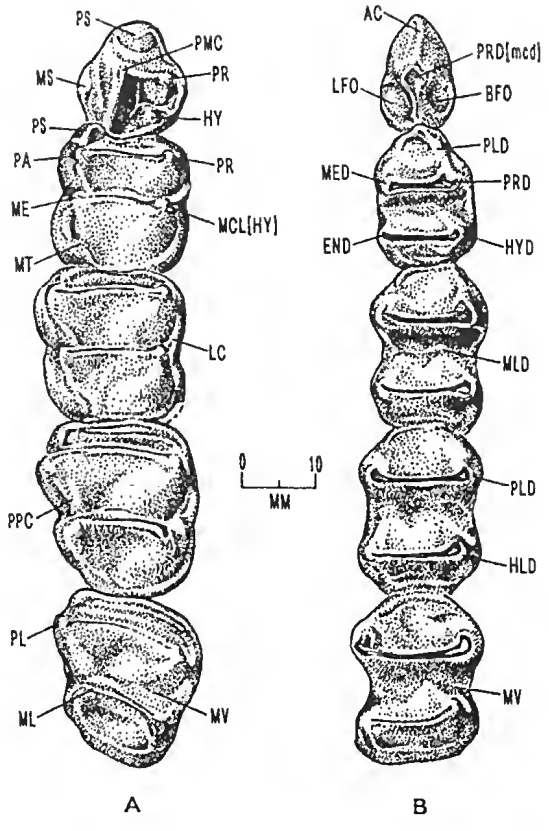

Fig. 9. A, upper, and **B**, lower cheek tooth rows of *Neohelos* spB.

Neohelos tirarensis Stirton, 1967a

Holotype. Posterior part of left P^3, South Australian Museum P13848 (Stirton 1967, fig. 1A–G).

Type locality and age. Leaf Locality (UCMP Loc. V6213), poorly indurated Wipajiri Formation, consisting of ferruginous, conglomeratic sandstone interbedded with dark grey claystone, cut into the Etadunna Formation, Lake Ngapakaldi, South Australia. Kutjamarpu Fauna, estimated to be latest Oligocene or early Miocene, as discussed below.

Referred specimens and localities. *N. tirarensis* is known from the Leaf Locality, Lake Ngapakaldi, South Australia and from several sites on Riversleigh Station Queensland.

Leaf Locality, Lake Ngapakaldi, South Australia: AM F87625, right P^3; AM F87626, left M^2; AR263, right M_2; AR456, M^1; AR3340, I^3; AR3358, I^3; AR3459, right M^2; AR3468, right P^3; AR4221 left M^3; AR5339, I^3; SAM/UC465, right M^1; UCMP 69977, left M^1; UCMP 69978, right M^2; UCMP 69979, M_3.

300BR, Riversleigh Station, Queensland: NTM P91171-5, left I^1; NTM P91171-6, right I^3; NTM P942-1 M^4; NTM P91171-2 left P^3 parastyle, left M^2; NTM P91171-4, right M_4.

Burnt Offerings, Riversleigh Station, Queensland: NTM P91166-1, right maxilla, canine alveolus, P^3; NTM P91166-2, edentulous premaxilla; NTM P91166-6, crushed braincase, Zygomatic arch, palate missing; NTM P91166-7, left I_1, NTM P91166-3, edentulous premaxilla.

Table 1. Summary of diagnostic features of the genus *Neohelos* Stirton

	Neohelos	*Zygomaturus*	*Maokapia*	*Kolopsis*	*Nimbadon*	*Kolopsoides*	*Plaisiodon*	*Alkwertatherium*	New zygomaturine genus from Riversleigh
I_1	lanceolate with ventrolabial groove and lingual longitudinal crest	tusk-like	tusk-like	V-L groove absent	unknown	spatulate	V-L groove and lingual crest absent	spatulate	unknown
I^1	mesially flattened, pointed crown	tusk-like	tusk-like	=*Neohelos*	unknown	=*Neohelos*	=*Neohelos*	unknown	=*Neohelos*
I^2	mesiodistally elongated, triangular occlusal surface with 1-2 vertical grooves labially	=*Neohelos*	=*Neohelos*	=*Neohelos*	unknown	unknown	elliptical occlusal surface	unknown	unknown
I^3	short triangular occlusal surface; shallow labial groove or sulcus	=*Neohelos*	=*Neohelos*	=*Neohelos*	unknown	unknown	=*Neohelos*	unknown	unknown
Canine	present or entirely absent	absent	absent	absent	present	absent	absent	absent	present
P^3	4 primary cusps, variable mesostyle, medium-large parastyle with labial crest separated from paracone by transverse sulcus; cuspate PMC with loph connected to protocone, small hypocone connected to protocone by short lingual crest	5 cusps	5 cusps	5 cusps	loph to cingulum	5 cusps, hypocone >protocone, parastyle conncected to paracone by crest	mesostyle, labial crest absent	hypocone absent	parastyle incipient, hypocone absent
M^1	length=P^3, narrow, curved protoloph, large parastyle and metastyle, wide IP contact	L>P^3, styles reduced	L>P^3, styles reduced	=*Neohelos*	styles small, narrow IP contact	L<P^3, styles small	L<P^3	styles small	styles small
P_3	conical main cuspid with anterior and posterior median crests and anterobasal cuspid or pit; crown shorter than M_1	=*Neohelos*	=*Neohelos*	=*Neohelos*	=*Neohelos*	anterior crest absent, L>M_1	anterior crest absent	anterior crest absent	unknown
M_1	narrow elongated trigonid, protolophid narrower than hypolophid; prominent paralophid crest, weak metalophid	=*Neohelos*	=*Neohelos*	=*Neohelos*	distinct protostylid	strong metalophid	strong metalophid	short trigonid, weak paralophid	unknown

Upper Burnt Offerings, Riversleigh Station, Queensland: NTM P91167-1 partial cranium with complete right cheek-tooth row and left M^{2-4}.

Sticky-beak, Riversleigh Station, Queensland: AR13795, right maxilla, canine alveolus, P^3-M^1; AR13994, left P^3.

Bone Reef, Riversleigh Station, Queensland: AR17470, left P^3; QM F24137, left maxilla M^{1-4}.

Camel Sputum, Riversleigh Station, Queensland: AR9947, left P^3; AR10362, left M^3; AR10641, right P^3; AR10706, right P^3; AR10726, right P^3; AR12120, left M^{3-4}; AR13360, left M_1; AR17443, left maxilla, M^{1-2}; AR24239, right M_1; AR10841, P^3.

D-Site, Riversleigh Station, Queensland: CPC 22558, right P^3, M^2; AR1685, right dentary P_3–M_{1-4}; AR1686, left dentary, P_3–M_{1-4}.

Inabeyance, Riversleigh Station, Queensland: QM F13088, palate, left P^3–M^{1-3}, right M^{2-4}.

Jim's Jaw Site, Riversleigh Station, Queensland: AR11858, right P^3; AR14393, M_3.

Mike's Menagerie, Riversleigh Station, Queensland: AR9925, left M^2; AR10668, left M_3; AR10669, left M^3; AR15119, left P^3; AR16492 + AR15751, right maxilla, P^3-M^{1-4}.

Neville's Garden, Riversleigh Station, Queensland: AR16656, left M_3; AR17291, right M^3; AR24240, right M_3; QM F12449, right M_1.

Wayne's Wok, Riversleigh Station, Queensland: AR10458, right dentary, P_1-M_{1-4}; AR15239, right M^3; AR16787, left dentary, P_3-M_1.

Species diagnosis. Small to medium-sized species, distinguished from *Neohelos* spA by wider, more rectangular molars, more consistent presence of transverse crest from parametacone to protocone on P^3, postcingulum continuous horizontally with the lingual cingulum of the metaconule on M^{1-2}; anterobasal cuspid or faint cingulid usually present on P_1, thicker, lower paralophid on M_1; protolophid does not overhang mid-valley. Differs from *Ni. scottorrorum* in having a horizontally continuous postcingulum on the metaconule; distinguished from *Neohelos* spB by smaller size, wider palate in proportion to molar crown size and presence of canine. Distinguished from *Neohelos* spC by smaller size, shorter, broader P^3 with simple pyramidal parametacone, upper molars with less overhang of lophs and by the presence of an anterior crest on P_3.

Remarks. Stirton (1967a) described *N. tirarensis* from a small collection of material from the Leaf Locality, Wipajiri Channel, on the eastern shore of Lake Ngapakaldi. His type specimen (SAM P13848) is the posterior part of a left P^3, supplemented by four paratypes: a left I^3 (UCMP69976) a left M^2 (UCMP 69977) a right M^2 and a left M_4. W. A. Clemens and M. O. Woodburne of The University of California collected additional *Neohelos tirarensis* material from the Leaf Locality in 1972. In 1982, more specimens were collected from the same locality by M. Archer although, as with previous collections, these consist only of isolated teeth. From these new collections we have selected four almost complete molar teeth (Fig. 10A–F, I) a complete right I^3 (Fig. 10G–H) a complete enamel cap of a right P^3 (Fig. 10J–K) and the posterior half of a right P_3 (Fig. 10L–N), all of which add considerably to our previous knowledge of the Wipajiri material.

The Riversleigh sample of *N. tirarensis* is more abundant and anatomically more informative, as some complete upper and lower cheek-tooth rows, a complete dentary, partial crania and fragments of maxillae have since been recovered. Despite the considerable geographic separation of the two localities, there are no apparent differences in the populations other than a greater size range in the larger and perhaps temporally more extensive Riversleigh assemblage. Initially we were able to divide the Riversleigh *Neohelos* specimens into what appeared to be two distinct species: a smaller form distinguished by smooth, thin enamel, weaker crests and cingulae, straighter cheek-tooth rows and weaker morphological and size gradient in the molars, from a somewhat larger more robust form, which we assumed to be typical *N. tirarensis*. As more specimens were added to the collection this distinction has become blurred to the extent that it is no longer possible to differentiate populations within the sample.

Description. *Incisors.* Specimens include a complete I^1 (NTM P91171-5), a heavily worn I^2 crown (NTM P91171-6), a complete I^3 (AR3340) and two heavily worn specimens (ARS339, AR3358) and a left lower incisor (NTM P91166-7) (Fig. 11).

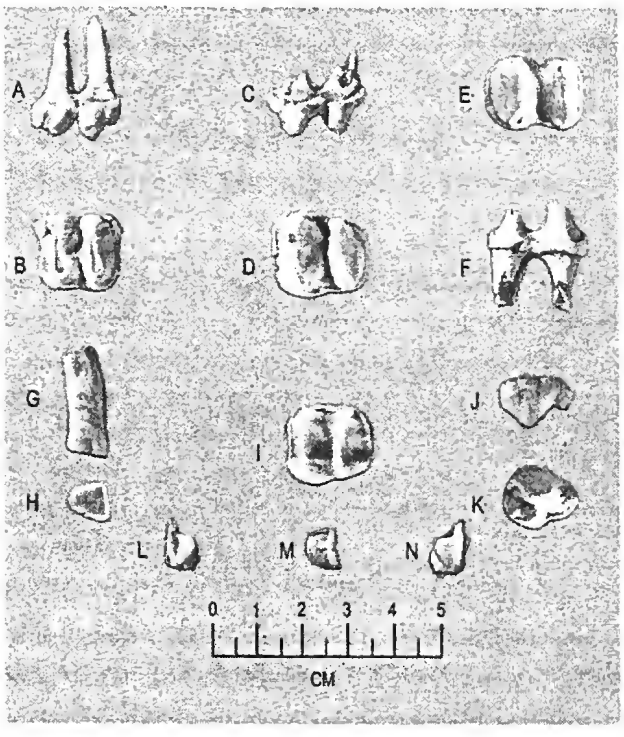

Fig. 10. Leaf Locality, Wipajiri Formation *Neohelos tirarensis* Stirton: **A-B**, right M^2 (SAM/UC 465); **C-D**, left M^3 (AM F87626); **E-F**, right M_5, **G-H**, right I^3, **I**, right M^3 (AM F87626); **J-K**, right P^3 (AM F87625; right P_3.

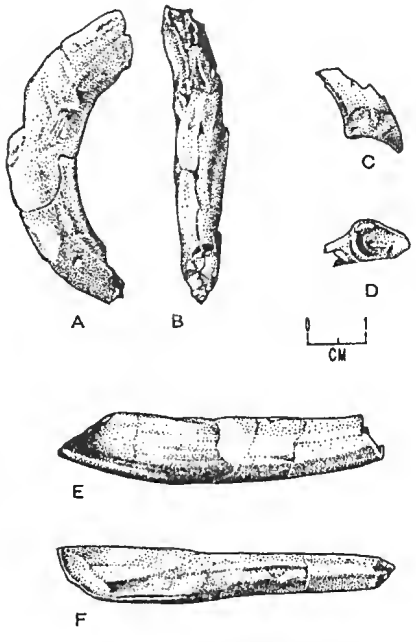

Fig. 11. *Neohelos tirarensis*, referred incisors: **A-B**, left I^1 labial and distal aspects (NTM P91171-5, 300BR, Riversleigh; **C-D**, right I^2, labial and occlusal aspects (NTM p91171-6, 300BR, Riversleigh; **E-F**, left I_1 labial and occlusal (dorsal) aspects (NTM P91166-7, Burnt Offerings, Riversleigh).

I^1. The I^1 is open-rooted, strongly curved and planoconvex in section, the internal surface being flat (Fig. 11A–B). The posterior surface of the distal end of the crown is marked by a deep occlusal notch. Enamel is present on the tip of the labial half of the tooth. It is damaged on the dorsolingual surface, where enamel may have been present. The root is 8.5 mm thick and 12.5 mm wide at its mid-point. The tooth tapers very gradually towards the tip, and again just slightly towards the root opening, being widest and thickest in the middle. The tooth is 52.0 mm long with a maximum distance of 9.5 mm from the concave side of the tooth perpendicular to a chord drawn between its ends. It does not differ, except for its smaller size, from those of *Neohelos* spB or *Neohelos* spC.

I^2. The I^2 crown is about half worn away, with a concave occlusal profile (Fig. 11C–D). The crown is transversely wide (10.0 mm) and tapers anteroinferiorly. The labial surface bears a faint indication of a groove or shallow sulcus, but the enamel is also split and eroded in this position. The enamel-dentine junction is a smooth curve, without a posterior salient. The occlusal outline is an elongated (10.0 mm by 7.0 mm), rounded triangle. An enamel thickening is present on its posterolabial corner. Except for its more feeble groove, the I^2 closely resembles that of *Neohelos* spB.

I^3. In occlusal pattern these teeth are very similar to Stirton's (1967a) description. All possess a well-defined lingual groove, a narrow, but well-defined, ridge anterior to the groove, and a weak groove on the labial surface. The diameter of the root is variable when measuring the largest dimension immediately above the crown (5.0, 6.3, and 8.6). The occlusal outline of the crown is an equilateral triangular shape.

I_1. The left I_1 (NTM P91166-7) bears a lanceolate crown, tapering anteriorly towards the tip from its junction with the root (Fig. 11E–F). The tooth is deepest (11.5 mm) across the root immediately behind the enamel-dentine junction. The tip and occlusal edge of the crown is twisted perpendicular to the axis of the root. The dorsal longitudinal crest is only slightly elevated and does not overhang the dentine exposure on the lingual side of the crown. The labial side of the crown is fully enamelled. A shallow groove runs parallel to the ventral labial border of the crown. On the lingual side, enamel is restricted to a narrow ventral strip closely corresponding to a slender, flattened appression surface. The occlusal facet is lenticular with a distal salient corresponding to a sharp, longitudinal dentine ridge situated about one-third of the depth of the crown below the dorsal crest. A less prominent ridge about 2.5 mm below, parallels the latter. The root is long, straight and elongated-oval in section. It tapers slightly towards the distal end. The enamel blade of the lower incisor of this species appears to be proportionally slightly narrower than in *Neohelos* spB.

Upper cheek teeth. P^3. The Leaf Locality P^3 (AM F87625) (Fig. 10J–K, Table 2) is an unworn enamel cap without roots. It is a little smaller than Stirton's figured holotype, the transverse basal width across the parametacone-protocone being 13.9 mm compared to 14.8 mm, while the height of the parametacone is exactly 11.0 mm. The posterior morphology of the tooth agrees in every way with Stirton's reconstruction. The parastyle is low (4.6 mm from the base of the enamel) and bluntly rounded.

A narrow, sharp ridge ascends from the parametacone but terminates at a commisure on the posterolabial side of the parastyle. A very small ridge ascends directly posteriorly from the parastyle but also terminates at the commisure slightly lingual to the anterior ridge of the parametacone. A slender cingulum connects the base of the protocone to the parastyle. There is a well-marked emargination in the lingual outline of the tooth just anterior to the protocone. In this specimen, the hypocone is small and directly behind the protocone, not posterolabial to it as in Stirton's (1967a) type specimen.

The P^3 of the Inabeyance specimen (QM F13088) is rather large in proportion to its molars (Figs 12I-J, 13). It is strongly lobate in occlusal outline, with a low parastyle, a well-developed mesostyle and a large hypocone. The parametacone and protocone are typical for the genus. The transverse link between the protocone and parametacone is strong and high; though the lingual emargination between the parastyle and the protocone is not well-developed. In contrast, QM F23137 (=*Nimbadon scottorrorum*) from the Fig Tree locality has a relatively small P^3 with a weak mesostyle, though the molars are very similar in size and morphology to the Inabeyance specimen.

A heavily-worn right P^3 (CPC 22558) from D-Site, Riversleigh is also relatively short and broad. The parastyle is low and transversely broad. The mesostyle is well-developed. The hypocone is small and situated close behind the protocone. The remnant of the very worn transverse link between the parametacone and protocone is robust, and the lingual emargination between the parastyle and the protocone is wide and strong.

The P^3 of AR16492 (Mike's Menagerie Site) is very similar to that of QM F13088 (Figs 12G–H, 14, 15). As in the latter, the parastyle is small. The lingual emargination and fossa between the parastyle and protocone is well–developed. A labially prominent, leaf-shaped mesostyle is nearly as large as the parastyle. P^3s from Camel Sputum (AR9947, AR10726) are both slightly larger, with more robust parastyles.

Table 2. Measurements (millimetres) of upper and lower cheek teeth of *Neohelos tirarensis* Stirton (estimations in italics).

UPPER CHEEK TEETH (mm)

SPECIMEN	SIDE	P^3		M^1			M^2			M^3			M^4		
		L	W	L	AW	PW	L	AW	PW	L	AW	PW	L	AW	PW
AR 9947	L	16.6	14.7	----	----	----	----	----	----	----	----	----	----	----	----
AR 10362	L	----	----	----	----	----	18.3	16.9	16.2	----	----	----	----	----	----
AR 10706	R	*16.5*	12.5	----	----	----	----	----	----	----	----	----	----	----	----
AR 10726	R	17.0	14.1	----	----	----	----	----	----	----	----	----	----	----	----
AR 11858	R	*15.8*	*12.9*	----	----	----	----	----	----	----	----	----	----	----	----
AR 12120	L	----	----	----	----	----	----	----	----	18.4	17.8	15.6	19.4	16.5	13.5
AR 13792	L	----	----	----	----	----	----	----	16.5	20.1	19.5	17.2	20.5	19.1	14.5
AR 13795	R	----	12.3	14.8	----	----	----	----	----	----	----	----	----	----	----
AR 13994	R	14.5	13.0	----	----	----	----	----	----	----	----	----	----	----	----
AR 15119	L	16.8	13.6	----	----	----	----	----	----	----	----	----	----	----	----
AR 15239	R	----	----	----	----	----	----	----	----	*18.8*	----	14.6	----	----	----
AR 16492 / 15751	R	15.6	14.8	16.4	14.7	15.4	17.2	16.4	15.4	19.6	16.8	15.5	*19.0*	*15.9*	13.0
AR 17291	R	----	----	----	----	----	----	----	----	19.5	*16.8*	14.6	----	----	----
AR 17443	L	----	----	16.9	15.0	15.1	17.0	15.9	15.0	----	----	----	----	----	----
AR 3459	R	----	----	----	----	----	18.5	17.3	15.8	----	----	----	----	----	----
AR 3468	R	15.8	13.7	----	----	----	----	----	----	----	----	----	----	----	----
AR 4221	L	----	----	----	----	----	----	----	----	20.9	18.9	15.2	----	----	----
AR 456	R	----	----	18.7	16.6	16.9	----	----	----	----	----	----	----	----	----
AR 9925	L	----	----	----	----	----	18.1	16.4	15.5	----	----	----	----	----	----
AR 9947	L	16.5	14.5	----	----	----	----	----	----	----	----	----	----	----	----
CPC 22558	L	15.4	13.7	----	----	----	19.2	17.1	15.7	----	----	----	----	----	----
NTM P91166-1	R	15.1	14.2	----	----	----	----	----	----	----	----	----	----	----	----
NTM P91167-1	L	----	----	----	----	----	16.5	15.1	14.9	16.9	15.5	14.0	17.2	15.6	13.5
NTM P91167-1	R	13.8	12.4	15.4	----	14.4	16.7	15.1	14.7	17.1	15.2	14.1	17.0	15.0	12.1
NTM P91171-2	L	----	----	----	----	----	18.3	16.7	15.5	----	----	----	----	----	----
NTM P942-1	L	----	----	----	----	----	----	----	----	----	----	----	20.0	16.5	14.5
QM F13088	L	16.4	14.3	17.2	14.6	14.9	17.3	16.2	16.0	17.1	16.7	15.0	----	----	----
QM F13088	R	----	----	17.2	14.5	14.8	17.0	16.0	15.8	----	----	----	----	----	----
SAM P13848 (TYPE)	L	----	14.8	----	----	----	----	----	----	----	----	----	----	----	----
SAM/UC 465	L	----	----	18.8	16.6	16.9	----	----	----	----	----	----	----	----	----
UCMP69977	L	----	----	17.0	15.5	15.6	----	----	----	----	----	----	----	----	----
UCMP69978	R	----	----	----	----	----	19.0	17.1	16.6	----	----	----	----	----	----

LOWER CHEEK TEETH (mm)

SPECIMEN	SIDE	P_3		M_1			M_2			M_3			M_4		
		L	W	L	AW	PW	L	AW	PW	L	AW	PW	L	AW	PW
AR 10458	R	13.0	10.0	17.4	10.8	12.2	18.5	13.9	14.4	18.7	15.4	14.4	18.2	14.1	*13.9*
AR 10668	L	----	----	----	----	----	----	----	----	*19.2*	*14.2*	13.6	----	----	----
AR 10841	R	13.0	8.5	----	----	----	----	----	----	----	----	----	----	----	----
AR 13360	L	----	----	17.8	12.0	13.7	----	----	----	----	----	----	----	----	----
AR 13634	R	----	----	----	----	----	18.0	----	14.4	21.2	----	15.8	20.4	----	14.4
AR 13969	R	12.5	8.6	17.3	11.6	12.2	----	----	----	----	----	----	----	----	----
AR 14393	L	----	----	----	----	----	----	----	----	19.6	*14.1*	*14.2*	----	----	----
AR 16656	L	----	----	----	----	----	----	----	----	19.6	14.1	12.9	----	----	----
AR 16787	L	11.5	8.1	16.5	10.5	11.8	----	----	----	----	----	----	----	----	----
AR 1685	R	12.0	8.4	15.3	10.5	11.6	16.0	12.3	12.7	17.0	13.0	12.2	16.2	12.1	10.5
AR 1686	L	11.7	8.1	15.3	9.5	11.5	16.2	12.0	12.5	17.0	13.4	12.6	17.3	12.7	11.9
AR 24239	R	----	----	17.0	10.8	11.3	----	----	----	----	----	----	----	----	----
AR 24240	R	----	----	----	----	----	----	----	----	19.7	14.9	13.8	----	----	----
AR 263	R	----	----	----	----	----	----	----	----	21.1	16.0	13.2	----	----	----
NTM P91171-4	R	----	----	----	----	----	----	----	----	----	----	----	----	----	14.3
QM F12499	R	----	----	16.5	10.8	11.9	----	----	----	----	----	----	----	----	----
UCMP69979	L	----	----	----	----	----	----	----	----	21.0	15.8	14.7	----	----	----

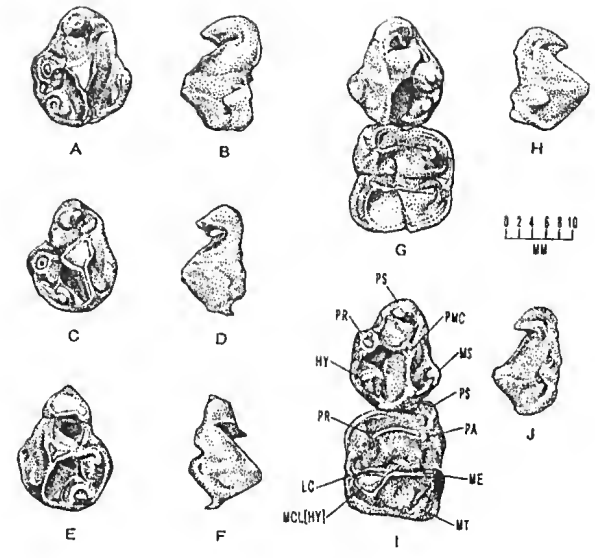

Fig. 12. *Neohelos tirarensis* Stirton, Riversleigh P^3-M^1 specimens: **A-B**, occlusal and labial aspects of left P^3 (AR9947, Camel Sputum, Riversleigh); **C-D**, labial and occlusal aspects of left P^3 (AR15119, Mike's Menagerie, Riversleigh); **E-F**, occlusal and labial aspects of right P^3 (AR10726, Camel Sputum, Riversleigh); **G-H**, occlusal and labial aspects of right P^3-M^1 (QM F13088, Inabeyance, Riversleigh).

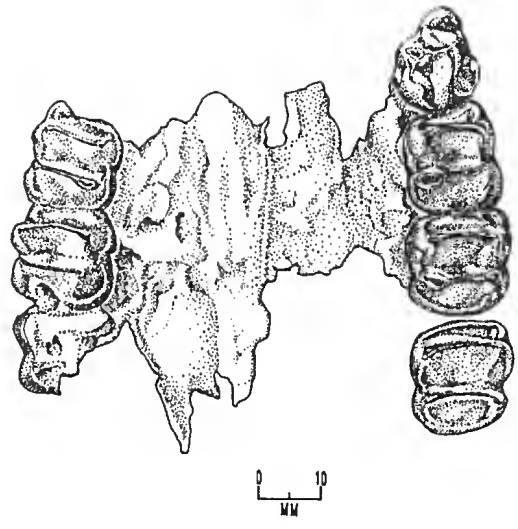

Fig. 13. *Neohelos tirarensis* Stirton; occlusal aspect of complete right tooth row, Mike's Menagerie Site, Riversleigh (AR16492)

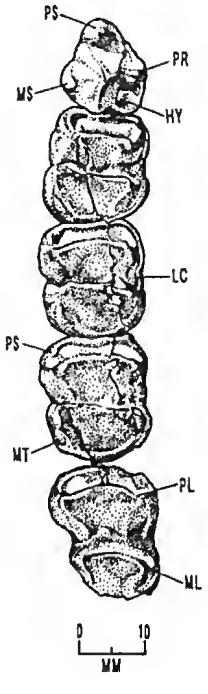

Fig. 14. *Neohelos tirarensis* Stirton; occlusal aspect of complete right cheek-tooth row, Mike's Menagerie Sitc, Riversleigh (AR16492).

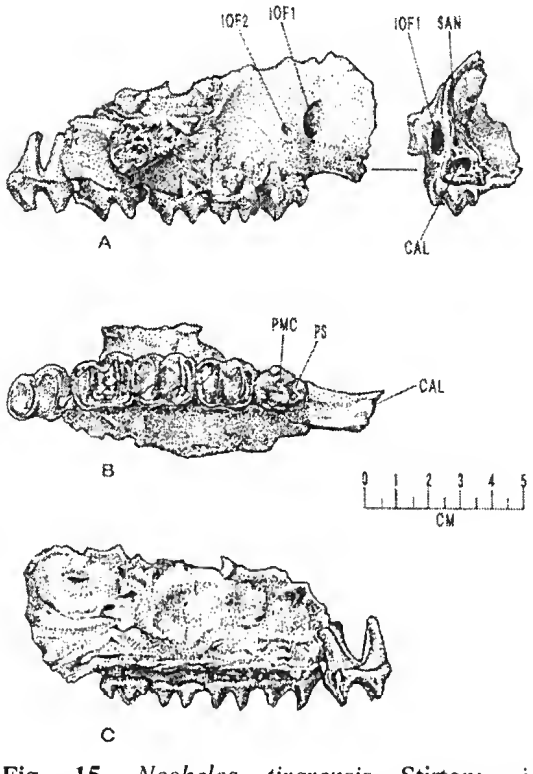

Fig. 15. *Neohelos tirarensis* Stirton; right maxillary fragment (AR 16492, Mike's Menagerie Site, Riversleigh: **A**, lateral aspect; **B**, occlusal aspect; **C**, internal aspect.

M^{1}. M^{1} SAM/UC 465 (Fig. 10A–B), while in general morphology, very similar to Stirton's (1967a) description, is considerably larger (anterior moiety 16.6 mm compared to 15.6; posterior moiety 16.9 compared to 15.7). The lophs are slightly crescentic and nearly transverse. The anterior loph is narrower than the posterior loph. There is a depression on the posterior surface of both the protoloph and the metaloph immediately labial to the longitudinal midline of the crown. The transverse median valley is V-shaped. A wide ridge descends from the median valley to the paracone tip. The parastyle, situated on the anterolabial corner of the crown is low, but well-developed, with weak crests anterior and posterior to it.

The precingulum traverses the anterior end of the crown from the base of the parastyle to the lingual base of the protocone. It commences again across the lingual mouth of the interloph valley, being briefly interrupted at the metaconule. The postcingulum commences at the tip of the metacone, below which, on the posterolabial corner of the crown, it is interrupted by a low metastyle. From the metastyle it continues toward the lingual side to terminate on the posterolingual base of the metaconule. The labial cingulum is absent. AR16492 has a larger parastyle and metastyle imparting a more trapezoidal shape to the crown (Fig. 12G). The lingual cingulum is strong and continuous horizontally around the loph bases to meet the postcingulum.

M^{2}. The M^{2} (AMF87626) is larger than M^{1} (Fig. 10I). The parastyles and metastyles are lower and smaller and the depressions on the posterior surfaces of the protoloph and metaloph are situated slightly more lingually than in M^{2}. The paraconal base is more rounded and the metaconal base is shorter than on the previous molar. The posterolingual cingulum rounds the base of the metaconule to make contact with a short lingual cingulum that traverses the median sulcus.

The D-Site (CPC 22558) M^{2} is from the same side and has the same degree of wear as the P^{3} with the same number, and probably represents the same individual. The crown is very similar to UCMP69978 in size and morphology. The anterior margin, including the parastyle, is abraded. The lingual cingulum traversing the mouth of the median valley is strong and laterally flared to produce a shallow basin. The posterolingual cingulum is strong where it swings around the base of the metaconule to meet the internal cingulum of the median valley.

AR10362 (Camel Sputum) is a left M^{2} retained in a fragment of maxilla. It is slightly shorter than the D-Site specimen (length 18.5 versus 19.0 mm) but resembles it closely morphologically. AR10362 has a large parastyle which is separated from the paracone by a deep notch.

The posterolingual cingulum is strong anterolateral to the metaconule base and nearly contacts the median valley cingulum. The metastyle is also relatively prominent, being visible as a small cuspule from the lateral aspect.

M^{3}. M^{3} is the largest and morphologically most variable molar in the series, sometimes resembling either the preceding or following molar (Figs 13–16). The parastyle and metastyle are smaller and lower than on the preceding molar. The protoloph is slightly wider than the metaloph, while the metaloph is slightly more oblique; otherwise the crown is typically more similar to M^{2} than it is to M^{4}. AR16492, a right maxilla containing P^{3}–M$^{1-4}$ (Figs 14, 15A–C) and a left maxilla fragment containing unworn M$^{3-4}$ (AR12120) show the size relationships and morphology of the otherwise isolated molar specimens

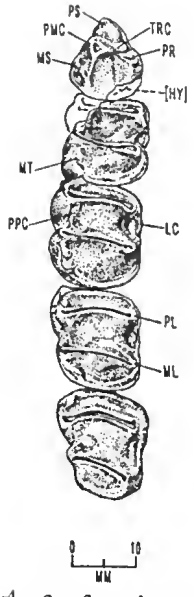

Fig. 16. *Neohelos tirarensis*, right P^3-M^{1-4} of referred cranium from Burnt Offerings Site (NTM P91167-1 possibly representing an early chronomorph of the species.

representing the series. In these specimens the protocone and metaconule are more bulbous near their tips than the paracone and metacone. The parastyle is low and pressed close to the base of the paracone. The metastyle is low, scarcely more than a widening of the postcingulum. The posterolateral lingual cingulum is weaker and interrupted at the loph bases. The lingual cingulum of the median valley mouth is short.

NTM P91171-2 is an isolated M^3, that while nearly identical to the previous description, both lophs are about the same width. A well-preserved isolated left M^3 (AR10669) is the largest *N. tirarensis* molar (20.3 mm long) in the collection. This molar also retains some of the features normally confined to M^2 such as a well developed posterolingual cingulum and a fairly high, though crest-like parastyle. It conforms to the M^3 morphology in having more bulbous tips of the protocone and metaconule, distinctly narrower and more obliquely oriented metaloph and feeble metastyle. NTM P942-1, AR17291 and AR12120 show more asymmetry of the crown, a narrower, more oblique metaloph and a short buccal cingulum across the mouth of the median valley similar to, but expressed to a lesser degree than in M^4.

M^4. M^4 is distinctly asymmetrical, with a bulbous paraconal base, strongly curved, obliquely oriented lophs and with the protoloph being much wider than the metaloph (Fig. 14). The parastyle is reduced to a low cuspule rising just above the precingulum. The metastyle is scarcely visible. A short buccal cingulum across the median valley is often, though not always present. M^4 is usually about the same length as M^3, but is slightly longer in some individuals, e.g. AR12120.

A complete upper cheek-tooth row of NTM P91167-1 represents one of the smallest and perhaps least derived examples of the *N. tirarensis* population sample (Fig. 16). It closely resembles QM F24137 from Bone Reef in the proportions of its lophs and expression of its cingulae and crests except it shows even less morphological differentiation of M^{1-3} from front to back, and the molar row is almost straight. The smaller *N. tirarensis* with less differentiation and curvature of the molar row may represent chronomorphs of the species.

Lower cheek teeth. P_3. The P_3 of *N. tirarensis* was previously unknown. Archer's 1982 collection of Wipajiri specimens contains an un-numbered posterior half of an unworn enamel cap which is a right P_3 (Fig. 10L–N, table 3). The tooth has a single high main cuspid. A ridge descends posteriorly from the cuspid with a tight, dorsally convex curve, then becomes vertical for 3.0 mm, at which point it turns through 90° to become horizontal. There is usually no posterior cuspid at the termination of this ridge. Lingual and labial crests descend from just below the end of the posterior ridge. The lingual crest forms a weak cingulid which delimits the edge of a shallow posteromedian basin and terminates anteriorly at a vertical ridge which descends from the main cuspid, while the labial crest descends, curving anteriorly to the edge of the enamel midway between the back of the tooth and a vertical line from the apex of the main cuspid. At this point it is joined by a weak ridge, which descends vertically from the main cuspid but which curves posteriorly over the last two millimetres.

Complete Riversleigh specimens confirm the identity of the Wipajiri P_3 fragment (Fig. 17A–B, E–F). The Camel Sputum specimen AR10841, differs from the Wipajiri example in having a cuspid-like termination of the posterior crest. In all larger *N. tirarensis* specimens (AR16787, AR10841 and AR10458) the anterior crest curves lingually and ascends the crown base forming a short precingulid which encloses a small, tear-drop-shaped fossa In smaller, possibly geologically older, less derived specimens such as AR1685-6 (D-Site) there is no precingulid.

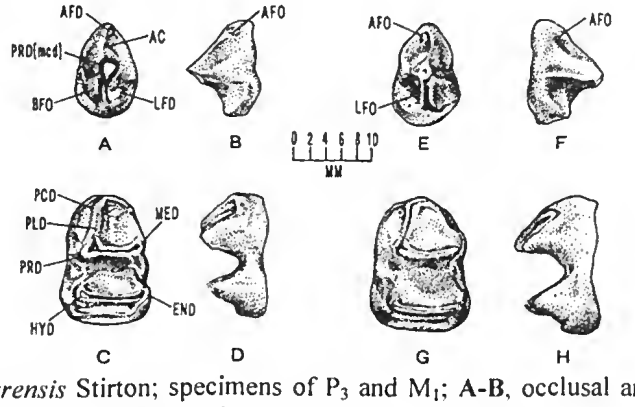

Fig. 17. *Neohelos tirarensis* Stirton; specimens of P_3 and M_1; **A-B**, occlusal and lingual aspects of left P_3 (AR16787 Wayne's Wok, Riversleigh); **C-D**, occlusal occlusal and lingual aspects of left M_1 (AR16787 Wayne's Wok, Riversleigh); **E-F**, occlusal and lingual aspects of right P_3 (AR10841, Camel Sputum, Riversleigh); **G-H**, occlusal and lingual aspects of left M_1 (AR13360, Camel Sputum, Riversleigh).

M_1. The M_1 trigonid of *N. tirarensis* is relatively shorter than in *Neohelos* spA and the entire crown is slightly broader relative to its length (Fig. 17C–D, G–H). The protolophid is narrower than the hypolophid. The paralophid originates from a short, strong, horizontal precingulid that sometimes partially ascends the metaconid base to enclose a U-shaped basin (e.g. AR16787, QM F12449). The paralophid is a thick, short crest, more steeply inclined than in *Neohelos* spA. The protolophid crest is nearly vertical in unworn specimens and does not overhang the interlophid sulcus. A short, rounded labial cingulid is sometimes formed across the mouth of the interlophid valley as a continuation of the postprotocristid and prehypocristid, which encloses a small basin in combination with the cristid obliqua. The lingual cingulid is short and weak.

M_2. In M_2 the lophids are about equal width, and as with M., the crown is broader relative

to its length than in *Neohelos* spA. The tips of the protoconid and hypoconid are bulbous. A faint labial cingulid is present, the lingual cingulid is poorly developed or absent. The precingulid is wide and inclined labially. It is thickest at the base of the metaconid. The postcingulid is elevated in the centre, and extends across the posterior lophid bases. In AR14393, the posthypocristid and postentocristid meet the ends of the postcingulid, emarginating the posterior face of the hypolophid.

M_{3-4}. M_3 is the largest molar in the series. The transversely oriented protolophid is much wider than the hypolophid. The entoconid is shifted posteriorly, resulting in a distinct obliquity of the hypolophid, a feature sometimes even more marked in *Neohelos* spB in which the M_2 hypolophid is also slightly oblique. Weak labial and lingual cingulids traverse the interloph valley. M_4 is nearly identical to M_3 but slightly smaller. The protolophid and the hypolophid show the same extent of obliquity and the hypolophid is only slightly narrower than the protolophid. The metalophid or cristid obliqua is usually more crisply defined on this molar.

Dentary. The dentary of *N. tirarensis* is known from two nearly complete specimens from D-Site (AR1685, AR1686). The horizontal ramus is long and slender, tapering gradually towards the incisor alveolus (Fig. 18A–C). The profile of the inferior border is smoothly convex, with a weak digastric process. The depth of the ramus at the level of M_{3-4} is 33.0 mm. The lateral surface of the horizontal ramus is rounded in the mid region, becoming shallowly concave anteriorly below the diastema. A small posterior mental foramen is present at the level of M_{2-3}. A round, 4.0 mm diameter mental foramen is located 5.0 mm anterior to the foremost P_3 root, 8.5 mm below the diastemal crest. The diastemal crest is sharp and arcuate with a convex lateral profile.

The lower incisor is procumbent, essentially following the curvature of the inferior border of the ramus to its tip. The coronoid crest is relatively straight and inclined posteriorly. The condyle is approximately 33.0 mm wide transversely; flattened and broad laterally (16.5 mm) and more cylindrical internally (10.0 mm). The masseteric fossa is smooth and deep, bounded posteroinferiorly by a low, thick masseteric eminence. A 3.0 mm diameter masseteric foramen is located in the inferior basin of the masseteric fossa. Internally, the surface of the horizontal ramus is flat. The symphysis is long, narrow and unankylosed. The digastric fossa extends anteriorly to the level of M_{2-3}, and is confluent with the pterygoid fossa posteriorly.

AR10458 is a well-preserved horizontal ramus fragment of the dentary (Fig. 19, Table 3). This specimen and its dentition are larger than AR1685-6. The jaw is 45.0 mm deep at the symphysial eminence below P_3 / M_1. The incisor alveolus is comparatively deep and oval in section, with a shallow notch in the inferior margin, commencing immediately anterior to the symphysial eminence. The incisor root is implanted about 20° from horizontal. The mental foramen is situated immediately anterior to, and 12.5 mm below, the P_3 anterior root exposure. The lateral surface of the dentary anterior to M_2 is gently convex, becoming concave anterior to P_3 above the incisor root. The diastemal crest is slightly elevated with a thick dorsal ridge. The internal surface is nearly flat. The sublingual fossa above the symphysis is a shallow groove indicating that the fossa was narrow (Fig. 19C). The symphysis is unankylosed; elongated, and oval-wedge-shaped. A large 5.0 mm diameter genial pit is present on the posterointernal surface.

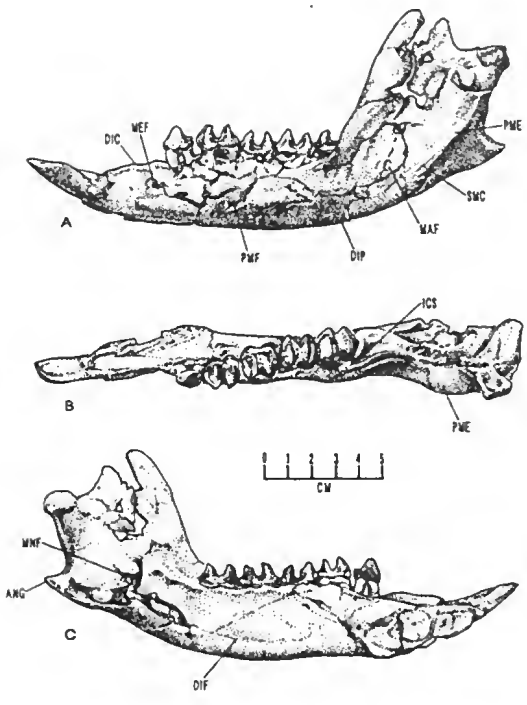

Fig. 18. *Neohelos tirarensis* Stirton, referred left dentary (AR1686) from D-Site, Riversleigh: **A**, lateral aspect; **B**, occlusal aspect; **C**, internal aspect. This is a small and apparently plesiomorphous specimen, with similar attributes to the small Burnt Offerings, Riversleigh, cranium.

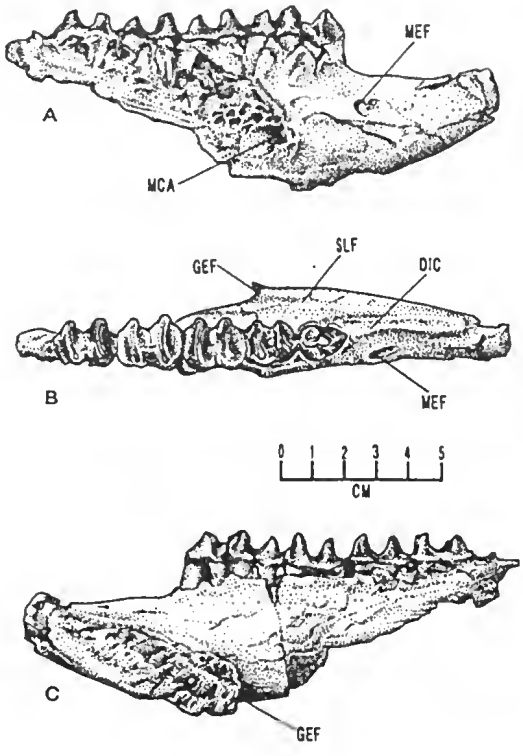

Fig. 19. *Neohelos tirarensis* Stirton, right dentary fragment (AR10458) from Wayne's Wok locality: **A**, lateral aspect; **B**, occlusal (dorsal) aspect; **C**, internal aspect. This more robust specimen is similar in size and appearance to the Lake Ngapakaldi material and is typical of the larger *N. tirarensis* specimens from Riversleigh.

Table 3. Measurements of palate and dentary of *Neohelos tirarensis* Stirton.

MEASUREMENT	millimetres
Width palate (QM F13088)	50.0
P_3 to canine alveolus (AR16492)	18.0
Diameter IOF1 (AR16492)	12.0 x 0.6
Length cheek tooth row (AR16492)	85.3
Dimensions lower incisor alveolus (AR10458)	9.0 x 15.6
Length (minimum) diastema dentary (AR10458)	31.5
Depth dentary at P_3/M_2 (AR10458)	41.5
Estimated length of dentary symphysis (AR10458)	66.2
Depth of dentary symphysis (AR10458)	22.6
Thickness (transverse section) of dentary at P_3/M_2 (AR10458)	15.0

Cranium. NTM P91167-1 is a partial cranium with a complete right cheek-tooth row (Fig. 20, Table 4). It is missing most of the left side, on which only M^{2-4} are preserved. The left side of the palate is crushed. The right side of the neurocranium is preserved to just behind the squamosal root of the zygomatic arch. The basicranium is missing up to the base of the right pterygoid crest. The right premaxilla is fairly complete but broken in half longitudinally between the orbit and the premaxillomaxillary suture.

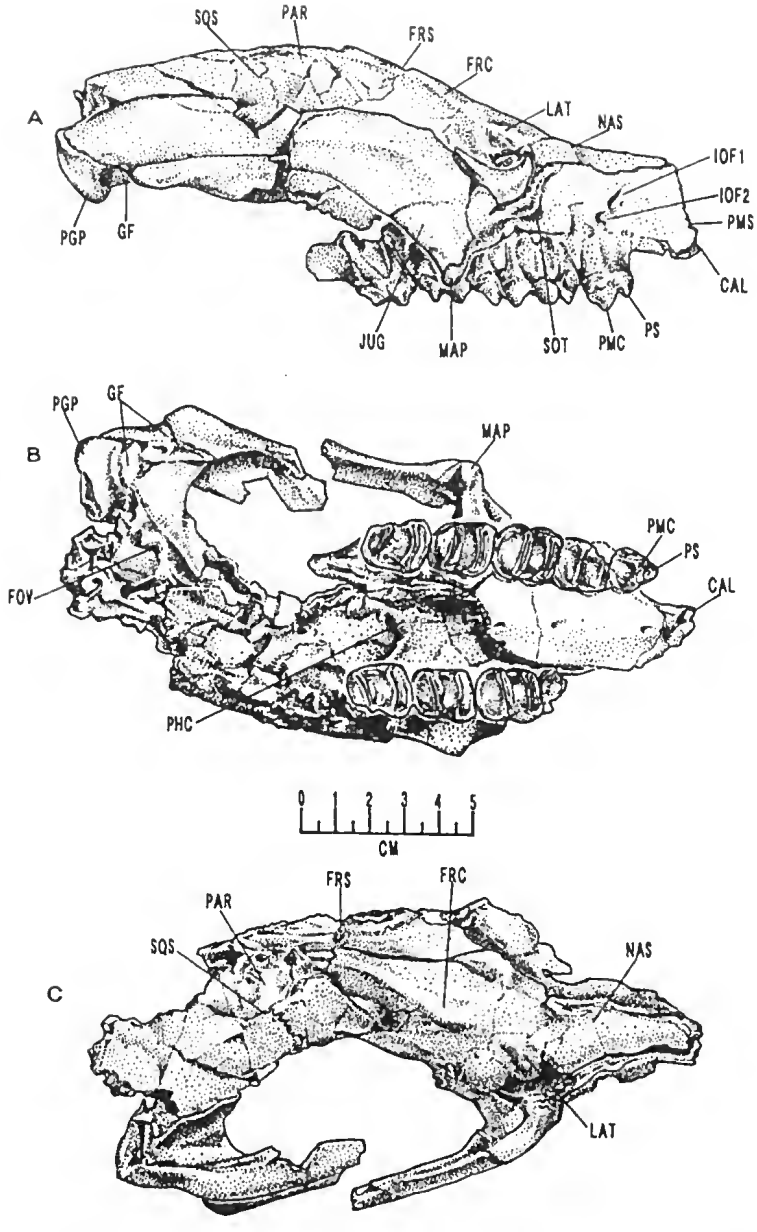

Fig. 20. Referred cranium of *Neohelos tirarensis* (NTM P91167-1) from Burnt Offerings, Riversleigh; **A**, lateral aspect; **B**, ventral aspect; **C**, dorsal aspect; the posterior part of the cranium is sheared off behind the squamosal root. Anteriorly the break follows the premaxillary suture. The upper half of the maxilla is crushed downwards and the left half of the palate is crushed inwards, being considerably overlapped by the right half, resulting in the illusion of a narrow palate, which is actually very wide in *N. tirarensis*.

In lateral aspect, the profile of the cranium is low and elongated (Figs 20A, 23). The frontal crests are sharp, prominent ridges that ascend steeply towards their posterior convergence to form a distinct vertex. A small portion of the anterior end of the sagittal crest is preserved on the specimen, indicating that it was well developed. The frontal crests are divided by a 10.0 mm deep, 50.0 mm by 25.0 mm oval median depression commencing at the long, narrow V-shaped frontonasal suture and ending immediately anterior to the frontoparietal vertex. A low, sharp postorbital eminence is present about 40.0 mm posterodorsal to the orbital margin. A prominent, elongated lacrimal tubercle, about 12.0 mm long by 8.0 mm wide is situated on the anterodorsal corner of the orbit.

Table 4. Measurements of the cranium of ?plesiomorphic chronomorphs of *Neohelos tirarensis* used in the restoration sketch in Figure 2; specimens from various sites, Riversleigh.

MEASUREMENT	millimetres
Dimensions of frontal fossa (NTM P91167-1)	25.0 x 50.0
Dimensions of lacrimal tubercle (NTM P91167-1)	08.0 x 12.0
Dimensions of suborbital fossa (NTM P91167-1)	15.0 x 20.0
Dimensions of infraorbital foramen (NTM P91167-1)	03.5 x 09.0
Dimensions of glenoid articular surface (NTM P91167-1)	30.0 x 35.0
Dimensions of postglenoid process (NTM P91167-1)	10.0 x 26.0
Length of squamosal-jugal suture (NTM P91167-1)	100.0
Depth (maximum) of zygomatic arch (NTM P91167-1)	30.0
Length of massteric process (NTM P91167-1)	11.0
With of submassteric notch (NTM P91167-1)	12.4
Distance anterior orbital margin to maxillary suture (NTM P91167-1)	48.0
Distance maxillary suture to postglenoid process (NTM P91167-1)	190.0
Distance maxillary suture to postalveolar process (NTM P91167-1)	115.5
Depth orbital margin to submasseteric notch (NTM P91167-1)	27.7
Estimated width of palate at M^2/M^3 (NTM P91167-1)	48.0
Distance anterior P^3 to canine alveolus (NTM P91167-1)	15.3
Length cheektooth row (NTM P91167-1)	81.5
Estimated bizygomatic width (NTM P91167-1)	150.0
Dimensions canine alveolus (NTM P91167-1)	06.0 x ---
Dimensions canine alveolus (AR 13795)	06.0 x 06.0
Dimensions I^1 alveolus (NTM P91166-3)	07.0 x 11.0
Dimensions I^2 alveolus (NTM P91166-3)	06.0 x 09.0
Dimensions I^3 alveolus (NTM P91166-3)	06.3 x 06.9

The missing nasal bones, delimited by the intact right maxillary margin, were slender, and judging from our composite restoration, elongated. The anterior orbital crest is thick and rounded, protruding anterolaterally into the facial region. It terminates in a prominent, angular infraorbital tuberosity inferiorly and continues superiorly as a weak facial crest or torus. The suborbital fossa is a 15.0 mm by 20.0 mm crescentic depression that extends down the anterior face of the zygomatic process. The infraorbital foramen is situated above the P^3 in the lower half of the maxilla. In *N. tirarensis* the foramen sometimes has two separate, nearly confluent orifices. The main foramen is tear-drop-shaped, 9.0 mm by 3.5 mm. Below and behind the main infraorbital foramen is a large auxiliary which opens immediately above the posterior root of P^3. The auxiliary foramen is slightly smaller and more separated from the main foramen in AR13795 (Fig. 21E). The auxiliary foramen appears to be absent in QM F24137, but this may be due to its slightly more anterior position, as the foramen is visible in the broken section. It is present, but reduced, in AR16492 (Fig. 15A). The facial fossa is broad and shallow, flaring slightly on its inferior margin around the canine alveolus.

The maxillary palate is broad and flat with a wide, though shallow median sulcus. The alveolar border is flush with the plane of the palate. The maxillopalatine suture is U-shaped, extending anteriorly to between the level of M^{2-3}. The posterior palatine margin is C-shaped and emarginated by a rugose pharyngeal crest (Fig. 20B). Small, elliptical posterolateral palatine foramina are located in shallow clefts developed in the posterolateral processes of the palatine. The pharyngeal or interpterygoid fossa is missing on the specimen. The anterior portion of the pterygoid fossa is a shallow, elongated sulcus perforated by a round, 5.0 mm diameter foramen of the transverse canal.

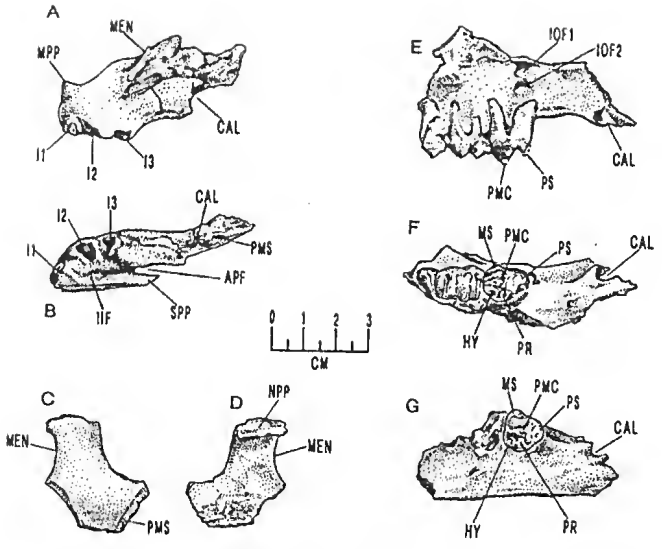

Fig. 21. Referred *Neohelos tirarensis*, premaxillae (A–D) and maxillae (E–G): **A–B**, lateral and palatal aspect of incisor alveoli, NTM P91166-2 (Burnt Offerings, Riversleigh); **C–D**, lateral and internal views of apertual process, NTM P91166-3 (Burnt Offerings, Riversleigh); **E–F**, fragment with labial halves of P^3–M^{1-2}, AR 13795, (Sticky-beak, Riversleigh)—note canine alveolus (CAL); **G**, palatal view of fragment NTM P91166-1 (Burnt Offerings, Riversleigh) with P^3 and canine alveolus.

The glenoid articular surface is transversely wide (approximately 35.0 mm) and about 30.0 mm long anteroposteriorly, extending forward onto a transversely expanded (15.0 mm by 15.0 mm) jugal eminence. The articular surface is flat and slightly obliquely oriented relative to the axis of the cranium. The postglenoid process is transversely wide (26.0 mm) and 10.0 mm thick, being extensively invaded by squamosal sinuses. Its inferior margin extends at least 18.5 mm above the glenoid surface. The posterior surface of the postglenoid process is missing as are all elements and relations of the middle ear and the medial glenoid eminence. A small fragment of bone preserves part of what appears to be foramen ovale and the posterior half of the pterygoid fossa. If this is the structure in question, the foramen ovale is formed entirely within the alisphenoid indicating that an alisphenoid tympanic process was present.

The squamosal root of the zygomatic arch is dominated dorsally by a long, deep squamosal sulcus. The squamosal zygomatic process is relatively thin and sharp on its dorsal margin. The squamosojugal suture is long and only slightly curved over its 100.0 mm extent. The maximum depth of the zygomatic arch (30.0 mm) is situated immediately anterior to the glenoid articular surface of the jugal. A deep masseteric sulcus extends from immediately anterior to the glenoid fossa to the posterior margin of the zygomatic process. A sharp masseteric crest defines its dorsal margin. A low elevation of the anterior zygomatic process of the squamosal immediately behind the rounded orbital margin, represents a rudimentary postorbital eminence. The 13.0 mm long zygomatic process is slender and conical, terminating inferiorly about 4.0 mm above the occlusal line of the cheek teeth. It is composed predominantly of the maxilla. The subzygomatic notch is 14.0 mm wide.

AR13795 is a fragment of right maxilla with the labial halves of P^3–M^1 and M^2 protoloph in place (Fig. 21E–F). The specimen is assigned to *Neohelos tirarensis* on the basis of its size and cheek-tooth morphology, including broad interproximal contact and large parastyle and metastyle on M^1. As in P91167-1, this specimen possesses a 6.0 mm diameter canine alveolus located behind the premaxillomaxillary suture, though further forward at about 20.0 mm anterior to P^3. The diastemal margin between the canine alveolus and the P^3 is more distinctly concave than in the type specimen. The alveolus is

strongly deflected anterolaterally. It also possesses an auxiliary infraorbital foramen and shows a remnant of a strongly expressed suborbital tuberosity. NTM P91166-1 is a right maxillary fragment containing P^3. The 6.0 mm diameter canine alveolus is 15.0 mm from the P^3, closely matching the proportions of the type specimen.

ARl6492 preserves part of the right maxilla, extending from the premaxillary suture to the M^4 alveolus (Fig. 15, Table 3). The 38.0 mm long maxillo-premaxillary suture is nearly vertical. The suture transects the proximal part of a canine alveolus, 20.0 mm anterior to the P^3 root and extending obliquely 10.0 mm into the bone (Fig. 15A). The alveolus, which is slightly curved and slanted inwards, is about 6.0 mm in diameter at the point of intersection. Immediately above the alveolus is the superior alveolar nerve foramen. The main infraorbital foramen, situated 13.0 mm above the anterior edge of the P^3, is a large 13.0 x 6.0 mm, anteriorly-opening, teardrop-shaped fissure set within a shallow, oval 13.0 x 15.0 mm fossa. A small, 2.0 mm diameter, elliptical auxiliary infraorbital foramen is located 9.0 mm behind the inferior margin of the former.

The 47.0 mm long maxillojugal suture obliquely transects the maxilla at an angle of about 30°. It is slightly curved with no indication of an infraorbital tuberosity as seen in NTM P91167-1. The subzygomatic notch is 6.0 mm above the alveolar margin of M^2. Only the alveolar margin of the palate is preserved, indicating that the palate was flat and slightly constricted at the diastema immediately anterior to P^3. The Inabeyance specimen (QM F13088) preserves the mid-palatal region of *N. tirarensis*, which is about 50.0 mm wide at the level of M^2. The palate is flat with a pair of indistinct shallow grooves situated on either side of the median suture (Fig. 13, Table 3).

NTM P9 1166-2 is an edentulous left half of the premaxilla (Fig. 21A–B) tentatively assigned on the basis of its size and *Neohelos*-like morphology. The canine alveolus is damaged. A fragment of I^1 is present in its alveolus. Although it is broken off nearly flush with the alveolar margin, the section of tooth is enamelled, indicating that the crown had not fully erupted. The section of the crown is 10.5 mm x 6.5 mm at the level of the alveolus. Another indication of its subadult age is that I^2 alveolus (6.0 mm x 9.0 mm) is larger than that of I^3 (6.3 mm x 6.5 mm). The occlusal or sectional shape of these partially erupted crowns are clearly reflected in the outer margins of the sockets.

The premaxilla has a well-developed, conical median crest or eminence, accentuated laterally by a smooth sulcus leading posteroinferiorly into the anterior palatal fenestrae. The premaxillary crest is continuous posteriorly with the septal process. Laterally, the apertural process, which is missing on the specimen, arises behind a small sulcus. The interincisive fossa is narrow. The incisive foramina are elongated and elliptical, separated by a stout septal process. In lateral profile, the inferior margin of the diastemal palate appears to have been straight, though slightly decurving immediately behind the I^3 alveolus. A long, narrow spur of the premaxillomaxillary suture extends anteriorly to 6.5 mm behind the I^3 alveolus. Restored, the incisor arcade viewed in ventral aspect would have been U-shaped with both halves present.

NTM P91166-3 is a left premaxilla fragment preserving the margin of the narial aperture anteriorly and the pre-maxillomaxillary suture on its posteroinferior half (Fig. 21C–D). The internal dorsal margin is greatly thickened (about 7.0 mm) along the nasal contact zone. The walls of the narial aperture are contrastingly thin (about 3.5 mm) and smoothly convex externally. The surface contour of the fragment indicates that the rostrum flared laterally just behind the narial opening. The narial aperture is smoothly emarginated by a

rounded thickening. The 18.5 mm notch is C-shaped in lateral profile and the margin does not seem to recede posterodorsally. The maximum distance perpendicular from a chord across the narial notch is 5.5 mm.

NTM P91166-6 is the posterior half of a cranium missing the palate and rostrum, preserving the frontals, parts of the parietals, the occipital, cranial base and right zygomatic arch (Fig. 22, Table 5). The specimen is crushed and compressed dorsoventrally. Lacking dentition, the specific identity of the cranium is based on its similarity to NTM P91167-1 and specimens of *Neohelos* spB. Corresponding preserved elements of the cranium are very similar to NTM P91167-1 except for their greater robusticity, particularly in the development of the zygomatic arch and glenoid fossa which are larger relative to the overall proportions of the rest of the cranium than in *Neohelos* spB. As in *Neohelos* spB crania, NTM P91166-6 has a vertical, low, transversely broad occipital plane; an ovo-rectangular foramen magnum; large, transversely narrow occipital condyles that protrude posteriorly beyond the profile of the occiput; large sinus-inflated mastoids; low rectangular entoglenoid eminence and tympanic bulla; ventral tympanic process composed of the alisphenoid; transversely wide, oblique glenoid fossae; evidence of large, sinus-inflated, obliquelyoriented postglenoid processes that partly displace or overlap the epitympanic fenestrae and short, rugose, blunt superiorperiotic process of the petrosal.

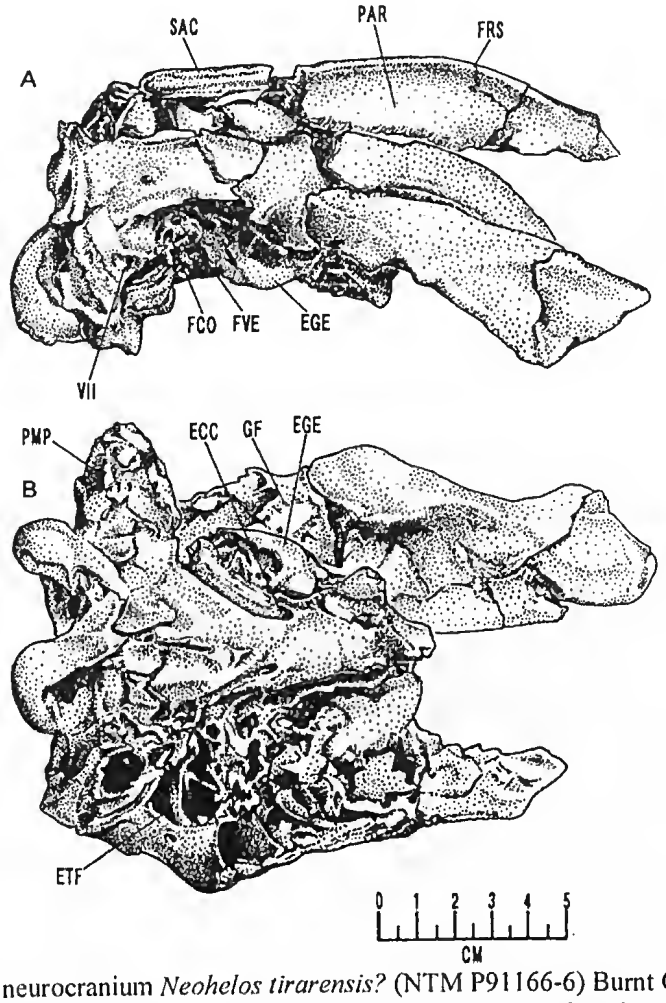

Fig. 22. Zygomaturine neurocranium *Neohelos tirarensis?* (NTM P91166-6) Burnt Offerings, Riversleigh: **A**, lateral aspect; **B**, ventral aspect. The specimen is similar to *N. tirarensis* referred cranium NTM P91167-1 but is larger, has deeper zygomatic arches and larger epitympanic fenestrae. Based on analogy with sexually dimorphic Bullock Creek *Neohelos* spB, this specimen might represent a male *N. tirarensis*.

Table 5. Measurements of *Neohelos tirarensis?* (NTM P91166-6) cranium.

MEASUREMENT	millimetres
Width occiput	113.5
Estimated height of occiput	75.0
Dimensions of right occipital condyle	13.5 x 35.0
Dimensions of foramen magnum	18.5 x 23.5
Depth (maximum) of zygomatic arch	47.5
Length from convergence of frontal crests to lambdoid crest	130.0
Estimated bizygomatic width	170.0
Length squamosal-jugal suture	90.0
Dimensions entoglenoid eminence	13.3 x 29.2
Dimensions mastoid-paroccipital process	23.0 x 28.0

The cranium was probably elongated relative to its width, judging from the distance between the convergence of the frontal crests and the back of the occiput (approximately 130.0 mm). The transverse width of the occiput from squamosal to squamosal is 113.5 mm. The posterior profile of the cranium is a low rectangle. The occipital condyles are large (35.0 mm dorsoventrally) and narrow transversely (13.5 mm). They extend posteriorly about 20.0 mm beyond the vertical profile of the back of the cranium. A single, large condylar foramen is present in the condylar sulcus of each side. The foramen magnum is ovo-rectangular, with dimensions of 23.5 mm by 18.5 mm. The mastoids are large, globular sinus-inflated protuberances that terminate in small, conical mastoidparoccipital processes. The lateral wing of the mastoid is confined to the posterior surface of the cranium and does not wrap around the lateral side. The auditory arch of the squamosal is wide and rounded. Mesially, a large, oval (17.5 mm x 12.5 mm) epitympanic fenestra opens into posterior (mastoid) and anterior (squamosal) cavities of the epitympanic sinuses.

Only the bases of the postglenoid processes are preserved (Fig. 22B). The base of the left postglenoid process flares ventrolaterally before a break exposes a large squamosal sinus. On the right side, part of the anterolateral base of the process curves outwards and downwards indicating that a large, sinus-inflated postglenoid structure, similar to that of *Neohelos* spB was present. The large entoglenoid eminence (a crest-like swelling of the squamosal situated at the medial end of the glenoid articular surface) is an elongated-oval swelling that extends posteriorly to form the lateral wall of the ventral tympanic wing and a bullalike structure that forms the anterior wall of the tympanic cavity. The ventral surface of the bulla is broken, but a rugose sutural contact with the squamosal indicates that it was floored by an overlapping alisphenoid process as in *Neohelos* spB. The entire structure is displaced anteromedially, obscuring the relations of foramen ovale. Foramen ovale appears to have been arched by the alisphenoid and pterygoid crest. The tympanic cavity is small and open ventrally. The petrosal is tucked in over the basioccipital and is floored by a small process of the latter.

The ventrolateral surface of the petrosal is visible in lateral aspect. The petrosal is short, broad and blunt with a flattened pars cochlearis surface. The ventral surface of the promontory is rugose. The auditory fenestrae are situated on the posterodorsal portion of the lateral surface of the petrosal. The 2.0 mm by 1.6 mm fenestra cochlearis is located 2.0 mm posteroventral to the 1.5 mm by 1.0 mm vestibular fenestra. The facial foramen opens at about the same level as, and 4.0 mm anterior to the vestibular fenestra. A 4.0 mm wide, 20.0 mm long facial nerve sulcus is inscribed on the posteroventral (mastoid) side of the acoustic arch. A shorter groove above, and a low, rugose process below the facial sulcus, represent the attachments for the posterior crus of the missing ectotympanic bone, which when present,

would have completed the anterior margin of the stylomastoid foramen and the bony auditory meatus.

The small, approximately 3.5 mm diameter, 2.5 mm deep epitympanic recess or attic, which accommodated the auditory ossicles, is situated within the long, narrow tegmen tympani. The 2.0 mm wide, 6.5 mm long incisura tympanica is situated about 1.0 mm lateral to the margin of the tegmen and the attic. The crista tympanica forms the rounded internal margin of the epitympanic fenestra. The distance from the tympanic crest to the lateral edge of the superficias meatus is about 19.0 mm. Commencing immediately anterolateral to the promontorium of the petrosal is a 7.0 mm wide, 29.0 mm long, gutter-like groove for the internal carotid artery. A notch at the commencement of the internal carotid groove demarks an irregularly-shaped middle lacerate foramen or pyriform fenestra. The internal carotid foramina pierce the basisphenoid immediately mesial to the pterygoid crest. The basisphenoid-basioccipital suture is not discernible on this specimen.

Part of the right glenoid fossa is preserved, indicating that it was transversely wide and oblique. The anterior articular eminence is flat to slightly concave, extending anterolaterally to a broad expansion (25.0 mm across) of the jugal. The zygomatic arch is deep and robust in proportion to the relatively light construction of the rest of the cranium. The zygomatic arch is 47.0 mm deep immediately anterior to the glenoid expansion of the jugal. The masseteric crest of the jugal is prominent and deeply excavated below. Most of the bones of the cranial wall are shattered. The parietals are partly intact. These were long and narrow, commencing anteriorly from just behind the convergence of the frontal crests. A strong sagittal crest is highest immediately behind the frontoparietal suture.

The appearance of the cranium of *N. tirarensis* has been restored in Figure 23 based primarily on the small cranium NTM P91167-1 with information on the back of the cranium taken from NTM P91166-6. The fragments of maxilla and premaxilla illustrated in Figure 21 were used to restore the rostrum. The dentaries are restored from the D-site specimens, AR1685-6.

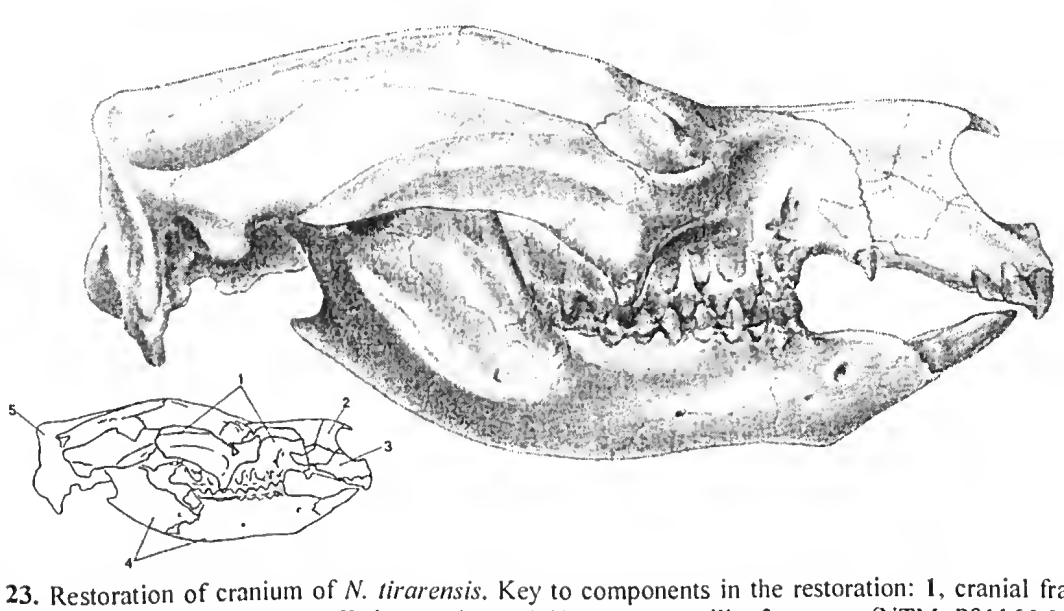

Fig. 23. Restoration of cranium of *N. tirarensis*. Key to components in the restoration: **1**, cranial fragment (NTM P91167-1 Upper Burnt Offerings, Riversleigh); **2**, premaxilla fragment (NTM P91166-3 Burnt Offerings, Riversleigh); **3**, premaxilla fragment (NTM P91166-2 Burnt Offerings, Riversleigh), **4**, dentaries (AR1685 D-Site, Riversleigh); **5**, cranial fragment (NTM P91166-6 Burnt Offerings, Riversleigh). Canine shape, dorsal nasal profile and I^3 are conjectural.

Comparisons with *Nimbadon scottorrorum* Hand, Archer, Godthelp, Rich and Pledge, 1993. [*Nimbadon scottorrorum* Hand, Archer, Godthelp, Rich and Pledge 1993 p. 204; fig. 5. Holotype: QM F23137, maxillary fragment with right P^3–M^{1-4}; the labial sides of M^{2-4} are damaged. Type locality and age: Fig Tree Site, adjacent to Godthelp's Hill, Riversleigh Station, north-western Queensland. Hand *et al.* (1993) interpret the Fig Tree assemblage to be ?late Oligocene - early Miocene in age.]

Nimbadon scottorrorum differs from other species of *Nimbadon* and resembles species of *Neohelos* in having broad, rectangular molars with wide interproximal contact and large parastyles and metastyles on M^{1-2}. It differs from *Neohelos* spA in having broader, more rectangular molar crowns and less morphological and size differentiation along the tooth row; though similar in having a vertical emargination of the metaconule by a continuation of the postcingulum; differs from *N. tirarensis* in having a vertical emargination of the metaconule by the postcingulum; differs from *Neohelos* spB and *Neohelos* spC in being smaller and in those features that differentiate it from *N. tirarensis*.

The apparent closeness of *Nimbadon scottorrorum* to *Neohelos* is one of the casualties of the merging of characters and character combinations resulting from the enlargement of the Riversleigh sample. The type specimen QM F23137 seems to have little in common with the other two species of *Nimbadon* and in most respects falls in more closely with small to medium-sized *Neohelos tirarensis* specimens (Fig. 24; Table 6). However, QM F23137 is unique among *N. tirarensis* specimens in having a weak, but clearly expressed upturn of the postcingulum along the side of the metaconule; similar to, but not exactly as in *Neohelos* spA (Fig. 25B), and its P^3, while having a well-developed transverse crest from the parametacone to the protocone, is small, has a weak mesostyle and exhibits a distinctive thegotic facet on the parastyle that is also present in *Neohelos* spA. Its molars are otherwise typical of *Neohelos tirarensis* in being broad, having wide interproximal contact, the parastyle and metastyle is large, the paracone and metacone bases do not bulge conspicuously, the meristic gradient and other details of the crown are almost identical to Inabeyance (QM F13088) and Camel Sputum (AR17443) specimens. The intermediate character combinations and states expressed by this specimen compels us to align the Cleft of Ages material within *Neohelos*, rather than to assign the Cleft of Ages specimens to a species of *Nimbadon* (forcing the retention of *Nimbadon scottorrorum*) or to assign both species to a new genus (ignoring the intermediate and blended morphological states). The practical implication of these remarks is that the smallest specimens of *N. tirarensis* overlap with *Neohelos* spA and *Ni. scottorrorum* considerably in size and in many morphological features. At the time of writing, *Neohelos* spA specimens were known only from the Cleft of Ages locality, Riversleigh, Station. As the relative age of the Cleft of Ages locality is in doubt, confusion of these species could result in an erroneous biocorrelation or biochronological estimation.

Table 6. Measurements (millimetres) of upper cheek teeth of *Nimbadon scottorrorum*; Fig Tree Site, Riversleigh Station.

UPPER CHEEK TEETH (mm)

SPECIMEN	SIDE	P^3		M^1			M^2			M^3			M^4		
		L	W	L	AW	PW	L	AW	PW	L	AW	PW	L	AW	PW
QM F23157	R	14.3	13.4	17.1	15.0	15.8	17.9	—	—	18.5	—	—	18.1	—	—

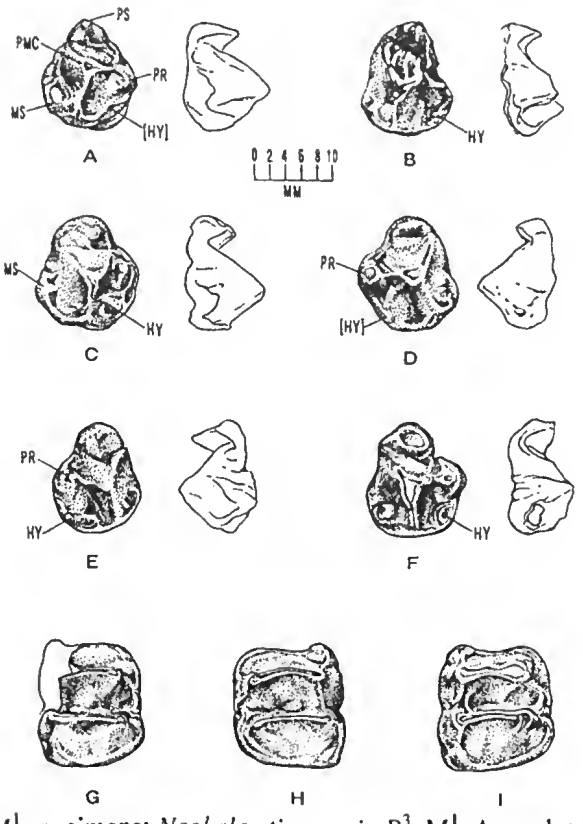

Fig. 24. Small *Neohelos* P^3–M^1 specimens; *Neohelos tirarensis*, P^3–M^1, **A**, occlusal and labial aspects of right P^3 (NTM P91167-1) from Upper Burnt Offerings, Riversleigh; **B**, occlusal and labial aspects of damaged right P^3 of *N. tirarensis* (AR13795) from Sticky-beak locality, Riversleigh; **C**, *N. tirarensis* occlusal and labial aspects of right P3 (NTM P91166-1) from Burnt Offerings locality, Riversleigh; **D**, *N. tirarensis*, occlusal and labial aspects of left P^3 (AR17470) from Bone Reef, Riversleigh; **E**, *Neohelos* spA left P^3 (QM F23247) Cleft of Ages, Riversleigh; **F**, *Neohelos* spA occlusal and labial aspects of right P^3 (QM F20584) from Cleft of Ages Site, Riversleigh; **G**, *N. tirarensis*, occlusal aspect of right M^1 (NTM P91167-1) from Upper Burnt Offerings, Riversleigh; **H**, *N. tirarensis* occlusal aspect of left M^1 (QM F24137) from Bone Reef, Riversleigh; **I**, occlusal aspect of right M^1 of holotype *Nimbadon scottorrorum* Hand *et al.* (1993) (QM F23157) from Fig Tree, Riversleigh (drawn from a cast).

Neohelos spA

Reference specimen. QM F30878 left maxillary fragment with P^3–M^{1-3}.

Type locality and age. Cleft of Ages locality Riversleigh Station. Cleft of Ages is a fissure-fill deposit within poorly constrained strata ranging in age from late Oligocene to early Miocene.

Referred specimens and localities. Cleft of Ages: AR16810, right M^3; AR16955, right M_1; QM F12432, left M_3 QM F12433, right M^4; QM F20488, left M^2; QM F20489, left M_3 QM F20584, right P^3; QM F20585, left M^2; QM F20709, right M_3; QM F22765, left maxilla, M^{2-3}; QM F22767, right M^3; QM F22771, right M^4; QM F22773, right P^3; QM F22774, right P_3; QM F23274, left P^3; QM F23407, left M^1; AR16957, right M^1; AR17453, right M^2; AR17454, left M^1; AR17469, left M^4; QM F12434, left M^1; QM F20831, left M^3; QM F20852, right M^1; QM F22765, left M^{2-3}; QM F23195, right M^1; QM F23197, right M^1; QM F23408, right M^3; QM F23472, right M^1; QM F24270, left M^{1-3}; QM F24731, right M^1; QM F29739, right M^1; QM F29740, right M^1; QM F30305, left maxilla, M^{1-3}; QM F30556, left M^1; QM F30558, right M^1; QM F30734, right P^3; QM

F24230, left dentary, M^{2-3}; QM F24298, right $P^3$6=; QM F24299, right M^3; QM F24300, right P_3; QM F24433, right M_3; QM F24435, left M_1; QM F24741, left M^3; QM F29738, left P_3; QM F30231, left dentary, M_{1-3}; AR16596, left M_1; QM F20486, left M_1; QM F20490, right M_3; QM F20491, right M_1; QM F20830, right M_2; QM F20832, left M_3; QM F20838, left M_1; QM F22766, right M_2; QM F23198, right P_3; QM F23199, right P_3; QM F24432, right M_2; QM F24440, left M_4; QM F24667, right P_3; QM F30306, right M_2; QM F30554, right M_1; QM F30560, right M_1.

Species diagnosis. Differs from *Nimbadon* species in larger size, broader molars, large stylar cusps on M^3. Cheek teeth range from slightly smaller than, to about equal in size to the smaller specimens of *N. tirarensis*; differs from *Ni. scottorrorum* and *N. tirarensis* in having proportionally longer upper and narrower lower molar crowns with much narrower M^1 protoloph, which is more deeply cleft on the posterior surface; differs from *N. tirarensis* in having a strong continuation of the postcingulum up the postcrolingual flank of the metaconule to the apex of the cusp; and from *Ni. scottorrorum* and *N. tirarensis* in that the margins of the paracone and metacone are more convex and the postcrior moiety of the crown is distinctly elongated and tapered towards the back. Differs from other *Neohelos* species in its smaller size, proportionally more elongated M^1; narrow, deeply clefted protoloph; conspicuous emargination of the metaconule by the postcingulum and the tapering posterior moiety of crown (Figs 25A, 26; Table 7).

Remarks. Though wc initially recognised many of the specimens from Cleft of Ages as being subtly different from the smallest specimens of *N. tirarensis*, our determinations were based entirely on isolated cheek. teeth, some of which, particularly P^3 and M^3, seemed indistinguishable from the latter. As only the M^3 consistently differed we were not sure whether one or two species were represented.

Newly discovered partial toothrow QM F30878 (Fig. 26) provides the information necessary to distinguish *Neohelos* spA from other small species of *Neohelos*. The recognition of this species is biochronologically important because of its similarity with smaller *N. tirarensis* and *Ni. scottorrorum* specimens. Only the upper molars, particularly M^{1-2}, can be consistently distinguished from those of small *N. tirarensis* or *Ni. scottorrorum*. At present, we cannot provide infallible distinctions for the P^3 or for the lower cheek teeth for these species which means that any critical determinations of these forms should be made on specimens of M^{1-2}.

Description of reference specimen, QM F30878. Cheek-tooth row with slight curvature and fairly strong meristic and morphological gradient in the molars; enamel thick and marked by numerous vertical ridgelets and shallow grooves. P^3 small, short and broad (length 14.4 mm, width 12.9 mm); parastyle low, erect, separated from parametacone by deep transverse cleft; transverse crest from paramctacone to protocone absent; protocone separated from parametacone by a deep anteroposterior cleft; pair of strong ridges extend down anterior face of the parametacone to the base of the parastyle; hypocone small; faint mesostyle represcnted by a series of low vertical ridges. M^1 elongated (length 15.4 mm, anterior width 12.7 mm, posterior width 13.5 mm) distinct trapezoidal outline with large parastyle and metastyle set low on the crown; protoloph narrow and deeply clefted on its posterior surface; lingual cingulae ascend protocone and metaconule bases on either side of the midvalley; postcingulum continuous ventrolingually to the apex of the metaconule;

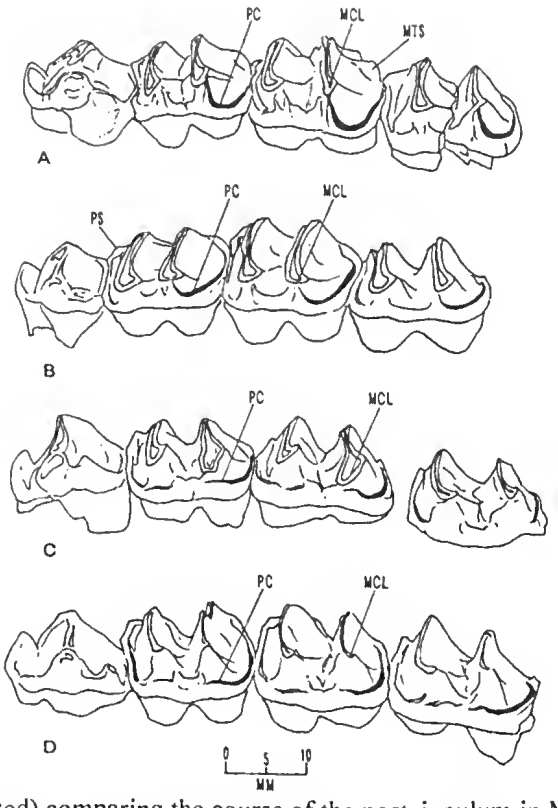

Fig. 25. Oblique views (inverted) comparing the course of the postcingulum in M^{1-3} of **A**, *Neohelos* spA (QM F30878) Cleft of Ages, Riversleigh; **B**, *Nimbadon scottorrorum* (QM F23137) Fig Tree (reversed), Riversleigh; **C**, *N. tirarensis*, (QM F13088) Inabeyance, Riversleigh; **D**, *N. tirarensis* (AR16492) Mike's Menagerie, Riversleigh (reversed). A, shows the typical condition in *Neohelos* spA in which the postcingulum ascends the lingual side of the metaconule to the apex of the cusp on M^{1-3}; in B, *Nimbadon scottorrorum*, the postcingulum ascends the side of the metaconule but fades out about half-way up to the cusp. In *N. tirarensis* examples C and D, the postcingulum courses anteriorly around the base of the metaconule in a horizontal plane.

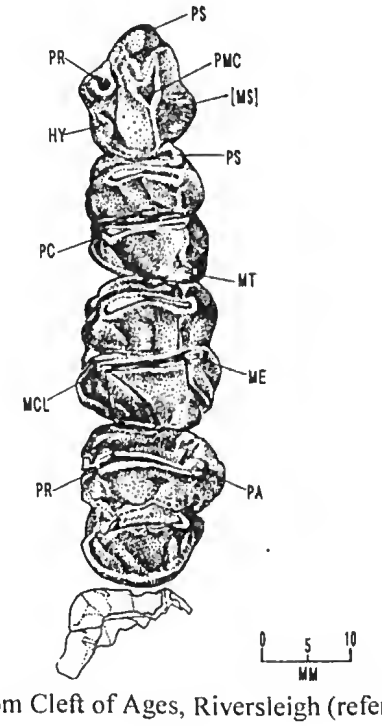

Fig. 26. *Neohelos* spA. Left P^3–M^{1-3} from Cleft of Ages, Riversleigh (reference specimen, QM F30878).

Table 7. Measurements (millimetres) of upper and lower cheek teeth of *Neohelos* spA, Cleft of Ages Site, Riversleigh Station (estimations in italics).

UPPER CHEEK TEETH (mm)

SPECIMEN	SIDE	P^3		M^1			M^2			M^3			M^4		
		L	W	L	AW	PW	L	AW	PW	L	AW	PW	L	AW	PW
AR 16957	R	—	—	16.9	13.8	14.2	—	—	—	—	—	—	—	—	—
AR 17453	R	—	—	—	—	—	17.4	15.3	14.5	—	—	—	—	—	—
AR 17454	L	—	—	16.9	13.7	13.3	—	—	—	—	—	—	—	—	—
AR 17469	L	—	—	—	—	—	—	—	—	—	—	—	19.1	16.9	13.4
AR 17470	L	14.3	13.4	—	—	—	—	—	—	—	—	—	—	—	—
QM F12433	R	—	—	—	—	—	—	—	—	—	—	—	17.6	15.0	12.0
QM F12434	L	—	—	17.1	14.0	14.0	—	—	—	—	—	—	—	—	—
QM F20488	L	—	—	—	—	—	17.6	15.8	14.5	—	—	—	—	—	—
QM F20584	R	14.8	13.4	—	—	—	—	—	—	—	—	—	—	—	—
QM F20585	L	—	—	—	—	—	17.0	15.3	14.9	—	—	—	—	—	—
QM F20831	L	—	—	—	—	—	—	—	—	18.3	16.3	14.2	—	—	—
QM F20852	R	—	—	16.8	13.1	13.1	—	—	—	—	—	—	—	—	—
QM F22765	L	—	—	—	—	—	17.0	14.5	14.0	17.5	15.0	13.5	—	—	—
QM F22765	L	—	—	—	—	—	17.1	14.7	14.3	17.8	15.2	13.8	—	—	—
QM F22767	R	—	—	—	—	—	—	—	—	17.4	15.9	13.7	—	—	—
QM F22771	R	—	—	—	—	—	—	—	—	—	—	—	17.5	14.6	11.5
QM F22773	R	14.1	12.6	—	—	—	—	—	—	—	—	—	—	—	—
QM F23195	R	—	—	17.3	14.1	14.1	—	—	—	—	—	—	—	—	—
QM F23197	R	—	—	16.7	14.0	13.9	—	—	—	—	—	—	—	—	—
QM F23274	L	14.6	12.6	—	—	—	—	—	—	—	—	—	—	—	—
QM F23407	L	—	—	16.0	13.8	14.1	—	—	—	—	—	—	—	—	—
QM F23408	R	—	—	—	—	—	—	—	—	18.1	16.1	14.2	—	—	—
QM F23472	R	—	—	16.0	13.2	13.3	—	—	—	—	—	—	—	—	—
QM F24137	L	—	—	16.8	14.5	14.8	17.5	15.9	15.0	18.7	16.0	14.0	—	—	—
QM F24270	L	—	—	16.1	14.0	13.9	17.2	15.7	14.0	17.2	15.5	13.6	—	—	—
QM F24299	R	—	—	—	—	—	17.5	15.0	14.6	—	—	—	—	—	—
QM F24731	R	—	—	15.5	12.9	12.4	—	—	—	—	—	—	—	—	—
QM F24741	L	—	—	—	—	—	—	—	—	18.3	—	14.4	—	—	—
QM F29739	R	—	—	17.7	15.0	14.7	—	—	—	—	—	—	—	—	—
QM F29740	R	—	—	16.0	13.1	13.7	—	—	—	—	—	—	—	—	—
QM F30305	L	—	—	16.7	13.9	14.0	16.9	15.5	14.3	18.1	15.3	13.7	—	—	—
QM F30556	L	—	—	15.7	13.5	13.8	—	—	—	—	—	—	—	—	—
QM F30558	R	—	—	16.9	14.3	14.2	—	—	—	—	—	—	—	—	—
QM F30734	R	15.5	13.8	—	—	—	—	—	—	—	—	—	—	—	—
QM F30878	L	14.4	12.9	15.4	12.7	13.5	16.7	14.3	15.6	17.2	15.5	13.6	—	—	—

LOWER CHEEK TEETH (mm)

SPECIMEN	SIDE	P_3		M_1			M_2			M_3			M_4		
		L	W	L	AW	PW	L	AW	PW	L	AW	PW	L	AW	PW
AR 16955	R	—	—	17.1	10.2	11.4	—	—	—	—	—	—	—	—	—
AR 16956	L	—	—	17.1	10.3	11.6	—	—	—	—	—	—	—	—	—
QM F20830	R	—	—	—	—	—	17.1	12.1	12.0	—	—	—	—	—	—
QM F12432	L	—	—	—	—	—	—	—	—	18.5	12.6	12.2	—	—	—
QM F20486	R	—	—	14.8	08.8	10.3	—	—	—	—	—	—	—	—	—
QM F20489	L	—	—	—	—	—	—	—	—	16.8	13.0	12.8	—	—	—
QM F20490	R	—	—	—	—	—	—	—	—	18.8	13.9	12.7	—	—	—
QM F20491	R	—	—	14.7	09.7	10.3	—	—	—	—	—	—	—	—	—
QM F20709	R	—	—	—	—	—	—	—	—	17.8	13.3	12.2	—	—	—
QM F20832	L	—	—	—	—	—	—	—	—	18.0	12.0	11.2	—	—	—
QM F20838	L	—	—	16.0	10.4	12.0	—	—	—	—	—	—	—	—	—
QM F22766	R	—	—	—	—	—	17.6	12.7	12.5	—	—	—	—	—	—
QM F22774	R	13.5	9.4	—	—	—	—	—	—	—	—	—	—	—	—
QM F23198	R	14.1	9.1	—	—	—	—	—	—	—	—	—	—	—	—
QM F23199	L	12.9	8.3	—	—	—	—	—	—	—	—	—	—	—	—
QM F24230	R	—	—	—	—	—	—	—	—	17.2	12.5	12.0	—	—	—
QM F24298	R	10.5	7.0	—	—	—	—	—	—	—	—	—	—	—	—
QM F24300	R	12.0	8.5	—	—	—	—	—	—	—	—	—	—	—	—
QM F24432	R	—	—	15.7	09.2	10.8	—	—	—	—	—	—	—	—	—
QM F24433	R	—	—	—	—	—	—	—	—	17.2	12.2	12.0	—	—	—
QM F24435	L	—	—	16.0	9.5	10.7	—	—	—	—	—	—	—	—	—
QM F24440	L	—	—	—	—	—	—	—	—	—	—	11.8	17.4	13.3	10.7
QM F24667	R	11.0	07.4	—	—	—	—	—	—	—	—	—	—	—	—
QM F29738	L	12.0	9.5	—	—	—	—	—	—	—	—	—	—	—	—
QM F30231	L	—	—	16.8	10.2	11.3	17.3	12.6	12.5	—	14.4	—	—	—	—
QM F30306	R	—	—	—	—	—	17.0	11.8	11.5	—	—	—	—	—	—
QM F30554	R	—	—	17.0	10.0	11.7	—	—	—	—	—	—	—	—	—
QM F30560	L	—	—	15.4	09.8	10.5	—	—	—	—	—	—	—	—	—

paracone and metacone bases expanded labially, postcingulum expanded posterolabially lengthening the crown and narrowing the interproximal contact with M^2. M^2 distinctly wider crown, protoloph much wider than in M^1; parastyle and metastyle reduced (length 16.7 mm, anterior width, 14.3, posterior width 15.5 mm). M^3 protoloph wider than metaloph; posterior margin of the crown more squared-off (length 17.2, anterior width 15.5, posterior width, 13.6). Maxillary palate flat, nearly horizontal, not conspicuously wide.

Infraorbital foramen large (9.5 x 4.5 mm), single; suborbital crest rounded with no evidence of a distinct tuberosity. With 16.5 mm of the diastema present, there is no indication of a canine alveolus.

Extended description and comparisons. *Lower incisor.* Three lower incisors (QM F69257, QM F20828, QM F30557) belonging to *Neohelos* are known from Cleft of Ages. These are similar in size and morphology to those of *N. tirarensis* (NTM P91166-7 and AR1686) having slender (12.0 mm deep) lanceolate crowns and possessing a shallow but distinct longitudinal ventrolabial groove (Figs 11, 18). As no undoubted specimens of *N. tirarensis* are known from Cleft of Ages, we have assigned these incisors to *Neohelos* spA.

Upper cheek teeth. P³. The P^3 of *Neohelos* spA is small and variable. The transverse crest from the protocone to the parametacone appears to be absent or poorly developed. The posterolabial cingulum and mesostyle also appears to be weak or absent. In QM F30734, the parastyle is represented by a tiny conical cuspule developed on an anterior cingulum, whereas in other Cleft of Ages specimens, the parastyle is well-developed, though varying from small to large-sized (Fig. 24; Table 7). The hypocone is poorly developed on the type (QM F30878) whereas it is large on QM F20584, and high and conical on QM F23274.

M¹. M^1 exhibits the diagnostic features of the species. However, all of the discriminating features are rarely present on a single specimen The most consistent character is the overall form of the crown, which is usually smaller, slightly narrower, lower, and more trapezoidal in outline, with a more elongated posterolabial corner in the region of the metastyle than in *N. tirarensis* (Fig. 26). In the majority of the specimens the postcingulum ascends the lingual side of the metaconule forming a strong vertical crest extending to the tip of the loph (Figs 25, 26). In some individuals the crest is poorly developed (QM F20852, QM F23197), but the posterior surface of the metaconule is somewhat flattened to produce a sharp posterolingual ridge. The points of the individual cusps appear sharper and more angular than in *N. tirarensis*. The protoloph is very short, with a deep posterior fossa or cleft (QM F23197). The unworn loph has a shallow V-shaped profile. The postprotocrista and postmetaconulecrista are strongly developed and sometimes sharply accentuated by thegotic facets (QM F30305). The styles are conspicuously developed. These are set slightly lower than on *N. tirarensis* and the metastyle is often distinctly conical and offset from the postcingulum by a sulcus (QM F20852, QM F23197). No examples of *N. tirarensis* M^1s appear to be present in the Cleft of Ages assemblage.

M². M^2 differs from M^1 in having a wider protoloph and weaker ascending postcingulum. There is one specimen of M^2 from Cleft of Ages that seems to resemble *N. tirarensis* more than it does *Neohelos* spA. QM F20585 lacks the characteristic *Neohelos* spA features, but also differs from typical *N. tirarensis* in having slightly more overhanging lophs and thinner loph bases. Although considerably smaller, QM F20585 closely resembles AR9925 (Mike's Menagerie) in other morphological details. QM F20488 is a rather large specimen, but otherwise resembles the type *Neohelos* spA more than *N. tirarensis*.

M^3. In M^3 the protoloph is usually wider than the metaloph and the styles are greatly reduced. *Neohelos* spA shows a stronger gradient in molar size and morphology than do some specimens of *N. tirarensis*. However, three specimens of M^3 from Cleft of Ages cannot be discriminated from *N. tirarensis* on the characteristics available (QM F24741, QM F24299, AR16810). QM F24741 is similar in size and basic form to QM F 23137 (Fig Tree) and AR17443 (Camel Sputum), lacking the ascending postcingulum and having a squared-off posterior margin. QM F24299 also lacks the ascending crest of the postcingulum and otherwise appears indistinguishable from *N. tirarensis*.

M^4. Species discrimination with M^4 is even more difficult with four equivocal specimens (AR17469, QM F23408, QM F20831, QM F2271). It is, therefore, possible that *N. tirarensis* specimens are present in the Cleft of Ages assemblage. However, given that none of the M^{1}s from the Cleft of Ages sample could be undoubtedly assigned to *N. tirarensis*, it seems more likely that these specimens of M$^{3-4}$ represent *Neohelos* spA and consequently we have assigned the entire Cleft of Ages *Neohelos* sample to the latter species.

Lower cheek teeth. P$_3$. The main cuspid of the P$_3$ of *Neohelos* spA is short with a steep convex anterior profile. The anterior crest is low and slightly sinuous, and as in the smaller *N. tirarensis* specimens, it does not terminate in a basal cuspid, cingulid or pit. The posterior crest is high and sharp with a slightly concave profile. The lingual fossa is large, bordered posterolabially by a steeply ascending cingulid that meets the posterior crest on the midline of the crown where the confluence of the structures forms a cuspid-like thickening. The labial fossa is shallow. Though sometimes smaller, there are no obvious features that distinguish these P$_3$s from those of *N. tirarensis* (Fig. 27).

M$_1$. As in the smaller specimens of *N. tirarensis*, the trigonid is elongated and narrow with a high paralophid crest (Fig. 27). In unworn specimens, the paralophid crest may be slightly thinner and higher than in *N. tirarensis*. The tips of the protolophid are curved backwards and overhang the mid valley. The hypolophid is wider and straighter than the protolophid. The hypolophid in this species may be slightly narrower in proportion to the protolophid than in *N. tirarensis* comparing AR1685-6 (D-site) with QM F30231 (COA4).

M$_{2-4}$. M$_{2-4}$ closely resemble those of *N. tirarensis*, except that they appear to be slightly narrower in proportion to their length comparing AR1685, and AR1686 (D-site) with QM F24230 (COA1) and QM F30231 (COA4). Given the known range of variation in *Neohelos* species, these proportional observations are probably not adequate for consistent differentiation of *Neohelos* spA from *N. tirarensis*.

Other Cleft of Ages specimens. Among the Cleft of Ages specimens is a zygomaturine P^3 (QM F20713) with an elongated parametacrista, incipiently divided at the tip by shallow longitudinal labial and lingual sulci, and lacking a mesostyle and labial cingulum; all apparently derived states (Fig. 28). While the incipient division of the parametacrista is considered to be an advanced condition, the state is not unique to the genus *Neohelos*, but is also present in *Kolopsoides cultridens* (Plane 1967) and *Plaisiodon centralis*. Though the size of the specimen (length, 16.0 mm; width, 13.8 mm) is within the range of *N. tirarensis*, and generally resembles the P^3 of *Neohelos* species, it shares several characters with *Plaisiodon* and *Kolopsoides*. These include the distinctive form of its hypocone which consists of a low, broad, posteriorlyinclined elevation of the posterolingual corner of the longitudinal valley, with no development of a distinct cusp. We cannot absolutely rule out

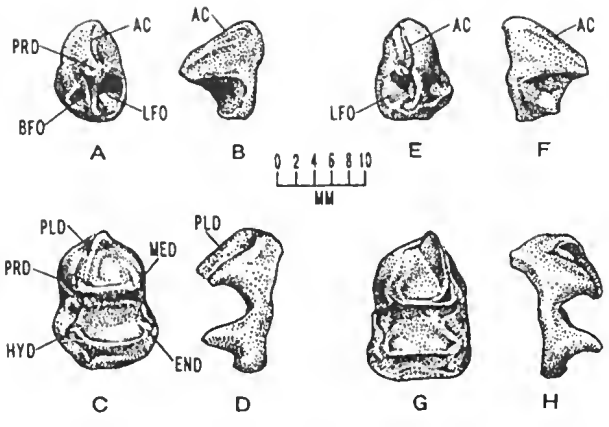

Fig. 27. Small *Neohelos* P_3–M_1 specimens; **A–B**, *N. tirarensis*, occlusal and lingual aspects of left P^3 (AR1686) from D-Site, Riversleigh; **E–F**, *Neohelos* spA occlusal and lingual aspects of right P^3 (QM F24300) Cleft of Ages, Riversleigh; **C–D**, small *N. tirarensis* occlusal and lingual aspects of left M^1 (AR1686) D-Site, Riversleigh; **G–H**, occlusal and lingual aspects of right M^1 (AR16955) Cleft of Ages, Riversleigh. In *Neohelos* spA the anterior cristid of P^3 fades into the base of the crown. The paralophid crest of M^1 is high and flange-like and the protolophid crest overhangs the interlophid valley more than in other *Neohelos* species.

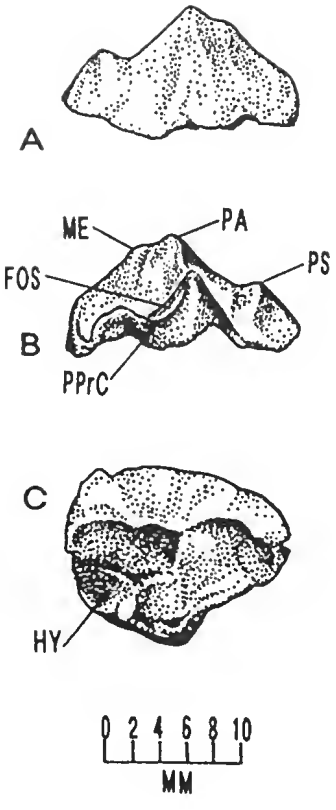

Fig. 28. Unassigned zygomaturine right P^3 crown (QM F20713) from Cleft of Ages Site, Riversleigh showing divided parametacone and parastyle connected to the paracone by a crest. This is an advanced character in zygomaturines equivalent in stage-of-evolution to that of *Plaisiodon centralis*, *Kolopsoides cultridens* or *Neohelos* spC, i.e. mid Miocene to early Pliocene.

the possibility that QM F20713 is a dP^3. However, if so, it would suggest an even more derived state of the P^3.

As in *Kolopsoides*, there is a high preparacrista which, in conjunction with the longitudinal crest of the parametacone forms a long ectoloph. A similar crest occurs in a few specimens of *Neohelos* spB but is always accompanied by a strong labial crest on the parastyle, which, as in *Plaisiodon*, is absent on QM F20713. Some *Plaisiodon* specimens also possess a low crest from the parametacone to the parastyle. While QM F20713 consists of a partially encrypted enamel cap, there is no indication along its labial margins that a labial cingulum and mesostyle were present. These features suggest that QM F20713 most likely represents a close relative of *Plaisiodon* and *Kolopsoides*. It seems to represent an advanced state of development and, therefore, provides an interesting possible stage of evolution age estimation for the Cleft of Ages material.

Neohelos spB

Reference specimen. CPC 22200 cranium with complete right and left cheek-tooth rows; parts of the right squamosal, parietal and zygomatic arch, and right and left I^{2-3} are missing (Fig. 29).

Reference specimen locality and age. Small Hills Locality, 26 km east south-east of Camfield Station Homestead on Bullock Creek, Northern Territory (approximately Latitude 17° 07' S, Longitude 131° 31'E). Tertiary limestones of the Camfield Beds are considered to be mid Miocene on the basis of stage-of-evolution biochronology as discussed below.

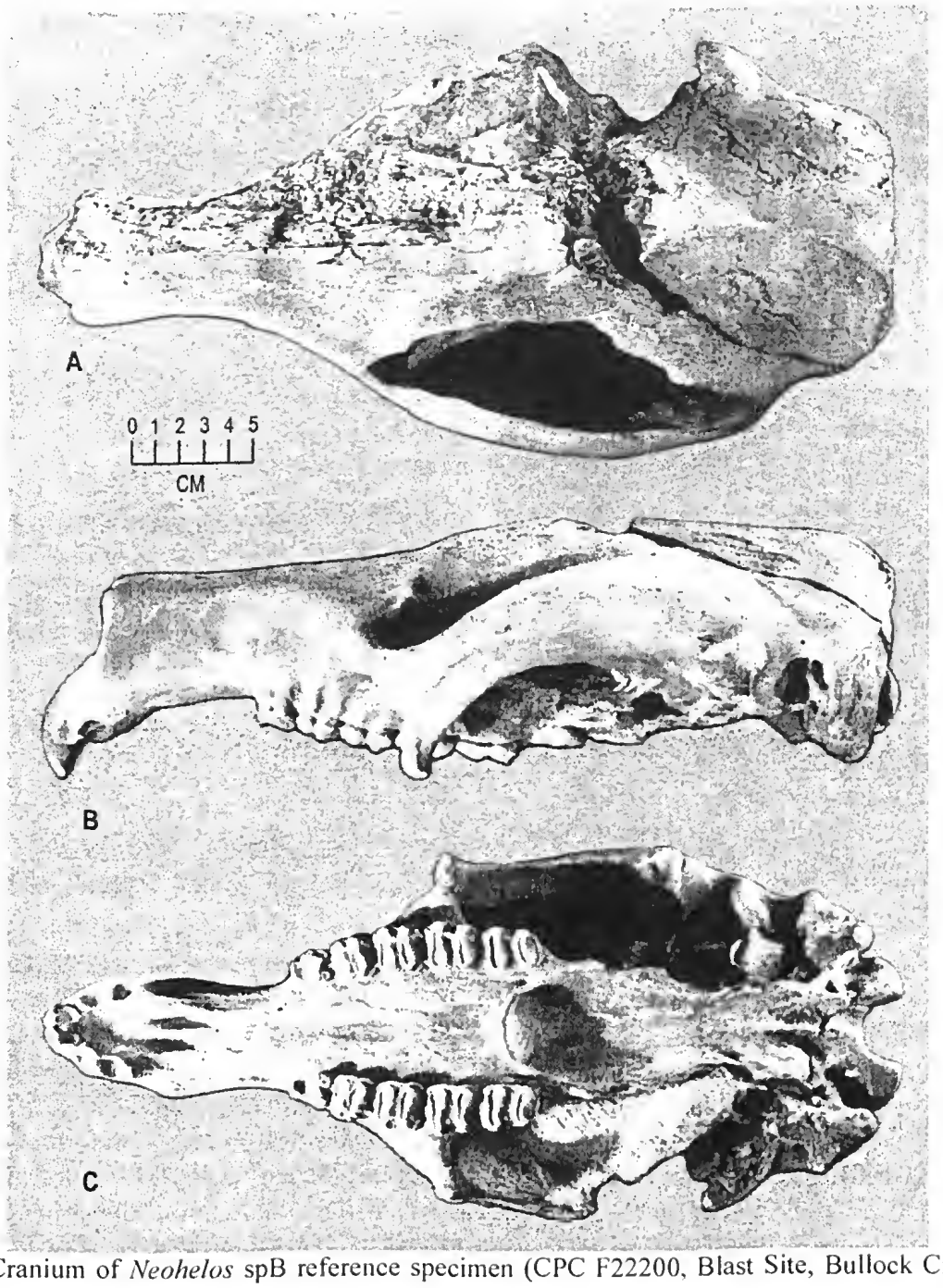

Fig. 29. Cranium of *Neohelos* spB reference specimen (CPC F22200, Blast Site, Bullock Creek); **A**, dorsal aspect; **B**, lateral aspect; **C**, ventral aspect.

Referred specimens and localities. *Neohelos* spB is known from localities in north-western Queensland and north-western Northern Territory.

Gag, Riversleigh, north-western Queensland: AR3878, right maxilla, P^3–M^{1-3}; AR 4294, maxilla, M^{1-2}.

Henk's Hollow, Riversleigh, north-western Queensland: AR5896, left P^3; AR3850, left P^3; AR7726, right P_3; AR6685, right M_3; AR13791, right dentary, M_{1-4}.

Sticky-beak, Riversleigh, north-western Queensland: AR138791, right dentary, M_{2-4}; AR13969, right dentary, P_3–M_1.

Blast Site, Bullock Creek, north-western Northern Territory: CPC 34301, left dentary, P_3–M_{1-3}; CPC 34302, left maxilla, P^3–M^{1-2}; CPC 34300, left dentary, P_3–M_{1-3}; CPC 22189, right dentary, M_{1-2}; CPC 22190, right dentary, P_3–M_{1-4}; CPC 22191, cranium with right and left P^3–M^{1-4}; CPC 22192, crushed cranium with right and left P^3–M^{1-4}; CPC 22193, right half of cranium and maxilla, P^3–M^{1-4}; CPC 22194, right and left premaxilla and maxilla, I^1, P^3; CPC 22188, anterior half of cranium, left and right P^3–M^{1-4}; CPC 22196, edentulous premaxilla; CPC 22199, right dentary, M^{1-4}; CPC 22525, braincase and latex endocast; CPC 22526, cranium with top sheared-off, right and left P^3–M^{1-4}; CPC 22529, right maxilla, M^2 CPC 22530, left dentary, P_3–M_{1-3}; CPC 22537, left dentary, P_3–M_{1-2}; CPC 22539, palate and rostrum, right and left I^1, I^3, P^3–M^{1-4}; CPC 22540, left premaxilla, I^1; CPC 22541, left dentary, M_3; CPC 22542, right dentary, M_{3-4}; CPC 22544, palate and posterior half of cranium, right M^{1-4}, left P^3–M^{1-4}; CPC 22545, right dentary, P_3 –M_{1-4}; CPC 22546, left dentary, P_3–M_{1-4}; CPC 22549, left dentary, M_{3-4}; CPC 22551, left dentary, P_3–M_{1-4}; CPC 22552, right M^1; CPC 22555, left dentary, M_{2-3}; CPC 22556, right dentary, M_{3-4}; CPC 22557, left maxilla, P^3–M^1; CPC 22987, right maxilla, P^3–M^{1-2}; NMV P179368, right dentary, P_3–M_1; NMV P179862, left dentary, P_3–M_{1-4}; NMV P187283, cranium, left and right P^3–M^{1-4}; NMV P194537, left M^3; NMV P198541, left dentary, M_3; NMV P198542, left dentary, M_{1-4}; NMV P201031, left dentary, M_{3-4}; NTM P862-1, right I^3; NTM P862-6, right dentary, M_{1-4}; NTM P862-25, right I^2; NTM P868-1, right M_4; NTM P868-2, right maxilla, P^3–M^{1-4}; NTM P869-4, right P^3; NTM P8551-13, cranium, left and right P^3–M^{3-4}; NTM P859550, left premaxilla, I^{1-2}; NTM P8610-1, left dentary, P_3–M_{1-4} NTM P8612-1, left premaxilla, I^1; NTM P8612-3, right P^3; NTM P8619-1, right dentary, M_{1-4} NTM P8645-1, left I^3; NTM P8675-1, right I^2; NTM P8689, left maxilla, P^3–M^{1-2}; NTM P8690, maxillary palate, left P^3–M^{1-2}, right P^3–M^{1-4}; NTM P86911, left I^3; NTM P8691-23, left maxilla, M^{1-2}; NTM P8694-2, right maxilla, P^3–M^{1-4}; NTM P8694-3, left maxilla, orbit, jugal, P^3–M^{1-3}; NTM P8694-43, right I^1; NTM P8695-2, right I^1; NTM P8695-2, right I^3; NTM P8695-4, right dentary, P_3–M_1,M_{3-4}; NTM P8695-38, cranium missing left zygomatic arch, left P^3–M^{1-4}, right P^3–M^4; NTM P8695-39, left maxilla, P^3–M^{1-3}; NTM P8695-41, left maxilla, P^3–M^{1-2}; NTM P8695-42, left maxilla, M^{1-3}; NTM P8695-43, right maxilla, P^3–M^{1-3}; NTM P8695-44, right maxilla, P^3–M^1; NTM P8695-45, right M^2; NTM P8695-46, right maxilla, P^3–M^{1-2}; NTM P8695-47, left premaxilla, I^1; NTM P8695-49, juvenile premaxilla, I^1; NTM P8695-51, left and right edentulous premaxillae; NTM P8695-52, left and right premaxillae, I^1; NTM P8695-53, left and right edentulous premaxillae; NTM P8695-61, right P^3; NTM P8695-63, left P^3; NTM P8695-64, right M^2; NTM P8695-67, right dentary, P_3–M_{1-4}; NTM P8695-69, right dentary, P_3–M_{1-2}; NTM P8695-70, right dentary, M_{3-4}; NTM P8695-71, left dentary, P_3–M_{1-3}; NTM P8695-72, left dentary, P_3–M_{1-4}; NTM P8695-73, left dentary, M_{3-4}; NTM P8695-74, left dentary, P_3–M_{1-4}; NTM P8695-76, right P_3; NTM P8695-78, maxilla, M^{3-4};

NTM P8695-141, left P^3; NTM P8695-211, left I_1; NTM P8695-218, right I^2; NTM P8695-221, right I^3; NTM P8695-222, left I^1; NTM P8695-223, left I^1; NTM P8695-224, left I^2; NTM P8695-225, left I^2; NTM P8695-226, left I^3; NTM P8695-269, left edentulous premaxilla; NTM P8695-286, right premaxilla, broken I^1; NTM P8695-, left scapula, left femur, left innominate, left tibia, left epipubic bone; NTM P8695a-e, three right and two left isolated petrosals; NTM P8711-9, left half of anterior part of cranium; NTM P8792-9, right I^3; NTM P8792-15, braincase and latex endocast; NTM P8792-16, edentulous left premaxilla; NTM P8792-17, left dentary, P_3–M_{1-4}; NTM P8792-18, left dentary, M_{2-4}; NTM P8792-19, cranium, left P^3–M^{1-4}, right P^3–M^{1-2}; NTM P8792-20, right M^2; NTM P9295, braincase and cranial base; NTM P87103-20, right M_2; NTM P87103- left ulna. NTM P87104-27, right premaxilla, I^1; NTM P87108-1, cranium missing rostrum, right M^{2-4}, left M^{3-4}; NTM P87108-6 left premaxilla, I^1; NTM P87108- ( ), left humerus, sacrum; NTM P87108a, right premaxilla, I^1, I^3; NTM P87110, right dentary, P_3–M_{1-3}; NTM P87111-16, left and right premaxillae, 1^3; NTM P87113-5, right I^3; NTM P87113-11, left dentary, P_3–M_{1-4}; NTM P87115, right dentary, P_3–M_{1-4}; NTM P87115-8, left maxilla, P^3–M^1; NTM P87115-16, left dentary, P_3–M_{1-4}.

Camp Quarry, Bullock Creek, north-western Northern Territory: NMV P187289, right dentary, P_3–M_{1-4}; NMV P187290, left dentary, M_{2-4}; NMV P194538, right maxilla, P^3–M^{1-3} and left P^3–M^1; NMV P194539, left dentary, M_{2-3}; NMV P194541, right M_2; NMV P197896, maxillae, left M^3 and right M^4; NMV P198543, left maxilla, P^3–M^3.

Horseshoe West, Bullock Creek, north-western Northern Territory: NMV P179244, right P_3; NMV P179369, left dentary, M_{1-2}; NMV P194364, right maxilla, P^3–M^1; NMV P194530, right maxilla, M^{2-3}; NMV P194532, left maxilla, P^3–M^{1-4}; NMV P194540, left M^3; NMV P194546, right dentary, M_{2-4}; NMV P194547, right M_4; NMV P194548, right maxilla, P^3–M^{1-2}; NMV P194549, right dentary, P_3–M_{1-3}; NMV P194551, right maxilla, P^3–M^1; NMV P194552, left maxilla, P^3–M^1; NMV P194553, left maxilla, P^3–M^1; NMV P194554, right M^1; NMV P194555, left M_3; NMV P194556, left maxilla, P^3–M^1; NMV P194557, right M_3; NMV P194558, left P^3; NMV P194565, right M^3.

Top Quarry, Bullock Creek, north-western Northern Territory: NMV P179106, left P^3; NMV P179159, right P^3; NMV P179857, left dentary, M_{2-4}; NMV P187284, right maxilla, M^{2-4}; NMV P187285, left maxilla, P^3–M^{1-4}; NMV P187286, left maxilla, M_{3-4}; NMV P187287, left maxilla, P^3–M^1; NMV P194533, right M_3; NMV P194534, left M^4; NMV P194535, right M_1; NMV P194536, right M^4; NMV P194544, right M^4; NMV P194545, right P^3; NMV P194559, left M_3; NMVP197892, cranium, left and right P^3–M^{1-4}; NMV P197893, left dentary, M_{1-4}; NMV P197894, left maxilla, M^{1-2}; NMV P197895, right maxilla, M^{2-4}; NMV P201027, right maxilla, M_{2-4}; NMV P201028, left dentary, P_3–M_1; NMV P201029, right dentary, M_4; NMV P201030, left maxilla, M^{2-4}; NMV P205129, left maxilla, M^{2-4}; NMV P205130, right maxilla, M^{2-4}; NMV P205131, right dentary, M_{2-4}; NTM P8662-9, left maxilla, M^{1-2}; NTM P8694-1, rostrum fragment; NTM P8697-1, cranium, left and right P^3–M^{1-2}.

Species diagnosis. Molars larger than *Nehelos* spA and *N. tirarensis*; P^3 parametacone cusp blade-like rather than conical or pyramidal; canine absent. Loph bases thicker and less overhanging, P^3 parametacone less acute, and anterior crest of P_3 stronger than in *Neohelos* spC.

Remarks. Some specimens of *Neohelos* spB are among the best preserved Tertiary vertebrate fossils in Australia (Figs 29, 30). Because of the completeness of the material,

we have endeavoured to provide as detailed an anatomical study of the species as seems practical within the confines of a predominantly systematic paper. Unfortunately, we have not completed the study of the manus and pes, the addition of which would have considerably improved our restoration of the skeleton (Fig. 51).

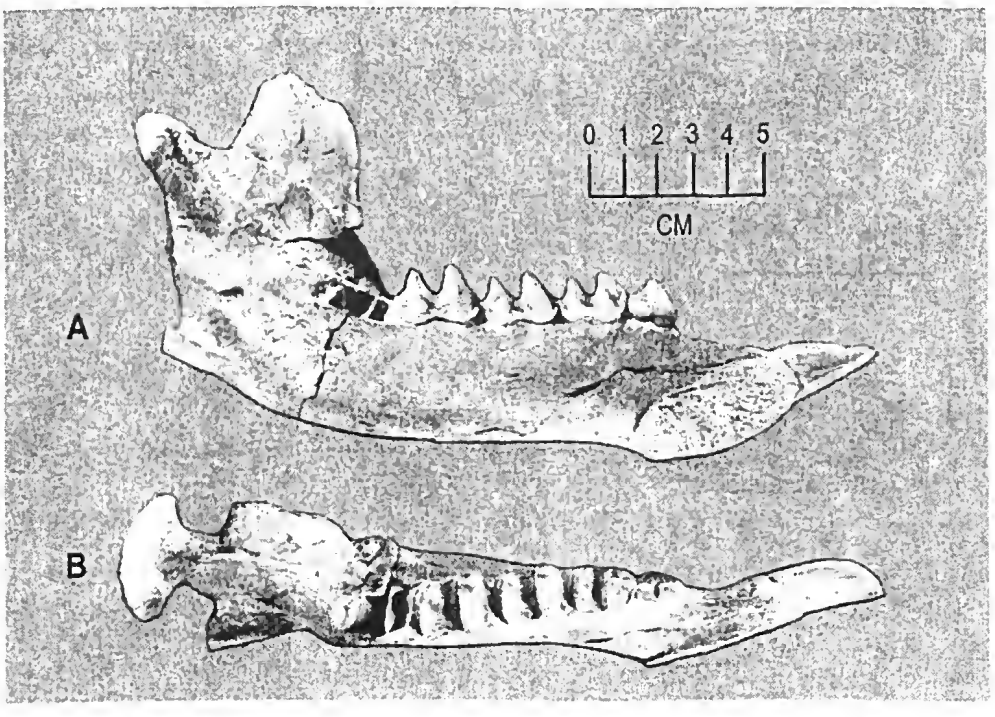

Fig. 30. *Neohelos* spB. Left juvenile dentary (CPC F23025 Blast Site, Bullock Creek); **A**, internal aspect; **B**, occlusal (dorsal) aspect.

Description. *Incisors.* The labial outline of the upper incisor series is C-shaped or U-shaped with the I^3 alveolus situated posterolateral to the I^2 alveolus (Fig. 31). The I^2 and I^3 have a horizontal wear surface while the I^1 is worn on its Posterior surface; consequently its tip extends below the occlusal plane of the other two teeth.

I¹. The I^1 was an ever-growing tooth with roots that remained open throughout most, if not all of the animal's lifetime (Fig. 32A–C). In a few highly worn examples, the apex of the root is partially closed, presumably indicative of extremely old individuals. The tip of I^1 bears a marked occlusal notch in all but the youngest specimens. Enamel is confined to the anterolateral surface of the tooth and to the distal one-fourth of the tooth in mature individuals. The mesial surface of the tooth is flat, the lateral surface concave and a section drawn midway between the tip and the root opening is D-shaped. A typical I^1 is 14.5 mm wide and 9.0 mm thick. When both first incisors are in place they converge at the tip, both emerging from the premaxilla in a ventromesial direction with a small gap between them.

I². I^2 is the least well represented of the incisors in the collection (Fig. 32D). Only one specimen of premaxilla retains an I^2 in its socket. The 13.5–13.8 mm wide I^2 crown is about a quarter to a third wider transversely than the I^3. In lateral aspect the crown is an asymmetrical trapezoidal shape with the anterior angle being acute and the posterior angle being obtuse. The pointed anterior margin of the I^2 crown slightly overlaps the posterolateral side of I^1, leaving a triangular gap between the contact and the alveolus above. The lateral surface of the crown is inscribed by one or more longitudinal grooves. The occlusal surface is lozenge-shaped with a slight lingual thickening just behind the midpoint. The entire crown has an enamel perimeter.

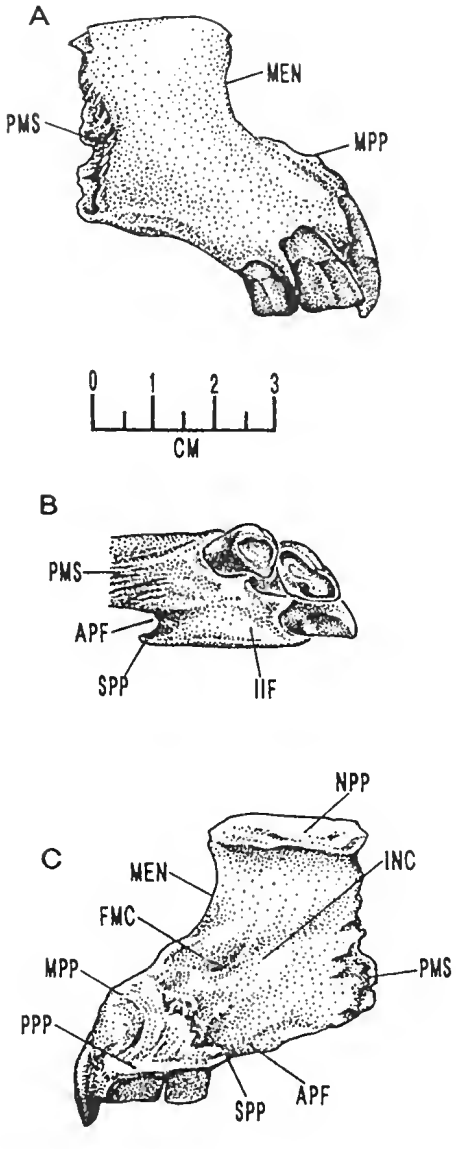

Fig. 31. **A–C**, *Neohelos* spB left premaxilla (NTM P87108-6, Blast Site, Bullock Creek); **A**, lateral aspect; **B**, ventral aspect; **C**, internal aspect.

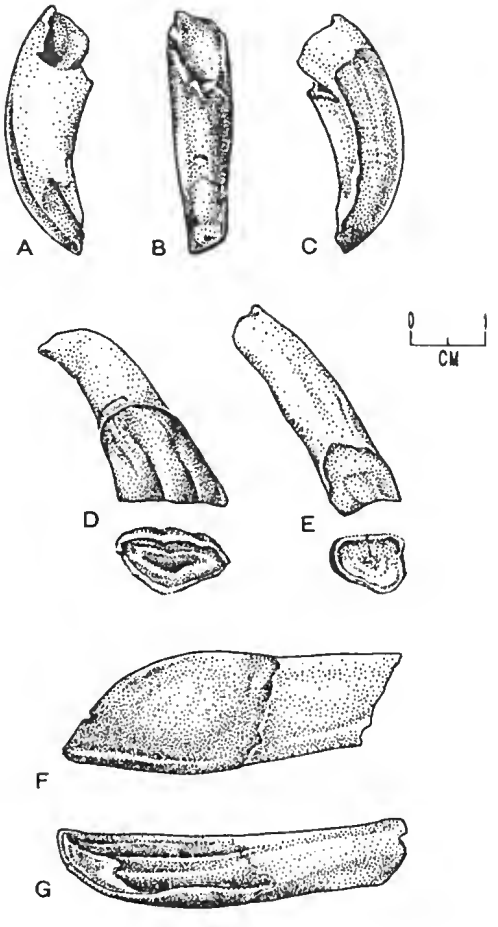

Fig. 32. *Neohelos* spB; incisors; **A–C**, mesial, distal and labial views, respectively of I^1 (NTM P8695-2 Blast Site, Bullock Creek); **D**, labial and occlusal aspects of right I^2 (NTM P862-25 Blast Site, Bullock Creek); **E**, labial and occlusal aspects of right I^3 (NTM P87113-5 Blast Site, Bullock Creek); **F–G**, labial and dorsal (occlusal) aspects of I_1 (NTM P8695-211 Blast Site, Bullock Creek).

I^3. The 9.0–10.5 mm wide I^3 crowns have an elongated triangular occlusal surface with the apex directed posterolaterally (Fig. 32E). A wide, shallow longitudinal groove divides the lateral surface of the crown into approximate halves. The crown is transversely narrow and tapers rapidly to the tip of the root. Enamel is developed on both labial and lingual surfaces and curves forward onto the anterior surface of the tooth.

I_1. The single paired lower incisors are broadly lanceolate (Figs 30A–B, 32F–G). The appression facet indicates that these incisors converge and touch only at their tips. They

curve gently upward and forward and bear enamel on the distal third of the tooth. The enamel is mainly confined to the ventrolabial surface but does curve around onto the lower third of the mesial surface near the tip. In little worn specimens, a ridge of dentine parallels the labial curve of the enamel. A deep, longitudinal groove is present on the internal dorsal surface. The ventral margin of the labial side of the crown also has a conspicuous longitudinal groove situated about 2.0 mm to 3.0 mm above a rounded enamel crest (Fig. 32F). The lower incisors occlude with all of the upper incisors meeting the posterior surface of I^1 and the horizontal occlusal surfaces of the I^{2-3}. Older individuals developed a marked occlusal notch. The root is ovate to subrectangular in cross-section, with the dorsal surface broader than the ventral. The tooth root does taper, but appears to have remained open, even in old individuals.

Upper cheek teeth. $\underline{P^3}$. The P^3 is a four-cusped tooth consisting of a protocone, parametaconc, parastyle and hypocone (Figs 9A, 33A–H; Table 8). A mesostyle is developed at the base of the parametacone. The crown is widest across the protocone, parametacone and mesostyle and tapers both anteriorly and posteriorly from this plane. The parametacone is the highest cusp and is distinctly pyramidal in shape. One plane of the pyramid is approximately labial, the anterior plane is transverse, and the posterior plane runs obliquely from the posterolabial corner of the tooth to, or just labial of, the protocone.

The protocone is conical and in unworn specimens has a transverse labial link of variable strength to the base of the parametacone. The parastyle is also conical and is lower than the parametacone and protocone. In some specimens three ridges ascend from the apex: labially, lingually and posteriorly; while in other specimens the labial and lingual ridges become cingulae. In some examples, the posterior ridge links with a ridge which ascends anteriorly from the parametacone. The hypocone is the smallest and lowest cusp, situated approximately midway between the protocone and the back of the tooth. It is conical with well-developed lingual cingulae anterior and posterior to it. In some specimens it is located slightly posterolabial to the protocone.

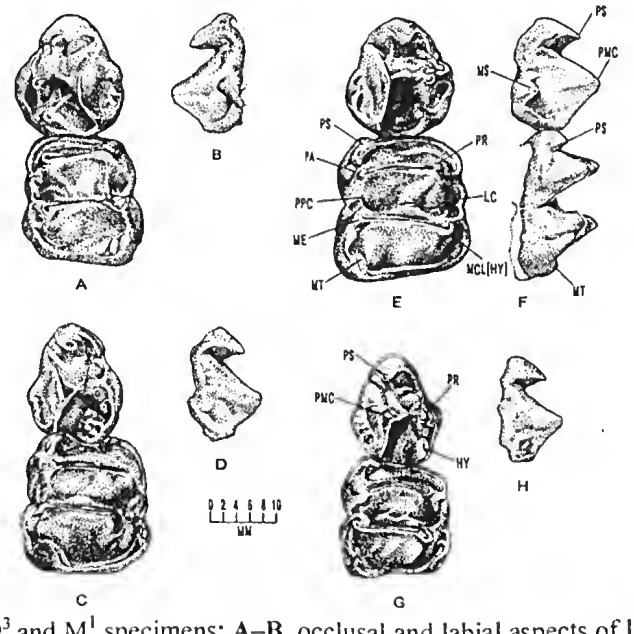

Fig. 33. *Neohelos* spB P^3 and M^1 specimens: **A–B**, occlusal and labial aspects of left P^3–M^1 (NTM P8695-41 Blast Site, Bullock Creek); **C–D**, occlusal and labial aspects of right P^3–M^1 (NTM P8695-44 Blast Site, Bullock Creek); **E–F**, occlusal and labial aspects of right P^3–M^1 (NTM P862-2 Blast Site, Bullock Creek); **G–H**, occlusal and labial aspects of right P^3–M^1 (AR3878) from the Gag Site, Riversleigh.

Table 8. Measurements (millimetres) of the upper cheek teeth of *Neohelos* spB (estimations in italics).

SPECIMEN	SITE	SIDE	P3		M1			M2			M3			M4		
			L	W	L	AW	PW	L	AW	PW	L	AW	PW	L	AW	PW
AR 3850	Gag Site	L	17.5	16.1	—	—	—	—	—	—	—	—	—	—	—	—
AR3878	Gag Site	R	17.1	14.4	17.8	15.6	16.3	20.2	18.0	18.2	22.2	21.2	18.6	—	—	—
AR4294	Gag Site	?	—	—	15.3	13.0	12.9	16.3	14.3	13.3	—	—	—	—	—	—
AR5896	Henks Hollow	R	19.2	—	—	—	—	—	—	—	—	—	—	—	—	—
CPC 22188	Blast Site	L	19.2	15.3	19.6	16.6	17.5	20.9	19.4	18.6	22.3	20.7	18.4	—	—	—
CPC 22188	Blast Site	R	19.4	15.8	18.8	16.7	17.5	21.0	19.0	19.1	22.0	20.2	18.3	—	—	—
CPC 22191	Blast Site	L	18.5	16.8	20.6	19.8	17.7	22.1	20.0	18.5	23.6	21.7	18.7	23.1	20.2	15.4
CPC 22191	Blast Site	R	17.8	17.6	19.6	18.0	17.9	21.8	20.6	19.0	24.2	21.7	19.6	23.5	20.0	15.1
CPC 22192	Blast Site	L	19.1	17.8	—	—	—	21.7	20.0	19.7	22.4	21.0	—	—	—	—
CPC 22192	Blast Site	R	—	—	20.0	—	—	21.5	—	—	22.4	—	—	22.1	—	—
CPC 22193	Blast Site	R	20.2	16.6	20.0	18.5	18.7	21.3	—	19.7	23.6	22.1	—	21.8	—	—
CPC 22200	Blast Site	L	19.4	16.3	20.4	19.4	20.2	22.1	21.9	21.5	24.4	22.3	20.5	24.2	20.0	16.9
CPC 22200	Blast Site	R	18.8	—	20.4	19.1	—	22.1	20.8	21.4	24.0	22.4	20.4	25.0	20.2	16.8
CPC 22525	Blast Site	L	—	—	—	—	—	—	—	—	23.0	—	—	23.9	—	15.9
CPC 22525	Blast Site	R	—	—	—	—	—	—	—	19.2	23.4	—	—	22.9	—	—
CPC 22526	Blast Site	L	17.9	15.5	20.5	16.3	17.6	23.0	19.6	18.7	24.6	21.0	18.6	23.8	20.1	15.0
CPC 22526	Blast Site	R	19.6	15.1	20.2	16.1	17.5	—	—	—	—	22.2	18.8	25.0	20.0	14.9
CPC 22529	Blast Site	R	—	—	19.8	18.0	17.9	—	—	—	—	—	—	—	—	—
CPC 22539	Blast Site	L	16.2	14.2	19.6	17.2	17.6	19.4	20.0	18.9	22.4	21.0	17.8	22.2	19.5	14.4
CPC 22539	Blast Site	R	18.3	15.5	19.6	17.5	17.9	21.0	19.4	—	—	—	—	—	—	—
CPC 22539	Blast Site	R	—	—	19.1	17.1	17.4	20.6	20.0	18.9	23.4	21.1	17.9	21.8	19.2	14.6
CPC 22552	Blast Site	R	—	—	—	—	—	22.7		20.6	—	—	—	—	—	—
CPC 22557	Blast Site	L	18.1	15.6	—	17.3	—	—	—	—	—	—	—	—	—	—
CPC 22987	Blast Site	R	18.0	16.8	20.5	18.6	19.6	22.1	20.7	19.9	—	21.1	—	—	—	—
CPC 34302	Blast Site	L	16.8	14.9	19.0	18.4	19.5		21.0	19.7	—	—	—	—	—	—
NMV P179106	Top Quarry	L	16.2	14.4	—	—	—	—	—	—	—	—	—	—	—	—
NMV P179159	Top Quarry	R	18.3	16.6	—	—	—	—	—	—	—	—	—	—	—	—
NMV P179159	Top Quarry	R	19.2	17.2	—	—	—	—	—	—	—	—	—	—	—	—
NMV P187283	Blast Site	L	16.2	15.4	17.4	16.4	17.0	—	—	—	—	—	—	—	—	—
NMV P187283	Blast Site	R	17.6	15.2	17.2	16.1	16.4	19.6	18.0	18.5	21.0	19.3	18.0	21.9	18.2	—
NMV P187284	Top Quarry	R	—	—	—	—	—	20.1	19.7	19.3	22.5	21.3	18.0	22.1	19.1	14.1
NMV P187285	Top Quarry	L	16.6	14.8	17.8	15.9	18.0	21.2	19.0	19.4	23.1	20.9	18.5	21.5	—	14.9
NMV P187286	Top Quarry	L	—	—	—	—	—	—	—	—	21.9	20.3	17.8	21.5	18.8	15.5
NMV P187287	Top Quarry	L	16.8	15.0	17.9	16.4	16.8	—	—	—	—	—	—	—	—	—
NMV P194364	Horseshoe W	R	18.1	16.1	18.9	18.1	19.0	—	—	—	—	—	—	—	—	—
NMV P194530	Horseshoe W	L	—	—	—	—	—	22.7	21.6	20.3	25.1	22.3	—	—	—	—
NMV P194530	Horseshoe W	R	—	—	—	—	—	22.9	21.7	19.9	—	20.7	—	—	—	—
NMV P194532	Horseshoe W	L	17.0	16.4	18.1	17.0	18.0	21.7	19.7	19.1	22.4	21.0	18.2	22.4	18.2	14.0
NMV P194534	Top Quarry	L	—	—	—	—	—	—	—	—	—	—	—	21.6	18.9	14.7
NMV P194536	Top Quarry	R	—	—	—	—	—	—	—	—	—	—	—	23.0	19.6	17.1
NMV P194537	Top Quarry	L	—	—	—	—	—	—	—	—	21.3	19.0	17.7	—	—	—
NMV P194538	Camp Quarry	L	16.4	14.7	19.0	17.1	18.5	—	—	—	—	—	—	—	—	—
NMV P194538	Camp Quarry	R	16.5	14.3	18.9	17.0	18.5	20.5	19.7	19.1	21.4	20.0	—	—	—	—
NMV P194540	Horse-shoe W	L	—	—	—	—	—	—	—	—	25.2	20.6	22.4	—	—	—
NMV P194544	Top Quarry	R	—	—	—	—	—	—	—	—	—	—	—	27.5	19.4	15.4
NMV P194545	Top Quarry	R	16.7	14.6	—	—	—	—	—	—	—	—	—	—	—	—
NMV P194548	Horseshoe W	R	—	—	19.0	17.5	17.6	20.1	18.0	18.4	—	—	—	—	—	—
NMV P194551	Horseshoe W	R	—	—	21.3	18.4	19.9	—	—	—	—	—	—	—	—	—
NMV P194552	Horseshoe W	L	—	—	19.5	16.8	17.7	—	—	—	—	—	—	—	—	—

The labial stylar cusp or mesostyle is variable in its development ranging from a small, sharp conical prominence to a larger, blunt swelling. A posterolabial cingulum is present in all specimens. The development of an anterolabial cingulum appears to be completely random. Lingual cingulae are always present between the bases of the protocone and hypocone. In most cases a posterior cingulum ascends from the posterior base of the hypocone across the back of the tooth and joins the postparametacrista or posterior shearing ridge.

Table 8 (cont). Measurements (millimetres) of the upper cheek teeth of *Neohelos* spB (estimations in italics).

SPECIMEN	SITE	SIDE	P3		M1			M2			M3			M4		
			L	W	L	AW	PW	L	AW	PW	L	AW	PW	L	AW	PW
NMV P194553	Horseshoe W	L	----	----	19.2	16.9	17.5	----	----	----	----	----	----	----	----	----
NMV P194554	Horseshoe W	R	----	----	19.1	16.5	16.5	----	----	----	----	----	----	----	----	----
NMV P194556	Horseshoe W	L	----	----	19.3	16.0	17.0	----	----	----	----	----	----	----	----	----
NMV P194558	Horseshoe W	L	17.8	15.5	----	----	----	----	----	----	----	----	----	----	----	----
NMV P194565	Horseshoe W	R	----	----	----	----	----	----	----	----	18.8	21.5	----	----	----	----
NMV P197892	Top Quarry	L	16.4	14.4	19.9	17.7	18.6	20.6	20.7	19.5	22.6	22.3	19.2	23.5	20.3	15.1
NMV P197892	Top Quarry	R	16.7	14.6	20.1	17.9	18.7	21.3	20.8	19.5	22.7	22.1	18.6	22.8	20.1	15.0
NMV P197894	Top Quarry	L	----	----	20.6	18.1	20.1	22.2	20.8	21.0	----	----	----	----	----	----
NMV P197895	Top Quarry	R	----	----	----	----	----	23.4	22.4	20.5	23.2	22.3	19.1	22.4	20.3	15.1
NMV P197896	Camp Quarry	L	----	----	----	----	----	----	----	----	23.0	20.1	17.4	----	----	----
NMV P197896	Camp Quarry	R	----	----	----	----	----	----	----	----	----	----	----	18.6	----	----
NMV P198543	Camp Quarry	L	16.7	14.8	18.6	17.9	18.8	20.9	20.2	18.2	----	----	----	----	----	----
NMV P201027	Top Quarry	R	----	----	----	----	----	20.4	21.3	19.7	22.4	22.1	18.8	22.4	20.5	15.8
NMV P201030	Top Quarry	L	----	----	----	----	----	19.4	18.4	18.0	21.1	19.4	17.5	21.1	18.7	14.8
NMV 205129	Top Quarry	L	----	----	----	----	----	18.9	19.0	17.9	21.5	20.8	----	21.2	18.9	13.8
NMV 205130	Top Quarry	R	----	----	19.2	17.9	18.2	21.0	20.3	18.4	22.5	21.0	18.1	21.2	19.6	14.8
NTM P8551-13	Blast Site	L	17.5	16.2	19.9	18.7	19.8	22.0	22.1	21.0	25.5	23.0	21.4	24.2	22.2	17.9
NTM P8551-13	Blast Site	R	17.6	16.3	19.4	18.0	18.9	21.9	20.9	19.2	24.2	20.1	19.0	24.1	20.6	15.6
NTM P8612-3	Blast Site	R	20.2	16.0	----	----	----	----	----	----	----	----	----	----	----	----
NTM P8662-9	Blast Site	L	----	----	----	----	----	20.1	----	18.0	22.3	----	----	----	----	----
NTM P868-2	Blast Site	R	18.7	16.7	21.7	19.1	20.2	21.9	20.6	21.0	22.0	20.8	20.3	----	20.5	----
NTM P8689	Blast Site	L	15.8	14.5	18.6	16.9	17.8	20.5	19.3	18.4	----	----	----	----	----	----
NTM P869-4	Blast Site	R	16.0	----	18.5	----	----	----	----	----	----	----	----	----	----	----
NTM P8690	Blast Site	L	----	----	19.0	16.1	16.9	20.5	18.9	18.4	----	----	----	----	----	----
NTM P8690	Blast Site	R	16.0	15.4	18.2	16.2	17.1	20.3	19.0	18.4	21.9	20.1	17.9	----	18.7	----
NTM P8691-23	Blast Site	L	----	----	----	----	----	20.7	----	----	22.8	----	----	----	----	----
NTM P8694-2	Blast Site	R	18.2	15.7	19.4	17.5	17.9	21.2	20.0	18.8	23.4	21.1	18.0	23.5	18.8	14.4
NTM P8694-3	Blast Site	L	18.7	----	18.4	----	----	20.2	----	----	21.6	19.3	----	----	----	----
NTM P8695-38	Blast Site	L	20.4	17.6	19.7	17.8	18.1	22.7	20.6	19.3	24.5	22.0	19.7	24.6	21.9	15.9
NTM P8695-38	Blast Site	R	19.6	16.2	----	----	----	----	----	----	----	----	----	----	----	16.2
NTM P8695-39	Blast Site	L	----	----	19.7	----	17.9	21.0	19.3	----	23.5	----	18.6	22.5	----	----
NTM P8695-40	Blast Site	L	----	----	----	----	----	----	----	----	24.0	7.0	19.0	7.0	21.0	1.0
NTM P8695-41	Blast Site	L	20.2	17.0	19.2	17.5	18.9	21.4	20.0	19.8	----	----	----	----	----	----
NTM P8695-42	Blast Site	L	----	----	----	----	----	21.6	----	----	24.0	22.0	----	----	----	----
NTM P8695-43	Blast Site	R	18.3	16.0	19.4	17.3	17.9	22.0	20.0	19.0	23.6	21.2	18.4	----	----	----
NTM P8695-44	Blast Site	R	18.7	15.3	19.8	17.0	17.9	22.1	----	----	----	----	----	----	----	----
NTM P8695-45	Blast Site	R	----	----	----	----	----	21.2	----	----	----	----	----	----	----	----
NTM P8695-46	Blast Site	R	19.2	17.0	20.9	18.5	18.6	22.2	21.3	19.8	----	----	----	----	----	----
NTM P8695-61	Blast Site	R	17.6	15.7	----	----	----	----	----	----	----	----	----	----	----	----
NTM P8695-63	Blast Site	L	18.6	15.7	----	----	----	----	----	----	----	----	----	----	----	----
NTM P8695-64	Blast Site	R	----	----	----	----	----	22.9	20.6	18.3	----	----	----	----	----	----
NTM P8695-65	Blast Site	L	----	----	----	----	----	----	----	----	----	----	----	21.3	19.3	15.6
NTM P8695-78	Blast Site	L	----	----	----	----	----	----	----	----	----	----	19.0	23.7	20.3	16.4
NTM P8697-1	Blast Site	L	17.5	15.3	20.0	----	18.3	21.8	20.3	20.1	----	----	----	----	----	----
NTM P8697-1	Blast Site	R	17.6	15.0	19.5	17.8	19.4	21.2	20.4	20.1	----	----	----	----	----	----
NTM P87108-1	Blast Site	L	----	----	----	----	----	----	----	----	23.8	23.0	21.0	22.8	21.8	17.5
NTM P87108-1	Blast Site	R	----	----	----	----	----	----	----	----	----	----	21.0	22.6	22.0	16.9
NTM P8792-19	Blast Site	L	15.1	----	19.0	19.0	19.1	21.4	19.9	19.1	23.0	21.6	19.0	22.3	----	----
NTM P8792-19	Blast Site	R	18.8	15.3	19.2	18.3	18.6	21.6	20.1	19.3	----	----	----	----	----	----
NTM P8792-20	Blast Site	R	----	----	----	----	----	20.7	18.9	18.1	----	----	----	----	----	----

M^1. The M^1 is slightly longer than it is wide in all specimens (Figs 33, 34D–E; Table 8). The transverse lophs of both moieties are slightly curved or convex towards the front of the tooth. The convexity of the lophs increase with wear, and in some specimens the depression on the posterior surface of the protoloph form well-defined circular basins in the median valley. The protoloph is transversely narrower than the metaloph and the tooth

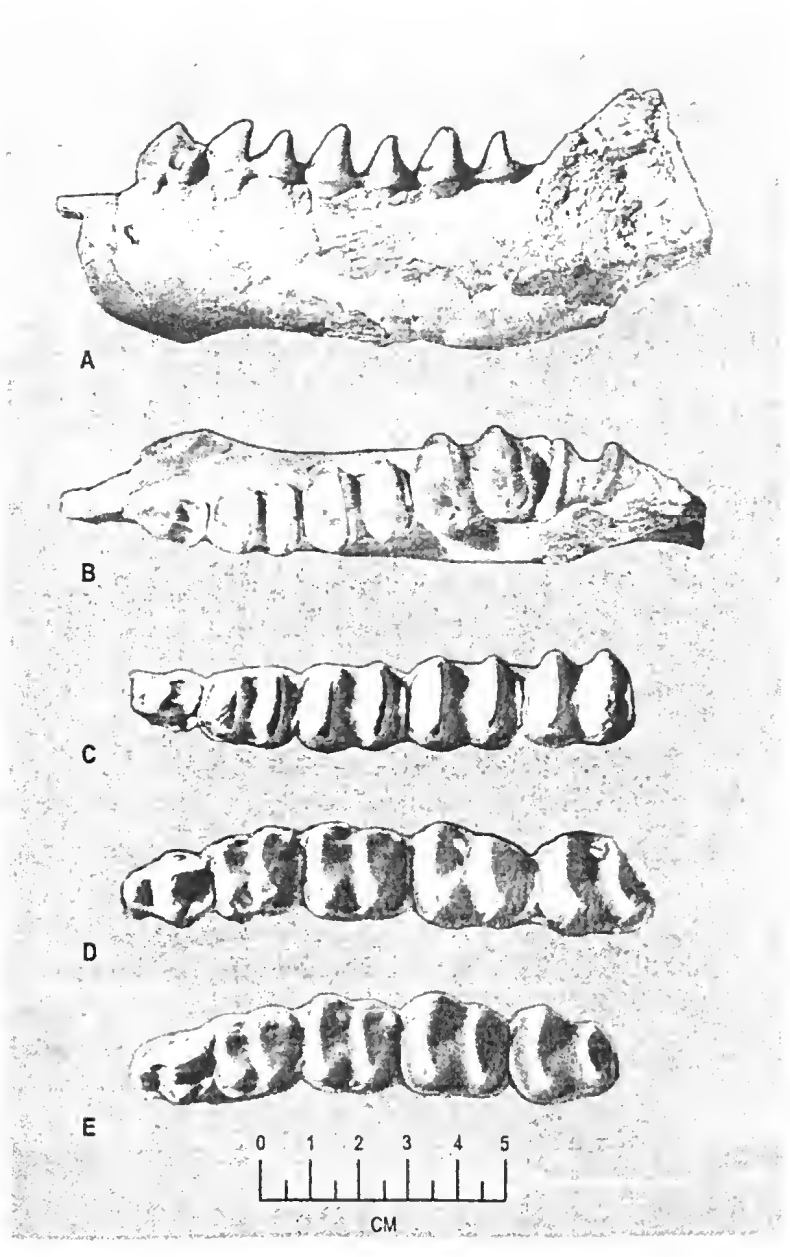

Fig. 34. *Neohelos* spB cheek tooth rows from the Blast Site, Bullock Creek: **A-B**, labial and occlusal aspects of left lower cheek teeth (CPC 22530); **C**, occlusal aspect of left lower cheek teeth (CPC 22551) **D**, occlusal aspect of left upper cheek teeth (CPC22525); **E**, occlusal aspect of left upper cheek teeth (CPC 22195).

tapers slightly towards the front. Anterior to the paracone is a strong parastyle, connected to the protoloph by a curved ridge. The parastyle also sends a ridge forward, ascending to the anterior cingulum. When viewed from the labial side of unworn specimens, the parastyle is separated from the protoloph by a deep, narrow commissure, and it is obvious that the parastyle forms a functional shear with the postparametacrista of P^1.

A small metastyle is found on the posterolabial corner of the metaloph. In most specimens it is a small cusp with an anterior and posterior ridge. The front ridge descends to the tip of the metacone while the back ridge rises in a posterolingual direction and continues across the base of the tooth to a lingual position above, and just lingual to the metaconule. In some cases a secondary cusp is found on the anterior ridge, halfway between the metastyle and the metacone. A weak link ascends from behind the paracone into the median valley

where it meets an even weaker ridge ascending forward from a point below and just lingual to the metacone on the anterior face of the metaloph. These weak crests merge just labial to the midline of the loph. A second, weak ridge ascends from the paracone to the labial edge of the median valley. At the lingual end of the transverse valley a cingulum connects the base of the protocone with the basc of the metaconule. This is a variable feature, being predominantly developed in specimens with strong ridges up onto the lingual ends of the proto- and metalophs, whereas in others, these ridges are totally absent. If the ridges are present, they are always strongest on the two anteriormost molars.

M^{2-4}. The posterior molars are generally similar to M^1. In M^2, the protoloph is slightly wider than the metaloph, the parastyle is reduced in size and does not have such well developed anterior and posterior ridges, nor does it form a functional shear plane with the posterior ridge on M^1 (Fig. 34D–E). The metastyle is considerably reduced as are the ridges in front of, and behind the metacone. In M^{3-4}, the protoloph is considerably wider than the metaloph, and in M^4 the metaloph is lingually offset, with the metaconule directly behind the protocone and the metacone considerably lingual to the paracone. In M^3 the metastyle is very small and lacks an anterior ridge, while in M^4 the metastyle is either completely missing or minute. The posterior cingulum is diminished in M^3 and often only faintly discernible in M^4.

Lower cheek teeth. P_3. The sectorial lower P_3 is oval in occlusal outline and is dominated by the large main cuspid or protoconid (Figs 34A–C, 35A–D; Table 9). The apex of the protoconid is situated in the center of the crown. In lateral aspect the anterior profile of the crown is convex and the posterior half, which forms a shearing blade, is concave. A sharp anterior blade extends to about three-quarters of the distance to the base of the crown. Anterolingually, a shallow, narrow longitudinal furrow that corresponds with a thegotic facet parallels the anterior crest, terminating inferiorly in a dimple emarginated by a short cingulid or cuspid. The posterior blade is formed by a steeply descending postprotocristid that unites with short labial and lingual basal cingulids to define a low posteromedial facet or ledge.

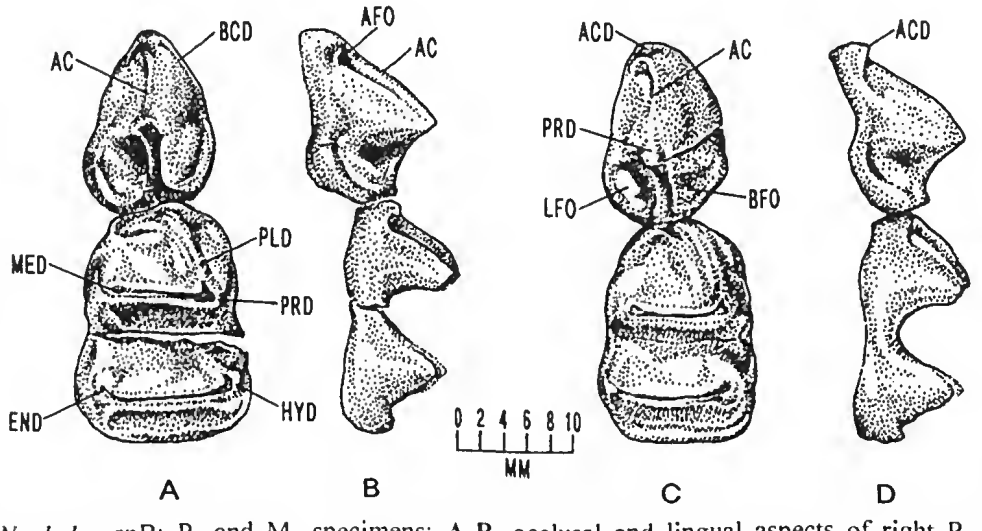

Fig. 35. *Neohelos* spB; P_3 and M_1 specimens; **A-B**, occlusal and lingual aspects of right P_3–M_1 (NTM P87103-26 Blast Site, Bullock Creek); **B**, occlusal and lingual aspects of right P_3–M_1 (NTM P8695-69 Blast Site, Bullock Creek). Note small cuspid (**ACD**) and short, low cingulid developed at the base of the anterior median cristid of P_3 in this species.

Table 9. Measurements (millimetres) of lower cheek teeth of *Neohelos* spB (estimations in italics).

SPECIMEN	SITE	SIDE	P3		M1			M2			M3			M4		
			L	W	L	AW	PW	L	AW	PW	L	AW	PW	L	AW	PW
AR13791	Sticky-beak	R	—	—	—	—	—	20.0	—	—	22.0	—	15.6	21.0	—	14.3
AR13969	Sticky-beak	R	12.5	8.6	17.3	11.6	12.2	—	—	—	—	—	—	—	—	—
AR 6685	Henks Hollow	R	—	—	—	—	—	—	—	—	22.2	16.7	16.4	—	—	—
AR 7726	Henks Hollow	R	14.0	10.5	—	—	—	—	—	—	—	—	—	—	—	—
CPC 22189	Blast Site	R	—	—	20.8	13.6	14.8	23.2	—	—	—	—	—	—	—	—
CPC 22190	Blast Site	R	14.8	10.6	19.8	15.1	15.6	22.5	17.9	—	24.4	—	—	23.1	18.5	16.0
CPC 22199	Blast Site	R	—	—	—	—	—	22.1	—	18.9	24.3	19.3	18.2	22.9	19.6	—
CPC 22530	Blast Site	L	14.6	11.6	19.1	14.3	15.8	21.9	18.3	17.0	23.9	20.1	18.0	—	—	—
CPC 22537	Blast Site	L	16.3	11.7	21.0	13.8	16.0	23.3	18.0	19.5	—	—	—	—	—	—
CPC 22541	Blast Site	L	—	—	—	—	—	—	—	—	—	—	17.4	—	—	—
CPC 22542	Blast Site	R	—	—	—	—	—	—	—	—	26.2	—	20.0	26.0	20.8	—
CPC 22545	Blast Site	R	13.1	—	8.9	—	—	20.1	—	—	22.3	—	—	22.9	—	—
CPC 22546	Blast Site	L	—	—	20.2	—	—	23.9	—	—	24.6	—	—	—	20.0	—
CPC 22549	Blast Site	L	—	—	—	—	—	—	—	—	25.1	18.9	17.4	24.9	18.5	—
CPC 22551	Blast Site	L	15.0	11.9	20.1	14.5	15.7	22.6	17.7	17.3	23.9	18.5	18.3	22.2	18.5	18.3
CPC 22555	Blast Site	L	—	—	—	—	—	22.4	—	18.0	23.8	—	—	—	—	—
CPC 22556	Blast Site	R	—	—	—	—	—	—	—	—	22.0	16.7	16.1	22.0	17.1	15.9
CPC 34301	Blast Site	L	13.8		19.7	13.3	15.6	22.1	18.1	17.3	24.4	18.8	17.8	—	—	—
CPC F34300	Blast Site	L	14.2	9.7	18.7	13.2	13.7	21.5	16.8	16.3	23.0	17.7	17.3	—	—	—
NMV P179244	Horseshoe W	R	17.9	13.0	—	—	—	—	—	—	—	—	—	—	—	—
NMV P179368	Blast Site	R	13.5	9.0	19.1	13.0	14.9	—	—	—	—	—	—	—	—	—
NMV P179369	Horseshoe W	L	—	—	19.8	12.9	14.9	21.9	16.9	—	—	—	—	—	—	—
NMV P179857	Top Quarry	L	—	—	—	—	—	21.8		17.8	24.4	19.9	18.6	25.0	20.3	—
NMV P179862	Blast Site	L	11.5	10.7	17.3	13.3	14.6	19.1	17.2	16.3	—	—	—	25.0	18.3	17.1
NMV P187289	Camp Quarry	R	13.0	9.3	17.4	12.5	14.0	19.6	16.0	15.9	22.4	18.1	17.6	22.7	—	—
NMV P187290	Camp Quarry	L	—	—	—	—	—	17.9	20.0	18.1	26.6	21.7	20.7	28.0	21.3	19.8
NMV P194533	Top Quarry	R	—	—	—	—	—	—	—	—	24.5	17.0	17.0	—	—	—
NMV P194535	Top Quarry	R	—	—	18.5	14.0	15.7	—	—	—	—	—	—	—	—	—
NMV P194539	Camp Quarry	L	—	—	—	—	—	—	—	16.5	23.9	18.8	18.7	—	—	—
NMV P194541	Blast Site	R	—	—	—	—	—	21.2	16.9	15.7	—	—	—	—	—	—
NMV P194546	Horseshoe W	R	—	—	—	—	—	—	—	—	20.8	—	16.5	23.5	—	15.5
NMV P194547	Horseshoe W	R	—	—	—	—	—	—	—	—	—	—	—	23.5	18.4	—
NMV P194549	Horseshoe W	R	—	—	19.7	14.6	16.1	22.7	18.6	12.8	24.8	19.7	18.7	—	—	—
NMV P194555	Horseshoe W	L	—	—	—	—	—	—	—	—	25.5	19.1	18.7	—	—	—
NMV P194557	Horseshoe W	R	—	—	—	—	—	—	—	—	22.3	16.7	15.9	—	—	—
NMV P194559	Top Quarry	L	—	—	—	—	—	—	—	—	23.9	18.2	16.6	—	—	—
NMV P197893	Top Quarry	L	—	—	19.9	13.7	16.4	24.2	17.7	18.2	—	—	—	—	—	—
NMV P198541	Camp Quarry	L	—	—	—	—	—	—	—	—	—	—	—	27.0	19.2	19.1
NMV P198542	Blast Site	L	—	—	21.2	13.9	15.6	23.2	17.3	17.3	25.9	19.1	19.3	—	—	—
NMV P201028	Top Quarry	L	—	—	19.8	—	—	—	—	—	—	—	—	—	—	—
NMV P201029	Top Quarry	R	—	—	—	—	—	—	—	—	—	—	—	22.5	16.3	14.8
NMV P201031	Top Quarry	L	—	—	—	—	—	—	—	—	—	—	—	23.3	17.8	14.9
NMV P205131	Top Quarry	R	—	—	—	—	—	21.7	17.3	16.9	23.5	17.8	17.2	23.5	17.7	
NTM 8695-71	Blast Site	L	—	—	22.7	16.7	18.7	—	—	19.4	25.5	21.4	19.7	—	—	—
NTM P8610-1	Blast Site	L	—	—	17.8	12.5	13.5	19.4	15.6	15.0	22.7	17.0	16.1	22.0	—	—
NTM P8612-2	Blast Site	L	14.1	10.3	—	—	—	—	—	—	—	—	—	—	—	—
NTM P8619-1	Blast Site	R	—	—	—	—	—	22.0	—	17.3	24.2	—	18.6	24.6	—	17.9
NTM P862-5	Blast Site	R	—	—	—	—	—	—	—	—	23.0	—	17.9	22.3	17.2	16.5
NTM P862-6	Blast Site	R	—	—	—	—	—	21.2	17.1	16.8	22.5	17.5	16.9	22.0	16.5	15.0
NTM P868-1	Blast Site	R	—	—	—	—	—	—	—	—	—	—	—	25.6	18.7	18.6
NTM P8695-4	Blast Site	R	14.2	10.4	18.8	13.6	14.8	—	—	—	23.3	17.6	16.4	24.2	17.7	16.3
NTM P8695-67	Blast Site	R	14.6	10.5	19.5	13.4	14.7	22.4	17.6	16.5	24.6	18.8	17.9	22.0	18.4	17.4
NTM P8695-69	Blast Site	R	16.8	11.3	20.6	13.8	15.1	21.4	17.1	16.5	—	—	—	—	—	—
NTM P8596-70	Blast Site	R	—	—	—	—	—	—	—	—	—	—	15.1	21.1	17.1	—
NTM P8695-72	Blast Site	L	—	—	18.1	12.4	13.2	21.3	16.4	15.1	24.0	17.6	16.4	23.5	17.8	15.9
NTM P8695-73	Blast Site	L	—	—	—	—	—	—	—	—	24.3	19.1	18.2	25.1	18.9	18.2
NTM P8695-74	Blast Site	L	14.7	10.7	19.7	13.7	15.0	—	—	—	—	—	—	—	—	—
NTM P8695-75	Blast Site	L	13.9	—	—	—	—	—	—	—	—	—	—	—	—	—
NTM P8695-76	Blast Site	R	15.2	10.3	—	—	—	—	—	—	—	—	—	—	—	—
NTM P87103-20	Blast Site	R	—	—	—	—	—	21.4	16.4	16.1	23.2	18.0	17.0	24.3	—	16.0
NTM P87110	Blast Site	R	14.9	10.4	20.3	14.5	15.9	22.0	18.0	17.0	23.7	19.0	17.3	—	—	—
NTM P87113-11	Blast Site	L	15.0	10.3	18.2	13.3	14.7	20.2	16.5	16.0	22.7	17.9	16.8	22.0	17.5	16.0
NTM P87115-116	Blast Site	L	15.0	10.1	20.4	14.5	16.0	23.0	18.0	17.6	24.3	19.0	17.9	24.5	18.5	16.6
NTM P87115-7	Blast Site	R	14.5	10.4	20.0	14.0	16.4	23.3	18.0	17.8	25.6	20.1	19.7	25.4	—	17.1
NTM P8792-17	Blast Site	L	—	—	19.2	—	15.6	21.7	—	—	23.6	18.0	16.9	22.7	17.2	16.5
NTM P8792-18	Blast Site	L	—	—	—	—	—	—	—	15.7	24.3	17.8	17.4	25.2	17.5	17.4

On worn specimens there is an illusion of a posteromedian cuspid, but unworn specimens demonstrate the apparent cuspid is an artefact or residual left when wear takes place on the crest that descends from the central cuspid. The posterolingual surface of the crown is a parabolic cavity extending from the apex of the protoconid down to a low, thick, obliquely-oriented lingual cingulid that emarginates a short, rounded posterolingual shelf. The labial posterior surface is also distinctly, though less concave. The posterolabial cingulid is divided by a vertical crease or furrow into posterior and anterior components. The posterior segment is longest and thickest. It ascends steeply towards the postprotocristid. The anterior segment is very short and usually less prominent. It is horizontal or may ascend towards the labial cristid of the protoconid. The posterolabial and posterolingual cingulids of P_3 terminate at the anterior margin of the posterior root in *Neohelos* spB. An anterolabial cingulid is present on some individuals.

M1. M_1 is a rectangular-crowned tooth, a little longer than it is wide (Figs 34A–C, 35A–D). The protolophid is narrower than the hypolophid. The tooth narrows to a blunt, steep interproximal face. A long, blade-like paralophid crest descends obliquely from the protoconid to a point between a third, to halfway from the labial edge of the tooth, to where it bends sharply onto the anterior cingulid. The anterior cingulid terminates at the anterolingual corner of the crown and is stronger on the lingual side of the tooth than on the labial. The paralophid crest extending from the protoconid to the anterior cingulid forms a functional shear in line with the postprotocristid of P_3. The metalophid is only weakly developed and descends anterolingually from the hypoconid.

A labial cingulid is present at the labial end of the transverse valley, and a very small cuspid on this cingulid is the origin of two slight ridges, which ascend towards the protoconid and the hypoconid. Similar ridges are present at the lingual end of the transverse valley. They meet at the base of the valley, the anterior ridge ascending towards the metaconid, but fading out approximately halfway up the lophid; while a similar ridge ascends posterodorsally towards the entoconid. A small posterior cingulid crosses the bottom of the tooth from the base of the hypoconid to the base of the entoconid. There is a slight thickening of the cingulid at the midline, and it terminates at the lingual end in a very small cuspid, only visible in lightly worn specimens. From the lingual view, the floor of the median valley is V-shaped, while in labial view it is more U-shaped.

M2-4. The M_2 is similar to M_1, as are M_{3-4}. However, the protolophid is wider than the hypolophid and the paralophid crest is short, descending only one-third the way down the crown (Fig. 34C). The lingual crests which ascend the entoconid and metaconid are weaker and do not meet in a sharp V, but rather are U-shaped, and the median valley when viewed from the lingual side is also U-shaped. M_3 is very similar to M_2 except that the protolophid is markedly wider than the hypolophid and both the protoconid and metaconid are more inflated and bulbous. A slight metalophid is apparent on unworn teeth. M_4 is similar in that the hypolophid is less wide than the protolophid, but not greatly reduced as in the metaloph of the uppermolars.

Cranium and dentary. General morphology of the cranium. Adult *Neohelos* spB crania range between 300 mm and 450 mm in condylobasal length, longer than any specimen of *Kolopsis torus* Woodburne (1967a) and smaller than, but also similar in appearance to *Plaisiodon centralis* Woodburne (1967a). The structural relations of the cranium of *Neohelos* spB are fundamentally wombat-like, though its elongated, narrow shape contrasts strongly with the dorsally flattened, rectangular crania of living wombats (Figs 29, 36; Tables 10, 11).

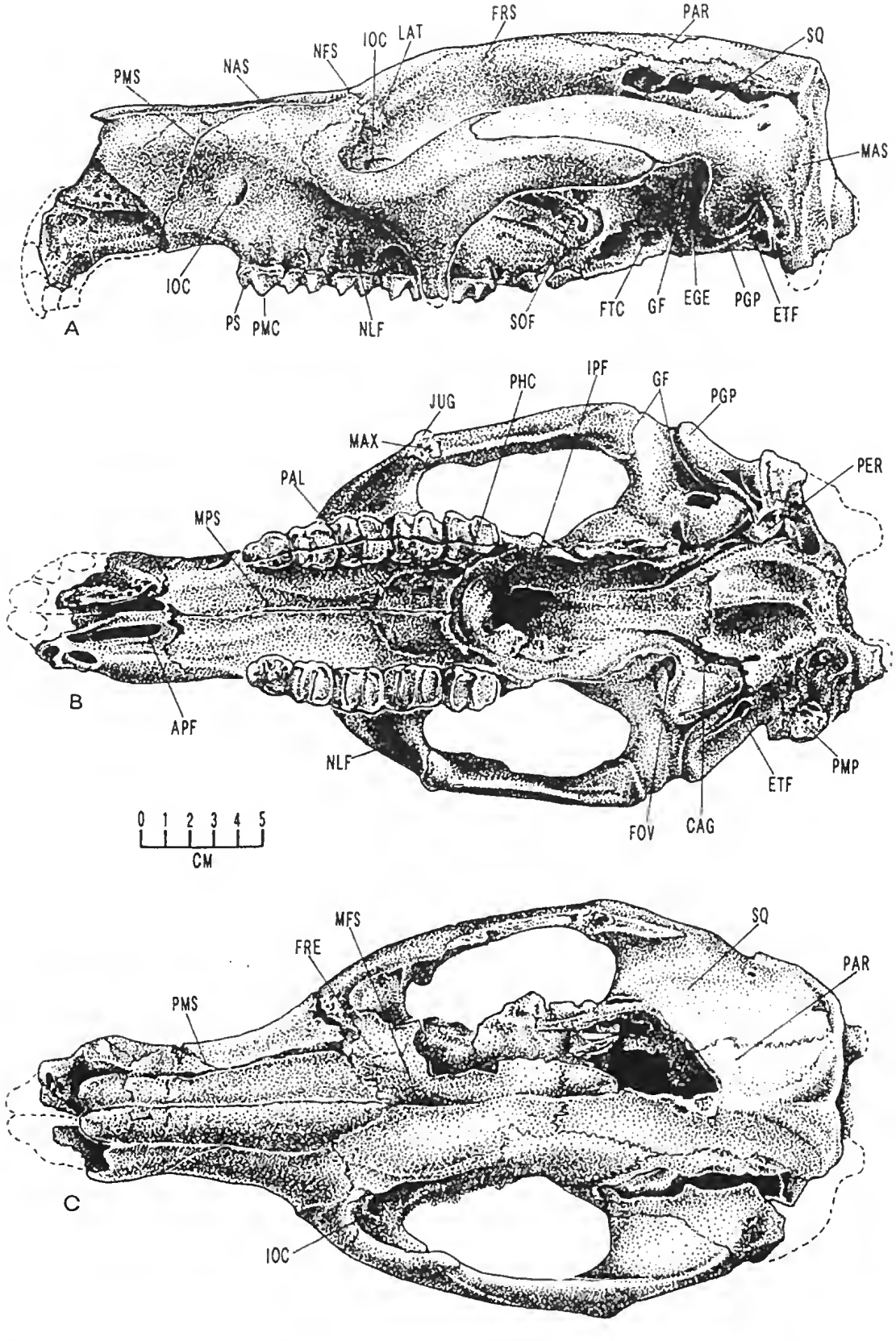

Fig. 36. Cranial anatomy of *Neohelos* spB (NTM P8551-13 Blast Site, Bullock Creek); **A**, lateral aspect; **B**, ventral aspect; **C**, dorsal aspect.

Table 10. Cranial measurements of *Neohelos* spB.

	CPC 22200	NTM P8697-1	CPC 2252	CPC22526	CPC 22192	CPC 22188	NTM P8551-13	NTM P8695-78	NTM P87108-1	NTM P8695-38
Width across masseteric processes	148	172	—	165	152	148	149		184	—
Width (minimum) between diastemal crests	17	20	—	26	21	—	25	—	—	24
Width of diastema between I^3 alveoli	23	27	—	30	22	—	24	—	—	29
Length diastema (ant. P^3 alveolus-post. I^3 alveolus)	66	65	—	72	60	67	61	—	—	84
Width of palate across posterolateral pal. for.	44	44	47	41	42	—	32	42	42	40
Length of basioccipital at midline	51	58	51	55	45	—	49	50	60	56
Length basicranium (pharyng. crest to for. magnum)	153	180	169	175	147	—	149	—	165	186
Width of glenoid fossa (entogl. pr. to lateral edge)	42	38	50	37	—	—	41	55	47	58
Length of glenoid fossa	28	22	—	27	22	—	21	22	23	23
Width between entoglenoid eminences	83	84	93	—	—	—	86	94	88	76
Length anterior palatal foramen	22	28	—	—	—	31	24	—	—	—
Width interpterygoid fossa	53	58	—	58	56	—	46	—	51	—
Length of palate (pharyngeal crest to P^3 alveolus)	176	181	—	—	170	—	166	—	—	207
Width (minimum) of rostrum at infraorbita lforamen	49	62	—	46	—	47	53	—	—	—
Length of nasals	131	129	—	—	—	118	122	—	—	152
Width across postorbital constriction	76	68	61	53	—	—	58	62	54	48
Width cranium (maximum) across zygomatic arches	182	182	—	178	—	—	175	—	207	224
Width cranium across occiput (at lambdoid crests)	128	129	156	—	136	—	127	152	143	—
Dorsal length of temporal fossa	169	184	176	137	157	—	162	183	182	207
Ventral length of temporal fossa	101	108	122	—	114	—	91	120	106	122
Width of temporal fossa	45	—	—	54	—	—	42	—	41	—
Width posterior cranium across glenoid fossa	65	72	76	—	—	—	62	80	67	83
Width rostrum at narial aperture	55	65	—	—	—	61	59	—	—	76
Width narial aperture	47	51	—	—	—	53	48	—	—	66
Height narial aperture	36	42	—	—	—	—	41	—	—	55
Height rostrum (dorsal surface nasals to I^1 alveolus)	70	86	—	—	—	—	72	—	—	100
Cranial length (maximum) condyles to I^1 alveolus	358	394	—	—	—	—	338	—	—	436
Height (maximum) of zygomatic arch	41	—	—	—	—	—	39	60	56	—
Cranial height (basioccipital suture to sagittal crest)	85	—	88	—	—	—	90	—	113	—
Length of masseteric processes (orbital margin - tip)	51	73	—	63	59	62	61	76	65	81
Projection of masseteric processes below tooth row	09	15	—	06	11	19	12	—	16	—
Occipital height (dorsal edge for. mag. – lambdoid cr.)	78	—	—	—	—	—	56	—	93	—
Diameter of orbit	30	31	—	—	—	26	31	—	35	—
Cranial length (dorsal) tip nasals – lambdoid crest	325	355	—	373	—	300	—	—	—	386
Height foramen magnum	19	—	22	—	21	—	22	25	26	—
Width foramen magnum	32	44	36	—	31	—	34	40	35	52
Height occipital condyle	34	41	40	—	34	—	34	39	35	47
Width occipital condyle	10	18	21	—	17	—	15	19	19	20
Length of cheek tooth row (P^3 to M^4)	108	107	—	108	102	—	103	—	—	110
Width of palate at hypoloph of M^2	47	46	58	50	45	47	44	—	54	48

The braincase of *Neohelos* spB is elongated, constituting over half of the total cranial length and overall, the cranium is relatively narrow transversely across the zygomatic arches (Figs 29A, 36B–C; Table 10). The cranial vault is convex in lateral profile and dome-like in the posterior aspect with prominent, inflated frontal bosses separated by a deep cleft that converge posteriorly into a low but stout sagittal crest. The broad occiput is outlined by smoothly arcing lambdoid crests. The zygomatic arches are elongated and fairly deep, flaring outward in smooth curves in dorsal aspect, whereas in ventral aspect they appear to be flat-sided and angular.

Table 11. Measurements of dentaries of *Neohelos* spB

	NTM P8695-74 / P87103-1	NTM P8695-67	NTM P8695-72	P8695-168	NTM P862-4	NTM P8695-71	NTM P 8695-4	NTM P8619-1	NTM P87112-2
Length of diastema	37	8	---	3	---	38	46	---	59
Width of jaw behind M_3	26	28	24	27	28	33	26	27	28
Transverse width of condyle	42	44	---	---	---	40	---	---	---
Anteroposterior width of condyle	13	17	---	---	---	16	15	---	---
Length from mandibular canal-postalveolar pr.	25	33	29	31	35	16	29	43	33
Length from behind condyle to edge asc. ram.	70	---	---	---	---	75	85	---	88
Depth of horizontal ramus below M_3	43	61	46	50	47	51	48	56	56
Depth horizontal ramus below M_1	45	63	45	45	47	55	48	55	54
Depth horizontal ramus at P_3	17	28	---	20	---	26	18	---	25
Distance ant. root P_3 to mental foramen	01	04	---	05	---	03	04	---	00
Length rear of symphysis to digastric process	76	114	96	91	93	111	80	100	87
Distance behind P_3 to behind condyle	186	229	---	---	---	206	201	---	220
Distance P_3 to mandibular canal	135	161	136	142	136	153	137	161	155
Distance P_3 to postalveolar process	114	134	112	117	109	138	117	125	125
Length tooth row P_3-M_4	105	107	101	102	98	111	102	103	106
Length from dorsal I_1 alveolus-behind condyle	225	280	---	---	---	246	248	---	278
Length from dorsal I_1 alveolus-postalveolar proc.	155	186	---	157	---	180	162	---	186
Length from dorsal I_1 alveolus to behind M_4	147	159	---	144	---	153	151	---	167
Length of symphysis	70	---	---	---	---	---	73	---	95

The masseteric processes are well-developed and elongated, though slender compared to *Plaisiodon* and *Zygomaturus*. The temporal fossae are large, egg-shaped vacuities, defined posteriorly by long squamosal sulci and anteriorly by the slight constrictions behind the posteriorly open orbits. The small orbits are situated about midway up the base of the rostrum. The snout is tubular, slightly flattened on the dorsal surface, gradually narrowing from anterior to the orbits to the infraorbital foramina, then gradually expanding anterior to the infraorbital foramina to flare out behind the narial opening. The floor of the narial aperture extends slightly anterior to the blunt termination of the nasal bones. The nasal bones are elongated, widest at their anterior and posterior extremities.

The cranial base is straight and only slightly elevated above the cheek-tooth row. The maxillary palate is flat, moderately expanded posteriorly and shallowly depressed in the midline. The median palatal sulcus becomes bounded on either side by sharp, parallel diastemal crests on the premaxillary palate, progressively deepening into a gutter-like interincisive fossa. In side view, the premaxillary alveolar process for the incisors is moderately to strongly decurved.

The interpterygoid fossa is a large, oval cavity that dominates the mid-region of the basicranium. Anteriorly, it is emarginated by rugose pharyngeal crests developed on the transverse palatal processes. Greater palatine fenestrae are absent. The glenoid fossae are rectangular, obliquely-oriented planoconcave surfaces bounded posteriorly by enormous, flap-like, sinus-inflated postglenoid processes and mesially by entoglenoid eminences and

bulla-like, sinus-inflated structures (Fig. 36B). The auditory arch is relatively small. The mastoidparoccipital processes are massive and sinus-inflated. The occipital condyles are large and protrude directly backwards, parallel to the basicranial axis. The lateral profile of the occiput is abruptly vertical, ascending to a low lambdoid crest dorsally and wrapping around the sides of the cranium to expose the mastoid surfaces in lateral aspect.

Braincase, cranial sinuses, endocranial casts. *Cranial walls.* The dorsal profile of the elongated braincase is a gently inclined convex surface dominated anteriorly by the large frontals and posteriorly by the long, narrow parictals. The frontal is expanded by large sinuses into a pair of smooth crests or tori, each of which are about 27 mm wide and separated by an 8 mm deep, 33 mm long median sulcus surrounded by an oval nasofrontal fossa. In lateral view, the anterior process of the frontal projects above the orbit and makes contact with the lacrimal about 15 mm behind the anterointernal rim of the orbit. The 84 mm long orbitofrontal suture passes obliquely posteroinferiorly to contact the alisphenoid. The posterior process of the frontal is wedge-shaped, dividing the squamosal and the parietal over a distance of about 50 mm (Fig. 37A). The descending posterior margin of the frontal is crescent-shaped, accommodating the low infratemporal process of the alisphenoid. The ventral border follows the dorsal margin of the infraorbital sulcus of the palatine to the orbital canal, to where it ascends up towards the lacrimal.

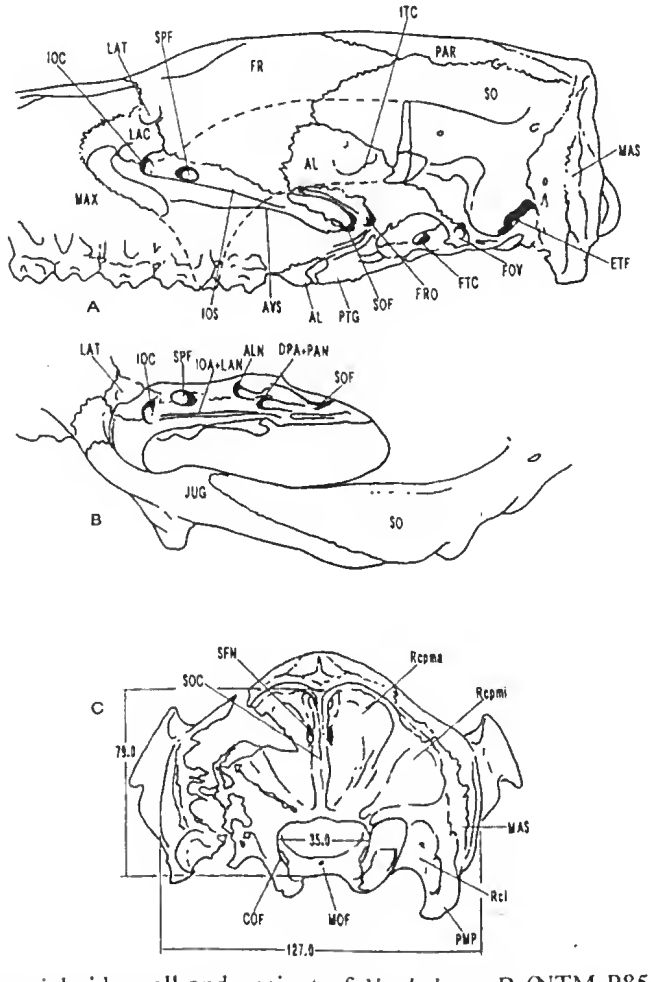

Fig. 37. Orbital fossa, cranial side wall and occiput of *Neohelos* spB (NTM P8551-13 Blast Site, Bullock Creek): **A**, lateral aspect showing structures within the orbit and lateral cranial wall; **B**, dorsolateral aspect showing structures in and around the infraorbital sulcus; **C**, occipital aspect.

The 120 mm long, narrow parietals contact the squamosal along a straight, obliquely oriented suture over a distance of 75 mm. The anterior processes terminate bluntly at the midline in a short, sinuous transverse suture line about 10 mm long. The squamosal lamina extends high up the braincase, comprising about three-fourths of the vertical extent of the lateral surface. The anterior process extends anteriorly to about the same level as the anterior process of the parietal. The squamosoalisphenoid suture parallels the parietofrontal suture, resulting in a Z-shaped sutural inscription. The anterolateral surface of the squamosal is slightly convex, steepening near the zygomatic root and deflecting inwards anteriorly to form the posterior margin of the infratemporal fossa. Continuous with the squamosal infratemporal crest is the anterior edge of a deep, wide 45 mm long squamosal sulcus that shallows posteriorly and grades into the posterolateral surface, where in combination with the parietals and interparietals, the braincase becomes widely gabled and slab-sided.

Posteriorly, the squamosal develops a low crest, the continuation of the lambdoid crest, which runs downwards to form the posterolateral margin of the auditory arch. The squamosal-mastoid contact is exposed on the lateral side of a wide, crescentic, rugose surface that grades inferiorly into the mastoid-paroccipital process. The squamosomastoid suture is highly irregular over much of its extent. Above and at the base of the zygomatic root are a pair of small foramina that lead into the vascular network associated with venous sinuses of the braincase.

Infratemporal and orbital fossae. The ascending process of the alisphenoid is poorly developed in *Neohelos* spB, the anterior margin of which terminates abruptly in an oblique, complex frontoalisphenoid suture that parallels the anteroinferior trend of the frontoparietal suture (Fig. 37A). The pillar-like descending process forms the anterior crest and dorsal half of the deep, oval pterygoid fossa posteriorly and the posterior crest of the foramen rotundum and sphenorbital fissure anteriorly. The posteroventral process of the alisphenoid extends a broad, posteriorly tapering lamina under a bulla-like structure that is situated immediately anterior to the middle ear cavity.

The squamosoalisphenoid suture follows the crest of the entoglenoid eminence (the lateral wall of the hypotympanic bulla) then ascends the wall of the infratemporal fossa at about a 45° angle, consequently bordering the inferior margin of the squamosal over a distance of about 80 mm. A 33 mm long by 17 mm wide and 11 mm deep pterygoid fossa is developed within the alisphenoid, encompassing the foramen of the transverse canal. The floor of the cavity is composed of the pterygoid. Opening posterolateral to the pterygoid fossa is the large 8.0 mm diameter foramen ovale.

The foramen rotundum is situated immediately posterolateral to the 30.5 mm long sphenorbital fissure (confluent lacerate and optic foramina). The orbitosphenoid suture is not discernible on any specimen of *Neohelos* spB. The orbital process of the palatine emerges along the anteroinferior margin of the sphenorbital fissure and continues anteriorly as a narrow strip in the base of the orbital wall, adjacent to the shelf-like extension of the maxilla, along which nerves and vessels emerging from foramen rotundum are conducted in a series of grooves. The anterior orbital process of the palatine appears to terminate at the sphenopalatine canal on the left side of NTM P8551-13 but forms part of the mesial wall of the infraorbital canal on the right side. In the type, CPC 22200, the infraorbital canal is entirely within the maxilla. The lacrimal is confined to the anteromesial corner of the orbit, extending dorsally to encompass the prominent lacrimal

tuberosity, the lacrimal foramen situated immediately anteroinferior to the tuberosity and a thumbnail-sized corner of the anterodorsal orbital margin.

The suborbital shelf is about 13 mm wide and about 25 mm deep from its dorsal margin to the molar alveoli (Fig. 37B). The dorsal surface of the shelf is inscribed with a series of narrow grooves, foramina and a wide sulcus for the infraorbital artery and nerve that passes through the large, 11 mm wide infraorbital canal. A more posteriorly positioned foramen appears to represent the posterior palatine that transmits the descending branch of the palatine artery and alveolar nerve. Lateral to the infraorbital sulcus are a pair of deep, narrow grooves that terminate in foramina at various points along the shelf. These relate to the blood supply of the alveolar region. A more medial, attenuated groove which does not terminate in a foramen probably conveyed the lacrimal nerve. The sphenopalatine canal which transmits the posterior nasal nerve, an artery and a branch of V^2, opens about 25 mm behind the infraorbital canal within the infraorbital sulcus.

Endocranial sinuses. An interesting feature of the neurocrania of the larger diprotodontid marsupials is the development of large sinuses that surround a thin inner table that actually encases the brain (Fig. 38). The extent to which these sinuses are developed appears to be partially size related, apparently as an allometric adjustment to provide additional external surface area for the attachment of the jaw muscles (Murray 1992). The neurocranial sinuses of *Neohelos* spB consist of two principle midline groups and three lateral groups. Anteriorly, the dorsolateral surfaces of the inner braincase are separated from the outer table by a series of frontal sinuses. Deep anterolateral sinuses encircle the lateral portion of the frontal lobes of the brain.

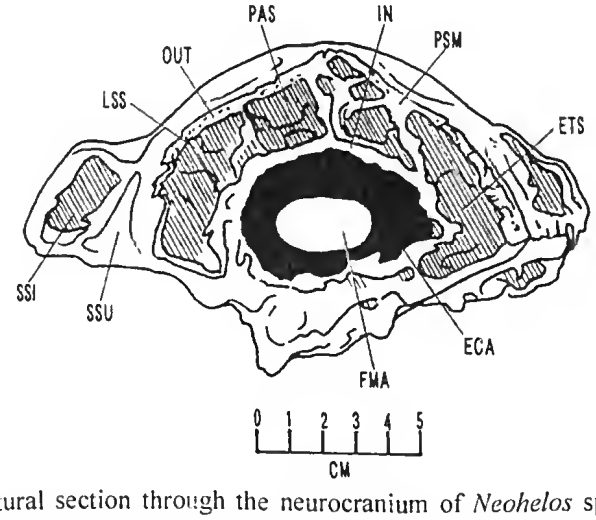

Fig. 38. Drawing of natural section through the neurocranium of *Neohelos* spB (CPC F23038 Blast Site, Bullock Creek) showing extent of endocranial sinus development (hachures) around the endocranial cavity (black).

The frontal sinus group is divided from the paired parietal sinus areas by a posteriorly curving transverse septum. The two parietal sinus groups, which are also subdivided, are separated by a short sagittal septum. The posterior parietal group is separated from the anterior parietals by a secondary transverse septum which curves in the opposite direction from the frontal septum, and in conjunction with the occipitomastoid septa, forms a large rhomboidal chamber in the posterior midline of the braincase. The squamosomastoid group form an interconnected network of chambers and passages surrounding the middle ear cavity and invading the zygomatic root. Particularly in the back of the cranium, these sinuses are closely associated with the endocranial venous circulation.

Endocranial casts. Two latex endocranial casts (Fig. 39A–B) were prepared from broken specimens (NTM P8792-15 and CPC F23038). Latex endocast CPC F23038 extends just anterior to the temporal lobes. NTM P8792-15 terminates immediately behind the frontal lobes. In dorsal aspect, the cerebellar outline is rectangular, with low, but broad oval protuberances of the parafloeculus. The cerebral cortex is broad transversely with little relief. The poles of the temporal lobes project laterally, suggesting a relatively thin neocortex. The brain is compressed dorsoventrally and roundly rectangular in transverse section immediately anterior to the temporal lobes. The endocranial surface representing the neocortex shows faint convolutions trending predominantly anteroposteriorly. In contrast to the strongly convoluted, gyrencephalic cortex of living vombatids, it is more similar to the lissencephalic Koala (*Phascolarctos cinereus*) in this respect. The frontal lobes and olfactory stalks and bulbs are not preserved on these endocasts.

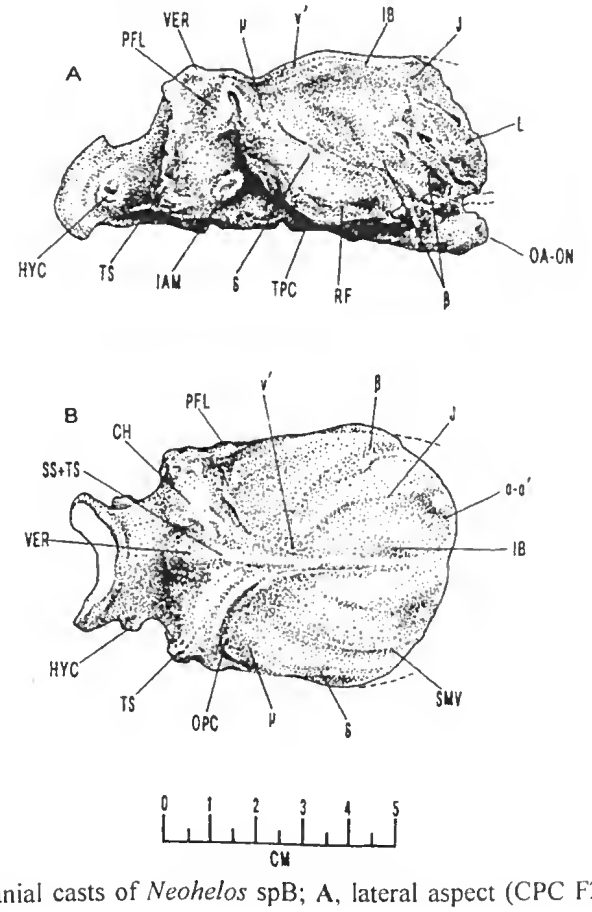

Fig. 39. Drawings of endocranial casts of *Neohelos* spB; **A**, lateral aspect (CPC F23038); **B**, dorsal aspect (NTM P8792-15).

The descriptive terminology below follows Haight and Murray (1981). The faintly visible rhinal fissure transects the lower third of the temporal lobe. Commencing dorsally from the sagittal sinus, a clearly defined interbrachial sulcus (IB) curves forward to isolate an elongated central gyrus on either side of the midline. A pair of dimples immediately anterior to the central gyri are interpreted to represent sulci α. The posterior part of the Jugular sulcus (J) is indistinctly present on both endocasts. Sulcus β for the middle cerebral artery is well defined. A short, straight sulcus L is present on CPC F23038. Sulcus δ is a shallow, rounded depression in the posterior portion of the temporal lobe and sulcus μ is represented by a smaller depression above and posterior to the former.

The morphology of these endocasts resembles that of living vombatids and phascolarctids. In basic outline shape, the resemblance is closer to that of *Vombatus* than *Phascolarctos*, while in terms of the sulcal morphology of the cerebral cortex, they are more like *Phascolarctos*. In terms of basic shape, proportions and sulcal development, the endocasts of *Neohelos* spB show a closer resemblance to *Vombatus* and to endocasts of the palorchestid *Propalorchestes novaculacephalus* than to the superficially phalangerid-like endocast of *Wynyardia bassiana* (Haight and Murray 1981).

Occipital region. The occiput of *Neohelos* spB is low and broad in posterior aspect and nearly vertical in lateral view (Fig. 37A, C). Its posterior surface is dominated by a large fossae for the attachment of the rectus capitus muscles. A median crest separates the two main surfaces, both of which are perforated by the supraoccipital emissary foramina. A small, shallow supracondylar fossa is present, in contrast with palorchestids, for example, in which the structure is large. The condylar sulcus is wide and deep, grading into a distinct lunate depression on the medial surface of the paroccipital process. This fossa may correspond to the insertion of the rectus capitus lateralis muscle. The occipital condyles are large and prominent but narrow transversely relative to their length. The foramen magnum is rectangular in shape and wider (35.0 mm) than high (23.5 mm). Large hypoglossal foramina are just visible in posterior aspect within the lateral walls of the foramen magnum.

A small median foramen opens posteriorly in the floor of the basioccipital. The paroccipital processes are stout, rectangular structures which have a mastoid contribution on the lateral side. The paroccipital-supraoccipital suture appears to course obliquely across the occiput from the median dorsal margin of the foramen magnum to converge dorsolaterally with the superior termination of the interposed mastoid bone. The external squamosomastoid suture is difficult to trace, but the anterior suture does not appear to contact the lambdoidsquamosal crest, and although it is fairly broad inferiorly, it remains confined to the lateral side of the occiput.

Basicranium and middle ear region. <u>*Tympanic cavity.*</u> The ear region of *Neohelos* spB is basically similar to that of *Ngapakaldia* Stirton, 1967b, and to that of the mid Miocene palorchestid *Propalorchestes* Murray, 1986. The relations of the auditory region of the basicranium include the glenoid fossa laterally, the roof of the middle ear cavity dorsally, the mastoid region posteriorly and the basioccipital and basisphenoid mesially (Fig. 40). Anteriorly the pterygoid and alisphenoid bones predominate. The floor of the middle ear cavity in *Neohelos* spB is open except for a small lobate process of the basioccipital.

The anterior wall of the tympanic cavity is represented by a shallow fossa in the posterior wall of the large hypotympanic swelling or bulla developed in the squamosal. The bulla is floored by a posteroventral process of the alisphenoid, which extends a few millimetres under the tympanic cavity as a short tympanic wing. A slightly concave or flattened lateral surface of the petrosal contributes the posteromesial wall of the cavity and a small, isosceles triangle-shaped process, the tegmen tympani, forms part of its roof (Fig. 41C). The tegmen is recessed with a 3.0 mm diameter fossa or attic accommodating the auditory ossicles; behind which a smaller, lower fossa accommodates the posterior ligament of the incus. A short (~5.0 mm) low tympanic crest defines the mesial end of a long, funnel-like acoustic arch which is breached dorsally by a slit-like (20 mm x 5 mm) epitympanic fenestra.

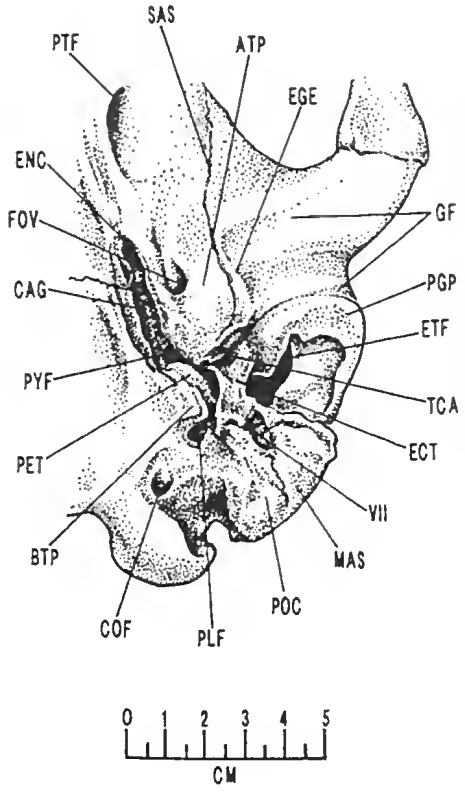

Fig. 40. Ventral aspect of left basicranial quadrant of cranium of *Neohelos* spB (CPC F23038 Blast Site, Bullock Creek).

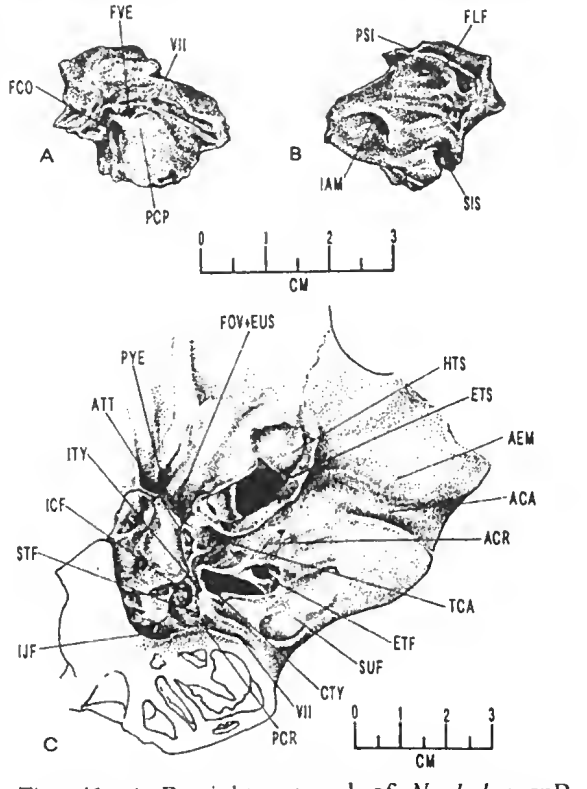

Fig. 41. **A–B**, right petrosal of *Neohelos* spB. (NTM P8695-78 Blast Site, Bullock Creek); **C**, ventral aspect of left basicranial aspect of cranium of *Neohelos stirtoni* showing structures surrounding the middle ear region revealed by missing ectotympanic and basioccipital tympanic process (NTM P8792-15 Blast Site, Bullock Creek).

The epitympanic recess is very confined mesially. The incisura tympanica is a narrow groove between the tegmen of the petrosal and the crista tympanica of the squamosal. Anterolaterally the incisura meets a perpendicular groove for the attachment of the anterior crus of the ectotympanic. The lightly attached ectotympanics (Fig. 40), which are usually missing, have remained in place in one specimen (CPC F22525). The ectotympanics are transversely narrow, 6.0 mm wide and 15.5 mm long anteroposteriorly, under the acoustic arch. The ventral surface of the ectotympanics are slightly arched, resembling small bridges. The internal contour of the bony meatus is an elliptical orifice about 8 mm high by 5 mm across. The posterior crus of the ectotympanic sends out a blunt dorsolateral process that surrounds the otherwise open groove for the facial nerve, to form a stylomastoid foramen.

Petrosal. In specimens lacking the ectotympanics, the ventrolateral aspect of the petrosal is fully visible (Fig. 41). The pars petrosus is a short, oval or even slightly cube-shaped structure approximately ~12 mm wide by ~15 mm long (Fig. 41A–C). The ventral surface is rugose, the pars cochlearis being nearly flat, bulging posteroventrally at the promontory. The superior periotic process is blunt, often terminating in an irregular pit. The cochlear fenestra opens posteroventrally towards the stapedial fossa of the posterior tympanic recess. The fenestra is elliptical, ~2.6 mm by ~1.6 mm, and is set in a smooth-walled

fossula. The cochlear fenestra is separated from the smaller ~1.5 mm by ~1.8 mm vestibular fenestra by a 2.0 mm rounded crest. In anatomical position, the vestibular fenestra, which opens posterolaterally towards the acoustic arch, is situated anterodorsal to the cochlear fenestra.

Dorsolateral to the vestibular fenestra, a shallow groove descends posteriorly to merge with a deep perpendicular groove in the anterior surface of the mastoid, which is the previously mentioned facial nerve sulcus. Immediately below this sulcus is a shallower, more irregular groove for the posterior crus of the ectotympanic. The facial groove continues anteriorly from above the vestibular fenestra for about 5 mm where it opens into the facial nerve foramen, which is up to about 2.0 mm by 1.5 mm in some specimens of *Neohelos* spB. In some specimens the groove continues anteriorly from the foramen parallel to the anterior periotic process, whereas in others a small canal leads anteriorly from the foramen to transmit the chorda tympani branch of the facial nerve.

The internal side of the periotic is divided by a low crest (prominence of the anterior and posterior semicircular canals) into two fossae: dorsally, a shallow floccular fossa and ventrally an approximately 6 mm diameter internal acoustic meatus with a slot-like fundus about 4 mm deep. A crista transversa between the facial and vestibulocochlear nerves is not visible on any of the specimens, but two channels can be visualised in the figure-eight-like recess, dorsally for the facial nerve and ventrally for the cochlear nerve.

Epitympanic fenestrae and glenoid processes. In *Neohelos* spB, the epitympanic fenestra is usually an oblique slit-like opening that extends from the tympanic crest, through the roof of the auditory arch to invade the base of the postglenoid process (Figs 29C, 36B, 40, 41C). Its shape and size is variable in the species. Located under the posterior margin of the fenestra is the postglenoid canal which is usually a large circular opening. Superolateral to the epitympanic fenestrae are variable fossae composed of merged circular depressions that occupy the dorsal surface of the superficies meatus and the posterior margins of the postglenoid processes. In some *Neohelos* spB specimens the posterior end of the fossa opens into the mastoid region to form a posterior epitympanic fossa. The postglenoid process is developed from an extensive swelling (a lateral or postglenoid hypotympanic sinus) about 50 mm long and 16 mm wide that extends from the tympanic crest to the lateral margin of the squamosal.

Mesially, the internal side of the base of the postglenoid process is separated from the posterior wall of the entoglenoid surface of the bulla by a 12 mm deep, 3 mm–6 mm wide, 32 mm long glenoid incisura. The glenoid incisura leads directly into the tympanic cavity and along its ventral margin are the roughenings for the attachment of the anterior crus of the ectotympanic. Anteriorly, the cleft opens into the mesial side of the 10 mm wide, 32 mm long transverse articular groove of the glenoid fossa, anterior to which is a flat, 40 mm wide by 20 long (anteroposteriorly) articular eminence that extends onto the ventral surface of the jugal.

Entoglenoid eminences and bullae. The base of the 26 mm by 32 mm bulla-like hypotympanic swelling which is continuous with a 20 mm wide, 16 mm deep entoglenoid eminence laterally and the anterior wall of the tympanic cavity posteriorly, is composed of the squamosal. Its ventral surface is sealed off by a V-shaped process of the alisphenoid which has the appearance of having folded itself around the structure (Figs 29C, 36B, 40). On the ventral anterolateral corner of the bulla, the alisphenoidsquamosal suture remains open, possibly for the transmission of the chorda tympani nerve. The course of the

alisphenoid-squamosal suture can be traced around the tympanic process where, on the anteromesial corner of the bulla, it forms an arch under the large 7.0 mm by 8.0 mm diameter foramen ovale, in combination with the posterior process of the pterygoid crest.

Basicranial structures. Anterolateral to the blunt, hollowed out superior periotic process of the petrosal, a deep irregular cavity, the pyriform fenestra, is composed of the middle lacerate foramen, the posterior end of the internal carotid groove, the mesial wall of the hypotympanic bulla and bounded laterally by a thin process of the squamosal. The 4 mm deep entocarotid groove extends some 25 mm along the lateral margins of the basioccipital and basisphenoid. The foramen for the internal branch of the internal carotid artery opens about 15 mm anterior to the basisphenoid-basioccipital suture in the lateral edge of the basisphenoid.

The basisphenoid-basioccipital suture lies 48 mm anterior to the foramen magnum. The basioccipital is broad, particularly where it is extended laterally to send a small process under the petrosal and tympanic cavity. The basisphenoid narrows within the interpterygoid fossa, extending anteriorly about 45 mm to meet the presphenoid along a clearly defined chevron-shaped suture. The pterygoid crests in *Neohelos* spB are low, thick laminae that form the floors of the deep, oval pterygoid fossae, perforated centrally by large transverse canal foramina. The crests deepen ventrally and widen laterally to form the walls of the pharyngeal cavity. The internal nares is a 34 mm deep, oval opening with smooth, steep walls laterally, bounded by a prominent, curving transverse palatine crest ventrally. Dorsally within the 60 mm long, 45 mm wide 35 mm deep interpterygoid fossa, the ventral surfaces of the basisphenoid and presphenoid are widely exposed.

Facial cranium. Palate. The posterior margin of the palatine bones are formed by high, posteriorly swept transverse palatine crests which blend into the pterygoids (Fig. 36B). Anterolaterally, the crests are deep, V-shaped clefts on either side, dorsomedial to the M^4 alveolus, into which open the orifices of the posterolateral palatine foramina. The palatine processes are devoid of greater palatal fenestrae. The maxillopalatine suture courses parallel to the molar alveoli for about 40 mm then turns mesially to meet in the palatal midline, level with interproximal M^{2-3}. The palatal surface is flat with a shallow median sulcus commencing at about the level of the posterior end of M^1. This furrow deepens as it continues onto the 60–65 mm long by 20–25 mm wide diastemal palate where its edges become more crisply delineated by low diastemal crests.

The straight, parallel diastemal crests become sharper and higher lateral to the anterior palatal fenestrae, the latter being encompassed by a deep, gutter-like interincisive fossa. The 23 mm long by 7 mm wide anterior palatal fenestrae are separated by a high, rounded premaxillary septal process. The overall proportion of the cheek-tooth bearing palate is a 2:1 rectangle. The diastemal palate narrows to about two-thirds of the width of the cheek-tooth palate, and constitutes slightly less than half of the total palatal length. The incisive arcade is U-shaped and expands laterally behind the I^3 alveoli to about twice the width of the diastema. The premaxillomaxillary suture commences in the midline immediately behind the premaxillary septal process. The suture courses anteriorly on the lateral palatal surface to about 20 mm behind the I^3, then runs posteriorly at an acute angle to the mesial suture line to form a narrow V. The suture then makes a nearly vertical ascent of the lateral side of the rostrum about midway between the I^3 and the P^3.

Rostrum. The tubular rostrum comprises about one-third of the total length of the cranium of *Neohelos* spB. The nasals are elongated. The proximal surface is gently arched and

widest immediately above the orbits, where the tapering frontal processes terminate at the anterior edge of the median frontal fossa. The nasals contract to their minimum width (10–15 mm) at the level of the infraorbital foramen, then expand laterally again to their maximum anterior width just behind the margin of the narial aperture (15–18 mm) and maximum posterior width of 20 to 24 mm. The nasals terminate in blunt, slightly rounded margins above the level of I^3.

The narial aperture is a large, transversely oval opening, 45 mm to 65 mm wide, with smooth, thick premaxillary lateral margins that thin dorsally to agree with the lateral margins of the nasal bones (Fig. 42A–B). The floor of the narial aperture is divided by a deep, wide trough through which the anterior palatine fenestrae open directly into the nasal cavity. The inferolateral margins of the nares are produced into wide, shelf-like processes, the inferior nasal crests, each of which bears a large oval sulcus that accommodated the anterior portion of the middle concha of the turbinate bones (Fig. 31C). Bending forces on the anterior premaxillary processes, which support the incisor roots, appear to have been distributed through the floor of the narial aperture via the robust inferior nasal crests. The superior crest or process of the premaxilla is a variable triangular to rhomboidal protuberance representing the anterior-most prominence of the cranium. This low protuberance is sometimes perforated by small foramina and appears to have supported a dense connective tissue mass possibly serving as the median attachment for a large mobile upper lip and / or the lower portion of a large rhinarium.

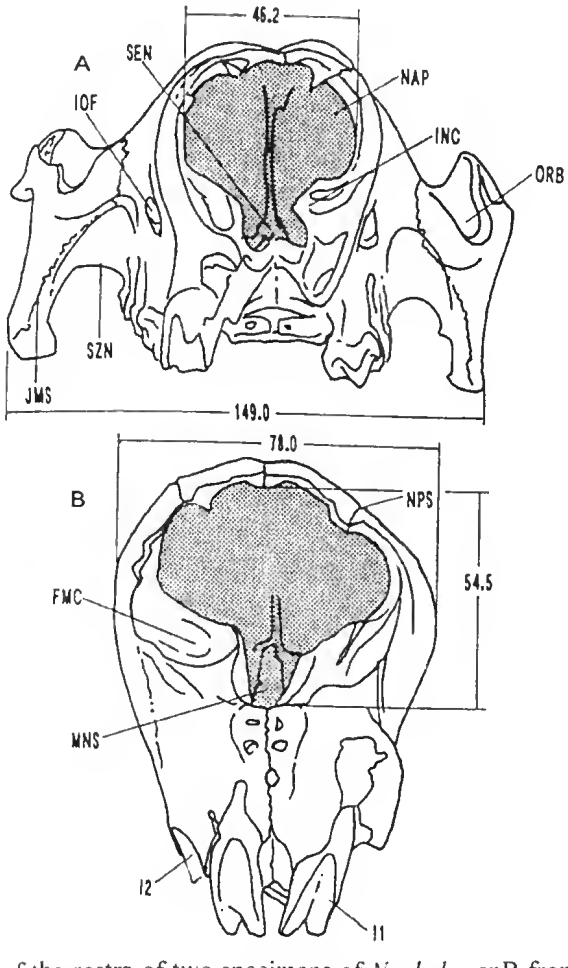

Fig. 42. Anterior views of the rostra of two specimens of *Neohelos* spB from the Blast Site, Bullock Creek; **A**, NTM P8551-13; **B**, NTM P8695-38. Note differences in the size and shape of the narial apertures.

Small nasopremaxillary notches are present on the dorsolateral margin of the nares. This area is vascularized via a foramen that emerges from within the internal nasal crests. The lateral aspect of the rostrum is dominated by the broad maxilla. The maxilla is divided from the premaxilla by an initially nearly vertical suture that commences in lateral aspect behind the mid point of the diastema. About two-thirds of the way to the nasals, the suture sharply bends posteriorly in a shallow arc to terminate dorsally about midway along the span of the nasals. A large infraorbital foramen opens in the lower half of the maxilla about 26 mm posterior to the premaxillomaxillary suture.

Orbit and zygomatic arch. Anterior to the infraorbital foramen is a shallow, approximately 20 mm by 30 mm fossa, above Which there is a distinct, rounded facial crest that flows posteriorly into the orbital margin. Anterodorsal to the orbital margins, the maxilla becomes slightly inflated and attains its greatest breadth at the root of the jugal. The maxillojugal suture follows the anterior contour of the rounded anterolaterally protruding orbital margin down to the masseteric process which is neatly formed by approximately equal contributions of both the maxilla and the jugal. The subzygomatic notch between the cheek-tooth alveolus and the masseteric process is 32 mm deep and 17 mm wide. Immediately below the orbital margin is a 35 mm by 20 mm maxillolabial fossa.

The orbit is small, about 27 mm to 30 mm wide, set off posteriorly by a low, thin, postorbital process of the jugal. A prominent lacrimal tubercle is located on the dorsomedial orbital wall. There are no distinct postorbital processes of the frontal. A deep masseteric sulcus and crest is confined to the lower half of the entire length of the jugal. The zygomatic process of the jugal is long and relatively deep posteriorly, tapering anteriorly to a rounded process that fits into the corresponding notch in the postorbital process of the jugal. The jugal-squamosal suture is nearly straight and relatively long, about half the total length of either zygomatic process. The maximum width of the cranium of *Neohelos* is across the lateral glenoid eminences of the jugals. In lateral profile, the glenoid fossa forms a right angle notch in the lower squamosal root, bounded posteriorly by a massive postglenoid process. The auditory arch is an inverted U or V-shaped notch.

Dentary. The dentary is long with a slender horizontal ramus (Figs 30A, B, 43A–C; Table 11). The body of the dentary usually tapers anteriorly from the inferior coronoid crest to the level of P_3. The longitudinal axis of the horizontal ramus is fairly straight. In lateral aspect, the inferior border of the dentary is sinuous and the alveolar border is nearly straight to slightly concave. A weak digastric eminence is invariably present. The horizontal ramus is strongly convex in section just anterior to the ascending ramus, after which it becomes much flatter in section. The diastemal crest is short and sharp on its superior margin. The mental foramen is situated immediately anteroinferior to the anterior root P_3. The lower incisor is procumbent. The long, shallow symphysis is oval to trapezoidal in outline and remains unankylosed throughout the animal's lifetime. Deep round or oval genial pits are present. A small posterior mental foramen is present in the middle of the horizontal ramus at about the level of interproximal M_{2-3}. A distinct mid-ramal torus extends a short distance forward from the base of the coronoid crest.

The ascending ramus comprises one-third to one-quarter of the total length of the dentary. The coronoid process is high and blade-like with a blunt, transversely wide tip. The coronoid notch is short and shallow. The condyle is situated high above the occlusal line of the cheek teeth. The posterior edge of the ascending ramus is constricted at the neck of the

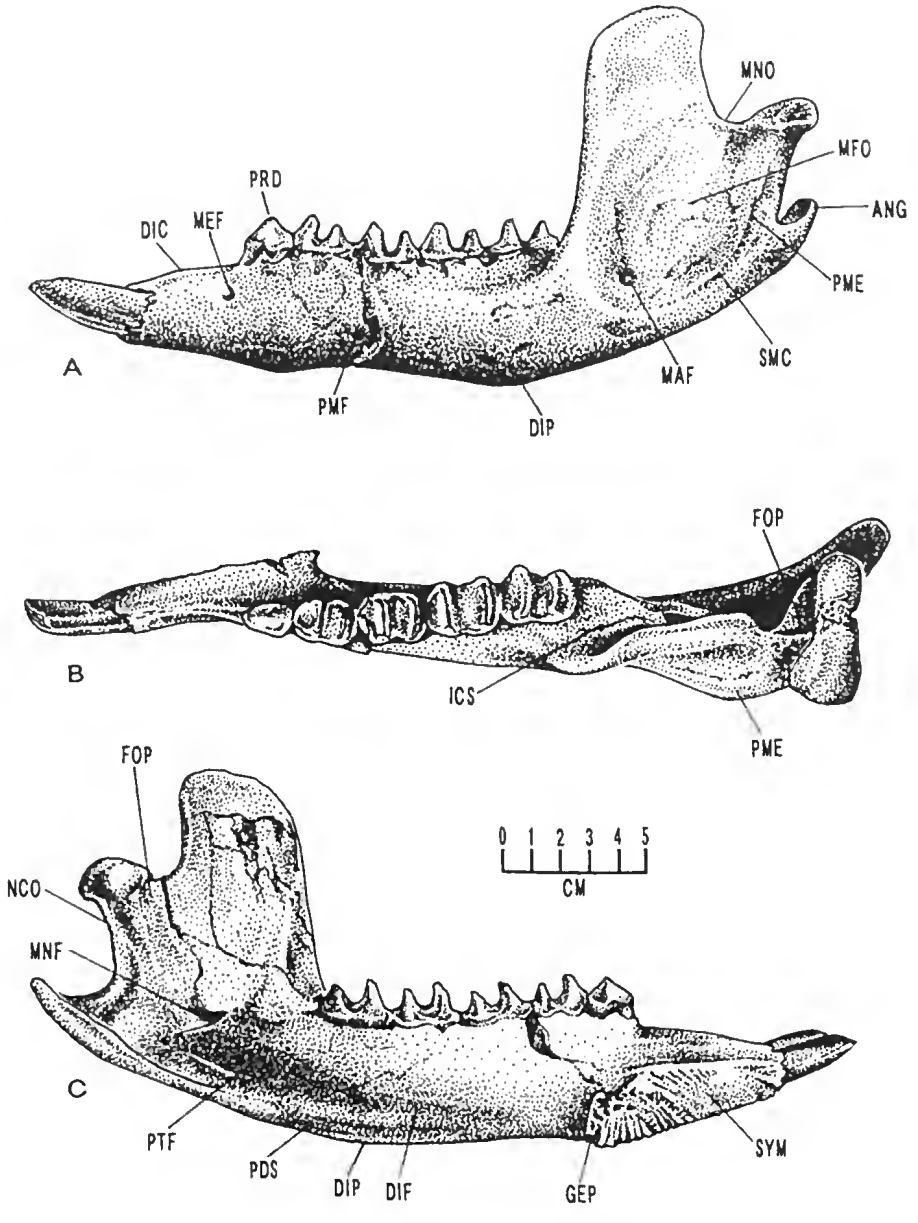

Fig. 43. *Neohelos* spB left dentary (NTM P8695-74 Blast Site, Bullock Creek) broken incisor tip and coronoid process tip restored; **A**, lateral aspect; **B**, occlusal (dorsal) aspect; **C**, internal aspect.

condyle to about 20 mm, then expands to a condylar width of about 50 mm. The condyle is transversely wide, convex posteriorly and presents an anteriorly inclined, flat articular surface laterally, narrowing medially to a more conical process. The masseteric fossa is a crisply defined concavity bounded inferiorly by a distinct submasseteric crest. The posterior masseteric crest is prominent and flange-like. A small, oval 3.5 mm to 4.5 mm diameter masseteric foramen is present.

The digastric fossa is elongated, extending anteriorly to below the level of interproximal M_{1-2}, and is usually posteriorly confluent with the pterygoid fossa, but rarely, a faint crest partially divides the two cavities. The medial edge of the pterygoid fossa is marked by a strong flat border about 10 mm wide that terminates dorsally at the angular process. The angular process projects slightly above the level of the tooth row and the posterior

masseteric eminence on the lateral side. The pterygoid fossa is deep and rugose. The mandibular foramen opens posterodorsally in line with the base of the tooth row. It is ovoid with its largest dimension varying from 8 mm to 15 mm. A postalveolar process is present 20 mm to 23 mm behind M_5.

Intermediate specimens. Here we describe a few specimens from Riversleigh and Bullock Creek that appear to be somewhat intermediate in size and in some morphological features between *N. tirarensis* and *Neohelos* spB, and *Neohelos* spB and *Neohelos* spC.

Gag maxilla. AR3878 (Fig. 44) is a right maxilla fragment from the Gag Site, Riversleigh Station, with P^3-M^{1-3}. The enamel is lightly worn on P^3 and the lophs of M^1. The P^3 is small but within the range of variation in size and morphology for *Neohelos* spB. As in *Neohelos* spB, the parastyle is large, but the parametaconal crests are steep and short. The M^{1-2} are slightly smaller than those of NTM P8690, but the M^3 is broader. The cingulae are not as strong, nor is the enamel as thick as in NTM P8690. Subjectively, the resemblances between AR3878 and NTM P8690 are compelling, though, due to the small sample involved, not sufficient grounds to propose a chronological basis for the similarities.

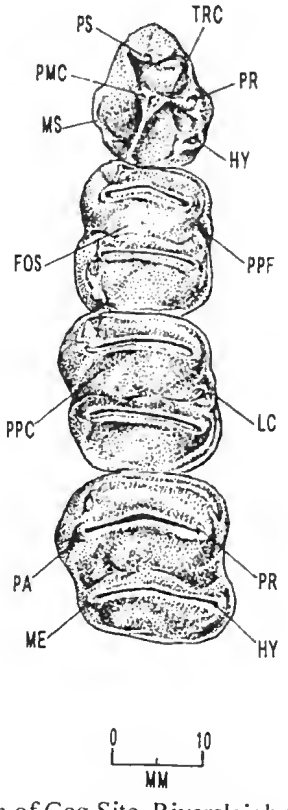

Fig. 44. *Neohelos* spB; right cheek teeth of Gag Site, Riversleigh specimen (AR3878).

Sticky-beak dentaries. AR13969 and AR13791 appear to be chronomorphs of *Neohelos* spB (Fig. 45). These dentaries contain mature adult dentitions with breached enamel on all molars. AR13791, a partial right dentary with M_{1-4} is about the same size as a juvenile dentary of *Neohelos* spB (CPC F23025) with a fully encrypted M_4. Its cheek teeth have matching occlusion with AR3878 (Gag) confirming that its morphological states are very similar and that the Sticky-beak dentaries are more appropriately included among *Neohelos* spB than among *N. tirarensis*. AR13969, a second right dentary fragment preserves the dentary symphysis, lower incisor alveolus and P_3–M_1. Because of their intermediate size,

the molar dimensions of these specimens are similar to those of *Bematherium*. However, they differ from *Bematherium* in having an elongated, well-developed paralophid crest on M_1 and otherwise conform more closely to all other characters of *Neohelos* spB.

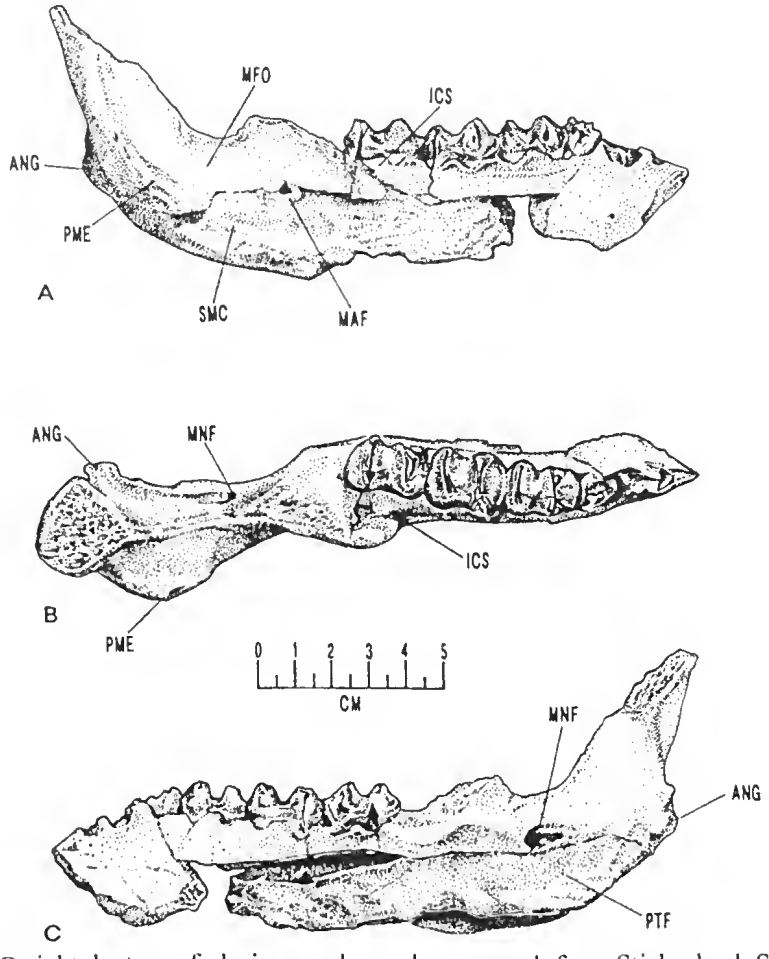

Fig. 45. *Neohelos* spB right dentary of plesio-morphous chronomorph from Sticky-beak Site, Riversleigh; **A**, lateral aspect; **B**, occlusal aspect; **C**, internal aspect.

Bullock Creek P^3s with incipient bilobation of parametacone. Two P^3 specimens of *Neohelos* spB (NTM P8695-46, NTM P8695-61) from Bullock Creek, Camfield Station show possible incipient division of the parametacone into two cusps (Fig. 46A–D). In NTM P8695-46 the postparametacrista is expanded into a small blade-like lobe behind a shallow indentation that is continuous with shallow, vertical creases on the buccal and lingual sides of the cusp. The parametacone is heavily worn in NTM P8695-61, though in this specimen the base of the parametacone is deeply lobate, much as in *Kolopsis torus*. Incipient lobation of the parametacone is not found in *N. tirarensis* and is rare and weakly developed in *Neohelos* spB (QM F20713, the twinned P3 cap from Cleft of Ages, Figure 28, does not appear to belong to *Neohelos*).

However, the weak presence of the trait in some individuals of *Neohelos* spB seems to *anticipate Neohelos* spC in which the characters seem to be a typical expression. Taking all specimens into account, *Neohelos* spB expresses a wide range of sizes and apparent morphoclinal states that to be smoothly transitional between *N. tirarensis* and *Neohelos* spC, indicative of gradual evolutionary morphogenesis.

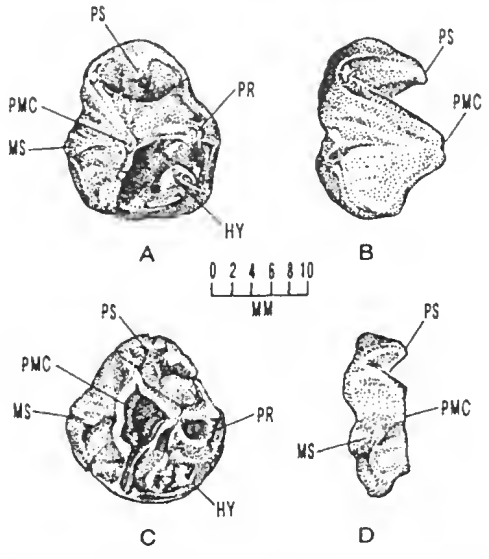

Fig. 46. *Neohelos* spB P^3's showing incipient bilobation of the parametacone; **A–B**, occlusal and labial aspects of left P^3 (NTM P8695-46 Blast Site, Bullock Creek); **C-D**, occlusal and labial aspect of P^3 (NTM P8695-61 Blast Site, Bullock Creek). In A, the parametacone is shallowly divided into a small conical anterior cusp and a thin lobate crest behind, by a faint labial groove; in B, the parametacone is worn down to the level of the parastyle showing a distinctly bilobed section. This variation is rare in *Neohelos* spB and shows only the merest hint of the tendency. The typical trend in this species is the formation of a single blade-like parametaconal cusp continuous with a prominent preparacrista.

Postcranial skeleton. Some elements of the postcranial skeleton of *Neohelos* spB are described and compared with the few zygomaturine genera for which a substantial portion of the skeleton is known (Figs 47-50; Table 12). Manus and pes elements of *Neohelos* are represented in the Bullock Creek collection, but have not been studied sufficiently to include them in the description. The material described and illustrated here is primarily intended to provide an impression of the overall structure of *Neohelos* spB. Comparisons of the material with other zygomaturines gives some indications of structural changes in subsequent zygomaturine lineages.

Vertebral column. The cervical vertebral bodies are slightly compressed, but with low neural spines compared to those of *Zygomaturus*. The thoracic and lumbar vertebral bodies are fairly long with circular to slightly oval articular facets. The pedicals are stout and broad. The transverse processes of both the thoracic and lumbar vertebrae are relatively short. The neural spines of the anterior-most thoracic vertebrae are slender, elongated and tapered distally. They are not bifurcated as in *Diprotodon*. The neural spines of the hind-most thoracic and all of the lumbar vertebrae are low and longitudinally broad. The distal ends of the lower thoracic and lumbar neural spines are expanded to form large, oval tuberosities related to the insertion of the transversospinalis group of back muscles. Judging from the series of small caudal vertebrae assigned to the species, the tail was weak, rapidly tapering and short. Ribs are poorly represented and fragmentary, though the curvature and length of some of the fragments indicate that the rib cage was deep and relatively wide (Fig. 51).

Scapula. The blade of the scapula is ovo-rectangular, measuring 300 mm long by 153 mm wide (Fig. 47A–C). The vertebral, caudal and cranial borders are strongly emarginated. The cranial border is convex above a wide, is nearly straight The vertebral border is

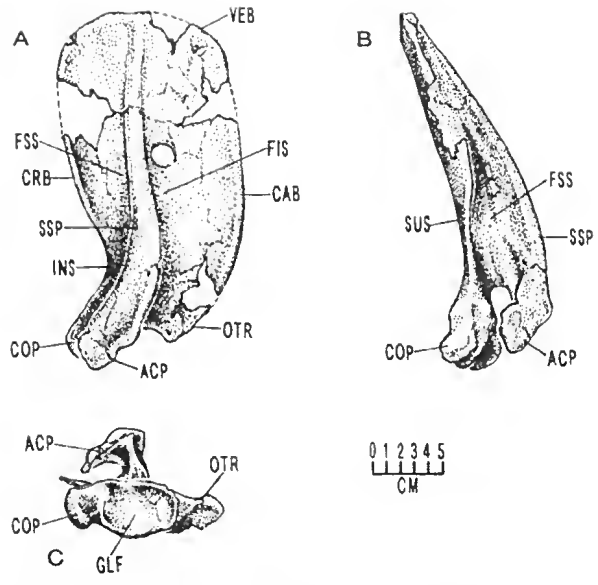

Fig. 47. *Neohelos* spB; left scapula **A**, lateral aspect; **B**, anterior aspect; **C**, glenoid aspect (NTM P8695-273 Blast Site, Bullock Creek).

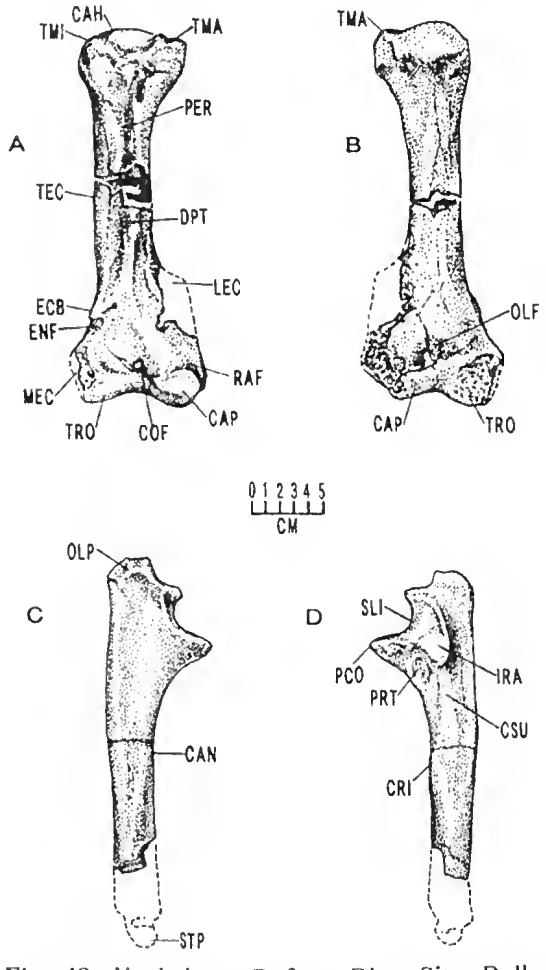

Fig. 48. *Neohelos* spB from Blast Site, Bullock Creek; **A–B** anterior and posterior aspect of left humerus (NTM P87108-30); **C–D**, lateral and internal aspect of left ulna (NTM P87103-45, P8695-278).

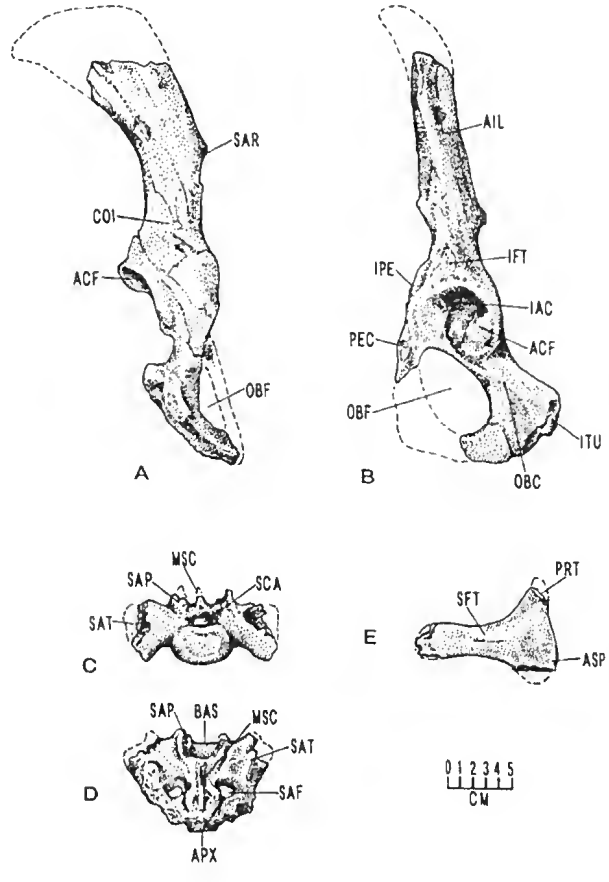

Fig. 49. *Neohelos* spB from Blast Site, Bullock Creek; **A–B**, posterior and lateral aspects of left innominate (NTM P8695-274); **C–D** anterior and dorsal aspects of sacrum (NTM P87108-31); **E**, left epipubic bone (NTM P8695-277).

Table 12. Measurements of postcranial elements of *Neohelos* spB.

ELEMENT	MEASUREMENT	millimetres
Scapula (NTM P8695-273)	Length	300.0
	Width	153.0
	Length vertebral border	125.0
	Width suprascapular fossa	58.0
	Width infrascapular fossa	87.0
	Depth (maximum) scapular spine	51.5
	Width (maximum) acromion	42.0
	Dimensions glenoid cavity	45.0 x 60.0
Humerus (NTM P87108-30)	Estimated length	310.0-315.0
	Diameter above D-P tuberosity	40.0 x 45.0
	Dimensions head	55.0 x 55.0
	Dimensions coronoid fossa	30.0 x 39.0
	Dimensions radial fossa	20.0 x 20.0
	Width distal articulation	110.0
	Dimensions trochlea	27.0 x 40.0
	Dimensions capitulum	35.0 x 35.0
	Dimensions olecranon fossa	20.0 x 35.0
Ulna (NTM P87103-43)	Estimated length	270.0
	Length radial incisure	52.0
	Width coronoid incisure	39.2
	Length coronoid incisure	51.0
	Length olecranon process	47.0
	A-P width at coronoid process	82.5
	Distal A-P width of shaft	31.0
Innominate (NTM P8695-274)	Estimated length	400.0
	Dimensions acetabulum	67.0 x 73.0
	Diameter (maximum) obturator for.	94.0
	Width body of ilium	41.0
	Dimensions sacral articulation	50.0 x 115.0
	Length ischial tuberosity	88.0
Femur (NTM P8695-275)	Estimated length	320.0-325.0
	Dimensions head	65.0 x 65.0
	Width (middle) diaphysis	47.0
	Width medial condyle	37.0
	Depth medial condyle	47.2
	Width lateral condyle	47.0
	Depth lateral condyle	40.0
Tibia (NTM P8695-276)	Estimated length	260.0
	Dimensions tibial facet	18.0 x 35.0
	Dimensions astragalar facet	30.0 x 40.0
	A-P diameter shaft	32.6
	M-L width proximal end	89.0
	M-L width distal end	37.0
Epipubic bone (NTM P8695-277)	Length	125.0
	Proximal height	82.0
Sacrum (NTM P87108-31)	Length	82.5
	Width	120.0

convey, about 125 mm wide. The distinctly concave suprascapular fossa is about one-third the width (58 mm) of the infrascapular fossa (87 mm). The robust, slightly sinuous scapular spine traverses the entire length of the blade. It is greatly elevated proximally (51.5 mm), terminating in a 42 mm wide, strap-shaped acromion process. The coracoid process is short and blunt; divided from the glenoid fossa by a transverse groove. The glenoid cavity is oval, measuring 45 mm by 60 mm. An infraglenoid tuberosity is absent.

In *Kolopsis torus* the scapular blade is narrower overall and more acuminate at the vertebral border. A well developed infraglenoid tuberosity is present and the coracoid process is elevated into a low crest. In *Plaisiodon centralis* the infraglenoid region is

expanded, but does not develop a distinct process or tuberosity. Its scapula otherwise resembles an enlarged version of that of *Neohelos*. In *Zygomaturus trilobus* the infraglenoid tuberosity is greatly elongated, extending below and behind the glenoid fossa in the form of a flange-like process. The vertebral border is distinctly pointed and rugose.

Humerus. The humeral diaphysis is robust, straight and triangular in section for most of its length. Its estimated length is 310–315 mm and its transverse dimensions are 40 mm by 45 mm above the deltopectoral tubercle (Fig. 48A–B). The head is a broad, partial hemisphereabout 55 mm by 55 mm, bounded laterally by a massive, rectangular major tuberosity and anteromedially by a thick transverse crest forming a minor tuberosity. A deep intertubercular sulcus is present between the two tuberosities, accentuated inferiorly by a sharp, very prominent pectoral crest that descends from the anterior side of the major tuberosity to the middle of the shaft. The pectoral crest merges with a flange-like deltopectoral eminence, which is buttressed distally by a pair of low crests originating from the entepicondylar bridge medially and from the lateral margin of the coronoid fossa laterally. The deltopectoral eminence is probably homologous to the deltoid tuberosity in vombatids, but it is not separated from the pectoral crest as in the latter.

Though damaged in the illustrated specimen, the supinator crest of the ectepicondyle is a wide, thin flange extending proximally for about one-third the length of the entire bone. The coronoid fossa is a large (39 mm x 30 mm x 3 mm), shallow, oval depression situated directly above the trochlea. The radial fossa immediately above the capitulum is smaller (20 mm x 20 mm x 3 mm). The distal articular surfaces are transversely wide, about 110 mm across. The arc of the articular surface of the trochlea is slightly flattened. It is relatively broad (>27 mm) and elongated (40 mm). The capitular articular surface is also slightly flattened, measuring approximately 35 mm by 35 mm.

The posterior surface of the humerus is nearly flat, being bordered by two crests; medially, a short low crest for the teres major muscle and laterally, by a longer crest for the brachioradialis muscle. The olecranon fossa is a sharplydefined, oval depression measuring 35 mm by 20 mm x 5 mm. The humerus of *Neohelos* spB closely resembles that of *K. torus* in its basic morphology, but is relatively more robust. In both genera the pectoral component of the deltoid tuberosity is only weakly developed, whereas in *Zygomaturus trilobus*, a distinct pectoral tuberosity is developed adjacent to the deltoid tuberosity, similar to the condition in vombatids. Separate deltoid and pectoral tuberosities are also present in *Plaisiodon centralis*.

Ulna. The estimated length of the illustrated specimen is approximately 270 mm. The entire bone is compressed mediolaterally and tapers strongly toward the distal end. The olecranon process is short, terminating in a rugose, elliptical, superomedially-directed tuberosity (Fig. 48C–D). The entire bone is gently bowed laterally and posteriorly. The medial surface of the ulna is predominantly concave and the lateral surface is flat to convex. A strong crest for the interosseous membrane overlaps the anterolateral margin of the shaft. The interosseous crest is continuous proximally with the supinator crest, which terminates at the ventral margin of the greatly expanded radial incisure of the semilunar cavity.

The coronoid process is a massive flange surmounted by a large, concave, circular articular surface for the trochlea. The radial incisure is shaped like a human ear, about 52 mm long; below which there is a large circular scar, the ulnar tuberosity, for the attachment of the brachialis muscle. Distally, the styloid process is a large hemispherical process situated in

the centre of the ulnar capitulum. As with the other bones of the forelimb, the ulna of *Neohelos* is most similar to that of *Kolopsis torus*. The ulna of *Kolopsis* differs from that of *Neohelos* in being more lightly constructed and in having a short, transversely broader olecranon process. It is structurally intermediate between *Neohelos* and *Zygomaturus* in the state of this particular attribute.

Innominate. The estimated length of the innominate is approximately 400 mm from the base of the pubic ramus to the restored iliac crest. The iliac blade is relatively long and narrow, flaring distally into a crescentic iliac crest (Fig. 49A–B). The iliac body is stout and triangular in section. The acetabulum is large, 67 mm x 73 mm. The dorsal acetabular crest is laterally expanded, greatly overhanging the acetabular fossa. A large, oval acetabular notch is present in the lower half of the acetabular fossa. The ischial ramus is relatively elongated, terminating in a short ischial tuberosity. The obturator foramen is a large ovo-triangular-shaped vacuity 94 mm long. A low iliopectineal eminence is present. The innominates of both *Neohelos* spB and *Kolopsis torus* are much narrower than that of *Zygomaturus trilobus* in which the iliac alae are greatly expanded laterally and the body of the ilium is short. The ischial ramus in *K. torus* is considerably shorter than that of *Neohelos* spB.

Femur. The proximal and distal ends of the femur are greatly expanded transversely relative to its shaft. The greater trochanter terminates in a rugose, conical tuberosity, expanding laterally into a thick, convex crest that extends down about one-third the length of the bone (Fig. 50A–C). The large 65 mm x 65 mm, hemispherical femoral head projects dorsomedially about 65 mm beyond the midline axis of the diaphysis and overhangs the anteromedial surface of the diaphysis by approximately 35 mm. The lesser trochanter is a thin, convex flange extending from immediately below the medial side of the head to about the same level as the termination of the lateral crest of the greater trochanter.

On the posterior surface, the lesser and greater trochanters are united by a strong intertrochanteric crest for the iliofemoral ligament. The diaphysis is planoconvex to oval in section, about 47 mm minimum width. The posterior surface of the diaphysis is marked by a faint linea aspera with irregular, oval scars for the attachment of the adductor magnus muscle. A low ridge continues distally onto the popliteal surface, extending to the base of the medial condyle. Proximally, a deep, thickly emarginated trochanteric fossa extends about 40 mm into the trochanteric crest.

The condylar surfaces are complex and asymmetrical. Distally, the medial condyle is transversely narrower but anteroposteriorly longer than the lateral condyle. The condyles are separated posterodistally by a 30 mm deep, 20 mm wide intercondylar sulcus. The distal articular surface is greatly expanded anteriorly by an extensive rotular surface. The medial side of the rotular sulcus is elevated into a prominent, rounded crest. The lateral margin of the rotular sulcus is defined by a lower, sharper crest arising anteromedial to the ectepicondyle.

The estimated maximum length of the illustrated specimen is 320–325 mm. The femora of *Kolopsis torus* are more slender relative to their length than in *Neohelos* or *Zygomaturus trilobus*. The diaphysis in *K. torus* is more compressed anteroposteriorly than in *Neohelos* spB, but not to the extent seen in *Zygomaturus trilobus*, which has a more flattened oval section to its wider relative to length, femoral shaft.

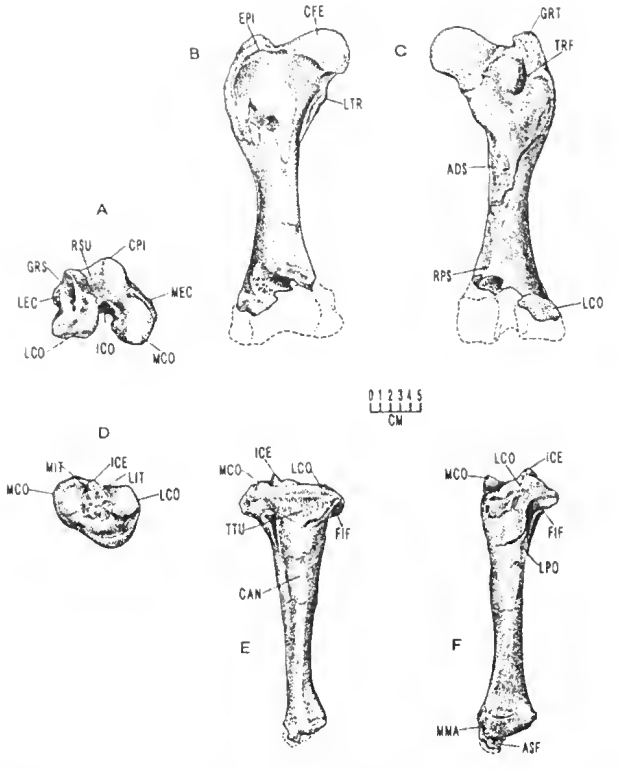

Fig. 50. *Neohelos* spB from Blast Site, Bullock Creek; **A–C**, anterior and posterior aspects of right femur (NTM P8695-275, P87103-44); **C–D**, distal articular surfaces of femur; E, proximal articular surface of left tibia; **F–G**, anterior and fibular (lateral) aspects of tibia (P8695-276/P87103-45).

Tibia. The proximal surface of the tibia is transversely wide. The medial condylar surface is concave and the lateral condylar surface is convex. The intercondylar eminence is a very prominent, 20 mm high triangular structure composed of a medial and a lateral tubercle separated by an oval pit. The tibial tuberosity is low and wide (Fig. 50D–F). The tibial facet is 35 mm by 18 mm, overhanging the lateral surface of the diaphysis approximately 25 mm. The anterior (tibial) crest is smoothly rounded proximally, narrowing and merging distally with the interosseus crest. A strong popliteal crest runs down the proximal third of the posterolateral border of the diaphysis. Medially, about midway down the shaft, a sharp crest and rugose scar denotes the probable attachments of the tibialis anterior musculature.

The distal articular surface is elongated anteroposteriorly. The medial malleolus is a short, broad conical process situated directly in line with the tibial crest. The astragalar facet is an oval convex surface 40 mm by 30 mm. The total length of the illustrated specimen is 260 mm. The tibia *of Neohelos* spB is essentially identical to that of *Kolopsis torus* except for its greater robusticity. In *Zygomaturus trilobus* the tibial shaft is relatively more slender mediolaterally relative to its proximal and distal ends, than in *Neohelos* and *Kolopsis*. *Zygomaturus* has a more prominent tibial tuberosity and the entire bone is much shorter in relation to its anteroposterior width than in *Neohelos* and *Kolopsis*.

Intermembral proportions between *Neohelos* spB and *Kolopsis torus* are similar: the ulna is 0.86 of the length of the humerus in both species. The tibia is 0.80 of the length of the femur in *Neohelos* spB and 0.70 in *K torus*. In *Zygomaturus trilobus* the ulna is 0.70 of the length of the humerus and the tibia is 0.60 of the length of the femur. In *Plaisiodon centralis* the ulna is 0.75 of the length of the humerus and the tibia is 0.79 the length of the

femur, its intermembral proportions being more like those of *Neohelos* spB than the other zygomaturine species noted.

Weight estimations of *Neohelos* spB calculated from Anderson *et al.*'s (1985) formula, which is based on upper limb bone diameters for quadrupedal mammals, suggest a mass of 250 kg for a large (male?) individual. For comparison, the same formula yields a mass of 673 kg for *Zygomaturus trilobus*. A small (female?) *Kolopsis torus* specimen may have weighed about 112 kg and a larger specimen (male?) may have weighed about 200 kg. Upper limb shaft diameters *of Plaisiodon centralis* indicate that this animal weighed about 550 kg. The postcranial elements have not been examined from a functional perspective, thus the characteristic standing posture of the animal is not known. *Neohelos* spB was about the size of a large ram, though more heavily built and shorter-limbed (Fig. 51).

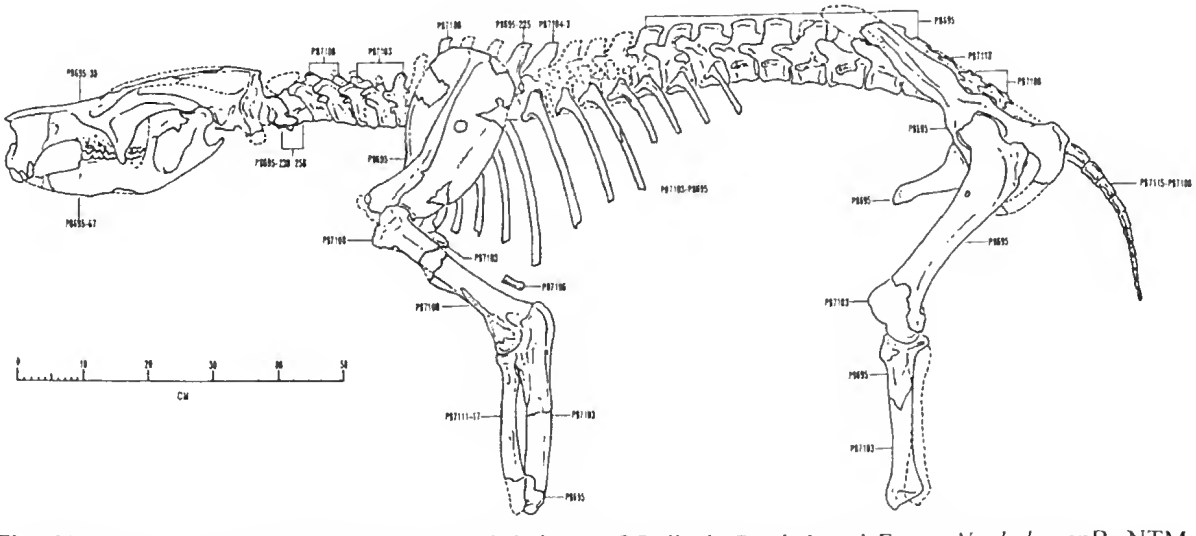

Fig. 51. *Neohelos* spB; partial restoration of skeleton of Bullock Creek Local Fauna *Neohelos* spB. NTM catalogue numbers of referred specimens are given on the illustration. No attempt has been made to restore the posture of the animal.

Neohelos spC

Reference specimen. AR5797, partial cheek-tooth row consisting of right P^3, right DM^1, right M^{1-2}.

Reference specimen locality and age. Jaw Junction Site, Riversleigh, Queensland; mid to late-Miocene based on stage of evolution biochronology.

Referred specimens and localities. *Neohelos* spC is known only from Riverslcigh, north-western Queensland.

Jaw Junction Site, Riversleigh Station, Queensland: AR5621, left M_{1-3} and dentary fragments; AR5797, right P^3-DM^1-M^{1-2} and maxilla fragments; AR5989, left M_{2-3} AR5989, left M^4; AR6343, right I_1; AR7851, right P^3; AR7857, right M_2; AR7859 right M_1 protolophid; AR7860, right M'; AR 7858, right P_3; NTM P91168-3 left I^1; NTM P91168-4, right I_1; NTM P91168-5, left M_1 protolophid; NTM P91168-2, right M^3.

Species diagnosis. Teeth larger than *NEOHELOS* spA and *N. tirarensis*, equal in size to *Neohelos* spB and distinguished from the latter by its higher, more slender molar lophs; higher, narrower, bilobed P^3 parametacone and lack of anterior crest on P_3.

Description. *Incisors,* $\underline{I^1}$. I^1 in isolation is probably not distinguishable from that of *Neohelos* spB (Fig. 52A–C). The depth of the crown at the cemento-enamel contact is 12.5 mm and it is 7.5 mm thick: bucco-lingually.

$\underline{I_1}$. The lower incisor crown is deep, thickly enamelled with a rounded, overhanging dorsal crest (Fig. 52D–E). As in *Neohelos* spB there is a strong longitudinal dentine ridge extending from the root to the tip of the crown on the lingual side, and a conspicuous groove paralleling the ventral border of the crown on the labial side. The maximum depth of the crown is 18.5 mm and its maximum thickness is 11.0 mm.

Upper cheek teeth, $\underline{P^3}$. The P^3 is elongated with a large parastyle. In profile, the lower half of the parametacone is like that of N. stirtoni, but the upper portion is prolonged into a narrow, blade-like pinnacle (Fig. 53A–D; Table 13). InAR7851 the parametacone is just perceptibly divided by faint lingual and labial furrows. In AR5797 the division of the parametacone is completed by a transverse groove extending from the base of the longitudinal basin lingually to the base of the crown labially. Vertical crests on either side of the groove correspond to the enamel thickening at the cusps. Although there is a distinct swelling of the postmetacrista in the position of the metacone, it does not appear to be fully cuspate and the metacone is much smaller and situated below the paracone. The attenuated parametacone accentuates the lobate posterior part of the postmetacrista, which when actually measured, is only slightly longer and higher than that of *Neohelos* spB. Other features of the P3 crown are within the range of variation known for *Neohelos* spB.

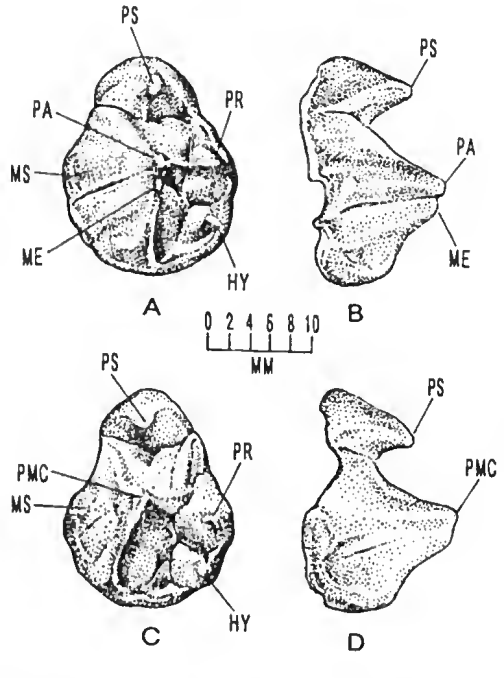

Fig. 52. *Neohelos* spC from Jaw Junction Site, Riversleigh; incisors; **A–C**, labial, distal and lingual, respectively, aspects of left I_1 (NTM P91168-3); **D–E**, labial and occlusal (dorsal aspects of right I_1 (NTM P91168-4).

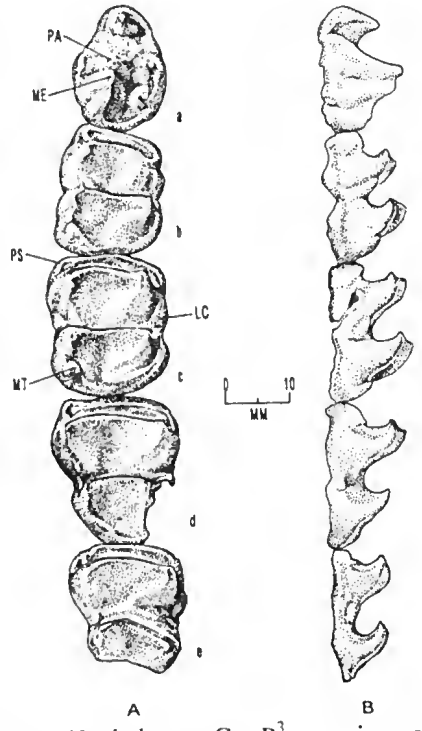

Fig. 53. *Neohelos* spC; P^3 specimens; **A–B**, occlusal and labial aspects of right P^3 (type, AR5797 Jaw Junction, Riversleigh); **C–D**, occlusal and labial aspects of right P^3 (AR7851 Jaw Junction, Riversleigh). The pinnacle-like parametacone is clearly divided in the type by a labial and lingual groove whereas AR7851 is less distinctly bilobed. The mesostyle is also poorly developed in this species.

Table 13. Measurements (millimetres) of upper and lower cheek teeth of *Neohelos* spC (estimations in italics).

UPPER CHEEK TEETH (mm)

SPECIMEN	SIDE	P^3		M^1			M^2			M^3			M^4		
		L	W	L	AW	PW	L	AW	PW	L	AW	PW	L	AW	PW
AR 5797	R	20.7	16.6	20.5	17.1	18.0	23.0	20.2	19.1	----	----	----	----	----	----
AR 5989	L	----	----	----	----	----	----	----	----	----	----	----	21.0	20.4	15.5
AR 7851	R	20.8	*16.8*	----	----	----	----	----	----	----	----	----	----	----	----
AR 7860	R	----	----	----	20.0	----	----	----	----	----	----	----	----	----	----
NTM P91168-2	R	----	----	----	----	----	----	----	----	24.4	21.4	----	----	----	----

LOWER CHHEK TEETH (mm)

SPECIMEN	SIDE	P_3		M_1			M_2			M_3			M_4		
		L	W	L	AW	PW	L	AW	PW	L	AW	PW	L	AW	PW
AR 5621	L	----	----	*21.2*	----	15.1	23.1	17.5	----	*25.0*	----	----	----	----	----
AR 5989	L	----	----	----	----	----	25.2	18.7	18.0	24.2	19.4	17.6	----	----	----
AR 7857	R	----	----	----	----	----	----	----	----	22.2	16.7	16.4	----	----	----
AR 7858	R	16.8	10.7	----	----	----	----	----	----	----	----	----	----	----	----
AR 7859	R	----	----	*21.0*	----	----	----	----	----	----	----	----	----	----	----

M^1. M^1 is basically as in *Neohelos* spB, but with slightly higher, more slender and more overhanging lophs (Fig. 54Ab–B). The parastyle is represented by a thickened, tightly curving enamel crest rather than as a distinct cuspule. It is set off from the paracone by a distinct vertical groove. The metastyle is represented by an elevated thickening of the postcingulum, separated from the postmetacrista by a small, labially indented notch. The pre- and postcingulae are well developed, but separated by short gaps at the bases of the protocone and metaconule. The lingual cingulum is short but strongly developed, traversing the lingual transverse valley. A mesostyle is absent.

M^2. M^2 is markedly larger than M^1 and closely resembles that of *Neohelos* spB (Fig. 54Ac-B). Except for its more overhanging lophs, which if made less apparent with light wear, the M^2 *of Neohelos* spC might not be reliably distinguished from those of *Neohelos* spB. In AR5797 the parastyle is a slight thickening of the precingulum and the postparastylar crest is faint. The lingual cingulae are much the same as on M^1. The postparastylar crest is low, thick and rounded. The metastyle is nearly identical to that on M^1. The protoloph is slightly wider than the metaloph.

M^{3-4}. M^3 is represented by NTM P91168-2, a molar cap missing its metaconule. It too, except for its more overhanging lophs, does not differ in any significant way from the M^3 of *Neohelos* spB (Fig. 54Ad–B). The protoloph is wider than the metaloph. The parastyle is represented by a tiny cuspule on the labial extreme of the precingulum. The metastyle, as such, is absent. A short labial cingulum traverses the interloph valley. M^4 (AR5989) is essentially identical to that of *Neohelos* spB. The lophs are slightly lower than on the preceding molar and the crown is markedly asymmetrical with a much narrower metaloph which is three-quarters the width of the protoloph. The protoloph is approximately as wide as that of the preceding molar. The parastyle is represented by a tiny salient on the precingulum. The postparaconal crest is a strong ridge extending from the tip of the parastyle to end at the interloph sulcus, just short of the base of the metaconule. A small stylar cusp and a weak cingulum is present in the lingual mouth of the median valley. The labial cingulum is absent.

Lower cheek teeth, P_3. The P_3 (AR7858) of *Neohelos* spC is very distinctive in its shape and in lacking an anterior crest (Fig. 55A–B; Table 13). The crown is elongated and

ovo-triangular in occlusal aspect. Commencing at a prominent bulge above the first root, the long, conical anterior part of the crown tapers smoothly to the apex of the main cuspid at an angle of about 45°. The slender, attenuated apex of the main cuspid is situated a considerable distance behind the midpoint of the crown. The upper part of the posteromedian crest is almost vertical, sharply turning posteriorly on its descent in the form of a high, thin, nearly horizontal ridge which merges with the lingual postcingulid.

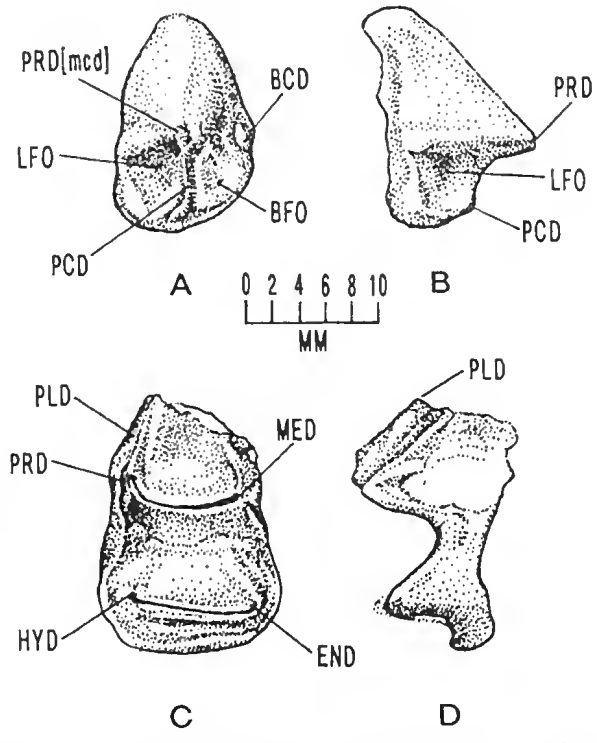

Figure 54. *Neohelos* spC from Jaw Junction, Riversleigh; right upper cheek tooth row (reconstructed) **A**, occlusal aspect, a–c, P^3–M^{1-2} type specimens (AR5797) d, M^3 (NTM P91168-2) e, left (reversed) M^4 (AR5989); **B**, labial aspect; amount of curvature of tooth row is conjectural; note slender, overhanging lophs, wide interloph valleys.

The lingual postcingulid makes a steep, arcing descent to just above the crown base, then continues horizontally forward to contact the base of the main cuspid, enclosing a large L-shaped lingual fossa. The labial fossa is shallow and small, being confined anteriorly by a vertical buttress from the protoconid and posteriorly by a bulge in the short, thick labial cingulid. A second small fossa is developed anterior to the labial postprotoconid buttress, emarginated anteroinferiorly by a small, isolated basal cingulid.

M_1. The M_1 (AR5621, AR7859, NTM P91168-5) protolophid in *Neohelos* spC is narrower and more slender in profile than in *Neohelos* spB (Fig. 55C–D). The paralophid is higher and steeper. The premetacristid is sharply defined and the crest of the protolophid is curved, strongly accentuating the anterior furrow of the lophid. As in *Neohelos* spB, the hypolophid crest is nearly straight and much wider than the protolophid.

M_{2-4}. The M_2 (AR5621, AR7857) lophids are slightly higher and more overhanging than in *Neohelos* spB. The interlophid valley is distinctly U-shaped in labial aspect and wider than in *Neohelos* spB. The lophids are slightly narrower in proportion to the length of the crown and the precingulid is proportionally narrower transversely. The anterior sulcus of the protolophid is confined and gradually narrowed by the preproto- and premetacristids down

to the precingulid. The protolophid is more curved than the hypolophid. The protolophid and hypolophid ere about equal width, with a slight obliquity to the hypolophid, which is also less curved than the protolophid.

The postcingulid is strongly lobate and deeper anteroposteriorly than in *Neohelos* spB. M_3 (AR5989) is the largest molar in the series. It is asymmetrical, the hypolophid being oblique and offset to the lingual side of the crown. The protolophid is about 25% wider than the hypolophid. Both lophids are slightly more curved and the interlophid valley is distinctly wider than in typical *Neohelos* spB. The postcingulid is thick and lobate in the midline of the hypolophid. M_4 (AR5989) closely resembles M_3 except that the hypolophid is only slightly narrower than the protolophid.

VARIABILITY IN *NEOHELOS*

By variation, we are referring to predominantly minor differences in traits or characters that have no apparent phylogenetic utility, though some labile characters in *Neohelos* and other zygomaturines are applicable to systematic problems. Three types of variability occur in *Neohelos*: 1) random and variable (including continuously varying) expression; 2) sexual dimorphism and age-related character expression and 3) on-off distribution of character states within groupings at various taxonomic levels.

Variability in the morphology and size of *Neohelos* specimens caused some initial difficulties in the determination of its species. By far the largest sample of *Neohelos* comes from the Blast Site (Small Hills locality, Camfield). We have found no indication from the biological content or lithology of that quarry to suggest that more than one stratigraphic horizon is locally present, and can find no basis for the discrimination of more than one morphospecies from this source. Therefore, the Blast Site sample is regarded as representing a population, and its features are treated as analogous to the variations recorded within a large living population. As more specimens of other *Neohelos* species came to light, a pattern of variation, characteristic of the entire group became apparent.

Random and variable expression. Character lability is frequently seen in the morphology of the paroccipital-mastoid processes, which range from massive, inflated knobs in about one-third of individuals to slender, tapering projections in the majority. The expression of a supratympanic fossa ranges from absent in 28.6% of specimens, to well-developed, even multiple expressions in the rest. The posterior epitympanic fossa is absent in 43% of specimens. The tympanic bullae vary from relatively narrow and oval (50% of individuals), to broad and triangular in shape. Cranial nerve foramina vary considerably in size and expression, with accessory foramina being common.

Variability in palatal width and contour are not closely correlated with the overall size of the cranium or the cheek teeth, though there may be a tendency for small individuals to have broad palates. The palatal surfaces vary from nearly flat, to distinctly though shallowly, concave. Also apparently unrelated to the size of the individual, the frontal region varies considerably in its appearance ranging from smooth, roundly inflated frontal bosses in 40% of specimens to narrow, sharper crests in 60%.

The cheek teeth of *Neohelos* species are quite variable in appearance, particularly in the degree of development of cingulae, styles and minor proportions of the crowns. However,

the dimensional range of variation of the molars does not attract specific comments here,other than to point out that there is not a close correlation between the size of the teeth (either expressed as tooth row length or individual crown dimensions) and the overall size of the cranium.

Because of its systematic importance, variability of the P^3 of *Neohelos* is considered in more detail. The crowns vary in their expression of ancillary cusps, cingulae, overall shape, and form of their primary cusps (Fig. 56; Table 14). There is also considerable variation in absolute size and size of P^3 relative to M^2. Because the general impression of high variability is a somewhat subjective observation, we have compared the dimensions of the P^3 crown of *Neohelos* spB with those of the closely-related zygomaturine species *Kolopsis torus* from the late Miocene Alcoota Local Fauna. In terms of dimensions length by width, the *Neohelos* spB P^3 examples yield a low correlation coefficient of r=0.55. The Pearson's coefficient of variation for crown lengths is 7.9 and for crown widths it is 6.7.

Comparing these figures with *Kolopsis torus*, the scatter is less diffuse and the correlation coefficient is higher at r=0.74. The Pearson's coefficient of variation in *Kolopsis* is 5.1 for crown lengths and 5.0 for crown widths. These examples indicate that the P^3 of *Neohelos* spB is absolutely more variable than in *Kolopsis torus*, which is also very similar in size (*Neohelos* mean P^3 length=18.2 mm; width=15.8 mm; *Kolopsis* mean length=18.9 mm; width 15.3 mm). The differences in variability between the Alcoota sample and the Bullock Creek sample could be a reflection of a greater temporal range at Bullock Creek, or it could, as the remarkable variability in the P^3 crown morphology in all *Neohelos* species suggests, represent a condition inherent to the entire group.

The most interesting aspect of the P^3 variability in *Neohelos* is that certain occasionally expressed features are similar to characteristically fixed, often apomorphous characters of other genera. The more obvious variations include expression of a 'hooked' parastyle characteristic of *Nimbadon* and *Plaisiodon* in about 6% of the *Neohelos* population, and the presence of a high preparaconal crest like that of *Kolopsoides* in 13% of *Neohelos* specimens. Twenty-three per cent of *Neohelos* have a strong anterolabial cingulum as in *Kolopsis torus* P^3s; 3% have incipiently divided parametacones anticipating the more derived genera *Kolopsis* and *Zygomaturus*. As a key character, the hypocone is absent in a small number of individuals of all Neohelos species for which there is a reasonably large sample. Size and morphological variations in the parastyle appear to have about the same frequency in all species of *Neohelos*. In fact, there are very few isolated otherwise 'apomorphous' P3 traits of other zygomaturine species that are not expressed to some degree by individual *Neohelos* spB specimens.

Sexually dimorphic and age-related traits. The *Neohelos* spB assemblage presents a striking range of sizes and shapes, some crania being nearly twice the size of others; some broad and low with deep maxillae; others being narrow, elongated or 'stretched' variants. Some individuals have strong sagittal crests, whereas others have none; some individuals have broad, distally flared snouts while others are narrow or even somewhat pointed (Figs 57–59). The zygomatic arches of some individuals are deep and strongly convex, whereas in others they are shallow and relatively straight.

The masseteric processes range from elongated and transversely flattened to short, slender and conical. In 50% of the specimens with the snout preserved, the anterior end of the rostrum is elevated and dorsoventrally expanded overall, from the incisor alveoli to the top

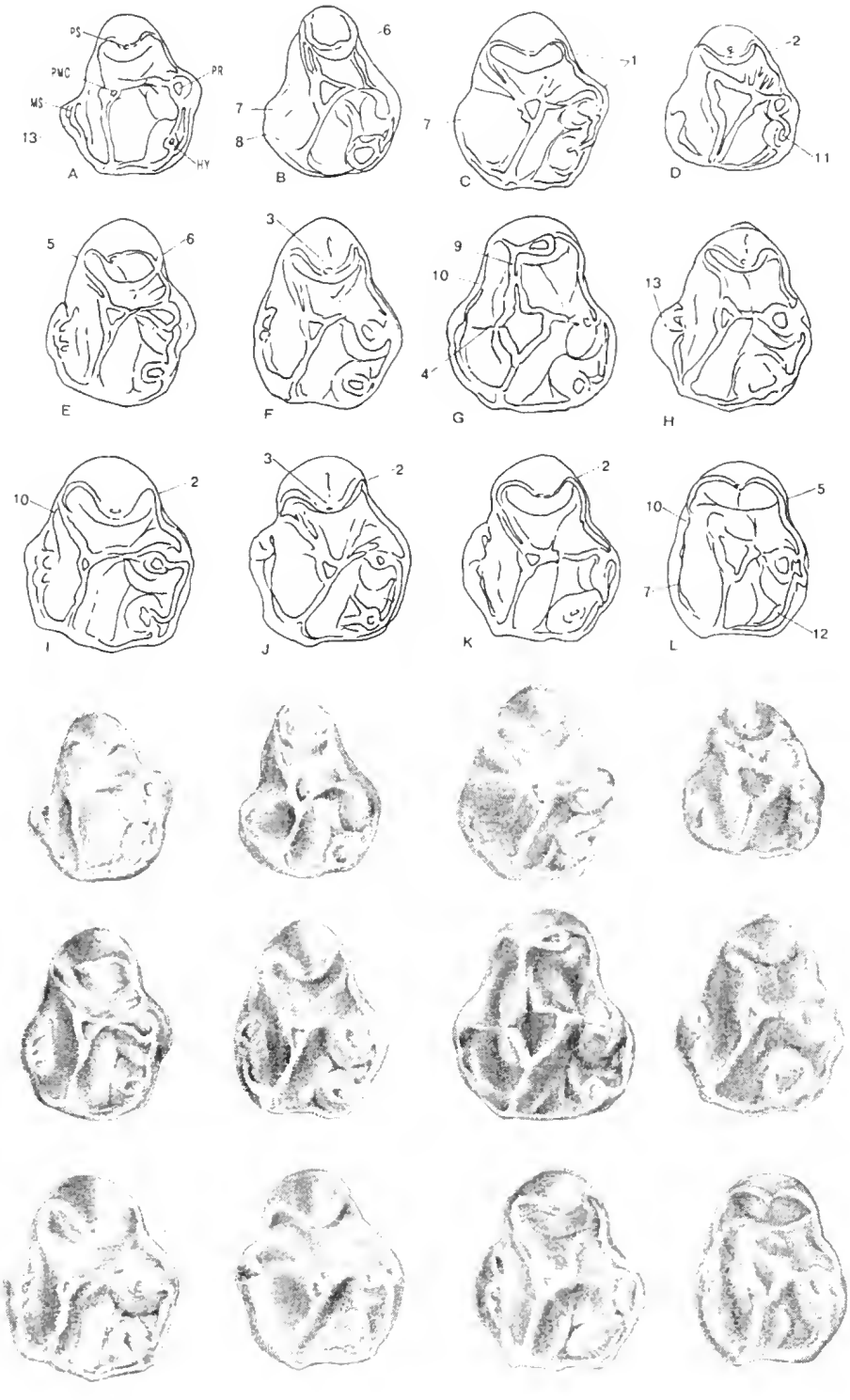

Figure 56. Line and shaded drawings of some morphological variations of the right P^3 of *N. stirtoni*. Numerals on line diagrams denote specific character variations: 1, strong compared to 2, weak emargination between protocone and parastyle; 3, posteriorly inclined or 'hooked' parastyle; 4, incipient division of paracone and metacone (note division of pair of enamel bulges by a faint sulcus on labial side of parametacone); 5, strong labial crest on parastyle; 6, strong lingual crest on parastyle; 7, absence of mesostyle; 8, weak-absent posterolabial cingulum; 9, elevated crest connecting parastyle with parametacone; 10, well-developed anterolabial cingulum; 11, small hypocone closely pressed to (twinned from?) the protocone; 12, hypocone absent; 13, large labially projecting mesostyle.

Table 14. Comparison of type (SAM P13848) and paratype (UCMP13848, UCMP69977, UCMP69978) material of *N. tirarensis* Stirton from the Leaf Locality (Wipajiri Formation of South Australia), Riversleigh, Queensland *N. tirarensis* (NTM P91167-1), *Neohelos* spB. (CPC 22200/BMR F23046), and *Neohelos* spC (AR5797, AR5989 and NTM P91168-2).

MEASUREMENT	Leaf Locality *N. tirarensis*	Riversleigh *N. tirarensis*	*Neohelos* spB	*Neohelos* spC
Dimensions frontal fossa	-----	25.0 X 50.0	30.0 X 65.0	-----
Dimensions lacrimal tubercle	-----	8.0 X 12.0	7.0 X 15.0	-----
Dimensions suborbital fossa	-----	15.0 X 20.0	12.0 X 27.0	-----
Dimensions infraorbital for.	-----	3.5 X 9.0	6.0 X 11.5	-----
Dimensions glenoid surface	-----	30.0 X 35.0	28.0 X 42.0	-----
Dimensions postglenoid pro.	-----	10.0 X 26.0	11.5 X 45.0	-----
Length squamosal-jugal sut.	-----	100.0	79.0	-----
Depth zygomatic arch	-----	30.0	40.5	-----
Length masseteric proces	-----	11.0	26.0	-----
Width submasseteric notch	-----	12.4	17.0	-----
Distance orbit to maxillary sut.	-----	48.0	77.0	-----
Distance max. sut. to postgl.	-----	190.0	237.0	-----
Dist. max. sut. to p. alv. proc.	-----	111.5	160.0	-----
Depth orb. to submas. notch	-----	26.7	25.0	-----
Width palate	-----	48.0 (est.)	51.0	-----
Length cheektooth row	-----	81.5	108.1	-----
P^3 length	-----	13.8 (R)	19.4	20.7
P^3 width	14.8 (Holotype)	12.4 (R)	16.3	16.6
M^1 length	17.0 (Paratype)	15.4 (R)	20.4	20.5
M^1 anterior width	15.5 (Paratype)	-----	19.4	17.1
M^1 posterior width	15.6 (Paratype)	14.4 (R)	20.2	18.0
M^2 length	19.0 (Paratype)	16.7 (R)	22.1	23.0
M^2 anterior width	17.1 (Paratype)	15.1 (R)	21.9	20.2
M^2 posterior width	16.6 (Paratype)	14.7 (R)	21.5	19.1
M^3 length	-----	17.1 (R)	24.4	24.4
M^3 anterior width	-----	15.2 (R)	22.3	21.4
M^3 posterior width	-----	14.1 (R)	20.5	-----
M^4 length	-----	17.0 (R)	24.2	21.0
M^4 anterior width	-----	15.0 (R)	20.0	20.4
M^4 posterior width	-----	12.1 (R)	16.9	15.5

of the nasals (Fig. 58E–F). This configuration would result in a distinctive snout profile in a living animal. It is, therefore, possible that exaggeration of the anterior end of the rostrum in *Neohelos* anticipates the development of conspicuous nasal bosses in *Zygomaturus*. Some dentary horizontal rami are nearly twice as deep, though about the same length as others. The gonial angle of the ascending rami ranges from perpendicular to the longitudinal axis of the horizontal ramus to a distinctly obtuse angle of 120° or more (Fig. 59I–J). Variations also occur in the angle of the dentary symphysis and implantation angle of the lower incisors.

It is often difficult to substantiate sexual dimorphism in fossil populations due to small sample sizes and the difficulty of distinguishing sexually dimorphic characters from merely size-related allometric relationships. That a component of the variability of *Neohelos* may be due to sexual dimorphism can be drawn from analogy with other sexually dimorphic mammalian species. In the case of *Neohelos* spB, though the usable sample size of complete crania is small, the dimensions of the sagittal crest and the narial aperture show an indication of bimodality in their distribution, which is probably more indicative of sexual dimorphism than it is of simple growth allometry.

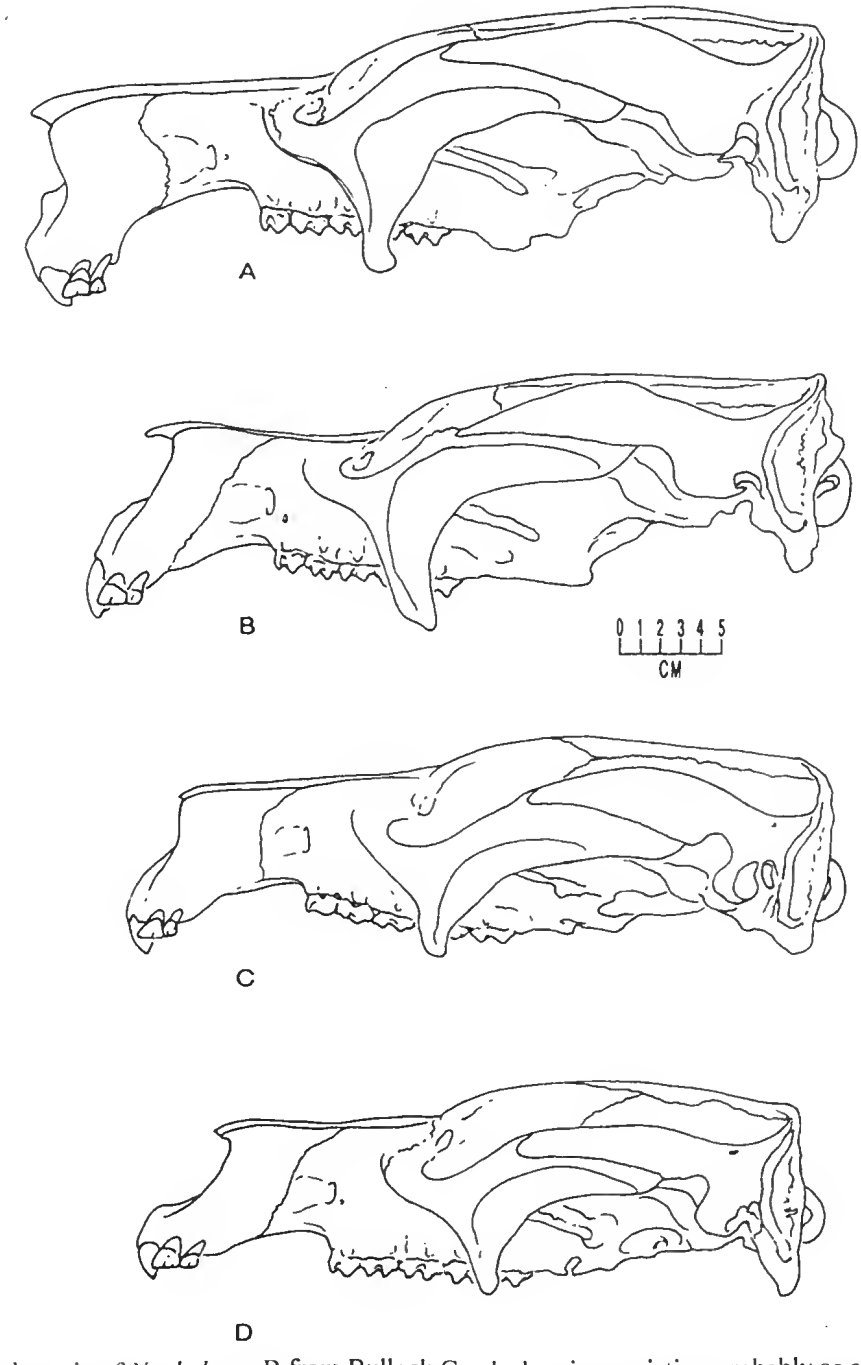

Fig. 57. Restored crania of *Neohelos* spB from Bullock Creek showing variation probably as an expression of sexual dimorphism; **A**, ? male (NTM P8695-38); **B**, ? male (NTM P8697-1); **C**, ? female CPC22200 (reference specimen); **D**, ? female (NTM P 8551-13).

Estimates of sexual dimorphism in cranial dimensions of Bulloek Creek *Neohelos* range from about 25% to 50%. Other variations in eranial and dentary shape seem to be related to stage of growth and a considerable range in individual body sizes and shapes in both sexes. The horizontal ramus tends to deepen as the animals mature, although the deepest and most robust jaws probably belong to males. It seems reasonable to assume that the deep dentaries would be assoeiated with crania having deep maxillae. The variation in the angle of the horizontal ramus may be eorrelated with extremes in eranial length, but there are no assoeiations of dentaries and erania to substantiate these remarks.

On / off distribution of character states. Certain characters appear to oscillate between genera, species or higher taxa with no apparent phylogenetic significance, though such characters may be consistently present or absent within a particular species and thus be useful in distinguishing a taxon. The presence or absence of the posterior mental foramen and the masseteric foramen are typical on / off traits in many diprotodontian groups. In *Neohelos* species the masseteric foramen is present, whereas it is usually absent in closely related *Kolopsis torus*. *Alkwertatherium webbi* lacks the foramen whereas it is present in *Plaisiodon centralis*.

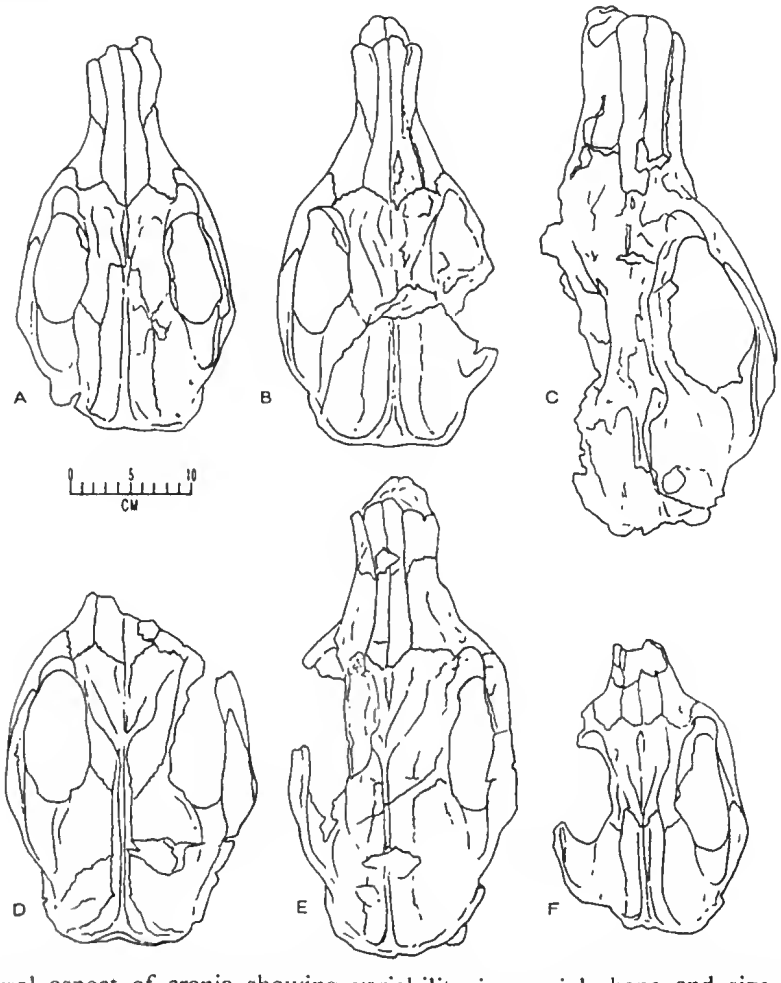

Fig. 58. A–F, Dorsal aspect of crania showing variability in cranial shape and size of adult crania of *Neohelos* spB from Bullock Creek suggestive of sexual dimorphism; **A**, NTM P8551-13; **B**, CPC 22200 (type); **C**, NTM P8695-38; **D**, NTM P87018-1; **E**, NTM P8697-1; **F**, NMV P187283.

More critical in the assessment of zygomaturine phylogeny are the states of certain characters of the P^3. *Neohelos* species express a range of states in the parastyle, parametacone and hypocone, which appear to have phylogenetic significance. The parastyle tends to be proportionally small in *Neohelos* spA and *N. tirarensis* compared to that of *Neohelos* spB, which could be interpreted as a phylogenetic trend. However, in *Alkwertatherium*, a structurally more primitive zygomaturine, the parastyle is very large, suggesting that a small parastyle is not necessarily a plesiomorphous state in *Neohelos*. Division of the parametacone into two cusps is another phylogenetically significant development in *Neohelos*, yet *Plaisiodon centralis* often has an incipiently divided parametacone and a well-developed elevation on the postparametacrista very similar to that of *Neohelos* spC.

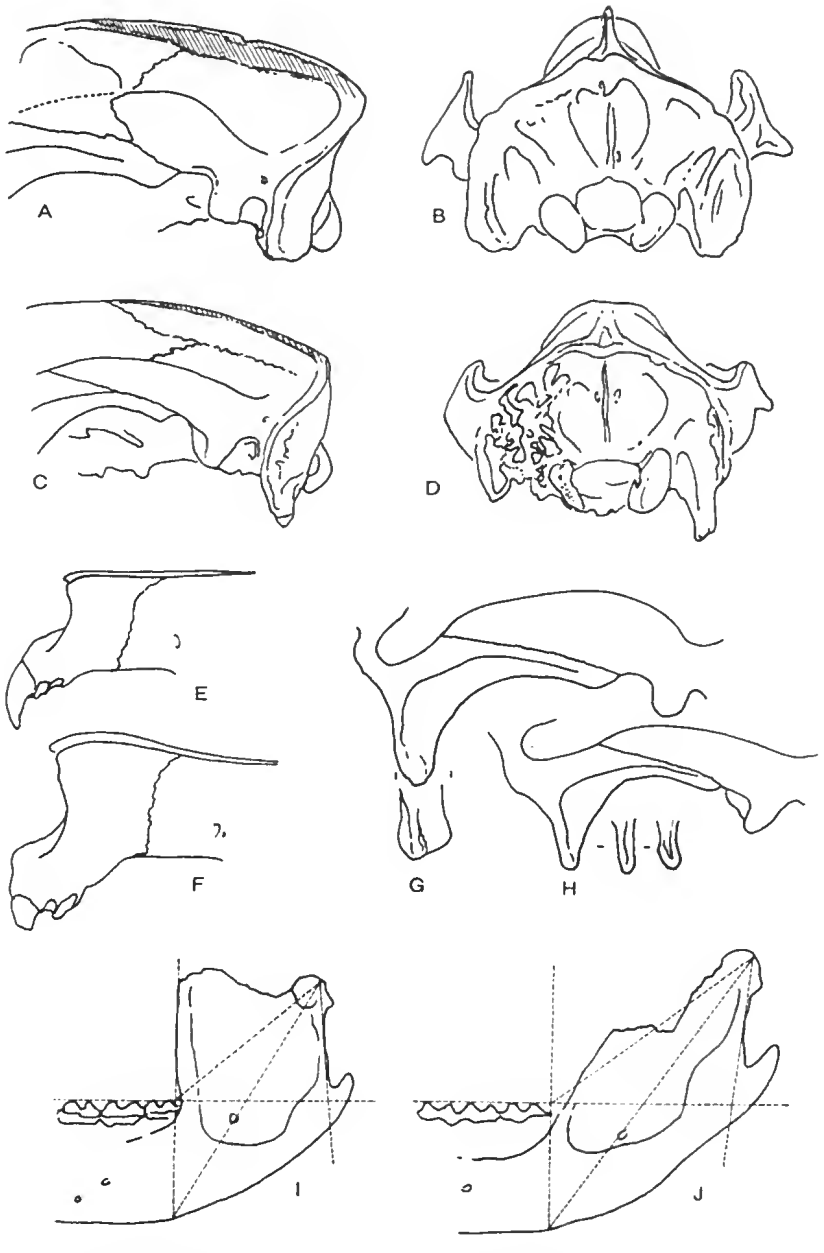

Fig. 59. Examples of variable attributes in the skull of *Neohelos* spB; **A–D**, sexually dimorphic variation in the sagittal crest; **E–F**, sexually dimorphic variation in shape of rostrum; **G–H**, variations in zygomatic arch depth and relative development of masseteric processes; **I–J**, variation in shape and inclination of posterior part of dentary.

Marshall *et al.* (1994, p. 12283) observe that in populations undergoing adaptive radiation '. . features may "flicker" on and off, resulting in a distribution of character states that does not reflect the phylogeny of the group.' They state that unexpressed genes and dormant developmental pathways for such traits may be successfully reactivated as long as six million years after their disappearance, but after ten million years, the possibility of reactivation of the character becomes remote. Marshall *et al.*'s (1994) conclusions have important consequences for cladistic methodology in that on-off character expression in rapidly speciating groups is likely to result in considerable homoplasy. Because cladistics favours the most parsimonious cladogram, a more complex, though perhaps more accurate phylogenetic reconstruction, is likely to be rejected.

The maintenance of a high degree of individual variability within the Neohelos population may have some significance in subsequent zygomaturine radiations. General heteromorphy could be linked to sexual selection for large body size in males resulting in extending overall morphological range of the species. A bull and harem type of mating pattern, often associated with sexual dimorphism, might result in smaller population isolates that would encourage a higher degree of individual variability within the general population.

However, it is likely that selection for sexual dimorphism and maintenance of individual variability within the *Neohelos* populations are subsets of predominantly environmental selective factors As indicated by recent palaeoenvironmental evidence (Murray and Megirian 1992), northern and central Australia was already undergoing vegetational changes in the early to mid Miocene. *Neohelos* spp. appear to have been the most widespread early zygomaturine, having taken advantage of more open, possibly more varied and correspondingly less predictable, though sporadically more productive habitat. As a pioneer species, its niche confines were relatively broad with perhaps correspondingly wide morphological constraints. Regardless of the particular selective agencies, it is often the case that groups undergoing rapid speciation show high individual variability.

SPECIATION AND SPECIES SUCCESSION IN *NEOHELOS*

Possibly because of the morphological variability associated with large size, combined with inadequate stratigraphic resolution and age determinations, the extent of speciation in many diprotodontid genera has not been determined satisfactorily. *Diprotodon* has been considered to have at least two species, *D. australis* Owen, 1838 and *D. minor* Huxley, 1862. The genus *Zygomaturus* has at least three species, *Z. trilobus* Owen, 1859, *Z. keanei* Stirton 1967c, *Z. gilli* Stirton 1967c, and the genus *Nimbadon* Hand *et al.* has two species, *N. lavarackorum* and *N. whitelawi*, Hand *et al.* 1993. The genus *Kolopsis* has three species: *K. torus* Woodburne 1967a, *K. rotundus* Plane 1967, and *K. yperus* Murray *et al.* 1993, although the latter two species may eventually be placed elsewhere (Murray 1993, Murray *et al.* 1993). As the largest sample of zygomaturine fossil material known, spanning by far the longest period of geological time of any diprotodontid genus, the presence of five species within *Neohelos* does not seem to be exceptional.

The characters that distinguish three of the five species of *Neohelos* have a distinct morphocline, which is primarily related to an overall increase in body size (allometry) (Figs 60, 61). With few exceptions, the specimens from a particular locality tend to be very similar in size and have specific morphological attributes. Because several localities have what appears to be essentially the same morphospecies, we infer that these collections represent distinct populations in time and space, hence a chronomorph within a morphospecies. In the cases of *Neohelos* spA and perhaps *Ni. scottorrorum*, some additional features indicate that they represent an isolate that arose from or near *N. tirarensis*. These species only partially conform to the morphocline for *N. tirarensis*, *Neohelos* spB and *Neohelos* spC. The Cleft of Ages *Neohelos* spA material is a unique population that has not been matched in any other locality.

Speciation in *Neohelos* is evaluated primarily on the basis of the states of the following characters or character complexes expressed by: 1) the main cuspid and its associated median crests of P_3; 2) the parametacone and its associated crests of P^3; 3) the lingual

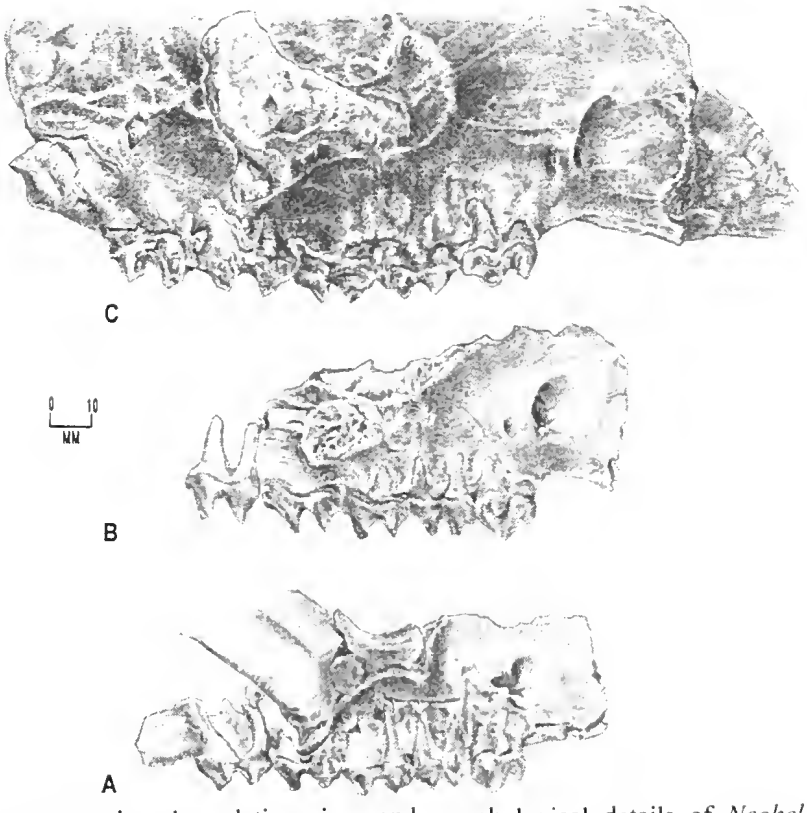

Fig. 60. Drawing comparing the relative sizes and morphological details of *Neohelos* maxillae in **A**, plesiomorphic chronomorph of *N. tirarensis* (NTM P91167-1) Upper Burnt Offerings, Riversleigh; **B**, *N. tirarensis* (AR16492) Mike's Menagerie, Riversleigh and **C**, *Neohelos* spB (BMR F20432) Blast Site, Bullock Creek.

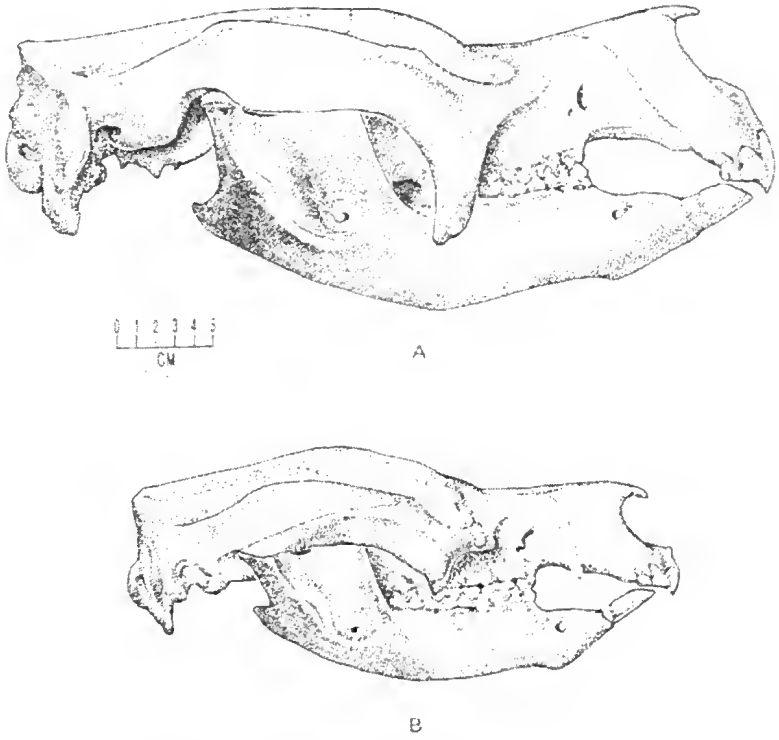

Fig. 61. Comparison of restored skulls of *Neohelos* species; **A**, lateral aspect of *Neohelos* spB (NTM P8697-1 cranium / NTMP8695-71 dentary, both from the Blast Site, Bullock Creek); **B**, *N. tirarensis* (NTM P91167-1 Upper Burnt Offerings, Riversleigh cranium / AR1695 dentary). Note allometric effects in orbit size, extent of sinus-inflation of frontals, depth of maxilla and zygomatic root.

cingulum of the upper molars; 4) the paralophid crest of M_1; 5) form of the lophs and lophids of the upper and lower molars; 6) amount of curvature of the upper cheek-tooth rows; 7) extent of size and morphological differentiation or individual molars in the upper cheek-tooth series; 8) reduction of canine and auxiliary infraorbital foramen; 9) modification of suborbital region.

Though relatively simple, the P_3 crown is systematically informative in zygomaturines (Fig. 62A,C,E,G,I). Outgroup comparison with closely related species of *Nimbadon* (crest present) and *Plaisiodon* (crest absent) indicates that the anteromedian crest is homoplasious in zygomaturines, though its presence is plesiomorphic. The crest is well developed, sharp and blade-like in *N. tirarensis* and *Neohelos* spA. The crest fades out at its termination near the base of the crown in *Neohelos* spA and among smaller examples of *N. tirarensis*. In more advanced *N. tirarensis*, a short, lingual extension of the anteromedian crest encloses a small basin. The crest is sharp and prominent in this species. In *Neohelos* spB the anteromedian crest, while usually strong, is lower and more rounded. The basal part forms a short cingulid defining a U-shaped basin. Frequently a small cuspid is present at the base of the crest. The anteromedian crest, cingulid and cuspid are autapomorphically absent in *Neohelos* spC. The absence of the anteromedian crest in this species is considered to be a character suppression having no phylogenetic significance beyond *Neohelos*.

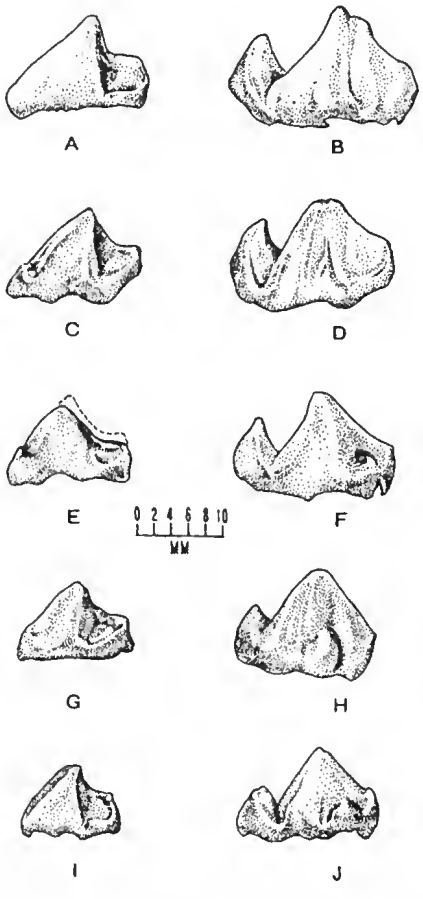

Fig. 62. Structural sequence in upper and lower P3 morphology in *Neohelos* species; **A–B**, *N.eohelos* spC Jaw Junction, Riversleigh (AR7858/AR5797); **C–D**, *Neohelos* spB Bullock Creek LF (NTM P87103-26/P8695-46); **E–F**, *N.eohelos* spB, Sticky-beak (AR13969) and Gag (AR3878); **G–H**, *N. tirarensis* (AR10841 Camel Sputum, Riversleigh / AR16492 Mike's Menagerie, Riversleigh); **I–J**, *N. tirarensis* (AR1685 D-Site, Riversleigh / NTM P91166-1 Burnt Offerings).

In the P^3 (Fig. 62B,D,F,H,J) the parametacone is very steep and short anteroposteriorly in *Ni. scottorrorum*, *Neohelos* spA and small *N. tirarensis*. The unworn parametacone cusp is bulbous. In larger *N. tirarensis* the parametacone is broader at its base relative to its height. The pre- and postparametacristae are more prominent and the unworn parametaconal cusp is elliptical anteroposteriorly. In *Neohelos* spB the unworn parametaconal cusp is made blade-like by its incorporation within the parametacrista. The preparametacrista is stronger and sharper than in *N. tirarensis*, often elevated into a prominent crest. In a few specimens, the postparametacrista forms a small lobe immediately posterior to the cusp and an incipient division of the cusps is foreshadowed by shallow lingual and labial grooves. *Neohelos* spC is autapomorphous in its development of a high, narrow lobe on the postparametacrista; a clear division of the parametacone in one individual is apomorphous, but less developed than in *Kolopsis* spp. The preparametacrista is less blade-like than in *Neohelos* spB.

The lingual cingulae of the upper molars (Fig. 63A–D) become increasingly stronger in the order *Neohelos* spA, *Ni. scottorrorum*, (absent) small *N. tirarensis*, (weak) large *N. tirarensis*, *Neohelos* spB (strong). The lingual cingulae of *Neohelos* spC do not differ from *Neohelos* spB. The paralophid crest of M_1 is highest and most blade-like in *Neohelos* spA and *N. tirarensis*, lowest and most rounded in *Neohelos* spB. In *Neohelos* spC it is slightly sharper and longer than in *Neohelos* spB. The protolophid of M_1 strongly overhangs in *Neohelos* spA, less so in *N. tirarensis* and *Neohelos* spB. However, in *Neohelos* spC, the lophids of all anterior molars have a slight overhang, at least more so than in *Neohelos* spB. The posterior faces of the molar lophs become increasing steeper (shorter) in the order: *Neohelos* spA, *N. tirarensis*, *Neohelos* spB. In *Neohelos* spC, this feature does not differ from that of *Neohelos* spB.

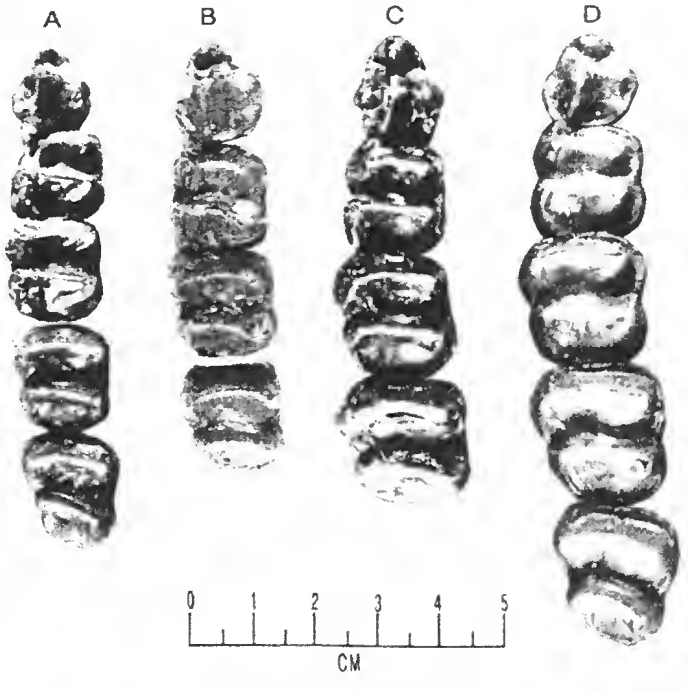

Fig. 63. Photographic comparison of *Neohelos* species upper cheek teeth: **A**, *N. tirarensis* plesiomorphic chronomorph (NTM P91167-1 Upper Burnt Offerings, Riversleigh) **B**, *N. tirarensis* (Inabeyance specimen, QM F13088) (reversed); **C**, *N.eohelos* spB plesiomorphic chronomorph (Gag Site, Riversleigh specimen, AR3878,) and **D**, *Neohelos* spB NTMP8551-13 (Bullock Creek, NT).

Curvature of the upper cheek-tooth rows increases from the essentially straight rows of small morphs of *N. tirarensis* to a distinct curvature in larger *N. tirarensis* to a stronger curvature in *Neohelos* spB (Fig. 64A–D). *Neohelos* spC is known only from isolated teeth. *Neohelos* spA appears to have slightly more curvature and more distinct gradient in the molars than in some *N. tirarensis*. Differentiation of the upper molars increases with the amount of curvature of the tooth row (Fig. 65A–D). The lower jaws and their dentitions show the same pattern (Figs 66, 67, 68).

The presence of upper canine alveoli in *N. tirarensis* is additional evidence of the plesiomorphous states of this species compared to *Neohelos* spB in which the alveolus is absent. The state of the canine is not known for *Neohelos* spA or *Ni. scottorrorum*. The progressive reduction of the auxiliary infraorbital foramen, and reduction of the infraorbital tuberosity (Figs 60, 61) also support the polarity of the morphocline through *N. tirarensis* to *Neohelos* spB to *Neohelos* spC. Although *Neohelos* spC shows three character states somewhat reminiscent of *Neohelos* spA (sharper, more elevated paralophid, overhanging lophids, slightly narrower molars) its otherwise extremely close similarities to*Neohelos* spB diminish the likelihood of a fundamental dichotomy. The evidence is overwhelmingly on the side of a gradual morphological succession of these species, originating from the smallest and earliest to culmination in the largest and latest.

Although the distinctions used to determine these palaeontological morphospecies are based on analogy with living mammalian species, we cannot determine solely on the basis of biological evidence, whether these are temporally circumscribed samples of a single, evolving species (anagenetic chronospecies) or if they represent adaptive branching within the genus. Very similar chronospecies successions are known for *Wakaleo* (Murray and Megirian 1990) and *Palorchestes* (Murray 1990a). The geological context of each species becomes an essential element in the formulation of an hypothesis of their evolutionary significance.

As discussed previously, assignments of some of the smaller species based on isolated cheek teeth are equivocal. The distinction between *Neohelos* spA and smaller *N. tirarensis* on any feature in the absence of $M_{1\text{-}2}$ must be considered tentative. There are several *Neohelos* specimens that are intermediate in size and morphology between *Neohelos* spA and *N. tirarensis* and between *N. tirarensis* and *Neohelos* spB. Given that there is considerable gradation, variability and sexual dimorphism within the normal range of each species, combined with the likelihood of the existence of some time depth within individual sites, it may not be possible to definitely assign some of these specimens either specifically or temporally.

However, the bulk of evidence supports a predominantly temporal explanation for the geological distribution of *Neohelos* species. *Neohelos* spA showing close, gradational similarities to *Neohelos tirarensis* particularly with reference to QM F23137 (=*Ni. scottorrorum*) could represent a derived form originating from an *N. tirarensis* population. Unfortunately, the polarity of this particular morphocline is not defined nor is there any good indication as to when such a cladogenic event might have commenced, other than to suggest the temporal equivalency of the Fig Tree assemblage (the absence of key *Neohelos* spA apomorphies among outgroup species strongly suggests that it is not a plesiomorphic zygomaturine). That the Cleft of Ages material might represent an extreme range of variation (e.g. subspecific) of *N. tirarensis* does not seem likely since the characters of *Neohelos* spA are confined to a population from a single locality in close geographic proximity to *N. tirarensis* localities.

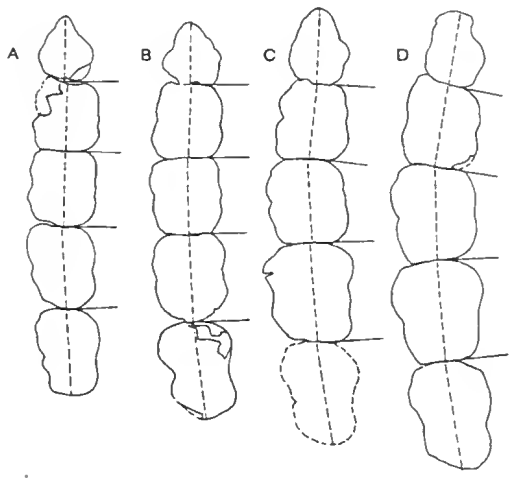

Fig. 64. Morphocline in curvature of cheek-tooth rows in *Neohelos* species; **A**, *N. tirarensis* (NTM P91167-1 Upper Burnt Offerings, Riversleigh); **B**, *N. tirarensis* (AR16492 Mike's Menagerie, Riversleigh) **C**, *Neohelos* spB (Gag Site, Riversleigh, AR3878); **D**, *Neohelos* spB (Bullock Creek, BMR F23041).

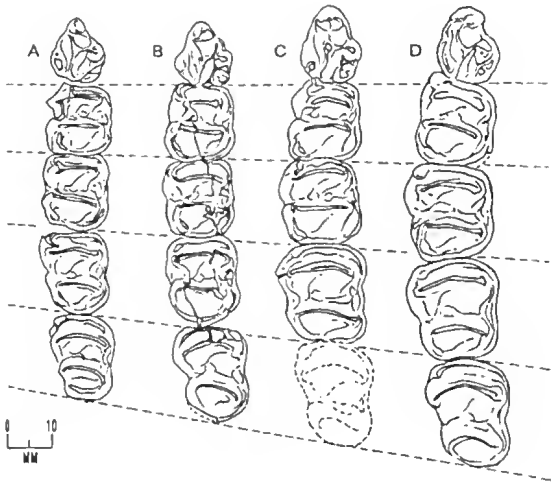

Fig. 65. Morphocline in gradient of upper cheek teeth in *Neohelos* species; **A**, *N. tirarensis*; **B**, *N. tirarensis*; **C**, *Neohelos* spB (Gag Site, Riversleigh); **D**, *Neohelos* spB, Bullock Creek.

Fig. 66. Comparison of right dentaries of *Neohelos* species; **A**, *Neohelos tirarensis*, plesiomorphic chronomorph (AR1685) D-Site, Riversleigh; **B**, *N. tirarensis* (AR10458) Wayne's Wok, Riversleigh; **C**, *Neohelos* spB, plesiomorphic chronomorph (AR13969) Sticky-beak, Riversleigh; **D**, *Neohelos* spB plesiomorphic chronomorph (AR13791) Sticky-beak, Riversleigh; E, *Neohelos* spB (NTM P8695-67) Blast Site, Bullock Creek LF.

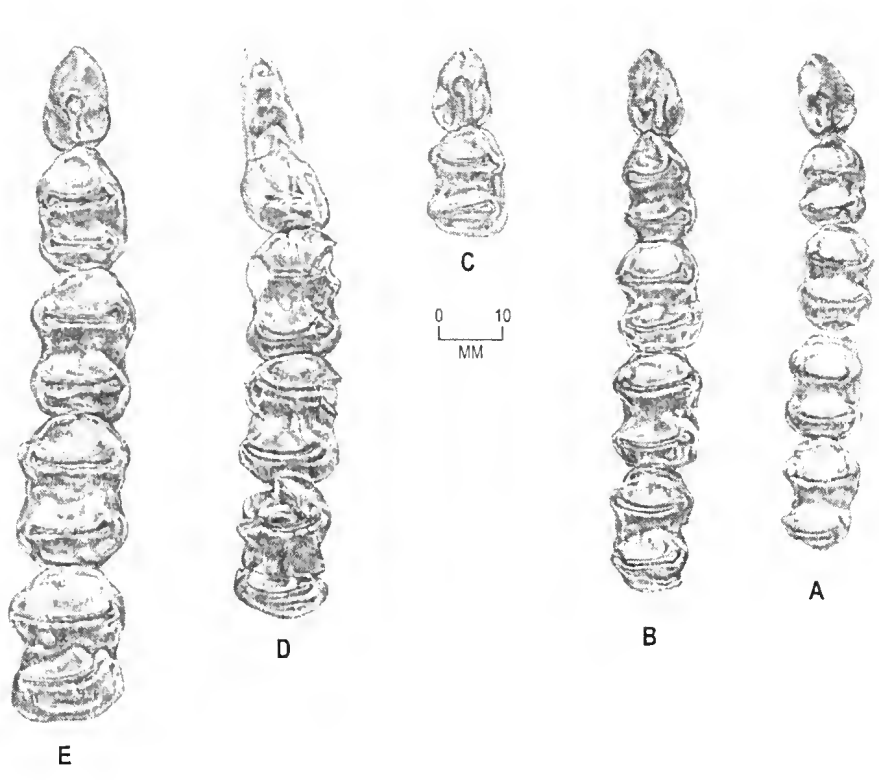

Fig. 67. Comparison of lower cheek dentitions of *Neohelos* species, occlusal aspect; **A**, *Neohelos tirarensis,* plesiomorphic chronomorph (AR1685) D-Site, Riversleigh; **B**, *N. tirarensis* (AR10458) Wayne's Wok, Riversleigh; **C**, *Neohelos* spB, plesiomorphic chronomorph (AR13969) Sticky-beak, Riversleigh; **D**, *Neohelos* spB plesiomorphic chronomorph (AR13791) Sticky-beak, Riversleigh; **E**, *Neohelos* spB (NTM P8695-67) Blast Site, Bullock Creek LF.

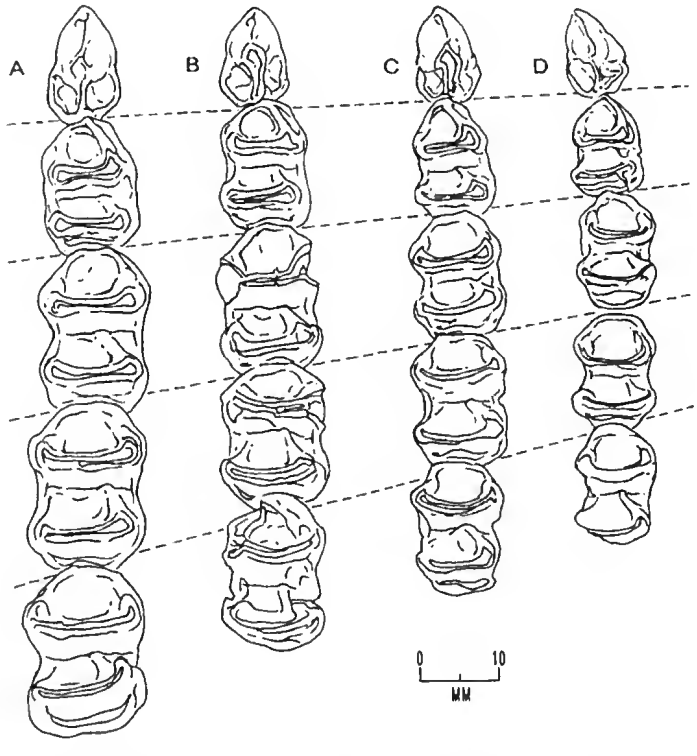

Fig. 68. Diagram showing progressive enlargement and proportional changes in lower molar crowns from *N. tirarensis* **D**, **C**, to *Neohelos* spB **B**, **A**; based on specimens in Figure 67; **B** has been restored by combining AR13969 with AR13791, both from Sticky-beak, Riversleigh.

Aside from the questions raised by the Cleft of Ages assemblage, the incremental nature of the morphocline of the remaining *Neohelos* species otherwise negates a fundamental dichotomy among the species or a near simultaneous ('bushy') radiation at a single node; structural (stage-of-evolution) successions in other genera from the same localities parallel the succession of *Neohelos* species. Consequently, we hypothesise, perhaps with the exceptions of *Ni. scottorrorum* and *Neohelos* spA, that species succession in *Neohelos* was predominantly gradualistic, perhaps with some minor temporal overlap of larger and smaller morphotypes. The localities in which these overlaps occur appear to be few (Table 18) and, as noted above, there are some alternative explanations for them besides the contemporaneous existence of more than one *Neohelos* species. We conclude that speciation within *Neohelos* is predominantly successional, chronologically significant and potentially useful for relative dating. The principle difficulties in the application of these observations is due to the high degree of individual variability within all species of this genus combined with the gradational nature of the characters that serve to distinguish one species from another.

NEOHELOS PHYLOGENY

Zygomaturines originated from the Diprotodontinae as originally suggested by Stirton *et al.* (1967). Stirton *et al.* constructed an intercalary lineage of diprotodontids, the Nototheriinae, to denote the closer relationships of the more primitive diprotodontines *Pyramios* and *Nototherium* to the zygomaturines. They were unable to further refine their hypothesis, because no structurally intermediate forms were known at the time. Two recently discovered zygomaturine genera provide evidence for the structural transition from primitive diprotodontine-like diprotodontids to primitive zygomaturines and from primitive zygomaturines to the typical zygomaturines represented by *Neohelos*. The structural succession from *Neohelos* to derived zygomaturine states found in Plio-Pleistocene genera, as proposed by Stirton and his colleagues, are supported by new evidence from anatomy and recently discovered structurally intermediate species (Fig. 69; Tables 15, 16).

Stirton *et al.* recognised the two-cusped P^3 of *Pyramios alcootense* as a structural predecessor to the zygomaturines because of its enlarged anterior lobe of the crown or presumptive parastylar base, and by the zygomaturine-like proportions of its protocone and parametacone (Fig. 5). The structure of the P^3 in other diprotodontines is derived or autapomorphous (e.g. lophodont in *Diprotodon*) or plesiomorphic (palorchestid–like, as in *Ngapakaldia* and *Pitikantia*).

The recent discoveries of two primitive zygomaturines, Gen. et sp. nov. (Archer, Hand and Godthelp 1991: 217) and *Alkwertatherium* Murray (1990a) (Fig. 69H, I) provide the previously lacking structural evidence for the origin of the Zygomaturinae from the Diprotodontinae.

Riversleigh Gen et sp. nov. shows two primary zygomaturine apomorphies in its possession of a small, but distinct parastyle, with strongly developed associated crests and a large, lobate parastylar extension of the crown on the P^3, and in the expression of an alisphenoid ventral tympanic process. The species otherwise shows many close structural similarities with the diprotodontines, particularly *Pyramios alcootense*.

Table 15. Character state polarities in the Zygomaturinae as determined by a diprotodontine outgroup (*Ngapakaldia tedfordi*) and ingroup comparisons based on primitive zygomaturines from Riversleigh and Alcoota.

	CHARACTER		APOMORPHIC	PLESIOMORPHIC	PRIMITIVE
Incisors	1	UPPER I^1	divergent tips	convergent tips	convergent tips
	2	UPPER I^{2-3}	small, buttress I^1	large, independant of I^1	large
	3	INCISOR ARCADE	narrow, U-shape	broad, C-shape	broad
C	4	UPPER CANINE	absent	present-vestigial	present
P^3	5	P^3 PARASTYLE	broad, low, close to PMC	large, separated from PMC	rudimentary
	6	HYPOCONE	large (variable)	small (variable) to absent	absent
	7	PARAMETACONE	differentiated PAC, MEC	undifferentiated-incipient	undifferentiated
	8	PARAMETACRISTAE	buccal side of crown	nearer mid-line of crown	poorly developed
	9	BUCCAL CINGULUM	weak	strong	present
	10	LINK PRC-PMC	strong	weak-absent	absent
M^1	11	OCCLUSAL SHAPE	square	trapezoidal	rectangular
	12	LOPH SHAPE	straight	slight curve, oblique	curved
	13	STYLES	reduced	large	small
Molars	14	OCCLUSAL PLANE	convex	straight	straight
	15	TOOTH ROW SHAPE	convex,	straight to slight curvature	straight
	16	ROW COVERGENCE	anterior	parallel	posterior
Cranium	17	ORBIT	frontated	lateral	lateral
	18	MASSETERIC PROCESS	long, wide	short, narrow	short, small
	19	ORBITAL PROCESS	narrow	wide	wide
	20	NASAL PROCESS	large	small-moderate	small
	21	UPPER DIASTEMA	short, constricted	long, wide to constricted	long, wide
	22	PALATE	deep, arched	shallow, flat	shallow, flat
	23	FRONTAL CRESTS	enlarged, vertical	moderately inflated	small
	24	POSTORBITAL PROCESS	absent	weak-absent	weak
	25	PMX-MX SUTURE	concave	straight, short	straight, long
	26	BASICRANIAL AXIS	marked flexion	slight flexion	straight
	27	ALISPH. TYMP. PROC.	complete, fused to mastoid	incomplete, elongated	incomplete, short
	28	POSTGLENOID PROC.	high, wide, thick, straight	high, wide, thick, oblique	low, narrow, thin
	29	EPITYMPANIC FENES.	absent	reduced, oval	large, circular
Dentary	30	ASCENDING RAMUS	elevated, upright	inclined, elevated	inclined, low
	31	DIGASTRIC EMINENCE	strong, posterior	low, mid-ramus position	weak
	32	MEDIAL FOSSAE	separated	confluent	confluent
	33	LOWER INCISOR	recumbent, pointed	procumbent, spatulate	procumbent
	34	SYMPHYSIS	long deep, fused	short, shallow, unfused	short, shallow
	35	MASSETERIC FOR.	absent	present	present
Other	36	VERT. BORD. SCAPULA	pointed, rugose	broad, thin	----
	37	INFRAGL. PR. SCAPULA	large	weak-absent	----
	38	OLECRANON PR. ULNA	wide, flange-like	narrow	----
	39	ALAE ILIUM	broad, short	narrow, long	----
	40	DELTOPECTORAL TUB.	differentiated	undifferentiated	----

Alkwertatherium webbi possesses a large parastyle, though its P^3 remains primitive in lacking a hypocone. The cranium and dentary of *Alkwertatherium* also expresses strong phenetic resemblances with both *Pyramios* (spatulate lower incisors, fused dentary symphysis, palatal shape, slight obliquity of molars) and *Plaisiodon* (cranial shape, similarity of cheek teeth, palatal form and cranial base), suggesting that *Alkwertatherium* originated from a species closely related to the antecedent of four-cusped P^3 zygomaturines (Murray 1990a).

Three genera of zygomaturines possessing a P^3 with four primary cusps are currently recognised: *Neohelos*, *Plaisiodon* and *Nimbadon*, each being distinguished from the previously discussed genera by possessing a hypocone on the posterolingual corner of the

Table 16. Distribution of character states in representative zygomaturine taxa; key: A=apomorphic; P=plesiomorphic; PV=primitive; AP=morphocline within genus ranges from plesiomorphic to apomorphic; (H)= homoplaisious characters, possible synapomorphies of *Plaisiodon* and *Kolopsoides*.

CHARACTER		*Maokapia*	*Hulitherium*	*'Kolopsis' rotundus*	*Zygomaturus* spp.	*Kolopsis* spp.	Beaumaris *'Kolopsis'*	*Neohelos* spp.	*Nimbadon* spp.	*Kolopsoides*	*Plaisiodon*	*Alkwertatherium*	Riversleigh zygomaturine	*Raemeotherium*
INCISORS	1	A	–	–	A	P	–	P	–	P	P	P	P	–
	2	A	–	–	A	P	–	P	–	–	P	P	P	–
	3	A	A	–	A	P	–	P	–	–	P	P	P	–
CANINE	4	A	A	A	A	A	–	AP	?	–	A	A	P	–
P^3	5	A	?	A	A	AP	–	P	P	A	P	P	P	–
	6	A	?	A	A	A	–	AP	P	A	P	PV	PV	–
	7	A	A	A	A	A	–	P	P	A	P	P	PV	–
	8	A	A	A	A	A	–	P	P	P	P	P	P	–
	9	A	A	A	A	A	–	P	P	A(H)	A	P	P	–
	10	A	?	A	A	A	–	AP	P	P	A	PV	PV	–
M^1	11	A	A	–	A	P	–	P	P	P	P	P	P	–
	12	A	A	–	A	P	–	P	P	P	P	P	P	–
	13	A	A	–	A	P	–	P	P	PV	PV	PV	PV	–
MOLAR ROW	14	A	A	A	A	P	–	P	P	P	P	P	P	–
	15	A	?	?	A	AP	–	AP	P	P	P	P	P	–
	16	A	A	?	A	P	–	P	P	P	P	P	PV	–
CRANIUM	17	A	A	?	A	P	–	P	–	–	P	P	P	–
	18	A	A	?	A	P	–	P	–	–	A(H)	P	P	–
	19	A	A	?	A	P	–	P	–	–	P	P	P	–
	20	A	A	?	A	P	–	P	–	–	P	P	P	–
	21	A	A	?	A	P	–	P	–	–	P	P	P	–
	22	A	A	?	A	P	–	P	P	–	P	P	P	–
	23	A	A	–	A	P	–	P	–	–	P	P	P	–
	24	A	–	–	A	P	–	AP	–	–	P	–	P	–
	25	A	–	–	A	P	–	P	–	–	P	P	PV	–
	26	A	–	–	A	P	–	P	–	–	A(H)	–	P	–
	27	–	–	–	A	AP	P	P	–	–	P	P	P	–
	28	–	–	–	A	A	P	P	–	–	P	P	PV	–
	29	–	–	–	A	A	P	P	–	–	P	P	PV	–
DENTARY	30	A	–	A	A	P	–	P	–	P	P	P	–	P
	31	A	–	A	A	P	P	P	–	P	P	P	–	P
	32	A	–	A	A	P	P	P	–	P	P	P	–	P
	33	A	–	A	A	P	–	P	–	P	P	P	–	P
	34	A	–	A	A	AP	P	P	–	A(H)	A(H)	A(H)	–	P
	35	A	–	–	A	A	P	P	–	A(H)	P	A	–	P
POSTCRANIAL	36	–	–	–	A	A	–	P	–	–	P	–	–	–
	37	–	–	–	A	A	–	P	–	–	A(H)	–	–	–
	38	–	–	–	A	A	–	P	–	–	A(H)	–	–	–
	39	A	–	–	A	A	–	P	–	–	P	–	–	–
	40	–	?	–	A	P	–	P	–	–	A(H)	–	–	–

crown (Fig. 69C, E, G). As of 1994, following the publication of *Nimbadon* (Hand *et al.* 1993) our assessment of *Neohelos* did not differ significantly from their conclusions (hypothesis A, Fig. 70A), which defined a *Neohelos tirarensis* crown group composed of four species and a *Plaisiodon centralis* crown group composed of four species and two genera.

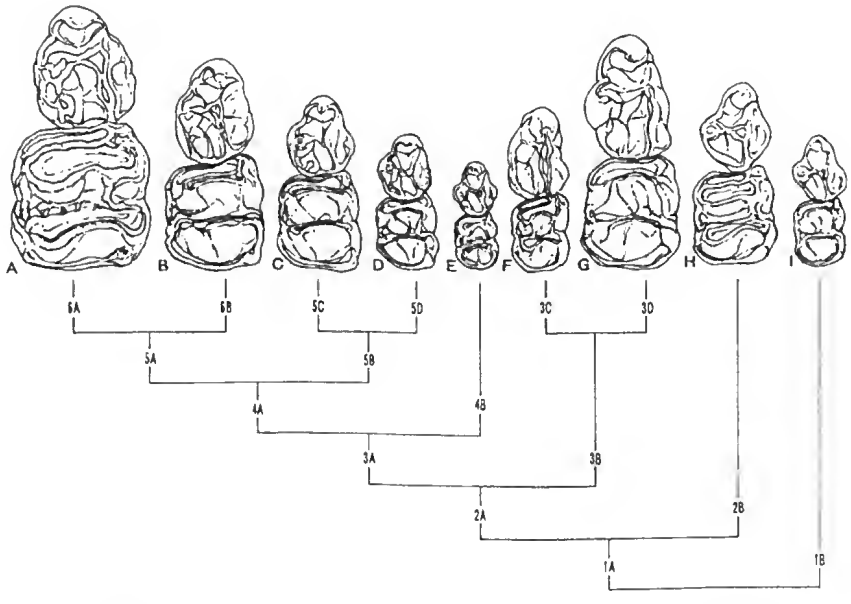

Fig. 69. Diagram depicting primary nodes (genera) in zygomaturine phylogeny based on P^3–M^1 morphology. Illustrated representative genera and species: **A**, *Zygomaturus trilobus*; **B**, *Kolopsis yperus*; **C**, *Neohelos* spB; **D**, *Nimbadon scottorrorum*; **E**, *Nimbadon whitelawi*; **F**, *Kolopsoides cultridens*; **G**, *Plaisiodon centralis*; **H**, *Alkwertatherium webbi*; **I**, Riversleigh Gen et sp. nov. Cladistic analysis for dendrogram as follows:

1: Anterior part of crown elongated, incipient parastyle evident
- 1A: P^3 parastyle large
- 1B: P^3 parastyle small, base from precingulum, hypocone absent

2: P^3 parastyle large
- 2A: P^3 hypocone present
- 2B: P^3 hypocone absent

3: Hypocone present
- 3A: P^3 with posterolabial cingulum and mesostyle
- 3B: Posterolabial cingulum and mesostyle absent on P^3
- 3C: P^3 parastyle conjoined to PMC by crest, hypocone>protocone
- 3D: P^3 parastyle hook-like, crown elongated

4: P^3 with posterolabial cingulum and mesostyle
- 4A: M^1 broad with large parastyle and metastyle
- 4B: M^1 narrow with reduced parastyle and metastyle

5: M^1 broad with large parastyle and metastyle
- 5A: P^3 parametacone divided into paracone and metacone
- 5B: P^3 parametacone undivided
- 5C: M^{1-3} postcingulum continuous horizontally around metaconule
- 5D: M^{1-3} postcingulum ascends lingual side of metaconule

6: Parametacone of P^3 divided
- 6A: M^1 parastyle and metastyle reduced, square outline
- 6B: M^1 parastyle and metastyle large, trapezoidal outline.

With the larger sample of *Neohelos*-like material at our disposal, it was apparent that *Nimbadon scottorrorum* was more similar to *Neohelos* species than to *Plaisiodon centralis* or to either of the remaining *Nimbadon* species. The P^3 morphology of the nearest outgroup species *Alkwertatherium webbi* suggests that *Plaisiodon* is no closer to *Nimbadon scottorrorum* than it is to *Neohelos* on the basis of its apomorphic loss of the posterolabial cingulum and mesostyle from the P^3. Retaining the rest of Hand *et al.*'s (1993) analysis, there are two genera united at the base by the symplesiomorphic retention of the posterolabial cingulum of P^3 as against its total loss in *Plaisiodon centralis* (Fig. 70B).

Hypothesis B (Fig. 70B) does not express the similarities of *Nimbadon scottorrorum* to specimens at the smaller end of the *Neohelos tirarensis* sample. The single known specimen of *Ni. scottorrorum* differs only subtly from typieal *N. tirarensis*, primarily in having a weak vertieal continuation of the postcingulum up the lingual side of the

metaconule. It could represent an individual variation within that species, so in hypothesis C (Fig. 70C) we have sunk the species under *N. tirarensis*, resulting in four *Neohelos* species united by the possession of large molar styles, broad rectangular molars and wide interproximal contacts. The *Nimbadon* species are united by the possession of small molar styles and narrow molars.

Simple statistical analysis of dental measurements of the *Neohelos* species outlined in detail in Appendix I reveals a close association of *Neohelos* spC with the bulk of *Neohelos* spB material. The other three *Neohelos* species plus two small samples of *Neohelos* spB form two additional clusters which are not as clearly distinct from one another as both are from the *Neohelos* spC–*Neohelos* spB group. This accords reasonably well with the phylogenetic hypothesis illustrated in Figure 70C which is based on analysis of qualitative characters of the teeth and skulls.

Hypothesis D (Fig. 70D) depicts the systematic description we have adopted for the genus. This scheme conservatively recognises *Ni. scottorrorum* as a separate species united with *Neohelos* spA on the basis of the extension of the postcingulum up the lingual flank of the metaconule. The hypothesis is preferred because it expresses the possibility that *Neohelos* spA might have originated from a form similar to *Ni. scottorrorum* for which we have a stage of evolution estimation of its age.

The relationships among these very similar genera are not completely resolved by phylogenetic analysis due to the obfuscation of characters by the derived states of *Plaisiodon* and the fineness of the character distinctions in question, which are at the level of species discriminations. *Plaisiodon* is so far known from only one late Miocene species. Although considered among the four-cusped P^3 forms, *Plaisiodon centralis* shows an elongation of the parametacone and an incipient lobate division of the parametaconal crest (Fig. 71E–F). As in *Neohelos* spC (Fig. 71A–B) the postparametacrista is elevated into a narrow secondary crest near the apex. Were it not for other characters (absence of a labial cingulum, absence of a lingual crest between the hypocone and protocone and absence of a labial crest on the parastyle) the labial profile of P^3 in some individuals of *Plaisiodon* bears a remarkable resemblance to that of *Neohelos* spC. Consequently homoplasious origins of parametaconal division in at least two zygomaturine lineages is indicated (Fig. 70).

The possibility of a close relationship between *Kolopsoides* and *Plaisiodon*, as first suggested by Archer (1984) is supported by a number of shared derived features of the P^3 including incipient division of the parametacone, reduction or loss of a posterolabial cingulum, elongation of the crown and posterior inclination of the parastyle. Other strong similarities include asymmetrically curved, pointed upper incisors and a rounded anterior cristid of the P_3 protoconid. It is, therefore, likely that the presence of a transversely divided parametacone in *Kolopsoides*, which was originally interpreted by Plane (1965) as apomorphous with *Kolopsis*, represents a homoplasious synapomorphy with *Plaisiodon* (Table 15). As the isolated, incipiently divided P^3 from Cleft of Ages, Riversleigh, (QM F20713) seems to indicate, the apomorphy character distinctions between *Neohelos* and *Plaisiodon–Kolopsoides* arose in a small species probably no later than mid-Miocene.

The fifth primary cusp of the zygomaturine P3 is represented by a transverse division of the parametacone into two distinct cusps (Fig. 69A–B). Five zygomaturine genera are known to share this apomorphic state: *Kolopsis* spp., *Zygomaturus* spp., *Maokapia*, possibly *Hulitherium* and the previously mentioned genus *Kolopsoides*. We have situated *Neohelos* as the morphological basis of a complex crown group represented by a cluster of species in the genera *Zygomaturus* Owen, *Maokapia* Flannery, *'Kolopsis' rotundus* Plane, *Hulitherium* Flannery and Plane and *Kolopsis* Woodburne.

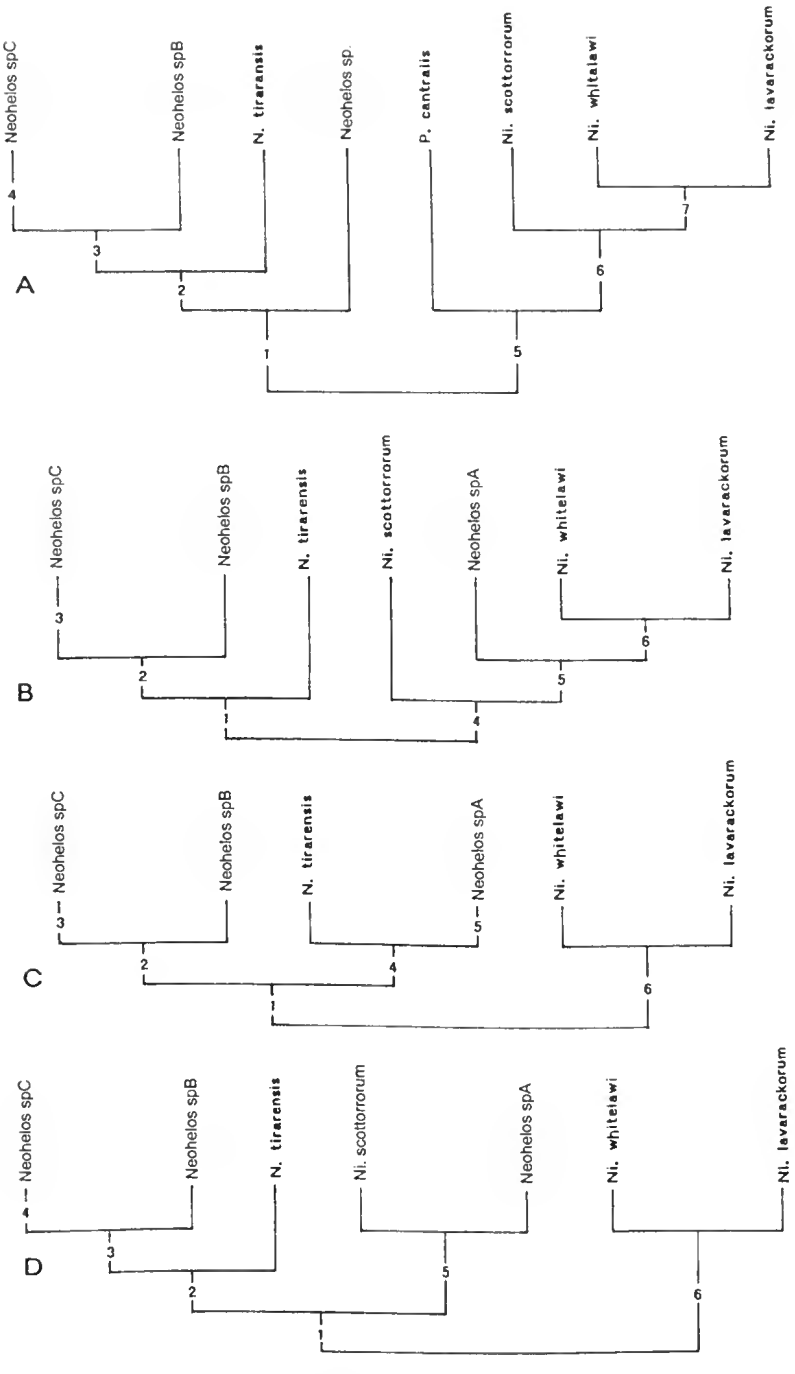

Fig. 70. Hypotheses of phylogenetic relationships of *Neohelos* species based on *Alkwertatherium webbi* outgroup comparison. **A**, dendrogram based on Hand *et al* (1993); cladistic analysis: 1) mesostyle on P^3 retracted towards cingulum; 2) larger size, more differentiation and curvature of cheek-tooth row; 3) loss of canine; 4) incipient division of P^3 PMC; 5) hooked parastyle; 6) apical blade and diagonal crest on P^3 parastyle; 7) elongation of molars; **B**, 1) increased curvature and differentiation of molar row; 2) loss of canine; 3) incipient division of P^3 PMC; 4) postcingulum ascends lingual side of metaconule; 5) elongation of molars; 6) reduction of styles on anterior molars; **C**, 1) large styles on M^{1-2}, wide IP contact, broad, rectangular molars; 2) loss of canine; 3) incipient division of P^3 PMC; 4) blend of characters via *Nimbadon scottorrorum*, incipient elevation of postcingulum; 5) postcingulum ascends lingual side of metaconule, elongation of molars; 6) reduction of styles on M^{1-2}, narrow molar crowns; **D**, 1) large styles on M^{1-2}, wide IP contact, broad, rectangular molars; 2) horizontal continuation of postcingulum around base of metaconule; 3) loss of canine; 4) incipient division of P^3 PMC; 5) postcingulum ascends lingual side of metaconule; 6) reduced styles on M^{1-2}, narrow molar crowns.

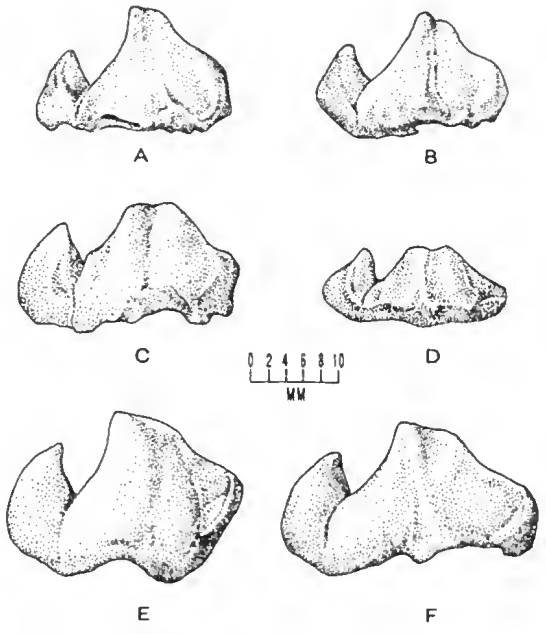

Fig. 71. Comparison of P^3's of zygomaturine species in which the parametacone is divided into two cusps; **A–B**, *Neohelos* spC; **C**, *Kolopsis yperus*; **D**, *Kolopsis torus*; **E–F**, *Plaisiodon centralis*. The resemblances between *Neohelos* spC (A–B) and *Plaisiodon centralis* (E–F) are independently derived as indicated by the presence of other distinctive characters. Twinning of the parametacone in *Kolopsis* species (C–D) appears to be derived from *Neohelos* spC, which however, possesses a higher, narrower crown in which the metacone is more accurately described as a blade-like salient rather than a cusp. Assuming that *Neohelos* spC gave rise to *Kolopsis*, the high-crowned Ongeva LF form *K. yperus*, is more similar to *Neohelos* spC than is the low-crowned *K. torus* (Alcoota LF). Alternatively, *Neohelos* spC may be too specialised to represent a direct ancestor of *Kolopsis* species.

Neohelos spC shows twinning of the P^3 as do, to a lesser degree, a few Bullock Creek specimens (e.g. NTM P87115-8 and P8695-61). The latter variants also possesses a strong anterolabial cingulum and an elevated crest between the parastyle and the anterolabial crest of the parametacone, which is frequently present in *Kolopsis torus*. Consequently there is an indication that *Neohelos* spB is potentially close to the ancestry of, if not directly ancestral to, *Kolopsis torus*. The phenetic resemblances between *K. torus* and *Neohelos* spB are about as compelling as between the lower-crowned *K. torus* and *Neohelos* spC, in which the P^3 is much higher-crowned and the labial cingulum is weak. With regard to the state of both of these characters, *Neohelos* spC bears a closer resemblance to *K. yperus* Murray *et al.* (1994), which is high-crowned and possesses a weak labial cingulum. It is thus possible that the two species of *Kolopsis* are independently derived from two species of *Neohelos* (Fig. 72A–B).

Fossil evidence from Alcoota (Ongeva Local Fauna) indicates that *Kolopsis yperus* Murray, Megirian and Wells 1993 is structurally antecedent to, or perhaps synonymous with *Zygomaturus gilli*. *Z. gilli* is known only from an isolated premolar, which we do not consider to be sufficient evidence for the assignment of the specimen to the genus *Zygomaturus* because the character states of its M^2 are not known. *Kolopsis yperus* has been retained in the genus *Kolopsis* because of certain symplesiomorphic similarities, which contrast with derived states of *Zygomaturus*; primarily in its retention of large styles on the M^2 and its retention of a large P^3 relative to M^2, the former being reduced in all Plio-Pleistocene members of the *Zygomaturus* clade (Murray 1993).

The Beaumaris '*Kolopsis*' specimens (MVP15911, P16279) variously assigned to *Z. gilli* (Woodburne 1969) or *K.* sp. (Rich 1976) remain taxonomically ambiguous, primarily due to the lack of an associated P^3. This species has relatively high-crowned, transversely narrow lower molars with strong metalophids and conspicuous apical crests on the anterolabial and anterolingual cuspids of each lophid. The P_3 is similar to that of *Kolopis torus* in possessing a strong anterolabial cingulid and to *Neohelos* spC in being somewhat elongated. Unlike *Kolopsis* spp., the Beaumaris species possesses a masseteric foramen. However, the lower molars of *Neohelos* spB and *Kolopsis torus* appear to be proportionally and structurally more alike than either species is to the Beaumaris form. Because a masseteric foramen is present in one specimen (the region is obscured by matrix in the other), and because the molar crowns are more narrow relative to their length in comparison to *Kolopsis torus* than compared to known *Neohelos* species, it is possible that it represents another, more derived species of *Neohelos*. However, it does not seem possible to resolve the position of this form without the evidence of the upper premolar.

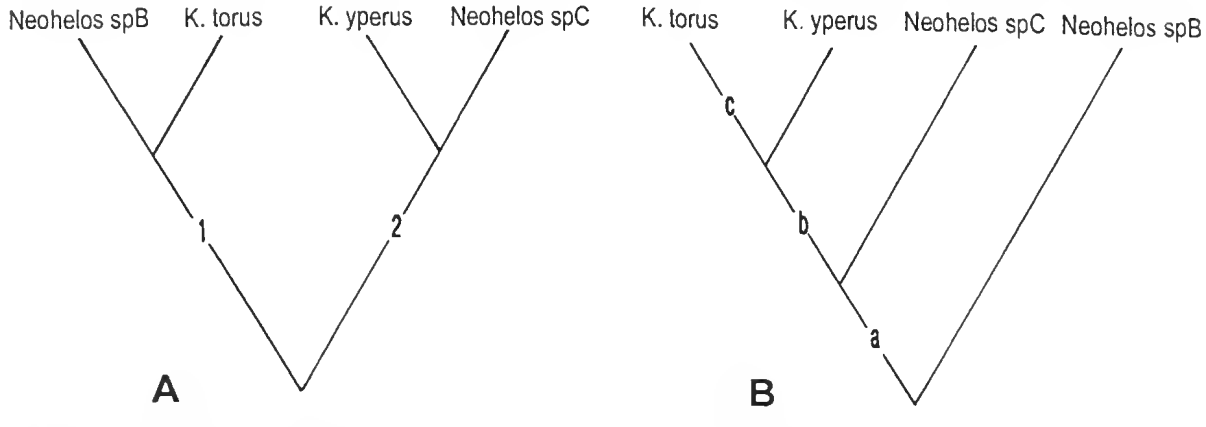

Fig. 72. Dendrograms depicting alternative hypotheses of *Neohelos* to *Kolopsis* transitions. **A**, assumes that a low crown (1) is a symplesiomorphous state shared between *Neohelos* sp**B** and *K. torus* and a high crown (2) is synapomorphous between *Neohelos* spC and *K. yperus*; **B**, suggests a more complex hypothesis in which *Neohelos* spB is the sister taxon of *Kolopsis* and *Neohelos* spC, the latter being too specialised to have been directly ancestral to *Kolopsis*; (a) is the apomorphous development of parametaconal twinning; (b) symplesiomorphous retention of more generalised, *Neohelos* spB-like P^3 crown proportions in *Kolopsis* ancestor; c) apomorphous reduction of height of P^3 crown.

An account of the morphological evidence for the proposed phylogeny of the later Zygomaturines is given by Murray (1992). In general, the available fossil evidence points to a radiation of heavy-bodied zygomaturine browsers with short, deep snouts, broad crania, with upward flexion of the basicranial axis, tusk–like, divergent upper central incisors and frontated orbits. Species of the *Zygomaturus* clade became gigantic on mainland Australia and Tasmania (*Z. trilobus*) and became dwarf-like in New Guinea ('*Kolopsis*' *rotundus*, *Hulitherium*, *Maokapia*). The immediate antecedent(s) of this group of genera (*Zygomaturus*, *Maokapia*, *Hulitherium*) have not been identified, although *Zygomaturus gilli* and *Z. keanei* remain in essentially the same basal relationship to the radiation that was postulated by Stirton *et al.* (1967).

The comparative anatomy of the cranial base in zygomaturines reinforces the broad outlines of gradual structural changes leading from primitive zygomaturines to the genus

Zygomaturus as proposed by Stirton *et al.* (1967). New evidence from the primitive Riversleigh diprotodontid Gen. et sp. nov. Archer *et al.* (1991) shows the plesiomorphous state of structures surrounding the middle ear (Figs 73A–74A). Its structural relations are fundamentally similar to that of *Ngapakaldia*: the epitympanic fenestra is large, the postglenoid process is poorly developed, low and thin, and the entoglenoid eminence and tympanic process is low and relatively small. Unlike *Ngapakaldia* and diprotodontines, the ventral surface of the tympanic process is composed of the alisphenoid instead of the squamosal, as in all members of the Zygomaturinae.

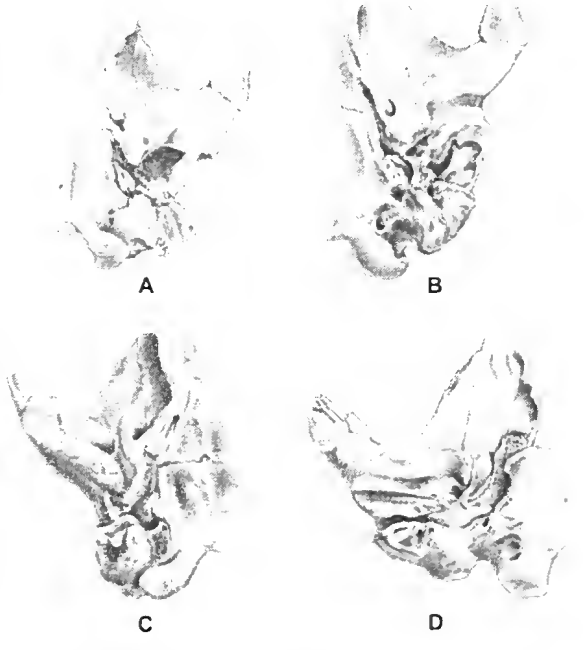

Fig. 73. Comparison of the structures surrounding the middle ear in the cranial bases of: **A**, Gen. et sp. nov. (Archer *et al.* 1991: 217); **B**, *Neohelos* spB; **C**, *Kolopsis torus*; **D**, *Zygomaturus trilobus*.

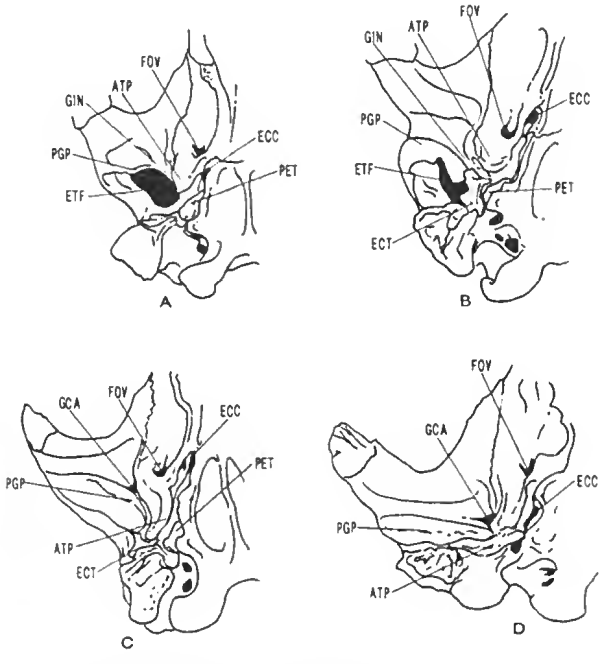

Fig. 74. Diagrams showing evolutionary trends in the middle ear structural relations in a chronological sequence from **A**, early Miocene primitive zygomaturine from Riversleigh (reversed for comparison with C-D); **B**, middle Miocene *Neohelos* spB; **C**, late Miocene *Kolopsis torus*; **D**, late Pleistocene *Zygomaturus trilobus*.

In *Neohelos* the basic structural relationships are similar to Gen. et sp. nov., but the hypotympanic sinus within the tympanic wing is enlarged and the postglenoid process has become elevated and expanded mesially and posteriorly (Figs 73B–74B). The ventral crest of the postglenoid process has overgrown its posterior margin to partially seal off the epitympanic fenestra.

In *Kolopsis torus* the posterior wall of the postglenoid process is complete, entirely sealing off the epitympanic fenestra (Figs 73C, 74C). The inner corner of the postglenoid process has encroached medially to contact the posteriorly elongated alisphenoid tympanic process, which is compressed into a narrow crest. The wide contact between the postglenoid process and the alisphenoid crest eliminates the ventrally open glenoid notch that connects the tympanic cavity with the glenoid fossa in *Neohelos* spB, but which, in *Kolopsis torus*, has become a partially enclosed glenoid canal.

In *Zygomaturus trilobus* the crest-like alisphenoid tympanic process has become fused with the base of the mastoid forming a complete tympanic wing over the tympanic cavity and has become situated parallel with, and posterior to the postglenoid process (Figs 73D, 74D). The postglenoid process has become oriented nearly at a right angle to the basicranial axis and all elements surrounding the middle ear are strongly fused.

The progressive fusion of the clements over the middle car cavity in zygomaturines is chronologically successive and non-disjunctive anatomically, providing clear evidence of gradual evolution over a period of 15 to 20 million years. An analogous process appears to have occurred in the Diprotodontinae, in which the PlioPleistocene genera *Euryzygoma* and *Diprotodon* have also undergone a process of fusion of the structures surrounding the middle ear (Fig. 75G–H).

Although much less is known of the evolution of the postcranial skeleton of the Zygomaturinae, especially the earlier forms, we have some evidence of a structural succcssion leading from *Neohelos* to *Kolopsis* and *Zygomaturus*. The postcranial skeletons of *Neohelos* and *Kolopsis* are very similar except for certain features of the forelimb, in which *Kolopsis* shows some similarities with *Zygomaturus*. In *Neohelos* the vertebral border of the scapula is broad, whereas it is narrower and morc pointed in *Kolopsis* (Fig. 76A, C). A rudimentary infraglenoid tuberosity is present in *Kolopsis* which is not present in *Neohelos*. In *Kolopsis* the olecranon process of the ulna is transverscly expanded in comparison to that of *Neohelos*. Each of these characters appear to be transitional states between *Neohelos* spB and *Zygomaturus trilobus* (Fig. 76A, C, D).

The postcranial morphology of *Plaisiodon centralis* is proportionally more similar to that of *Neohelos* than the other zygomaturine genera for which the postcranial skeleton is reasonably well-known (Fig. 76B). *Plaisiodon centralis* is derived relative to *Neohelos* and homoplasious relative to *Kolopsis* and Zygomaturus in possessing a broadened infraglenoid table of the scapula, which however, is not developed into a distinct process. As in *Neohelos*, the vertebral border is broad and relatively thin, rather than narrow and thickened, as characteristic of *Kolopsis* and *Zygomaturus*. The olecranon process of the ulna of *Plaisiodon* is broad compared to that of *Neohelos* but takes the form of a very short, flattened tuberosity, quite distinct from that of *Kolopsis* and *Zygomaturus*.

As in *Zygomaturus*, but not *Neohelos* or *Kolopsis*, a distinct pectoral tuberosity appears to have been present adjacent to a well-developed deltoid tuberosity. Because this region is damaged in all of the available specimens of *Plaisiodon*, a more detailed comparison with the humerus of *Zygomaturus* must await a morc perfect specimen. Comparisons of the available postcranial material indicatcs that *Neohelos* is the more suitable structural precursor to the lineage leading to *Zygomaturus*. *Plaisiodon centralis* is too derived in certain features, while otherwise retaining a majority of states closely resembling those of *Neohelos*.

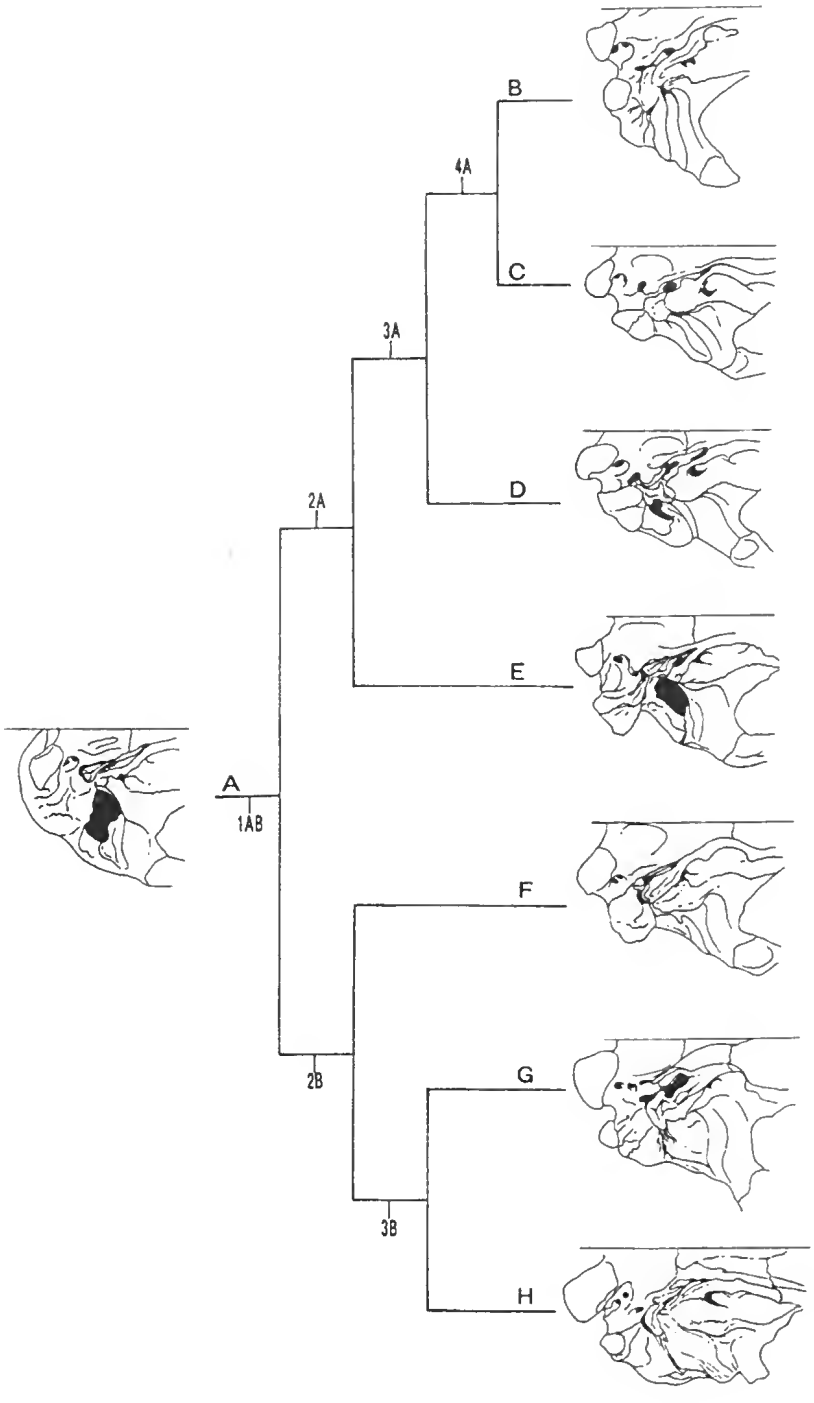

Fig. 75. Phylogeny of the Diprotodontidae determined by the morphology of the basicranium of representative genera: A, *Ngapakaldia tedfordi* is depicted as representing the plesiomophic state for the family Diprotodontidae. B–E, are members of subfamily Zygomaturinae; F–H, are members of subfamly Diprotodontinae. B, *Zygomaturus trilobus*; C, *Kolopsis torus*; D, *Neohelos* spB; E, primitive zygomaturine; F, *Pyramios alcootense*; G, *Euryzygoma dunense*; H, *Diprotodon sp.*; Apomorphies at designated nodes: 1AB=large epitympanic fenestra, weak postglenoid process and squamosal tympanic process; 2B=wider, deeper, but thin postglenoid process, not fused to posterior or mesial elements; reduced or absent epitympanic fenestra, squamosal tympanic process enlarged; 3B=posterior elongation and fusion of the postglenoid process mesially with the tympanic process and with the mastoid-squamosal posteriorly forming complete auditory meatus; 2A=alisphenoid tympanic process; 3A=reduced epitympanic fenestra, inflated entoglenoid eminence or bulla; 4A=loss of epitympanic fenestra, elongation and fusion of alisphenoid tympanic process and postglenoid process.

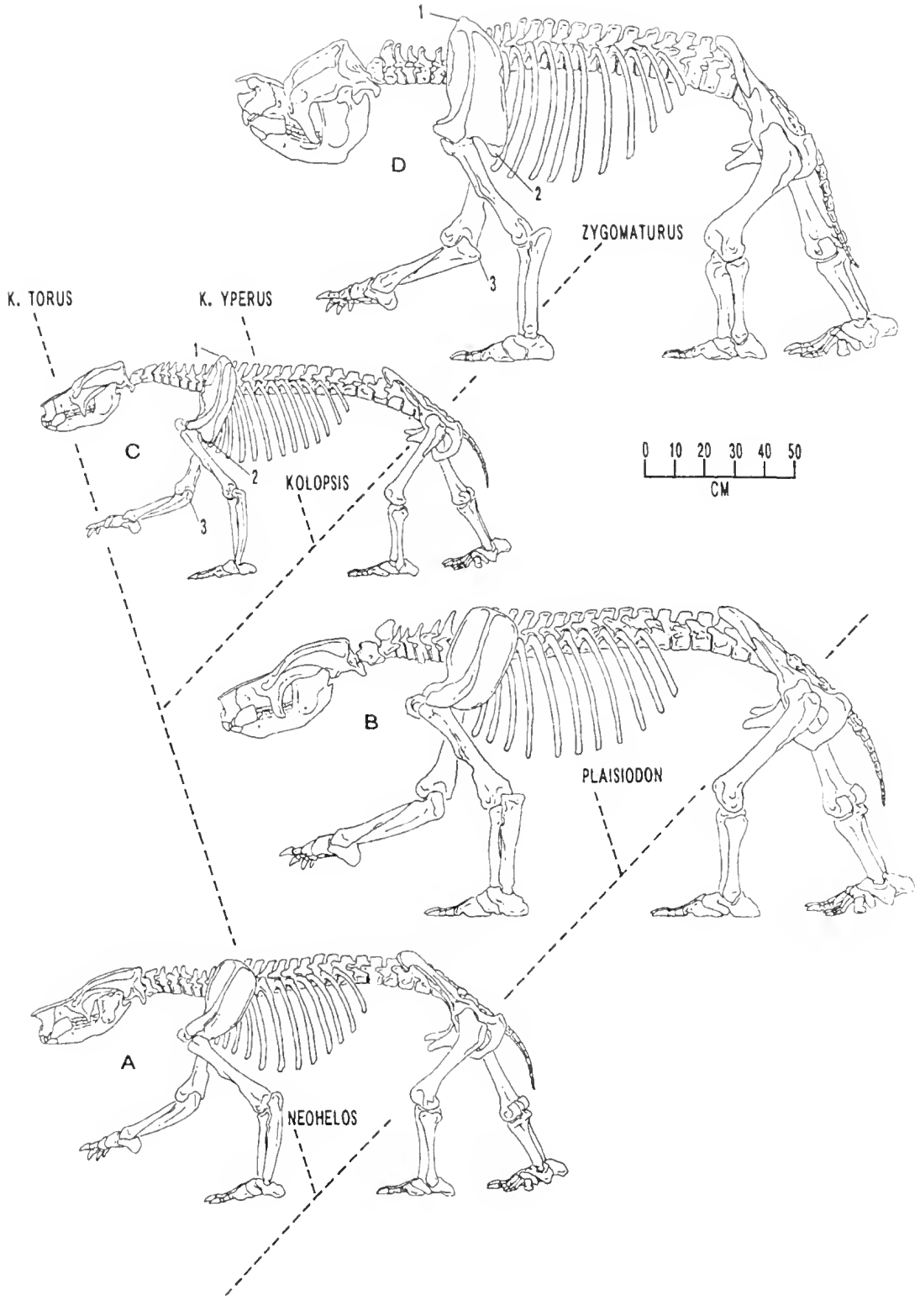

Fig. 76. Restored skeletons of **A**, *Neohelos* spB; **B**, *Plaisiodon centralis*; **C**, *Kolopsis torus*; **D**, *Zygomaturus trilobus*; broken lines indicate relationships based on postcranial morphology: *Neohelos–Plaisiodon*=symplesiomorphous; *Kolopsis–Zygomaturus*=synapomorphous: 1, similarity in olecranon process shape; 2, pointed, thickened vertebral border of scapula; 3, elongated infraglenoid process. The form of the manus and pes are inferred from incomplete material, some of which is known for each genus depicted. All of these genera have laterally flanged 5th metatarsals and metacarpals, large calcanei and pisiforms, large ungual phalanges on both manus and pes, short, broad phalanges and reduced metatarsals II–III.

BIOCHRONOLOGY OF THE ZYGOMATURINAE

Gingerich (1979) outlined an approach to the elucidation of evolutionary relationships between fossil species well–represented in a continuous stratigraphic record. To paraphrase Gingerich (1979: 49–50), detailed stratigraphic information combined with phenetic clustering of the fossil material provides an empirical record of phylogeny, which he termed a 'stratophenetic phylogeny'. He demonstrated the approach using richly fossiliferous mammal sequences of North America and Europe.

An empirical record of phylogeny is not simply a palaeobiological statement, but is a manifestation of geological time, and hence can have a practical application in correlation. Of course, it is not necessary to recognise phylogeny in a continuous stratigraphic sequence in order to apply palaeontological data to correlation (i.e. biostratigraphic correlation), but where a stratigraphic record is discontinuous and incomplete, a phylogenetic hypothesis based on the relative stage–of–evolution of closely related species can sometimes be used to correlate disjunct strata. In stage–of–evolution biochronology, stratigraphic superposition of taxa, where it can be observed, provides independent control on inferences of evolutionary trends within lineages.

Stirton, Woodburne and Plane (1967, fig. 2) produced a stage–of–evolution biochronology for the Diprotodontidae which represented a significant step in the development of a correlation framework for Australian continental sediments hosting vertebrate remains. As the Zygomaturinae remain one of the most useful clades for correlation in Australia and New Guinea, a revised biochronology is presented below.

Method. Information used in the construction of stage–of–evolution biochronologies, ranked from the observable to the inferential, includes:

1. Empirical evidence for organic evolution (evolutionary change between forms in chronostratigraphic succession).

2. The co-existence of related morphospecies within a bed (empirical evidence that cladogenesis has occurred at some earlier time).

3. Geochronometry (techniques of calibrating observations of relative age derived from stratigraphy, and determining ages of chronostratigraphically unconfined fossil occurrences).

4. Phenetic clustering of taxa (e.g. Rich 1991, Fig. I–1, or the clusters developed in this paper on the basis of dental measurements – Appendix 1).

5. Co–existence of closely related forms within an inferential isochron (implying cladogenesis occurred at some earlier time).

6. Hypotheses of evolutionary relationships based on shared, derived, morphological character states.

In graphical terms, a stage–of–evolution biochronology consists of a phylogeny of fossil species superimposed on a succession of time planes (horizons). Information sets 1 to 5 either wholly or in part determine the time planes (fixed points of reference) that an evolutionary hypothesis must satisfy.

In the absence of chronostratigraphic or geochronological control, anagenetic speciation is presumed if a form interpreted to represent a more primitive stage–of–evolution possesses

no derived features which precludes its direct ancestry of a more derived form. These data, for the zygomaturines are summarised below with short commentaries accompanying Tables 17 to 24. The status of additional named Pliocene and Pleistocene diprotodontids (e.g. Archer *et al.* 1984: 1041, 1045) are under investigation (Brian Mackness pers. comm.), and most are excluded from this review because they are either poorly known, synonymous, or of uncertain affinity (Murray 1991). *Zygomaturus trilobus*, a well established form, is included, though Murray (1991: 1098) observed that it was either "...highly variable, or there was more than one species".

Superposition, coexistence of taxa, and geochronometric control. *Lake Eyre Basin, South Australia* (Table 17). The late Oligocene Etadunna Formation of the Lake Eyre Basin is taken here as the reference standard for zygomaturine succession. The Etadunna Formation itself contains only fragmentary remains of *Neohelos* sp. (Woodburne *et al.* 1993 and N. Pledge written comm.), but the formation unconformably underlies the Wipajiri Formation, type stratum for *Neohelos tirarensis* Stirton. The Etadunna Formation is thought to span 24 to 26 MY BP on the basis of a radioisotopic date on illite, foraminiferal biostratigraphy and palaeomagnetic data, as discussed in Woodburne *et al.* (1993). The Wipajiri Formation is thought to be only slightly younger than the Etadunna Formation: Woodburne *et al.* (1993) suggest an age based on palaeomagnetic data as old as 23.8 MY.

Table 17. Summary of superpositional relationships, geochronology and taxonomy of Lake Eyre Basin Zygomaturinae. Abbreviations: I, calibrated invertebrate biostratigraphy; P, palaeomagnetic; R, radioisotopic; *, type locality for taxon.

Lithostratigraphy	Age (MY) and basis	Fauna (F) Local Fauna (LF) Zone	Zygomaturinae	Source
Katipiri Formation	0.04 P	Malkuni F	*Zygomaturus* sp.	Tedford and Wells 1990
		Kalamurina F	*Zygomaturus* sp.	
unconformity				
Tirari Formation	3.9 - 3.4 P	Palankarinna F	*Zygomaturus keani**	Stirton 1967;
		Kanunka F	cf. *Kolopsis* sp.	Tedford *et al.* 1992
			cf. *Zygomaturus* sp.	
		Toolapinna F	*Zygomaturus* sp.	
unconformity				
Wipajiri Formation	?23.8 P	Kutjamarpu LF	*Neohelos tirarensis**	Stirton 1967
unconformity				
Etadunna Formation	26 – 24	zone E	*Neohelos* sp.	Woodburne *et al.* (1993)
	P, R, I	zone D / Ngama LF	*Neohelos* sp.	
		zone B / Ditjimanka LF	*Raemeotherium* sp.	

Raemeotherium yatkolai, described from a lower jaw, two isolated I^3s and two isolated lower molars from the Namba Formation (Ericmas Fauna) of the Tarkarooloo Basin, is a possible zygomaturine, and / or one of the most structurally-primitive diprotodontids known (Rich *et al.* 1978). The Ericmas Fauna is correlated with zone B of the Etadunna Formation, which contains a possible representative of the genus (Woodburne *et al.* 1993). The Ericmas Fauna pre-dates the Etadunna *Neohelos* occurrences, but because of the small difference in age, and in the absence of a third upper premolar which might be instructive about the sub-familial affinities of the taxon, it is regarded here as a plesiomorphic sister taxon of all other zygomaturines, rather than as a direct ancestor of any other taxon.

Karumba Basin, Carl Creek Limestone, Queensland (Table 18). No explicit account of stratigraphic superposition of *Neohelos* morphospecies is available for the Carl Creek Limestone. Demonstration of chronostratigraphic relationships between fossil assemblages (Fig. 77) thought to be of significantly different age has so far not been possible because of a lack of marker beds or discontinuities traceable through the formation (Tedford 1967, Megirian 1992).

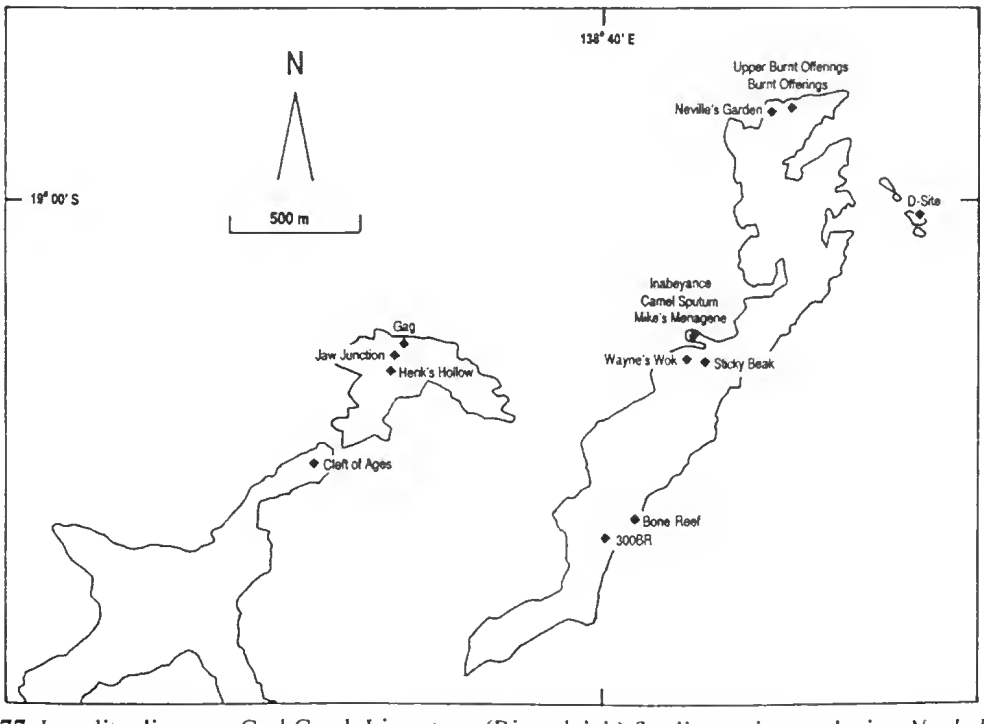

Fig. 77. Locality diagram, Carl Creek Limestone (Riversleigh) fossil quarries producing *Neohelos*.

Based on stage–of–evolution criteria, the occurrence of *Neohelos* spB at Gag Site, Sticky–beak and Henk's Hollow together with even more advanced *Neohelos* spC at Jaw Junction, suggests that those four Riversleigh sites are younger than all other localities in that area where *Neohelos tirarensis* is known to occur; namely 300BR, Burnt Offerings, Camel Sputum, Fig Tree, Inabeyance, Mike's Menagerie, Neville's Garden, Bone Reef, Cleft of Ages, Jim's Jaw Site, Upper Burnt Offerings, D-Site and Wayne's Wok. Statistical analysis of this material, detailed in Appendix I further reinforces the distinctiveness of the Henk's Hollow and Jaw Junction *Neohelos* specimens, for they consistently cluster with the large assemblages of *Neohelos* spB from Bullock Creek.

Within *Neohelos*, the structural progression, from the most plesiomorphic to the most derived, is *N. tirarensis*, *Neohelos* spB, *Neohelos* spC. Does this morphocline represent an evolutionary succession with geochronological significance, or does it reflect spatial factors, where the geographic distribution of contemporaneous species was perhaps controlled by palaeoecological factors?

There are no structural features present in a more plesiomorphic form that precludes its direct ancestry to the more derived form, and thus no grounds for postulating unknown common ancestors to link representatives of the five species. Although one of the Riversleigh assemblages (Sticky–beak) contains material assigned to two species of *Neohelos* (Table 18) the apparent 'contemporaneity' of any two forms may not be genuine.

The suggestions of temporal overlap in *Neohelos* species can be challenged on the basis of possible sample error, diachronous assemblages, and ambiguities in the assignment of poorly preserved material, as discussed previously. Certainly the data are far too sparse to present a definite case for the co–existence of two *Neohelos* populations.

The observed morphocline of *Neohelos* species is similar to that documented in the palorchestids (*Propalorchestes ponticulus–P. novaculacephalus–Palorchestes painei*: Murray 1990a) and thylacoleonids (*Wakaleo* sp. nov.– *Wakaleo oldfieldi–Wakaleo vanderleueri*: Murray and Megirian 1990); that is, gradual evolution of dental and cranial characters primarily in conjunction with an overall increase in body size. The indications are that *Neohelos* species represent a chronocline (Table 18).

Table 18. Carl Creek Limestone fossil sites grouped according to the biochronologically-useful species of *Neohelos*, from *N. tirarensis* (primitive stages–of–evolution) — *Neohelos* spB (intermediate stages–of–evolution) — *Neohelos* spC (advanced stage–of–evolution). As discussed in the text, *Neohelos* spA and *Nimbadon scottorrorum* possibly represent relative stage–of–evolution closer to *Neohelos tirarensis* than *Neohelos* spB or *Neohelos* spC. The only quarry apparently containing two morphospecies of *Neohelos* (Sticky-beak) is inderlined. (*) is the type locality of the species.

Species	Site	Co-occuring zygomaturine species	Species at an equivalent stage-of-evolution?
Neohelos spC	Jaw Junction		
Neohelos spB	Henk's Hollow	*Nimbadon lavarackorum*	
	Gag		
(plesiomorphic form)	Sticky-beak		
N. tirarensis			*Neohelos* spA (Cleft of Ages) *Nimbadon scottorrorum* (Fig Tree*)
	Camel Sputum		
	Wayne's Wok		
	Nevilles Garden		
	Mike's Menagerie		
	Jim's Jaw Site		
	Inabeyance		
(plesiomorphic form)	D-Site		
	Bone Reef		
	Sticky-beak		
	300 BR		
	Upper Burnt Offerings		
	Burnt Offerings		

Camfield Beds, Northern Territory (Table 19). The palaeontology of the Camfield Beds was most recently summarised by Murray and Megirian (1992). The stratigraphic relationships between various fossil quarries in the Camfield Beds remain unresolved. There is no evidence that an evolutionarily significant period of time is represented by vertebrate fossils from the Camfield Beds, which are united into a single local fauna (Bullock Creek LF). The only age constraint on the local fauna comes from stage-of-evolution comparisons. The Bullock Creek LF is interpreted to be younger than the Kutjamarpu LF (Wipajiri Formation, Lake Eyre Basin), but older than the Alcoota LF (Waite Formation, Waite Basin) on the basis of palorchestids (Murray 1990b), thylacoleonids (Murray and Megirian 1990) and zygomaturines (this work).

Table 20. Summary of co-existence of Camfield Beds Zygomaturinae. The 'Horseshoe West Locality', one of many assemblages assigned to the Bullock Creek LF, contains both *Neohelos* spB and *Nimbadon whitelawi*. The age of the Camfield Beds are bracketted only on the basis of stage-of-evolution as discussed in the commentary. * denotes the type locality of the taxon.

Lithostratigraphy	Age (MY) and basis	Local Fauna (LF)	Zygomaturinae	Source
Camfield Beds	-	Bullock Creek LF	*Neohelos* spB	Murray *et al.*(this work)
			*Nimbadon whitelawi**	Hand *et al.* (1993)

Waite Basin, Waite Formation, Northern Territory (Table 20). The Waite Formation is a stratified deposit in central Australia. Fossils are known from two stratigraphic levels, neither of which have been dated. The Ongeva LF is unconformably above the Alcoota LF. On the basis of zygomaturine stage-of-evolution (Murray *et al.* 1993; Megirian *et al.* 1996), the two Waite Formation local faunas are considered to be slightly older than the Beaumaris LF of Victoria which is dated by invertebrate biostratigraphy.

Table 20. Summary of superpositional relationships and taxonomy of Waite Basin Zygomaturinae. The age of the strata are bracketted only on the basis of stage-of-evolution as discussed in the commentary. * denotes the type locality of the taxon

Lithostratigraphy	Age (MY) and basis	Local Fauna (LF)	Zygomaturinae	Source
Waite Ftn				
	-	Ongeva LF	*Kolopsis yperus**	Murray *et al.* (1993)
			cf. *Kolopsis* sp.	
unconformity				
	-	Alcoota LF	*Kolopsis torus**	Woodburne (1967a,b)
			*Plaisiodon centralis**	
			*Alkwertatherium webbi**	Murray (1990)

Black Rock Sandstone, Victoria (Table 21). The Black Rock Sandstone is a marine deposit containing the Chelthamian stratotype. The age of the Cheltenhamian is not entirely satisfactorily resolved but is accepted to be Mio-Pliocene. The presence of marsupials within the Stage makes the Beaumaris LF particularly significant in marsupial biochronology (Rich 1991: 1037).

Table 21. Summary of the marsupial palaeontology of the Black Rock Sandstone. * denotes the type locality of the taxon.

Lithostratigraphy	Stage and Age (MY)	Local Fauna (LF)	Zygomaturinae	Source
Black Rock Sandstone	Cheltenhamian c. 5	Beaumaris LF	*Zygomaturus gilli**	Stirton (1967)
			Kolopsis sp.	Rich (1976)

Allingham Formation, Queensland (Table 22). Basalt used for radioisotopic dating were collected about 10 km along strike from the source of the fossils (Rich *et al.* 1990: 1041). The validity of the minimum age of the Bluff Downs LF thus depends on the correctness of the interpretation of stratigraphic relationships between the basalt and the fossiliferous sediments.

Otibanda Formation, New Guinea (Tables 24, 25). The Awe Fauna represents the base of the marsupial record of New Guinea, which is the product of collision of the Australian–

Table 23. Summary of the age and taxonomy of the Bluff Downs Local Fauna zygomaturine.

Lithostratigraphy	Age (MY) and basis	Local Fauna (LF)	Zygomaturinae	Source
Allensleigh Flow, Nulla Basalt	4.5 , 4.0 R			
conformity				
Allingham Formation	> 4.5 , 4.0	Bluff Downs LF	*Zygomaturus* sp.	Rich *et al.* (1990)

Indian and Pacific plates. Early radioisotopic dates of Evernden *et al.* (1964) of 7.6 MY for the Otibanda Formation were subsequently revised upwards (Page and McDougal 1972; Hoch and Holm 1986). The Otibanda Formation dates provide minimum ages for the emergence of New Guinea as a discrete biogeographic zone, but as New Guinea shares no marsupial fossil species with Australia, the time, or times, of colonisation of the island can only be inferred by stage-of-evolution considerations.

Table 24. Summary of the New Guinean Otibanda Formation zygomaturine occurrences. R = radioisotopic date; * denotes type locality for the taxon.

Lithostratigraphy	Age (MY) and basis	Local Fauna (LF)	Zygomaturinae	Source
Otibanda Formation	3.3, 2.5: R Hoch and Holm (1986)	Awe LF	*Kolopsis rotundus** *Kolopsoides cultridens**	Plane (1967)

Table 25. Additional dated zygomaturine occurrences from New Guinea and Australia. P = palaeomagnetic date; R = radioisotopic date; * denotes type locality for the taxon.

Lithostratigraphy	Age (MY) and basis	Local Fauna (LF)	Zygomaturinae	Source
un-named formation, Pureni, New Guinea	0.038: palynology	un-named	*Hulitherium thomasettii**	Flannery and Plane 1986
fissure-filling in Moorabool Viaduct Sand, Victoria	2.03 - 2.48: P	Dog Rocks LF	*Zygomaturus* sp.	Rich *et al.* 1991
Comadai Limestone, Victoria	3.40 - 3.64: R, P	Coimadai LF	*Zygomaturus* sp.	Rich *et al.* 1991

Synthesis. A stage-of-evolution biochronology for the zygomaturines is shown in Figure 78. It incorporates ideas presented above about possible relationships and affinities of named and unnamed taxa, summarised as follows:

1. Because it is not certain that *Raemeotherium yatkolai* is a zygomaturine, it is shown as a plesiomorphic sister taxon to all other zygomaturines;
2. The zygomaturine Gen. et sp. nov. figured in Archer *et al.* (1991: 217) is the plesiomorphic sister taxon to all other zygomaturines;
3. One or more of the unnamed zygomaturines from Cleft of Ages show as close an affinity to *Plaisiodon* and *Kolopsoides* as to *Neohelos*;
4. *Nimbadon scottorrorum* may be a species of *Neohelos*.
5. *Zygomaturus* may have evolved from *Neohelos* through *Kolopsis yperus* rather than *Kolopsis torus*, which may share a common ancestor with a *Neohelos* species

(perhaps *Neohelos* spC). The Beaumaris zygomaturine identified by Woodburne (1969) as *Zygomaturus* and by Rich (1976) as *Kolopsis*, may be a *Neohelos* species;

6. Murray (1992) previously outlined reasons for including *Kolopsis rotundus* in the *Zygomaturus gilli* crown group.

These hypotheses should be well-tested before any taxonomic revisions are proposed. The taxonomy used in Figure 78 should be regarded as labels of convenience for morphotypes from specific strata, rather than as Linnaean binomials.

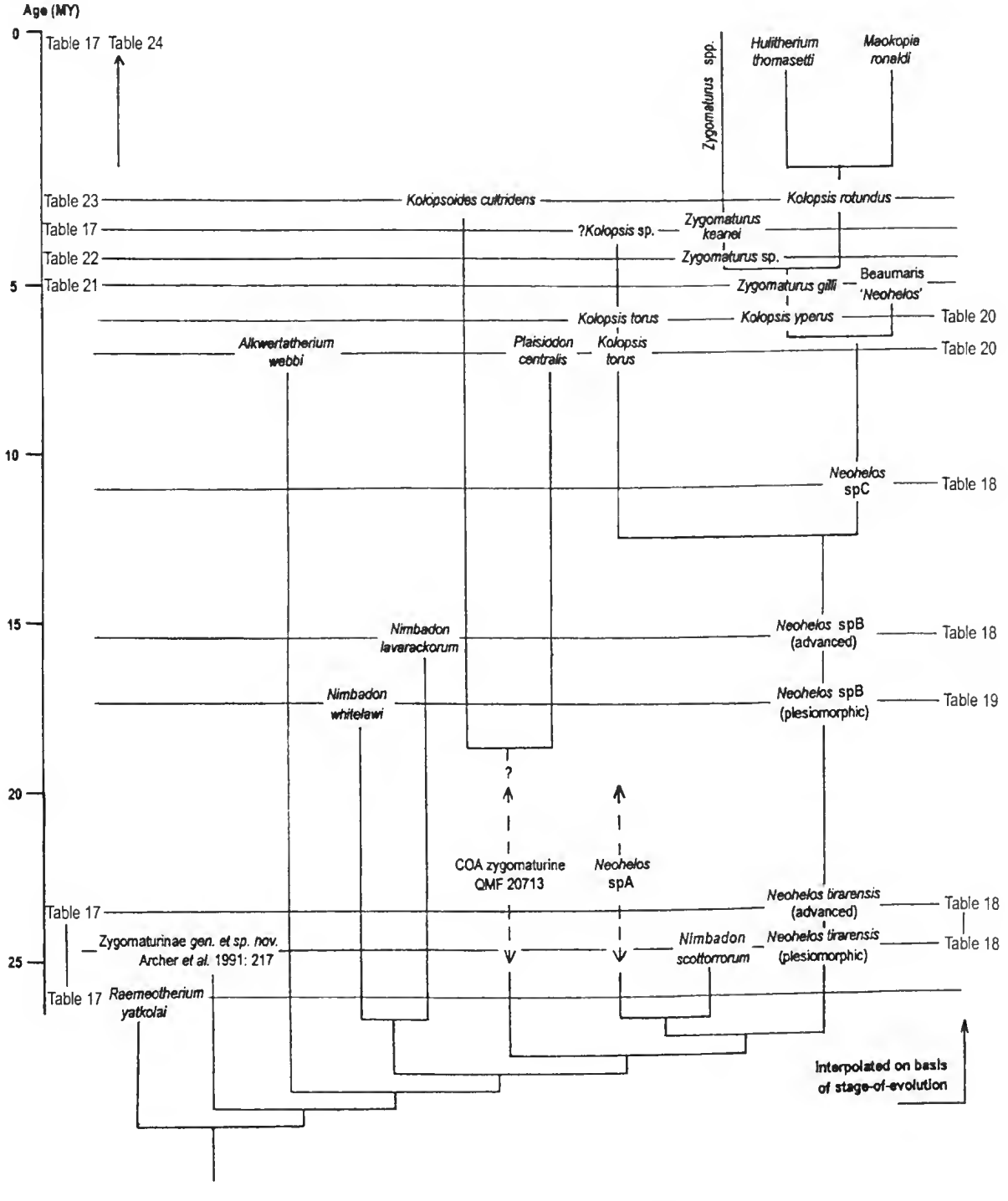

Fig. 78. Biochronology of the Zygomaturinae.

The available evidence indicates a significant radiation of the Zygomaturinae occurred before the late Oligocene (certainly before Wipajiri Formation time, and probably before Etadunna Formation time). Ancestor-descendent relationships have so far only been identified within the *N. tirarensis* crown group, which makes it particularly applicable to stage-of-evolution correlation even though many details of relationships within the group remain to be resolved. Apart from the placement of *Kolopsis torus* onto a collateral lineage in Figure 78, the succession originally proposed by Stirton *et al.* (1967, fig. 2) of *Neohelos tirarensis–(Kolopsis torus)–Zygomaturus gilli–Zygomaturus keanei–Zygomaturus trilobus* is retained.

The earliest evidence for cladogenesis within the crown group is in the Ongeva LF, with several later assemblages confirming the co-existence of at least two lineages. The indications are that significant faunal turnover occurred within the late Miocene / early-Pliocene interval. This turnover is marked by cladogenesis in the *N. tirarensis* crown group, coupled with other lineages apparently not continuing beyond the mid-Miocene (*Nimbadon*) or much beyond the Miocene / Pliocene boundary (*Alkwertatherium*, *Plaisiodon*, *Kolopsis torus* crown group, Beaumaris '*Neohelos*').

The existence at Riversleigh of a small *N. tirarensis* morph that appears to be more plesiomorphic than the Wipajiri Formation *N. tirarensis*, suggests that some strata of the Carl Creek Limestone are older than the Wipajiri Formation. Figure 78 was constructed on the assumption that the small *N. tirarensis* specimens are perhaps synonymous with the underlying Etadunna Formation *Neohelos* sp. Palaeomagnetic data suggest that the Wipajiri Formation is only marginally younger than the youngest Etadunna Formation (Woodburne *et al.* 1993), and these factors have the effect of implying a phase of rapid morphological evolution in *Neohelos* during Etadunna and Wipajiri Formation time, relative to that exhibited during later periods of the Tertiary (Fig. 78). On the other hand, an assumption that the rate of evolution of *Neohelos* was relatively constant over the time of the genus raises the possibility that the plesiomorphous *N. tirarensis* bearing strata of the Carl Creek Limestone predate the Etadunna Formation. These issues might be resolved by the recovery of diagnostic *Neohelos* material from the Etadunna Formation allowing stage-of-evolution comparisons, or chronometric calibration of the Carl Creek Limestone.

CONCLUSIONS

The palaeontology of the genus *Neohelos* has been a challenging study. The range of variation in size and morphology of the members of two geographically and temporally circumscribed species, *N. tirarensis* and *Neohelos* spB are very large. A continuously varying morphology in the Riversleigh sample, which combined with individual variation, a high level of character lability and the certainty of a high degree of sexual dimorphism, produced an excessive amount of random biological information with little in the way of consistent character expressions upon which to formulate even the most basic species discriminations. In the initial stages of the project we had an extremely biased sample of many specimens of *Neohelos* spB and very few specimens, consisting mostly of isolated teeth, of *Neohelos tirarensis*. There is a striking size range within the sample population of smaller *Neohelos*, which we considered might be a species separate from *N. tirarensis*. As the collection was expanded substantially at a much later stage in the study, it became apparent that the *Neohelos tirarensis* sample was a continuously varying population, which

seemed to be part of a morphocline that includes *Neohelos* spB and *Neohelos* spC. Although predominantly allometric, the several minor differences in the smaller forms of *N. tirarensis* seemed to be expressions of more plesiomorphic states, and because the majority of these examples showed a uniformity in size and morphology associated with their particular localities, we conclude that they probably represent chronomorphs of the species *N. tirarensis*. Consequently, we have presented a biochronological hypothesis based on the stage-of-evolution of this series of chronomorphic populations extending from the late Oligocene (Woodburne *et al.* 1993) to the middle Miocene and encompassing three species.

Adding to the high level of analytical noise in the assessment of this genus is the presence of several other zygomaturine species of similar size and morphology within the Riversleigh sample. Very small and conspicuous forms, *Nimbadon lavaradkorum* and *Ni. whitelawi* (Hand *et al.* 1993) are easily discriminated from the *Neohelos* population, but *Ni. scottorrorum* appears to blend into the *Neohelos tirarensis* population. *Nimbadon scottorrorum* differs slightly from the typical *N. tirarensis* sample in having an upward extension of the postcingulum to form a distinct crest on the lingual side of the metaconule. This character was never present in any member of the *N. tirarensis* sample, suggesting that while *Ni. scottorrorum* may belong in *Neohelos*, it is a little different than *Neohelos tirarensis* and hence, being the only specimen of its kind from Fig Tree (type locality), its species distinction has been retained.

In terms of stage–of–evolution, *Ni. scottorrorum* most closely resembles the more derived end of the smaller chronomorphs of *N. tirarensis*, such as that from Inabeyance (QM F13088) and is probably early Miocene in age. The assessment of the possible age of the Fig Tree specimen is important because the other small species of *Neohelos*, *Neohelos* spA, is from the Cleft of Ages locality, which consists of fissure fills within poorly constrained strata. There seems to be insufficient information on the other fauna associated with the Cleft of Ages *Neohelos* to provide a correlative estimation of its age, consequently it must be left to a stage-of-evolution estimation. *Neohelos* spA is readily distinguished from other small *Neohelos* species by its posterolabially elongated M^1 crown and the presence of an extension of the postcingulum up the labial side of the metaconule, similar to, but not exactly like that seen in *Ni. scottorrorum*. It also differs from *N. tirarensis* in having a very narrow protoloph. When in full expression, these characters are highly distinctive, but these traits do not always manifest themselves so clearly on the M^{3-4}. Some specimens from Cleft of Ages closely resemble *Neohelos tirarensis*. However, it is rather strange that among so large a sample, none of the molars belong to *N. tirarensis*, so we have concluded that all of the *Neohelos* material from Cleft of Ages belongs to *Neohelos* spA. While the evidence is circumstantial, it suggests that the Cleft of Ages material is not only specifically, but is also temporally, distinctive. This can be very problematic because of its close resemblance to the most plesiomorphic and inferentially earliest morphs of *N. tirarensis*.

There are three rather slim hypotheses that may help bracket the Cleft of Ages species. First, there is the evidence of the morphocline. The character states of *Neohelos* spA are clearly derived relative to the earliest *N. tirarensis*. Second, there is the similarity between *Ni. scottorrorum* and *Neohelos* spA in the morphology of the postcingulum. Since the Fig Tree locality is considered to be late Oligocene to early Miocene based on faunal correlation, and the stage of evolution estimation of the age of *Ni. scottorrorum* is closest to Inabeyance (early Miocene), we may have an indication of the earliest appearance of the

species if we assume that *Ni. scottorrorum* represents an *N. tirarensis* population in transition to *Neohelos* spA. The third line of evidence comes from the small, incipiently bilobed P^3 from Cleft of Ages. While this specimen may not represent a *Neohelos*, it does indicate an advanced state in the development of the crown otherwise known only among mid Miocene to early Pliocene zygomaturines. We, therefore, conclude that *Neohelos* spA is more likely to have occurred later than earlier, perhaps sometime in the early to mid-Miocene.

SUMMARY

The genus *Neohelos* represents four species ranging from the late Oligocene to the middle Miocene and occurring in widely separated localities in central and northern Australia. *Neohelos* spA known only from the Cleft of Ages locality at Riversleigh Station is the smallest species, differing from all other *Neohelos* species in its narrow M' protoloph, posterolabial elongation of the crown and vertical emargination of the lingual side of the metaconule by a continuation of the postcingulum. *Nimbadon scottorrorum* from the Fig Tree locality is morphologically intermediate between *N. tirarensis* and *Neohelos* spA., and may be a fifth species of *Neohelos*. Only one specimen of this species is known. The type species, *N. tirarensis* is considered to have chronomorphic elements. Smaller, plesiomorphous *N. tirarensis* from Burnt Offerings, D-Site and Bone Reef at Riversleigh Station, Queensland are approximately the same size as *Neohelos* spA and *Ni. scottorrorum*, but differ from those species in having a wide M' protoloph and a horizontal continuation of the postcingulum around the base of the metaconule. Typical, larger *Neohelos tirarensis* occurs in early to middle Miocene strata of both central and northern Australia. An unidentified species of the genus *Neohelos* has been recognised in the Ngapakaldi Local Fauna of South Australia and in several sites at Riversleigh.

Neohelos spB from the middle Miocene Bullock Creek Local Fauna and the Riversleigh, Gag and Henk's Hollow Sites is the best represented species, distinguished by marked differentiation of the molar dimensions along the tooth row, distinct curvature of the cheek-tooth arcade, total absence of a canine alveolus and larger size. The fourth species, *Neohelos* spC is the most derived in showing a division of the parametaconc of the P^3 into two cusps and higher, more overhanding loph and lophids on the molars. It is very similar in size and in other characters to *Neohelos* spB which appears to be directly ancestral to *Neohelos* spC.

At least from a structural point of view, the species of *Neohelos* represent the most complete and longest gradual evolutionary sequence documented for an Australian marsupial genus. The structural succession is no less incremental or gradual at generic boundaries than between species; from its first appearance as being only subtly different from its sister taxa in the late Oligocene to the attainment of a state very close to, and probably directly ancestral to, the late Miocene genus *Kolopsis*. On a larger scale, the structural succession within the Subfamily Zygomaturinae is similarly gradual, with parallelisms being a common occurrence.

Neohelos species appear to represent a chronological morphocline that may be useful in biocorrelation work on the late Oligocene through late Miocene of Australia. However, the proposition that a chronological morphocline existed in these species does not imply that the species could not have some degree of temporal overlap, where for example, one of the

smaller species could persist in suitable, perhaps isolated or relict habitat. However, the selection process responsible for this trend renders the possibility of sympatry of these species unlikely. Therefore, the likelihood of any two of these species occurring in the same assemblage would be low, and in general, the morphocline would correspond with a temporal, rather than a spatial framework.

REFERENCES

Anderson, J., Hall-Martin, A. and Russell, D. 1985. Long-bone circumference and weight in mammals, birds and dinosaurs'. *Journal of Zoology, London (A)* **207**: 53–61.

Archer, M. 1977. Origins and subfamilial relationships of Diprotodon (Diprotodontidae, Marsupialia). *Memoirs of the Queensland Museum* **18**: 37–39.

Archer, M. 1978. The nature of the molar-premolar boundary in marsupials and a reinterpretation of the homology of marsupial cheekteeth. *Memoirs of the Queensland Museum* **18**: 157–164.

Archer, M. 1984. The Australian marsupial radiation. In: Archer, M. and Clayton, G. (eds) *Vertebrate zoogeography and evolution in Australasia.* Pp 633-808. Hesperian Press: Carlisle, Western Australia.

Archer, M., Clayton, G. and Hand, S. 1984. A checklist of Australasian fossil mammals. In: Archer, M. and Clayton, G. (eds) *Vertebrate zoogeography and evolution in Australasia.* Pp 1027–1087. Hesperian Press: Carlisle, Western Australia.

Archer, M., Godthelp, H., Hand, S. J. and Megirian D. 1989. Fossil mammals of Riversleigh, northwestern Queensland: preliminary overview of biostratigraphy, correlation and environmental change, *Australian Zoologist* **25**(2): 29–65.

Archer, M., Hand S. J. and Godthelp, H. 1991. *Riversleigh. The story of animals in ancient rainforests of inland Australia.* Reed Books Pty Ltd: Sydney.

Bultitude, R. J. 1973. Wave Hill, Northern Territory 1:250 000 Geological Series. *Bureau of Mineral Resources, Geology Geophysics, Australia, Explanatory Notes* SE/52–8.

Eldredge, N. and Gould, S. J. 1977. Evolutionary models and biostratigraphic strategies. In: Kauffman, E. G. and Hazel, J. E. (eds) *Concepts and methods of biostratigraphy.* Pp. 25–40. Dowden, Hutchinson and Ross: Stroudsburg.

Evernden, J. F., Savage, D. E., Curtis, G. H. and James, G. T. 1964. Potassium-Argon dates and the Cenozoic mammalian chronology of North America. *American Journal of Science* **262**: 145–98.

Fisher, R. A. 1938. Statistical methods for research workers. Oliver and Boyd: Edinburgh.

Flannery, T. 1992. New Pleistocene marsupials (Macropodidae, Diprotodontidae) from subalpine habitats in Irian Jaya, Indonesia. *Alcheringa* **16**: 321–31.

Flannery, T. and Plane, M. 1986. A new Late Pleistocene diprotodontid (Marsupialia) from Pureni, Southern Highlands Province, Papua New Guinea. *BMR Journal of Australian Geology and Geophysic* **10**(1):, 65–76.

Folk, R. L. 1959. Practical petrographic classification of limestones. *Bulletin of the American Association of Petroleum Geologist* **43**(1): 1–38.

Gill, T. 1872. Arrangement of the families of mammals with analytical tables. *Smithsonian Miscellaneous Collection* **11**.

Gingerich, P. 1979. The stratophenetic approach to phylogeny reconstruction in vertebrate paleontology. In: Cracraft, J. and Eldredge, N. (eds) *Phylogenetic analysis and paleontology*. Pp. 41–77. Columbia University Press: New York.

Haight, J. and Murray, R 1981. The cranial endocast of the Early Miocene marsupial, *Wynyardia bassiana*: an assessment of taxonomic relationships based upon comparisons with recent forms. *Brain, Behavior and Evolution* **19**: 17–36.

Hand, S., Archer, M., Rich, T. and Pledge, N. 1993. *Nimbadon*, a new genus and three species of Tertiary zygomaturines (Marsupialia, Diprotodontidae) from northern Australia, with a reassessment of *Neohelos*. *Memoirs of the Queensland Museum* 33(1): 193–210.

Hays, J. 1967. Land surfaces and laterites in the Northern Territory. In: Jennings, J. N. and Mabutt, J. A. (eds) *Landform studies from Australia and New Guinea*. Pp 182–210. Australian National University Press: Canberra.

Hoch, E. and Holm, R. 1986. New K/Ar determinations of the Awe Fauna, Gangue, Papua New Guinea: consequences for Papuaustralian late Cenozoic stratigraphy. *Modern Geolog* **10**: 181–95.

Huxley, T. H. 1862. On the premolar teeth of Diprotodon, and a new species of the genus. *Quarterly Journal of the Geological Society, London* **18**: 422–27.

Illiger, C. 1811. *Prodromus systematis mammlian et avium additus terminus zoographicis utriudque classis*. C. Salfield: Berlin.

Lloyd, A. R. 1965. Possible Miocene marine transgressions in northern Australia. *Bureau of Mineral Resources, Geology and Geophysics, Australia, Bulletin* **80**: 87–103.

Luckett, W. R. 1993 An ontogenetic assessment of dental homologies in therian mammals. In: Szalay, F. S.M., Novacek, J. and McKenna, M. C. (eds) *Mammal phylogeny: Mesozoic differentiation, multituberculates, monotremes, early eutherians, and marsupials*. Pp 182–204. Springer-Verlag: New York.

McGowran, B. and Li, Q. 1994. The Miocene oscillation in South Australia. *Records of the South Australian Museum* **27**(2): 197–212.

Marshall, C. R., Raff, E. C. and Raff, R. A. 1994. Dollo's law and the death and resurrection of genes. *Proceedings of the National Academy of Science, U.S.A.* **91**: 12283–12287.

Megirian, D. 1992. Interpretation of the Miocene Carl Creek Limestone, northwestern Queensland. *The Beagle, Records of the Northern Territory Museum of Arts and Sciences.***9**(1): 219–248.

Megirian, D. 1994. Approaches to marsupial biochronology in Australia and New Guinea. *Alcheringa* **18**: 259–274.

Megirian, D., Murray, R. and Wells, R. 1996. The late Miocene Ongeva Local Fauna of central Australia. *The Beagle, Records of the Museums and Art Galleries of the Northern Territory* **13**: 9–38.

Murray, R. 1986. *Propalorchestes novacnlacephalus* gen. et sp. nov., a new palorchestid (Diprotodontoidea: Marsupialia) from the middle Miocene Camfield Beds, Northern Territory. *The Beagle, Occasional Papers of the Northern Territory Museum of Arts and Sciences* **3**(1): 195–211.

Murray, R. 1990a. *Alkwertatherium webbi*, a new zygomaturine genus and species from the late Miocene Alcoota Local Fauna, Northern Territory (Marsupialia: Diprotodontidae). *The Beagle, Records of the Northern Territory Museum of Arts and Sciences* **7**(2): 53–80.

Murray, R. 1990b. Primitive marsupial tapirs (*Propalorchestes novaculaceplialus* Murray and *P. ponticulus* sp. nov.) from the mid-Miocene of northern Australia. *The Beagle, Records of the Northern Territory Museum of Arts and Sciences* 7(2): 39–52.

Murray, R. 1991. The Pleistocene megafauna of Australia. In: Vickers-Rich, P, Monaghan, J. M., Baird, R. F. and Rich, T. H. (eds). *Vertebrate palaeontology of Australasia.* Pp 1070–1164. Pioneer Design Studio and Monash University Publications Committee: Melbourne.

Murray, R. 1992, 'The smallest New Guinea zygomaturines–derived dwarfs or relict plesiomorphs? *The Beagle, Records of the Northern Territory Museum of Arts and Sciences* 9(1): 89–110.

Murray, R. and Megirian, D. 1990. Further observations on the morphology of *Wakaleo vanderleueri* (Marsupialia: Thylacoleonidae) from the mid-Miocene Camfield Beds, Northern Territory. *The Beagle, Records of the Northern Territory Museum of Arts and Sciences* 7(1): 91–102.

Murray, R. and Megirian, D. 1992. Continuity and contrast in middle and late Miocene vertebrate communities from the Northern Territory. *The Beagle, Records of the Northern Territory Museum of Arts and Sciences* 9(1): 195–218.

Murray, R., Megirian, D. and Wells, R. 1993. *Kolopsis yperus* sp. nov. (Zygomaturinae, Marsupialia) from the Ongeva Local Fauna: new evidence for the age of the Alcoota fossil beds of central Australia', *The Beagle, Records of the Northern Territory Museum of Arts and Sciences* **10**(1): 155–72.

Owen, R. 1838. In: Mitchell, T. L. (ed.) *Three expeditions into the interior of eastern Australia, with descriptions of the recently explored region of Australia Felix, and of the present colony of New South Wales*. T. and W. Boone: London.

Owen, R. 1859. On some outline drawings and photographs of the skull of *Zygomaturus trilobus*, Macleay (Nototherium, Owen?). *Quarterly Journal of the Geological Society of London* **15**: 168–76.

Owen, R. 1866. *On the anatomy of vertebrates. 11, birds and mammals*. Erxleben: London.

Page, R. W. and McDougall, I. 1972. Ages of mineralization of gold and porphyry copper deposits in the New Guinea Highlands. *Economic Geology* **67**: 1034–48.

Plane, M. 1967. Two new diprotodontids from the Pliocene Otibanda Formation, New Guinea. In: Stirton, R., Woodburne, M., and Plane, M. (eds) *Tertiary Diprotodontidae from Australia and New Guinea*, Pp 107–228. Bureau of Mineral Resources, Geology and Geophysics, Australia, Bulletin **85**.

Plane, M. and Gatehouse, C. 1968. A new vertebrate fauna from the Tertiary of northern Australia', *Australian Journal of Science* **30**: 272–273.

Randal, M. A. and Brown, M. C. 1967. The geology of the northern part of the Wiso Basin. *Bureau of Mineral Resources, Geology and Geophysics, Australia, Record* **1967/110**.

Rich, T. H. 1976. Recent fossil discoveries in Victoria. Five Late Cenozoic fossil Marsupial sites in Victoria: a progress report. *The Victorian Naturalist* **93**(5): 198–206.

Rich, T. H. 1991. Monotremes, placentals, and marsupials: their record in Australia and its biases. In: Vickers-Rich, P, Monaghan, J. M., Baird, R. F. and Rich, T. H. (eds). *Vertebrate palaeontology of Australasia.* Pp 893–1069. Pioneer Design Studio and Monash University Publications Committee: Melbourne.

Rich, T., Archer, M., and Tedford, R. 1978. *Raemeotherium yatkolai* gen. et sp. nov., a primitive diprotodontid from the medial Miocene of South Australia. *Memoirs of the National Museum of Victoria* **39**: 85–91.

Rohlf, F. J. 1990. *NTSYS-pc. Numerical Taxonomy and Multivariate Analysis System, Version 1.60.* Exeter Software: Setauket, New York.

Savage, D. E. 1977. Aspects of vertebrate paleontologieal stratigraphy and geochronology. In: Kauffman, E. G. and Hazel, J. E. (eds) *Concepts and methods of biostratigraphy*. Pp. 427–442. Dowden, Hutchinson and Ross: Stroudsburg.

Smart, J., Grimes, K. G., Douteh, H. F. and Pinehin, J. 1980. The Mesozoie Carpentaria Basin and Cainozoic Karumba Basin, north Queensland. *Bureau of Mineral Resources, Geology and Geophysics, Australia, Bulletin* **202**.

Stirton, R. 1967a. A diprotodontid from the Mioeene Kutjamarpu Fauna, South Australia. In: Stirton, R., Woodburne, M., and Plane, M. (eds) *Tertiary Diprotodontidae from Australia and New Guinea*, Pp 45–51. Bureau of Mineral Resources, Geology and Geophysies, Australia, Bulletin **85**.

Stirton, R. A. 1967b. The Diprotodontidae from the Ngapakali Fauna, South Australia. In: Stirton, R., Woodburne, M., and Plane, M. (eds) *Tertiary Diprotodontidae from Australia and New Guinea*, Pp 1–44. Bureau of Mineral Resourees, Geology and Geophysies, Australia, Bulletin **85**.

Stirton, R. A. 1967e. New speeies of *Zygomaturus* and additional observations on *Meniscolophus*, Plioeene Palankarinna Fauna, South Australia. In: Stirton, R., Woodburne, M., and Plane, M. (eds) *Tertiary Diprotodontidae from Australia and New Guinea*. Pp 129–147. Bureau of Mineral Resourees, Geology and Geophysics, Australia, Bulletin **85**.

Stirton, R., Woodburne, M. and Plane, M. 1967. A phylogeny of the Tertiary Diprotodontidae and its signifieanee in correlation. In: Stirton, R., Woodburne, M., and Plane, M. (eds) *Tertiary Diprotodontidae from Australia and New Guinea*, Pp 151–160. Bureau of Mineral Resourees, Geology and Geophysics, Australia, Bulletin **85**.

Stirton, R. A., Tedford, R. H. and Woodburne, M. O., 1968. Australian Tertiary deposits containing terrestrial mammals. *University of California Publications in Geological Sciences* **77**: 1–30.

Sweet, I. R, Mendum, J. R., Bultitude, R. J. and Morgan, C. M. 1971. The geology of the Waterloo, Vietoria River Downs, Limbunya and Wave Hill 1 :250 000 Sheet Areas, Northern territory. *Bureau of Mineral Resources, Geology and Geophysics, Australia, Record* **1971/71**.

Tedford, R. H. 1967. Fossil mammal remains from the Tertiary Carl Creek Limestone, northwestern Queensland. *Bureau of Mineral Resources, Geology and Geophysics, Australia, Bulletin* **92**: 217–237.

Tedford, R. H. and Wells, R. T. 1990. Pleistoeene deposits and fossil vertebrates from 'the dead heart of Australia. *Memoirs of the Queensland Museum* **28**(1): 263–284.

Tedford, R. H., Wells, R. T. and Barghoorn, S. F. 1992. Tirari Formation and contained faunas, Plioeene of the Lake Eyre Basin, South Australia. *The Beagle. Records of the Northern Territory Museum of Arts and Sciences* **9**(1): 173–194.

Wells, R. T. and Callen, R. A. (eds) 1986. *The Lake Eyre Basin–Cainozoic sediments, fossil vertebrates and plants, landforms, silcretes and climatic implications*. Australasian Sedimentologists Group Field Guide Series No. 4: Geologieal Society of Australia, Sydney.

Wiley, E. O. 1977. Ancestors, speeies, and eladograms–remarks on the symposium. In: Cracraft, J. and Eldredge, N. eds) *Phylogenetic analysis and paleontology*. Pp 211-225. Columbia University Press: New York.

Woodburne, M. 1967a. Three new diprotodontids from the Tertiary of the Northern Territory, Australia. In: Stirton, R., Woodburne, M., and Plane, M. (eds) *Tertiary Diprotodontidae from Australia and New Guinea.* Pp 55–103. Bureau of Mineral Resources, Geology and Geophysics, Australia, Bulletin **85**.

Woodburne, M. 1967b. The Alcoota Fauna, central Australia. *Bureau of Mineral Resources, Geology and Geophysics, Australia, Bulletin* **87**.

Woodburne, M. 1969. A lower mandible of *Zygomaturus gilli* from the Sandringham Sands, Beaumaris, Victoria, Australia. *Memoirs of the National Museum of Victoria* **29**: 29–39.

Woodburne, M., Tedford, R., Archer, M., Turnbull, W., Plane, M., and Lundelius, E. 1985. Biochronology of the continental mammal record of Australia and New Guinea. *Special Publication of the South Australian Department of Mines and Energy* **5**: 347–363.

Woodburne, M. O., MacFadden, B. J., Case, J. A., Springer, M. S., Pledge, N. S., Power, J. D., Woodburne, J. M., Johnson, K. B. and Gwynn, T. C. 1993. Land mammal biostratigraphy and magnetostratigraphy of the Etadunna Formation (late Oligocene) of South Australia. *Journal of Vertebrate Palaeontology* **13**(4): 483–515.

APPENDIX I

STATISTICAL ANALYSIS OF *NEOHELOS* DENTAL MEASUREMENTS

THOMAS H. RICH

ABSTRACT

Length and width measurements of the cheek teeth of the mid-Tertiary Australian diprotodontoid *Neohelos* from three areas have been analysed statistically. The three areas were Lake Ngapakaldi, South Australia; Bullock Creek, Northern Territory; and Riversleigh, Queensland. Measurements of individual features were compared between populations of *Neohelos* from different localities utilising Student's t-test. These outcomes were subsequently summarised utilising means of the t-test values as the basis for assessing the degree of similarity between population pairs. This information was then expressed graphically by means of a dendrogramme showing the clustering of populations on the basis of the relative degree of similarity.

This mode of analysis is based solely on size and proportional differences in tooth measurements between populations. As such, its weakness in that two quite unrelated taxa would be judged as similar if their tooth dimensions happen to be the same. However, where a difference on this basis is recognised, it is to be anticipated that examination of other, perhaps quite subtle features will corrorborate that different taxa are present.

What examination of the dendrogrammes shows is that with two exceptions, the Bullock Creek *Neohelos* spB material stands quite apart from all other sites. The exceptions are from two sites at Riversleigh: Jaw Junction specimens of *Neohelos* spC, a species known nowhere else and three teeth of *Neohelos* spB from Henk's Hollow. It is solely on the basis of qualitative characters that *Neohelos* spB and *Neohelos* spC are split apart. Likewise, the Riversleigh Cleft of Ages *Neohelos* spA material and the single specimen of *Nimbadon scottorrorum* from the Fig Tree locality at Riversligh both group with one of the two distinct clusters of Riversleigh *Neohelos tirarensis* populations.

INTRODUCTION

The mid-Cainozoic diprotodontoid *Neohelos tirariensis* Stirton 1967a was named on the basis of a few isolated teeth from the Kutjamarpu Fauna collected at the Leaf Locality, Wipijari Formation at Lake Ngapakaldi, South Australia. Subsequently a large quantity of material referrable to *Neohelos* has been collected from four different sites (Blast Site, Camp Quarry, Horseshoe West, and Top Quarry) in the Camfield Beds on Camfield Station, Northern Territory, that form the Bullock Creek Fauna. A much smaller amount of material referrable to this same genus has been collected from seventeen different named areas on Riversleigh Station, Queensland (300 BR {300 metres from Bone Reef}, Bone Reef, Burnt Offerings, Camel Sputum, Cleft of Ages, D-Site, Fig Tree, Gag, Henk's

Hollow, Inabeyance, Jaw Junction, Jim's Jaw Site, Mike's Menagerie, Neville's Garden, Sticky-beak, Upper Burnt Offerings, and Wayne's Wok).

Beginning with Stirton, Tedford and Woodburne (1968), the chronological framework of Australian Cainozoic terrestrial mammal localities has been based to a great extent on evaluation of the remains of diprotodontoids. Thus, determing the relationships of the *Neohelos* material from the various sites is not only of interest in its own right but furthers understanding of the chronological relationships between the various localities as well.

METHODS

The fossils of *Neohelos* from Bullock Creek consist of numerous dentitions and whole skulls along with many post cranial elements. Quite in contrast, in the Lake Ngapakaldi and Riversleigh areas, the genus is represented solely by rare, fragmentary dental remains. For this reason, analysis of measurements of teeth was employed as one way of reaching conclusions regarding the relationships of *Neohelos*.

In order to extract as much information as possible from the measurements of the teeth, in addition to the measurements given in Tables 2, 6-9, 13 and 16 of the main text, several ratios of dental measurements were included in the analysis. These ratios which can be calculated from the data in those tables were length:width of P3, length:anterior width of M1-4, length of M2:length of M3, and anterior width of M2:anterior width of M3.

Because of fragmentary nature of the *Neohelos* material available, particular that from Lake Ngapakaldi and Riverslcigh, few comparable measurements are consistently possible among all the groups of specimens to be evaulated in order to determine the relationships of the genus. Of necessity, therefore, simple statistical procedures have been adopted which forego the sophistication possible with more elaborate modes of analysis that function best with data sets that have few if any gaps. Fortunately, a consistent pattern of clustering of sites emerged from the simple procedures utilised here.

First, every comparison possible between each population pair has been made utilising Student's t-test. Because of the fragmentary nature of many of the samples from the Leaf Locality and the Riversleigh sites, this meant that in practice in one case, it would be possible for example to compare the length and width of the P^3 but not M^3 and in another pair of populations length, anterior and posterior widths of M^3 but not P^3.

Second, the mean of the Student's t-test values was then used to evaluate all the comparisons that could be made and combine them in a meaningful way even if they were different measurements. That is, the assumption was made that if two populations were far apart in the size of the P^3 and another two populations were close in the M^3, was that not a reasonable basis to infer that the latter two populations were more alike?

So if one had ten t-test measurements for one pair of samples and the mean of the t-test values was 0.2 and for a second pair of poulations where twelve t-test measurements were possible and the mean of those t-test values was 0.8, one could could reasonably infer that the second pair was more alike than the first although the inference was not necessarily based on identical measurements.

Third, a matrix of such values for all population pairs was created and then the relative closeness of the various populations graphically portrayed as a dendrogrammes using the

UPGMA [Unweighted Pair Group Method, Arithmetic Average] and option of the SAHN [Sequential, Agglomerative, Hierarchial, and Nested] clustering programme of the NTSYS-pc [Numerical Taxonomy and Multivariate Analysis System] Version 1.60 system produced by F. James Rohlf, Exeter Software, 1990.

The SAHN clustering algorithm works as follows:

1. Search the imput matrix for the pair of objects (*i,j*) that are most similar....
2. Merge these objects into a new cluster.
3. Update the matrix to reflect the deletion of the pairs of objects, *i* and *j,* that were merged and the addition of a new "object" corresponding to the new cluster. Similarities have to be computed between the existing objects and the new cluster.
4. Go back to stcp 1, above, if the size of the new matrix is greater than 2 x 2--- else stop. Note that 2 objects are deleted and one is added at each so this algorithm must terminate. Rohlf (1990)

RESULTS

This first step, the Student's t-test, assumes that the population measurements are normally distributed. To check that this was a reasonable assumption, the biggest sample available, that from the Blast Site at Bullock Creek, was divided into sub-samples of various sizes and compared with onc another using thc t-test. Several thousand such comparisons were made. Table 26 summarises that work and compares the values at the various points in the distribution with thc corresponding ones in the t-test table for the samc number of degrees of freedom.

In the case of the upper dentition of *Neohelos* in Table 26 for example, the entire population from the Blast Site was divided in two at random 42 times. Because there are 14 comparisons possible in an upper dentition, this meant that a total of 588 t-test values were generated using the standard formula where X_1, s_1 and N_1 are the mean, standard deviation and sample size of one population and X_2, s_2 and N_2 are the same values for the second population.

$$t = \frac{|(X_1 - X_2)|\sqrt{\dfrac{N_1 N_2}{N_1 + N_2}}}{\sqrt{\dfrac{(N_1 - 1)s_1^2 + (N_2 - 1)s_2^2}{N_1 + N_2}}}$$

The 588 t-test values so measured were then ranked from highest to lowest. Because these two samples were known to be drawn from the same population, it was then possible to empirically estimate the frequency at which a particular t-test value should be equalled or exceeded in two samples of this nature that can be regarded as the same. In the case of the upper dcntition in Table 26a, beginning at the highest value of the t-test determincd and going down the listing of cver decreasing values, one interpolates between the 117th and the 118th measurement of the t-test value to obtain the value 1.3823 that is to be expectcd or exceeded one fifth of the time; *i.e.* at a frequency of 0.2, 117.6 being 20% of 588.

Examination of Table 26A shows that large samples of *Neohelos* spB can be relied upon to have a statistically normal distribution. In progession from Table 26A to Table 26E, the samples become progressively smaller. However, it is only in the case of the two smallest comparisons made, one individual in one population against three in a second, Table 26D, and one individual in one population against only two in a second, Table 26E, that serious departures from normality were observed. While this possible error in cases where samples are small must be kept in mind when examining resulting dendrogrammes, it is clearly established by these results that the assumption of normality in this case is justified in all but the smallest sample sizes compared.

Table 26. T-test Significance Values based on comparisons between of subpopulations of *Neohelos* from the Blast Site

A. Entire Blast Site population divided into two subpopulations based on random numbers.

Probability	.80	.60	.40	.20
Upper dentition, 588 t-test values	.2825	.5213	.9043	1.3823
Lower dentition, 588 t-test values	.2591	.5365	.8688	1.359
Student's t-test tables, 20 df (Table IV in Fisher 1938)	.257	.533	.860	1.325

B. Single individuals compared to remainder of sample from Blast Site

Probability	.80	.60	.40	.20
Upper, 665 t-test values	.2140	.4929	.8155	1.3062
Lower, 464 t-test values	.3105	.4975	.8738	1.3454
Student's t-test tables, 20 df (Table IV in Fisher 1938)	.257	.533	.860	1.325

C. One individual compared against six individuals from Blast Site

Probability	.80	.60	.40	.20
Upper, 455 t-test values	.2586	.5696	.8496	1.3458
Lower, 326 t-test values	.2865	.6069	.9379	1.5759
Student's t-test tables, 5 df (Table IV in Fisher 1938)	.267	.559	.920	1.476

D. One individual compared against three individuals from Blast Site

Probability	.80	.60	.40	.20
Upper, 1559 t-test values	.2950	.6475	1.0690	1.7453
Lower, 1156 t-test values	.4283	.8573	1.4174	2.5465
Student's t-test tables, 2 df (Table IV in Fisher 1938)	.289	.617	1.061	1.886

E. One individual compared against two individuals from Blast Site

Probability	.80	.60	.40	.20
Upper, 1533 t-test values	.3008	.6244	1.0677	2.3550
Lower, 1074 t-test values	.5935	1.2247	2.2540	5.1711
Student's t-test tables, 1 df (Table IV in Fisher 1938)	.325	.727	1.376	3.078

The t-test information is conveniently summarised in dendrogrammes for nine different combinations of populations presented in Figures 79-87. Seven population groups were required in order that every population be shown at least once because two populations which have no measurements in common cannot be on the same dendrogramme. Two more population groups were added to clarify the relationships of particular populations. The more material present in a population, the more likely it is to be represented in a given dendrogramme. This is because in that case it is more likely that such a population is more likely to have some measurement in common with every other population in a given dendrogramme. Those more frequent populations show a consistent pattern of clustering that carries through from one dendrogramme to another. By noting the placement of the

rarer populations in the one or few dendrogrammes they occur in, their positions relative to the overall clustering can be assessed.

Inspection of Figures 79-87 shows two consistent clusters together with a third, less obvious one plus two Riversleigh *Neohelos* populations that do not appear to strongly group with any other.

The largest, consistently distinct cluster is the *Neohelos* spB specimens from four sites at Bullock Creek (Blast Site, Camp Quarry, Horseshoe West, and Top Quarry) and Henk's Hollow at Riversleigh plus the *Neohelos* spC from Jaw Junction at Riversleigh. They clearly stand apart from the other Riversleigh populations of *Neohelos* and the *Neohelos tirarensis* material from the Leaf Locality in South Australia.

Central to the second consistent cluster, evident on all dendrogrammes where all three populations occur (Figs 79-82, 84) are the Mike's Menagerie and Camel Sputum *Neohelos tirarensis* material together with the Gag *Neohelos* spB specimens. They are more closely linked than the Bullock Creek plus Jaw Junction specimens are to one another. On the one dendrogramme where it appears, (Fig. 79), the 300 BR *N. tirarensis* material is more closely linked go the Gag *Neohelos.* spB than either is to the Mike's Menagerie and Camel Sputum *N. tirarensis.* Less closely linked to the Mike's Menagerie - Camel Sputum - Gag cluster is the Leaf Locality, Inabeyance, and Burnt Offering *N. tirarensis* material as well as the *Neohelos scottorrorum* specimen from the Fig Trec locality. On those dendrogrammes where the *N. tirarensis* from Camel Sputum is represented but the specimens from Mike's Menagerie and Gag are not, the Camel Sputum material is closely linked to the *Neohelos* spB material from Neville's Garden (Fig. 83) and Sticky Beak (Fig. 85).

The third, less clearly defined cluster is centred around the *Neohelos* spA material from the Cleft of Ages locality and the *Neohelos tirarensis* material from the Sticky Beak locality, the one site with more than a single species of *Neohelos,* the other being *Neohelos* spB. On the one dendrogramme where they occur, the *N. tirarensis* specimens from Upper Burnt Offerings (Fig. 82) and Jim's Jaw Site (Fig. 84) are nested within this cluster, being closer to the *N. tirarensis* specimens from Sticky Beak than they are to the *Neohelos* spA material from Cleft of Ages. On the one dendrogramme where it occurs (Fig. 80), the Bone Reef *N. tirarensis* material is weakly associated with the Cleft of Ages and *N. tirarensis* speciemsn from Sticky Beak.

On those dendrogrammes where the *Neohelos tirarensis* material from Sticky Beak is not represented, the Cleft of Ages *Neohelos* spA is noticeably closer to the Mike's Menagerie - Camel Sputum - Gag cluster.

The Wayne's Wok *Neohelos tirarensis* specimens clusters with the material of that species from Camel Sputum on those dendrogramme where the *Neohelos* spB material from Henk's Hollow is not represented. When both are present, the Wayne's Wok *N tirarensis* groups with the Henk's Hollow *Neohelos* spB.

The D-Site *Neohelos tirarensis* can be linked either to the Cleft of Ages *Neohelos* spA material or the Mike's Menagerie - Camel Sputum - Gag cluster. In some cases D-Site, Cleft of Ages, and the Mike's Menagerie - Camel Sputum - Gag cluster plus the Leaf Locality *N. tirarensis* specimens form a recognizable grouping (Figs 86-87).

In summary three population groupings as well as two populations are not obviously part of any cluster can be recognised by inspecting Figures. 79-87. In addition, elements of the

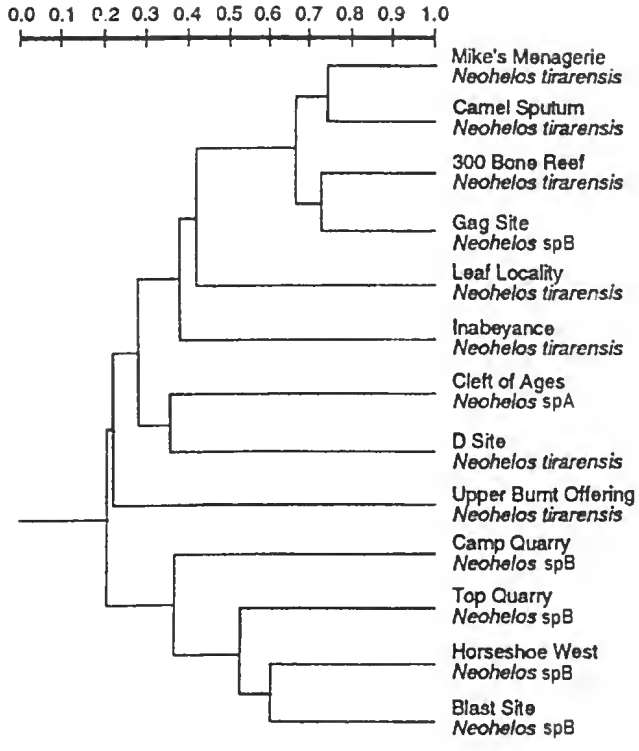

Fig. 79. Dendrogram depicting t-test information for one of nine different *Neohelos* population combinations; [this combination shows 300BR *N. tirarensis* more closely linked to Gag *Neohelos* spB than either is to Mike's Menagerie and Camel Sputum.]

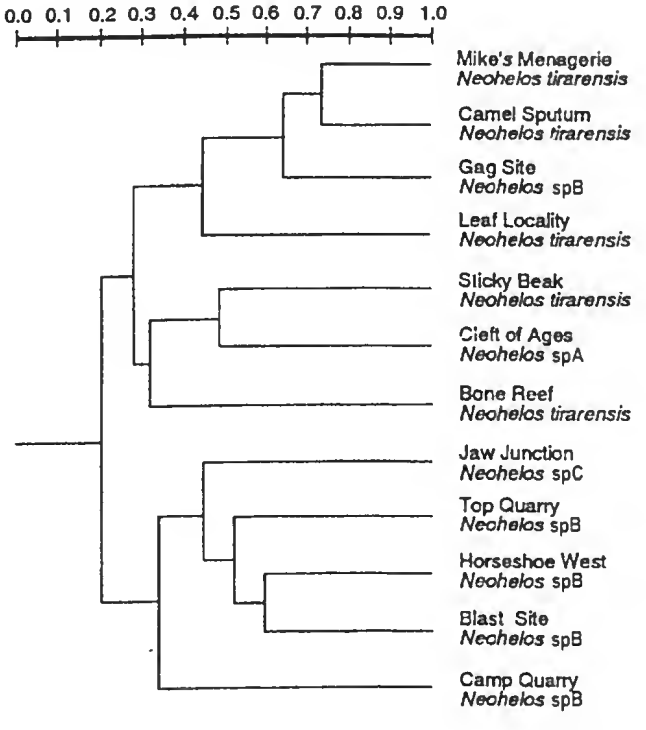

Fig. 80. Dendrogram depicting t-test information for one of nine different *Neohelos* population combinations; [this combination shows a weak association of Cleft of Ages *Neohelos* spA and Sticky-beak *N. tirarensis*.]

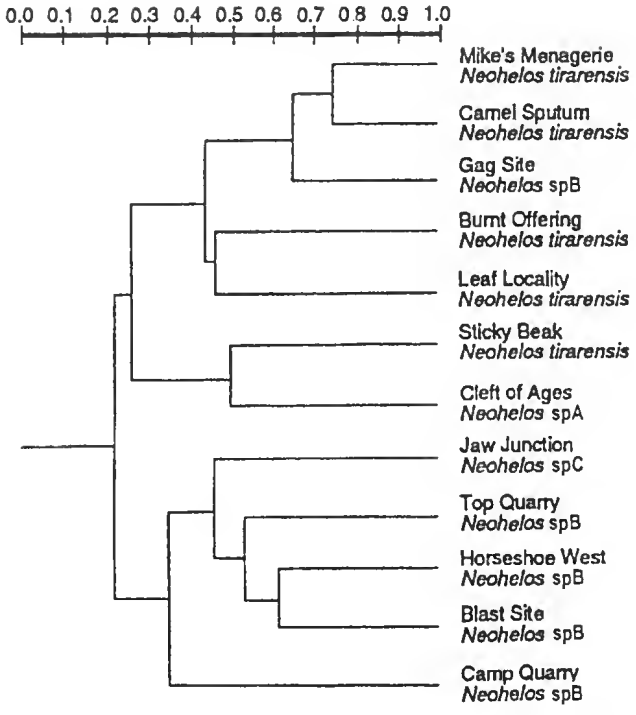

Fig. 81. Dendrogram depicting t-test information for one of nine different *Neohelos* population combinations; [this combination is similar to the previous one showing an association between Cleft of Ages and Sticky-beak.]

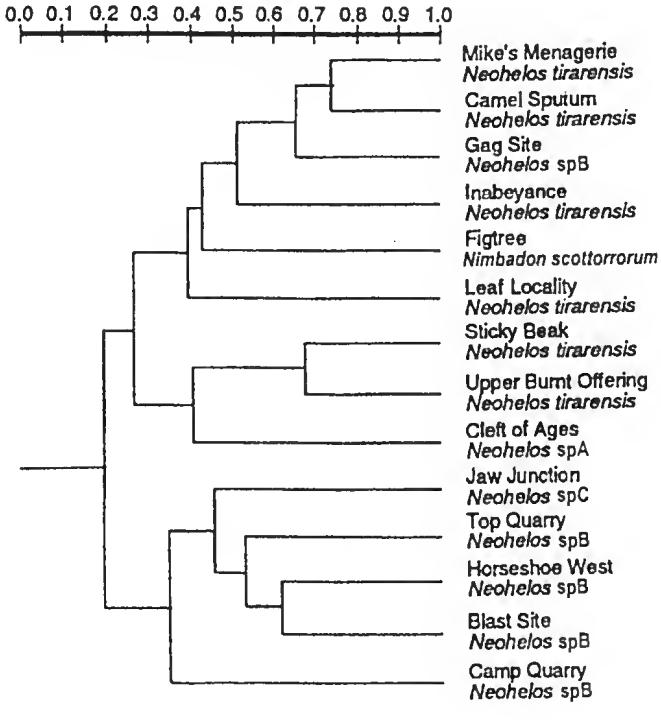

Figure 82. Dendrogram depicting t-test information for one of nine different *Neohelos* population combinations; [in this combination, Sticky-beak and Upper Burnt Offerings *N. tirarensis* are associated, with a weak link to Cleft of Ages *Neohelos* spA.]

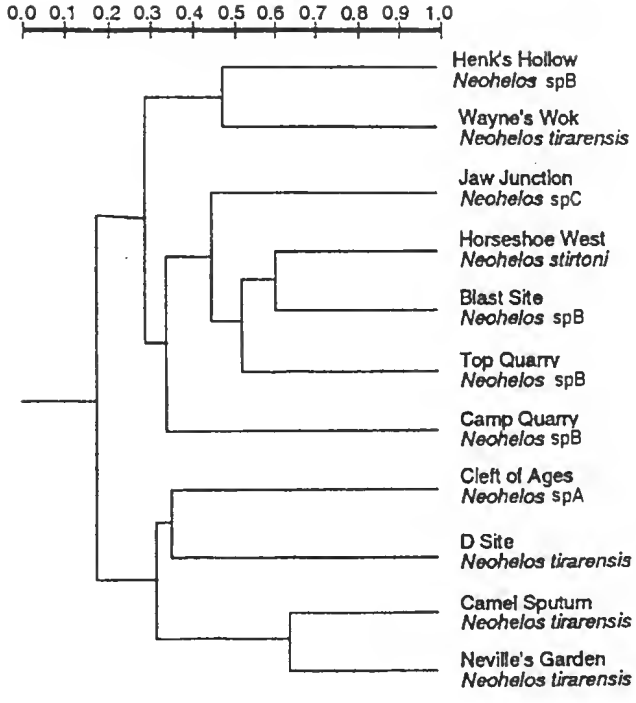

Fig. 83. Dendrogram depicting t-test information for one of nine different *Neohelos* population combinations; [this combination shows a link between Camel Sputum *N. tirarensis* and Neville's Garden *Neohelos* spB when Mike's Menagerie and Gag measurements are excluded.]

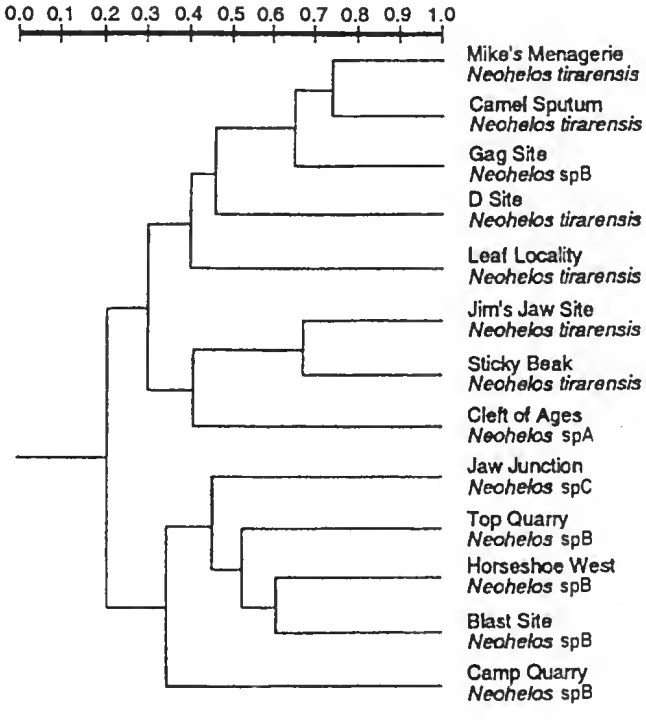

Fig. 84. Dendrogram depicting t-test information for one of nine different *Neohelos* population combinations; [in this combination, Jim's Jaw *N. tirarensis* are closer to Sticky-beak *N. tirarensis* than to Cleft of Ages *Neohelos* spA.]

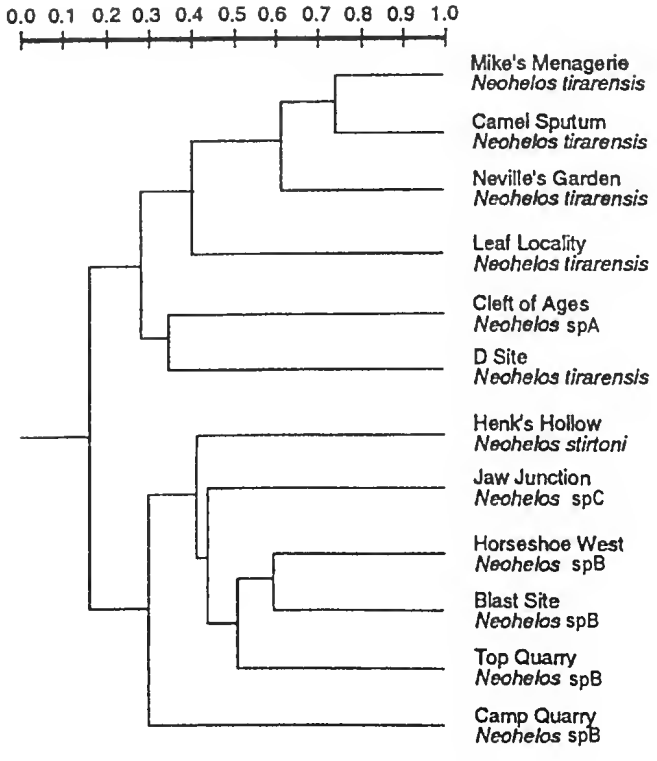

Fig. 85. Dendrogram depicting t-test information for one of nine different *Neohelos* population combinations; [showing that in the absence of Mike's Menagerie and Gag measurements, Camel Sputum is closer to Sticky Beak.]

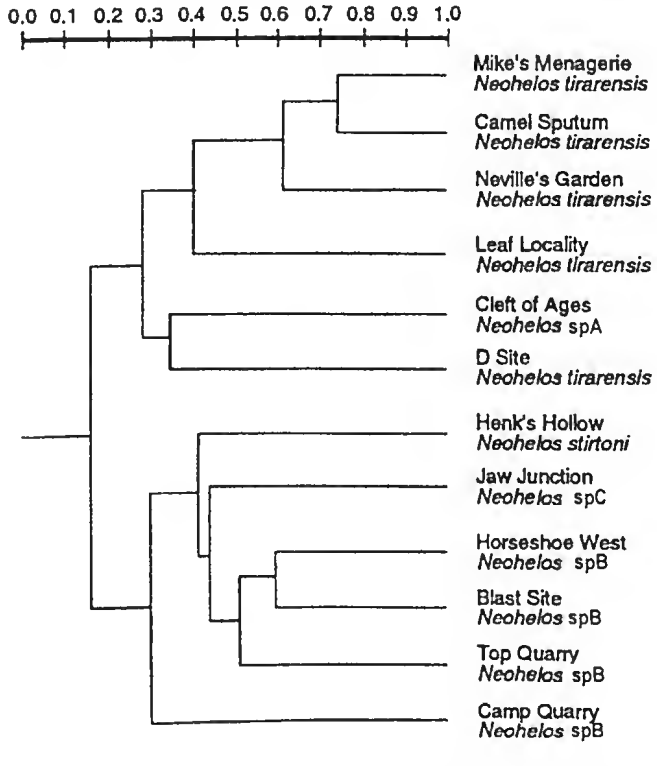

Fig. 86. Dendrogram depicting t-test information for one of nine different *Neohelos* population combinations; [this combination shows that with the omission of Wayne's Wok *N. tirarensis* sample (figure 85) the Leaf Locality *N. tirarensis* assumes a similar position.]

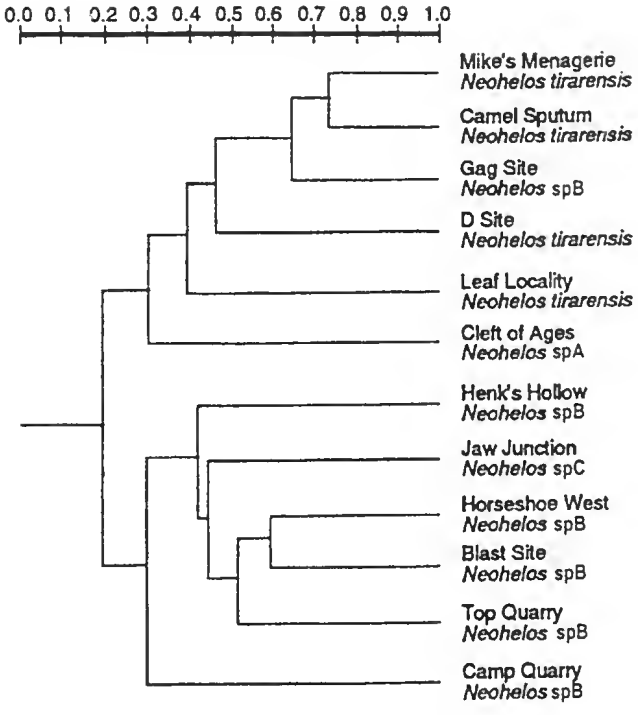

Fig. 87. Dendrogram depicting t-test information for one of nine different *Neohelos* population combinations; [this combination shows that despite the substitution of the Gag Site *Neohelos* spB in this dendrogram for the Neville's Garden *Neohelos tirarensis* in Figure 86, there is almost no difference between the two dendrograms.]

third cluster group with the second in some instances where the numbers of populations sampled are low and the two indeterminate populations in some instances show affinities for the second group and in other cases, the third. These groupings are as follows:

Group 1

Blast: *Neohelos* spB
Camp: *Neohelos* spB
Horseshoe W.: *Neohelos* spB
Henks Hollow: *Neohelos* spB
Jaw Junction: *Neohelos* spC
Top: *Neohelos* spB

Group 2

300 BR: *N. tirarensis*
Burnt Offerings: *N. tirarensis*
Camel Sputum: *N. tirarensis*
Fig Tree: *Nimbadon. scottorrorum*
Gag Site: *Neohelos* spB
Inabeyance: *N. tirarensis*
Leaf: *N. tirarensis*
Mike's Menagerie: *N. tirarensis*
Neville's Garden: *N. tirarensis*
Sticky Beak: *Neohelos* spB

Group 3

Bone Reef: *N. tirarensis*
Cleft of Ages: *Neohelos* spA
Jims Jaw: *N. tirarensis*
Sticky Beak: *N. tirarensi*
U. Burnt Offerings: *N. tirarensis*

Indeterminate

D-Site: *N. tirarensis*
Wayne's Wok: *N. tirarensis*

CONCLUSIONS

The *Neohelos* material analysed here falls into two quite distinct groups. The first includes all the *Neohelos* spB material from the Bullock Creek sites (Blast Site, Camp Quarry, Top, and Horseshoe West) plus a few specimens from two sites at Riversleigh: three isolated teeth of *Neohelos* spB from Henk's Hollow and ten specimens of *Neohelos* spC from Jaw Junction. The specimens from these six sites are always found distinctly clustered together on every dendrogramme they occur on and no other populations are associated with them.

The remaining specimens from the Leaf Locality, the type locality for the genus and species *Neohelos tirarensis*, plus that from fifteen other sites at Riversleigh do form two obvious clusters but the boundary between them is not as sharp. This blurring of the division is most apparent in the difficulty in characterising the association of the *N. tirarensis* material from D-Site and Wayne's Wok.

The method of analysis employed here was dictated by the structure of the data: (1) individual specimens could have up to fourteen measurements possible but typically many of them missing, (2) several populations with few individuals in them, and (3) there were a few populations with large number of individuals in them. The Blast Site at Bullock Creek was the largest population. Analysis of it enabled a study to be carried out which demonstrated that the distribution of t-test values in a sample population of *Neohelos* was reasonably close to theoretical expectations (Table IV, Fisher 1938). Inspection of the morphology of the specimens from that site justified the assumption that only a single species was likely to be represented in it. Sub-samples of it were then compared to one another to empirically measure the distribution to t-test values to be expected when different populations of a single species were compared to one another. The values were found to be close enough to the theoretical expectations that no corrections were made when that data was then analysed utilising study of the means of the Student's t-test values.

This method of analysis is conservative in that if a difference is found, it is likely to be meaningful but if populations are combined, it may be erroneous because only simple measurements of the cheekteeth are considered. An obvious example of the latter is the close similarity of the Alcoota *Kolopsis torus* to the Bullock Creek *Neohelos*, the clear difference between them being a feature not considered in this analysis, namely the condition of the paracone and metacone on the P^3.

The chronological framework of the Tertiary terrestrial mammal localities of inland Australia is poorly established (Stirton *et al.* 1968, Woodburne *et al.* 1985). Out of necessity, an ordering of these sites has been attempted utilising stage-of-evolution analysis. This procedure attempts to assign assemblages of a fossils from different localities to a relative chronological sequence by inferring which ones have members that are more advanced and thus presumably younger. The method has both its defenders (Savage 1977) and detractors (Eldredge & Gould 1977). Be that as it may, when no other method is available for chronologically ordering a series of sites, utilisation of this method does provide a reasonable working hypothesis.

In the evolution of diprotodontoids, the general trend within genera as well as between them has been towards larger size. *Neohelos* spB from Henk's Hollow and *Neohelos* spB from Jaw Junction are clearly similar in size to the four populations of Bullock Creek material of *Neohelos* spB and therefore all six populations clearly cluster together in Figures. 79-87. The fifteen other Riversleigh populations of *Neohelos* are clearly smaller, and may be in turn divisible into two groups. Therefore, it would appear that two of the Riversleigh *Neohelos* assemblages (Henk's Hollow and Jaw Junction) plus the *Neohelos* from Bullock Creek, being consistently larger are also younger than the *Neohelos* from the Leaf Locality, Kutjamarpu Local Fauna, Lake Ngapakaldi and the fifteen other Riversleigh sites where the genus is known.

REFERENCES

Eldredge, N. and Gould, S.J., 1977. Evolutionary models and biostratigraphic strategies. In: Kauffman, E.G. and Hazel, J.E. (eds) *Concepts and methods of biostratigraphy*. Pp 25-40. Dowden, Hutchinson and Ross: Stroudsburg.

Fisher, R.A., 1938. *Statistical methods for research workers.* Oliver and Boyd: Edinburgh.

Rohlf, F. J. 1990. *NTSYS-pc. Numerical Taxonomy and Multivariate Analysis System Version 1.60.* Exeter Software: Setauket, New York.

Savage, D.E., 1977. Aspects of vertebrate paleontological stratigraphy and geochronology. In: Kauffman, E.G. and Hazel, J.E. (eds) *Concepts and methods of biostratigraphy*. Pp 427-442. Dowden, Hutchinson and Ross: Stroudsburg.

Stirton, R.A., Tedford, R.H. and Woodburne, M.O., 1968. Australian Tertiary deposits containing terrestrial mammals. *University of California Publications in Geological Sciences* 77: 1-30.

APPENDIX II

KEY TO ABBREVIATIONS

Tooth structures:

ABC	Anterobuccal crest of parametacone
AC	Anterior cingulum
AG	Anterior groove I^2
ALC	Anterolingual cingulum
BC	Buccal cingulum
BCP	Buccal crest of parastyle of P^3
DEN	Dentine exposure
DEJ	Dentine-enamel junction
ENA	Enamel surface
FOS	Fossa and basin on posterior loph surfaces and median valley
HY	Hypocone, posterolingual cusp on upper cheek teeth
[HY]	Hypocone damaged or missing due to breakage or wear
[hy]	Approximate position of congenitally missing hypocone
I	Incisor
IGR, VG	Longitudinal groove on ventrolateral edge of lower incisor
LBA	Lingual basin on P^3
LC	Lingual cingulum
LCP	Lingual crest on parastyle of P^3
LS	longitudinal sulcus in posterior basin of P^3
M	Molar
ME	Metacone, posterolabial cusp on upper cheek teeth
ML	Metaloph, posterior transverse crest on upper molar
MS	Mesostyle, labial cuspule on P^3
MT	Metastyle, postcrolabial cuspule on upper molars
MV	Median vallcy or transverse sulcus between molar lophs
OR	Open-rooted tcrmination of upper central incisors (I^1)
P^3	Permanent upper premolar
PA	Paracone, anterolabial cusp on upper cheek teeth
PBA	Posterior basin of P^3
PC	Postcingulum or posterior cingulum of upper cheek teeth
PES	Posterior enamel salient on I^2
PG	Posterior groove on I^2
PMC	Paramctacone, large pyramidal labial cusp of P^3
PMCR	Post(Para-)metacrista, posterior crest of parametacone
PR	Protocone, anterolingual cusp of upper chcek teeth
PRD	Protoconid, large cusp on P_3; anterolabial cusp of lower molar
PPC	Postparacrista, a crest behind the paracone
PPF	Postprotoconal fossa or basin, a basin behind the protocone
PS	Parastyle, anterolabial cuspule on upper chcek teeth
TCR	Transverse crest or link, crest betwcen PMC and PR

TRS	Transverse sulcus, groove between parastyle and parametacone
VG, IGR	Ventral longitudinal groove on I_1

Cranial structures:

AIF, IOF2	Auxiliary infraorbital foramen
AL	Alisphenoid bone
ALN	Alveolar nerve foramen
ALS	Alveolar shelf or suborbital shelf
APF	Anterior palatal fenestra or incisive foramen
CAL	Canine tooth alveolus
COF	Condylar foramen, hypoglossal canal
DPA+PAN	Foramen for descending palatal artery and palatine nerves
ECC	Entocarotid canal, foramen for internal carotid Artery
EGE	Entoglenoid eminence, swelling or bulla medial to glenoid fossa
ETF	Epitympanic fenestra, opening into epitympanic sinuses
FCO	Fenestra cochlearis, ventral cochlear opening in petrosal
FMC	Fossa for middle concha within external nares
FOV	Foramen ovale, transmits mandibular branch of trigeminal N.
FR	Frontal bone
FRC	Frontal crest
FRO	Foramen rotundum, transmits maxillary branch of trigeminal N.
FRS	Frontal suture
FVE	Vestibular fenestra, dorsal vestibular opening in petrosal
GF	Glenoid fossa, articular surfaces for the dentary condyle
IIF	Interincisive fossa
INC	Inferior nasal crest
IOA+LAN	groove for great infraorbital artery and lacrimal nerve
IOF	Infraorbital foramen
IOC	Infraorbital canal
ITC	Infratemporal crest
JMS	Jugal-maxillary suture
JUG	Jugal
LAC	Lacrimal bone
LAT	Lacrimal tubcrosity
MAP	Maxillary portion of masseteric or zygomatic process
MAS	Mastoid bone
MAX	Maxillary bone
MEN	Margin of external nares
MNS	Median ventral sulcus of narial aperture
MOF	Median occipital foramen
MPP	Median premaxillary process or eminence
NAP	Aperture of the external nares
NAS	Nasal bone
NPP	Nasal articular surface of premaxilla
NPS	Nasopremaxillary suture
ORB	Orbit
PAL	Palatine bone

PAR	Parietal bone
PGP	Postglenoid process
PGT	Pterygoid bone
PHC	Pharyngeal crest of palatine bone
PMP	Paroccipital-mastoid process
PMS	Premaxillomaxillary suture
PPP	Premaxillary process of palate
Rcl	Fossa for rectus capitus lateralis muscle
Rcpma	Fossa for rectus capitus major muscle
Rcpmi	Fossa for rectus capitus minor muscle
SAC	Sagittal crest
SAS	Squamosal-alisphenoid suture
SFN	Emissary foramina in supraoccipital
SOC	Median crest of supraoccipital
SOF	Sphenorbital foramen (optic nerve+ophthalmic artery)
SOT	Suborbital tuberosity
SPF	Sphenopalatine foramen
SSP	Septal process of premaxilla
SQS	Squamosal suture
SQ	Squamosal bone
SZN	Subzygomatic notch
VII	Facial nerve groovc, foramen or stylomastoid foramen

Neurocranium and endocasts:

α–α′	Rostral-most sulcus separating prefrontal from parietofrontal lobes
β	Sulcus separating parietofrontal and temporal lobes
μ	Sulcus separating occipital lobe from temporal lobe
δ	Short sulcus in temporal lobe
ν′	Sulcus separating parietofrontal lobe from occipital lobe
CH	Cerebellar hemisphere
ECA	Endocranial cavity
ETS	Epitympanic sinus
FMA	Foramen magnum
HYC	Hypoglossal canal
IAM	Internal auditory meatus (acoustic+facial nerves)
IB	Interbrachial sulcus
IN	Inner table or internal capsule of braincase
J	Jugular sulcus
L	Labial sulcus
LSS	Lateral sinus of squamosal bone
OA-ON	Opthalmic artery+optic nerve
OPC	Optic pole of cerebrum
OUT	Outer table of neurocranium
PFL	Paraflocculus
PSM	Parietal septum
RF	Rhinal fissure
SMV	Superficial middle cerebral vein

SS+TS	Confluence of sagittal and transverse sinuses
SSI	Squamosal sinus in the zygomatic root
SSU	Squamosal sulcus
TPC	Temporal pole of cerebrum
TS	Transverse sinus
V	Vermis of cerebellum

Basicranium and ear region:

ACR	Attachment of anterior crus of ectotympanic bone
AEM	Articular eminence of glenoid fossa
ATP	Alisphenoid tympanic process
ATT	Attic of tegmen tympani
BTP	Basioccipital tympanic process or wing
CAG	Groove for carotid artery
COF	Condylar foramen
CTY	Crista tympanica
ECT	Ectotympanic
EGE	Entoglenoid eminence
ENC	Canal for internal carotid artery
ETF	Epitympanic fenestra
ETS	Epitympanic sinus
FLF	Floccular fossa of periotic bone
FCO	Fenestra cochlearlis
FOV	Foramen ovale
FOV+EUS	Mandibular nerve+eustacian tube
FVE	Fenestra vestibularis
GF	Glenoid fossa
HTS	Hypotympanic sinus
ICF	Incudal fossa
IJF	Internal jugular foramen (posterior lacerate foramen)
ITY	Incisura tympanica
MAS	Mastoid bone
PCP	Paroccipital-mastoid process
PCR	Attachment for posterior crus of ectotympanic bone
PET	Petrosal
PGP	Postglenoid process
PLF	Posterior lacerate foramen
POC	Paroccipital bone
PSI	Petrosal sinus
PTF	Pterygoid fossa
PYF	Pyriform fenestra (middle lacerate foramen)
SAS	Squamosal-alisphenoid suture
SIS	Sigmoid sinus
STF	Stapedial fossa
SUF	Supratympanic fossa or recess
TCA	Tympanic cavity
VII	Facial nerve foramina, grooves or stylomastoid foramen

Dentary:

ANG	Angular process
DIC	Diastemal crest
DIF	Digastric fossa
DIP	Digastric process
FOP	Fovea pterygoidea
GEP	Genial pit
ICS	Intercoronoid sulcus
MAF	Masseteric foramen
MEF	Mental foramen
MFO	Masseteric fossa
MNF	Mandibular foramen
MNO	Mandibular or coronoid notch
NCO	Condylar neck
PDS	Postdigastric sulcus
PME	Postmasseteric eminence
PMF	Posterior mental foramen
PTF	Pterygoid fossa
SLF	Sublingual fossa
SMC	Submasseteric crest
SYM	Symphysis
TRT	Transverse torus

Postcranial Structures:

ACP	Acromion process
ADS	Adductor muscle scar
AIL	Ala of ilium
APX	Apex of sacrum
ASF	Astragalar facet
ASP	Articular surface pecten pubis
BAS	Basis sacrum
CAB	Caudal border scapula
CAH	Humeral head
CAN	Anterior crest
CAP	Capitulum humerus
CFE	Femoral head
COF	Coronoid fossa
COP	Coracoid process
CPI	Conical process of inner condyle
CRB	Cranial border scapula
CRI	Interosseous crest
CSU	Sipinator crest
DTP	Deltopectora; tuberosity
ECB	Entepicondylar bridge
ENF	Entepicondylar foramen
EPI	Epiphyseal line

FIF	Fibular facet
FIS	Infrascapular fossa
FSS	Suprascapular fossa
GLF	Glenoid fossa (scapula)
GRS	Groove between rotular surface and ectepicondyle
GRT	Greater trochanter
ICE	Intercondylar eminence
ICO	Intercondylar notch
IFT	Iliofemoral tuberosity
INS	Incisura scapulae
IPE	Iliopectineal eminence
IRA	Radial incisure
ITU	Ischial tuberosity
LCO	Lateral condyle
LEC	Lateral epicondyle
LIT	Lateral intercondylar tubercle
LPO	Popliteal line
LTR	Lesser trochanter
MCO	Medial condyle
MEC	Medial epicondyle
MIT	Medial intercondylar tubercle
MSC	Median sacral spine
OBC	Obturator crest
OBF	Obturator foramen
OLF	Olecranon fossa
OLP	Olecranon process
OTR	Origin triceps muscle
PCO	Coronoid process ulna
PEC	Pecten
PER	Pectoral ridge
PRT	Pit (radial tuberosity) brachialis muscle scar
RAF	Radial fossa
RPS	Ridge popliteal surface femur
RSU	Rotualr surface femur
SAF	Sacral foramen
SAP	Superior articular process sacrum
SAR	Articular process for sacrum
SAT	Sacral tuberosity
SCA	Sacral canal
SFT	Shaft of epipubic bone
SLI	Semilunar notch ulna
STP	Styloid process
SSP	Scapular spine
SUS	Subscapular fossa
TEC	Teres muscle crest (humerus)
TMA	Major tuberosity humerus

TMI	Minor tuberosity humerus
TRF	Trochanteric fossa
TTU	Tibial tuberosity
VEB	Vertebral border scapula

Museum and university collection prefixes:

AMNH	American Museum of Natural History
AM	Australian Museum
CPC	Commonwealth Palaeontological Collection, Bureau of Mineral Resources
AR	Field designation for University of New South Wales
NTM	Northern Territory Museum (Museums and Art Galleries of the N.T.)
NMV	Museum of Victoria (formerly National Museum of Victoria)
MONASH	Monash University
SAM	South Australian Museum
UCMP	University of California Museum of Palaeontology
UC/SAM	Joint University of California / South Australian Museum field designation
QM	Queensland Museum

APPENDIX III

PHYLOGENETIC ANALYSIS OF *NEOHELOS*

PETER F. MURRAY

This appendix complements the sections on speciation and succession in *Neohelos* and *Neohelos* phylogeny in the body of the paper. Recognition of *Neohelos* spA and *Nimbadon scottorrorum as possibly* a species *of Neohelos* occurred after the final draft of the paper had been circulated.

The systematics were modified accordingly but a cladistic analysis of the new data was not carried out, as the paper had already been submitted and subjected to peer review. The addition of an appendix obviates the need to make extensive changes to the paper.

METHOD

Previous work on zygomaturine phylogeny (Stirton *et al* 1967, Stirton 1967, Woodburne 1967, 1969; Plane 1967, Hand *et al* 1993, Murray 1990, 1992, Murray *et al* 1993) provide a systematic and analytic framework for initial character assessment. Character definitions and polarity determinations are from Murray (1992), Hand *et al* (1993) and Murray *et al* (1993). Phylogenetic analysis of a 32-character matrix (Tables 1-2) was carried out with HENNIG 86 version 1.5 (Farris 1988) set at mhennig; bb; and nelsen. Comparable results were obtained with PHYLIP version 3.57c (Felsenstein 1995) using its Wagner algorithm (Mix). A bootstrapped consensus tree was generated with Seqboot and Consense. As Mix does not accept multistate characters, the consequently much larger PHYLIP discrete character matrix is not included.

Individual variability in character expression is an important factor in zygomaturine character assessment. Larger population samples (*Neohelos stirtoni*) indicate that there is a fair chance that the expression of some primary characters in small samples or single specimens of a species may not be representative of the species as a whole. Omission of variable characters is hardly an option, because few, if any, characters would remain for analysis. Consequently, the assessment contains an element of subjectivity in relation to determination of the intensity of expression and specific combination of states considered typical or representative of a particular species. Many different matrices representing a variety of character combinations and transformations were compiled and examined using the two parsimony programs at my disposal. All of these resulted in configurations similar to that described below.

RESULTS

The most parsimonious computer-generated HENNIG 86 dendrograms (Figs 1-2) point to the same problematic areas discussed in the paper: the position of *Kolopsoides-Plaisiodon* in relation to *Nimbadon* and the relationship of these genera to basal members of *Neohelos*. *Nimbadon* spp. are most often depicted as the sister group to *Neohelos* spA.

Table 1. Character states of zygomaturine taxa included in the analysis of the affinities of species of *Neohelos*. Polarity codes: 0, primitive, 1, 2, 3, derived. Definitions and polarity determinations from Murray (1992), Hand *et al* (1993) and Murray (1993).

1	Lower incisor form: lanceolate 0; tusk-like 1; spatulate 2.
2	Upper incisor tips: converge 0; diverge 1.
3	Canine: present 0; absent 1.
4	P^3 shape: rhomboidal 0; oval 1; pear-shaped 2.
5	P^3 length/M^1 length: L=M^1 0; L>M^1 1; L<M^1 2.
6	P^3 parastyle: absent 0; rudiment 1; small 2; large 3.
7	P^3 crown (parastyle and parametacone): vertical 0; slanted posteriorly 1.
8	P^3 parastylar crests: weak-absent 0; present lingually 1; lingual and labial 2.
9	P^3 transverse sulcus: wide 0; narrow 1.
10	P^3 posterior basin: broad, shallow 0; long, narrow 1.
11	P^3 hypocone: absent 0; small 1; large 2.
12	P^3 anterobuccal cingulum: absent 0; present 1; joined to posterobuccal cingulum 2.
13	P^3 posterobuccal cingulum: present 0; absent 1.
14	P^3 mesostyle: absent 0; small 1; large 2.
15	P^3 parastyle joined to metacone by high crest: no 0; yes 1.
16	P^3 parametacone: undivided 0; incipient division 1; fully divided 2.
17	P^3 parametacone: high 0; low 1.
18	P^3 transverse crest: absent 0; to anterolingual cingulum 1; low to protocone 2; high 3.
19	P^3 partial hypoloph blocking longitudinal sulcus absent 0; present 1.
20	M^{1-4} interproximal contact areas: narrow 0; wide 1.
21	M^{1-4} parastyle and metastyle: small 0; large 1; incorporated 2.
22	M^{1-3} metastylar corner expanded or lengthened: no 0; yes 1.
23	M^{1-3} postcingulum ascends side of posterolingual cusp: absent 0; partial 1; to tip 2.
24	M^{1-3} lingual cingulum: discontinuous 0; weakly continuous 1; strongly continuous 2.
25	M^{1-4} loph orientation: slightly oblique 0; straight 1; very oblique 2.
26	M^{1-4} mesio-distal gradient: weak 0; strong 1.
27	M^1 protoloph shape: wide, slight curve or straight 0; narrow, V-shaped 1.
28	M^1 shape: rectangular 0; trapezoidal 1; square 2.
29	M^{1-4} row curvature: straight 0; slight curve 1; very curved 2.
30	Tympanic wing: squamosal 0; squamosal-alisphenoid 1; alisphenoid 2.
31	Postglenoid and entoglenoid: thin 0; slightly inflated 1; very inflated 2.
32	Epitympanic fenestra: large 0; small 1; absent 2.

Plaisiodon and *Kolopsoides* are sister genera to *Nimbadon* spp. Bootstrapped strict consensus in PHYLIP unites *Plaisiodon-Kolopsoides* and *Nimbadon* spp in a sister clade to *Neohelos-Zygomaturus*, possibly reflecting the entirely dichotomised discrete character state matrix.

Ambiguity in the *Neohelos-Kolopsis-Zygomaturus* crown group is shown in an unresolved trichotomy in the HENNIG 86 Nelson consensus tree (Fig. 1). This issue is discussed and illustrated in the paper. *Neohelos* species, *Neohelos* spA to *Neohelos* spC, are depicted as a series of successively evolving species, possibly implying gradual fixation of synapomorphies within the lineage (Wiley 1979). Although *Plaisiodon centralis* shows a general resemblance to the larger species of *Neohelos* and *Zygomaturus* crown groups, Stirton *et al* (1967:155) consider *Plaisiodon* to be "...considerably removed from *Neohelos*..." [and] "...may represent an early branch of the Zygomaturinae..." , as confirmed here.

Though Stirton *et al* (1967) suggest that *Kolopsoides cultridens* appears to be more closely related to *Kolopsis* than to *Plaisiodon*, their hypothesis is based primarily on the divided parametacone of P^3 (character 16) which both (HENNIG 86 and PHYLIP)

Table 2. Character state matrix for species of Zygomaturinae; *Pyramios alcootense* (Diprotodontinae) outgroup species.

	Pyramios alcootense	*Alkwertatherium webbi*	Riversleigh zygomaturine	*Plaisiodon centralis*	*Kolopsoides cultridens*	*Nimbadon lavarackorum*	*Nimbadon whitelawi*	*Neohelos* spA	*Nimbadon scottorrorum*	*Neohelos tirarensis*	*Neohelos* spB	*Neohelos* spC	*Kolopsis torus*	*Kolopsis yperus*	*Zygomaturus trilobus*
1	2	2	0	0	0	-	-	-	-	0	0	0	0	0	1
2	0	0	0	0	0	-	-	-	-	0	0	0	0	0	1
3	1	1	0	1	-	-	-	-	-	0	1	-	1	1	1
4	0	0	1	1	1	2	2	2	2	2	2	2	2	2	2
5	0	0	0	1	1	1	0	0	2	0	0	0	0	2	2
6	0	3	1	3	3	2	2	2	2	2	3	3	3	3	3
7	0	0	1	1	1	1	1	0	0	0	0	0	0	0	0
8	0	0	0	0	0	0	0	1	2	2	2	2	2	2	2
9	0	0	0	0	1	0	0	0	0	0	0	0	1	1	1
10	0	0	0	1	1	1	1	1	1	1	1	1	1	1	1
11	0	0	0	2	2	1	2	1	1	1	2	2	2	2	2
12	0	0	0	0	0	0	0	0	0	0	0	0	1	0	1
13	0	0	0	1	1	0	0	0	0	0	0	0	0	0	0
14	0	0	0	0	0	1	1	1	0	1	2	1	1	2	2
15	0	0	0	0	1	0	0	0	0	0	0	0	0	0	0
16	0	0	0	0	2	0	0	0	0	0	0	1	2	2	2
17	0	0	0	0	1	0	0	0	0	0	0	0	1	0	0
18	0	0	0	0	0	1	1	0	2	2	2	0	0	3	3
19	0	0	0	0	0	0	0	0	0	0	0	0	0	1	1
20	0	0	0	1	0	0	0	0	1	1	1	1	1	1	1
21	0	0	0	1	0	0	0	1	1	1	1	1	1	1	2
22	0	0	0	0	0	0	0	1	0	0	0	0	0	0	0
23	0	0	0	0	0	0	0	2	1	0	0	0	0	0	0
24	0	0	0	2	0	0	0	0	0	1	2	2	2	2	2
25	2	2	1	0	0	1	1	1	1	1	1	1	1	0	0
26	1	1	0	1	1	0	0	1	0	0	1	1	1	1	1
27	0	0	0	1	1	1	1	1	1	0	0	0	0	0	0
28	0	0	0	0	0	0	0	1	1	1	1	1	1	2	2
29	2	1	1	1	1	0	0	1	1	1	1	-	1	2	2
30	0	1	1	1	-	-	-	-	-	1	2	-	2	-	2
31	0	1	1	1	-	-	-	-	-	1	2	-	2	-	2
32	2	1	0	1	-	-	-	-	-	0	1	-	1	-	2

parsimony algorithms recognise as homoplasious with *Kolopsis-Zygomaturus*. The species otherwise exhibits several autapomorphic features: 3-rooted P^3, widely emarginated labial outline of P^3, and well-developed paraconal-metaconal crest (character15). Possible synapomorphic states with *Plaisiodon* include elongated P^3 (character 5), absent labial cingulae and mesostyle on P^3 (characters 13, 14). Binding branch consistency between these species is relatively high (0.8).

Affinity of *Plaisiodon-Kolopsoides* with *Nimbadon* species is tenuous, based primarily on the shared possession of anteriorly-projecting crown base of P^3 (character 7 or "hooked parastyle" of Hand *et al* 1993). *Nimbadon* species more consistently bind to basal *Neohelos* species (0.6). While the P^3 morphology of *Nimbadon* species shows strong resemblances to those of *Neohelos*, the molars are generally narrower, with narrower interproximal contacts, weak molar gradient approaching 1.0 and smaller stylar cusps (characters 20, 21, 28) considered primitive zygomaturine states (Hand *et al* 1993).

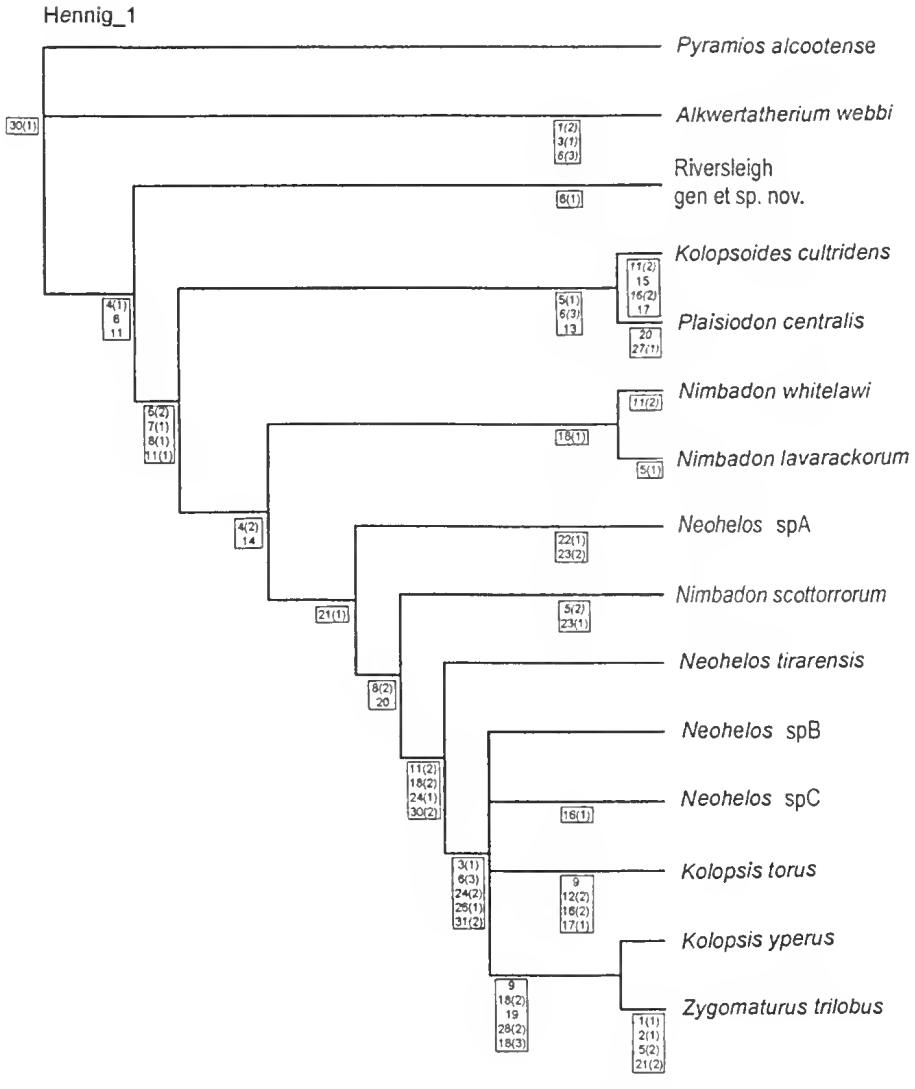

Fig. 1. Nelsen consensus tree (Hennig86: set at mhennig, bb, nelsen; length 89; c.i. = 0.58; r.i. = 0.72; 3 trees). boxed numerals indicate character states at nodes; italics denote inferred homoplasious states.

CONCLUSIONS

The HENNIG 86 result requires fewer steps than the PHYLIP-generated tree, and is therefore considered the most parsimonious reconstruction of *Neohelos* phylogeny. The reconstruction does not differ significantly from that of Hand *et al* (1993) except for the revision of *Nimbadon scottorrorum* to *Neohelos scottorrorum* (which may represent an individual variation of *Neohelos tirarensis*). The study confirms Stirton's (1967) and Stirton *et al*'s (1967) recognition of the intermediate position of the genus *Neohelos* between several early branches of the Zygomaturinae and the subsequent late Cenozoic radiation of zygomaturines leading to *Zygomaturus trilobus*. While the newly discovered species have added complexity to the record, the basic phylogeny of zygomaturines proposed by Stirton and his colleagues continues to be a robust hypothesis.

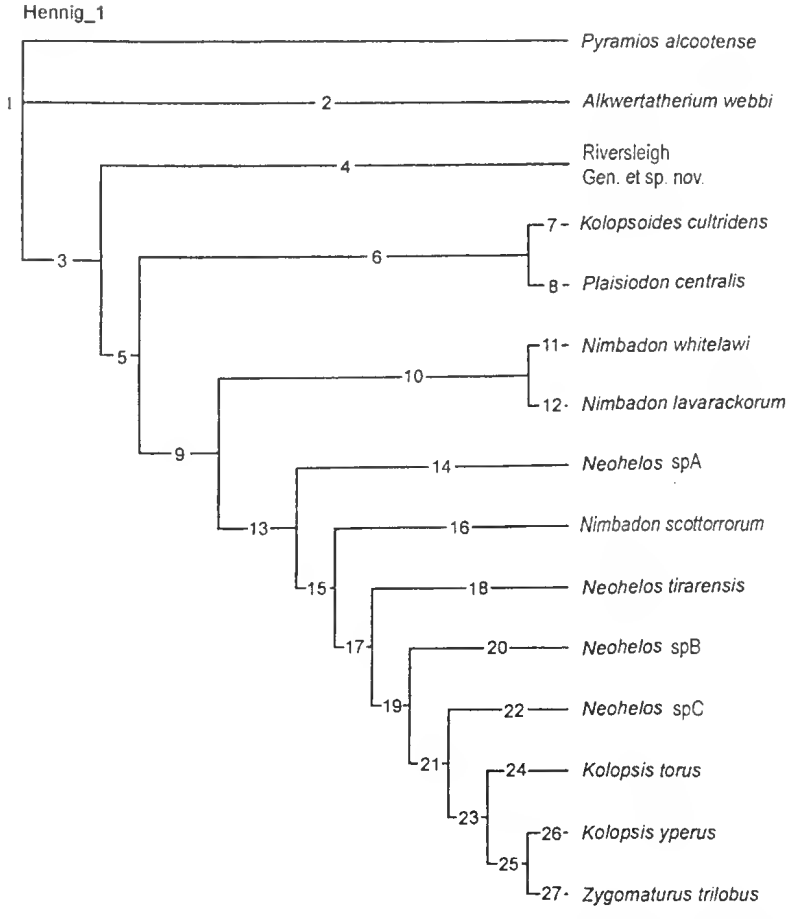

Fig. 2. Phylogram depicting most parsimonious reconstruction of *Neohelos* phylogeny, configuration selected from among three equally parsimonious trees; apomorphic character states at each node: **0)** outgroup species *Pyramios alcootense* (squamosal tympanic wing, P^3 parastyle absent); **1)** alisphenoid component of tympanic wing present; **2)** autapomorphic states: large P^3 parastyle, spatulate incisors, loss of canine; **3)**, ovo-triangular P^3 shape, parastyle or parastylar base present; **4)** rudimentary parastyle present; **5)** P^3 crown base projects anteriorly, weak lingual parastylar crests present, hypocone present; **6)**, P^3 elongated, posterobuccal cingulum of P^3 lost; **7)** autapomorphic states: P^3 hypocone enlarged (?homoplasious with *Nimbadon whitelawi*), P^3 parastyle joined to paracone by crest, fully divided parametacone (homoplasious with *Zygomaturus*); **8)** homoplasious broad interproximal contact of internal molars, homoplasious narrow, V-shaped or strongly curved M^1 protoloph (in some individuals); **9)** P^3 distinctly 'pear-shaped' and about equal in length to M^1, mesostyle distinct; **10)** P^3 transverse crest from parametacone descends to anterolingual cingulum; **11)** homoplasious enlargement of P^3 hypocone; **12)** P^3 considerably longer than M^1; **13)** $M^{1\text{-}3}$ parastyle and metastyle large, divided from paracone and metacone by distinct sulcus, M^1 trapezoidal outline shape; **14)** autapomorphic: M^1 elongated by expansion of metastylar corner , post cingulum continues continues as a strong crest to the tip of lingual side of posterolingual cusp; **15)** distinct labial and lingual parastylar crest on P^3, wide interproximal contacts of molars; **16)** homoplasious (or individual variation) P^3 much shorter than M^1, possibly synapomorphic (with *Neohelos* spA) presence of (weaker) crest from postcingulum ascending posterlingual cusps of anterior molars; **17)** lingual cingulum of molars weakly continuous, alisphenoid tympanic wing; **18)** no additional features; **19)** loss of canine, parastyle and hypocone large, lingual cingulum of molars strongly continuous; **20)** no additional features; **21)** divided P^3 parametacone; **22)** incipient or variable division of P^3 parametacone; **23)** narrow or congested transverse sulcus between base of paracone and base of parastyle; **24)** autapomorphic states: low paracone and metacone, anterobuccal cingulum joined to postcrobuccal cingulum; **25)** square M^1, P^3 longitudinal sulcus congested by partial hypoloph; **26)** no additional features; **27)** P^3 much shorter than M^1, parastyle and metastyle reduced or incorporated, tusk-like incisors with divergent tips.